



UNIVERSITY OF THE PELOPONNESE

KLADOURI NIKOLETTA KANELLA

(R.N. 1012201602004)

DIPLOMA THESIS:

**A TECHNOLOGICAL STUDY OF A BRONZE PINS COLLECTION OF
GEOMETRIC PERIOD FROM THE SANCTUARY OF ATHENA ALEA AT
TEGEA**

SUPERVISING COMMITTEE:

**-Professor Nikolaos Zacharias
-Dr Vana Orfanou**

EXAMINATION COMMITTEE:

**-Professor Nikolaos Zacharias
-Dr Vana Orfanou
-Assistant Professor Eleni Zimi**

KALAMATA, JANUARY 2018

Acknowledgements

I would like to thank and express my gratitude to my supervisors and members of the Examination Committee, Professor Nikolaos Zacharias, Dr Vana Orfanou (Aarhus University) and Professor Eleni Zimi, for all their support, useful critique and guidance, throughout the course of this research.

I would like to express my very great appreciation to Dr Vasiliki Kantarelou (NCSR Demokritos) and Dr Andreas-Germanos Karydas (NCSR Demokritos). Their guidance, targeted comments and immediate response provided me with valuable knowledge.

I was honoured to have the support of Professor Andreas Tsatsaris (TEI of Athens) to whom I am grateful, as I am obligated to the kindness of Professor Mary Voyatzis (University of Arizona) and Dr Georgios Steinhauer for their permission to study their archaeological material.

I am particularly grateful to Ms Vasiliki Valantou who in her own unique way kept supporting my spirit and very often my body, by providing a spare blanket and a soft couch and Dr Eleni Palamara for her advices and patience during the times I believed that Excel is a program made in hell (spoiler alert: It is not).

My special thanks are extended to my good friends Dr Grigoris Grigorakakis, Spiros Kiziridis, Dr Klaus-Valtin Von Eickstedt and Georgia Simbroukou for their overall support.

Above all I would like to express my love and dedicate this work to my kids Eleftheria and Konstantino, without whom this thesis would have been completed fifteen years earlier. Fortunately, it didn't.

Contents

List of tables, images and figures	v
Abstract	viii
Introduction	ix
I. The archaeological context	1
1.1. Tegea and the sanctuary of Athena Alea	1
1.1.1. History of the excavations	1
1.1.2. The Sanctuary	1
1.1.3. The bronze pin assemblage	3
1.1.4. The chronological context of the assemblage	4
1.2. Ancient copper alloys technology	5
1.2.1. Analysis of copper alloys	7
1.2.2. Copper alloys' corrosion products, selective corrosion and de-alloying phenomena	8
II. Materials and Methods	12
2.1. Classification of the assemblage	12
2.1.1. Dating of the assemblage	13
2.1.2. Bronze pins	15
2.1.3. Metallurgical wastes	41
2.2. Optical Microscopy	52
2.2.1. General principles	52
2.2.2. Devices and settings	53
2.3. X-ray Fluorescence Spectroscopy (XRF)	53
2.3.1. General principles	53
2.3.2. Devices and settings	57
2.4. SEM with Energy Dispersive Spectroscopy (EDS)	60
2.4.1. General principles	60
2.4.2. Devices and settings	63
III. Results and discussion	65
3.1. Stereomicroscopic observation	65
3.1.1. Bronze pins	68
3.1.2. Metallurgical wastes	82

3.2. Elemental analysis using p-XRF	94
3.3. Elemental analysis using μXRF	97
3.4. Elemental analysis using SEM-EDS	100
3.5. Methodology-comparison of the techniques	101
3.6. Results of the chemical analysis	108
3.7. Composition of the assemblage	119
IV. Conclusions	138
V. References	145
VI. Appendices	154
I. Charts and Images	155
II. Appendix-p-XRF	161
II.1. Reference samples	161
II.2. Bronze pins	162
II.3. Metallurgical wastes	166
III. Appendix-μXRF	168
III.1. Reference samples	168
III.2. Bronze pins	169
III.3. Metallurgical wastes	194
IV. Appendix-SEM-EDS	200
IV.1. Reference samples	200
IV.2. Bronze pins	201
IV.3. Metallurgical wastes	214

List of tables, images and figures

- Table 1.1.** *Major copper corrosion products* 9
- Images 3.1-10.** *Casting marks on pins ALEA-P1, -P3, -P4, -P5, -P5, -P6, -P7, -P8, -P11, -P26* 65
- Table 3.1.** *Classification of the corrosion types of bronze alloys* 67
- Table 3.2.** *Concentration of the mean values of the elements detected on the bronze pins with the p-XRF method* 94
- Table 3.3.** *Concentration of the mean values of the elements detected on the metallurgical wastes with the p-XRF method* 96
- Table 3.4.** *Concentration of the mean values of the elements detected on the bronze pins with the μ XRF method* 97
- Table 3.5.** *Concentration of the mean values of the elements detected on the metallurgical wastes with the μ XRF method* 99
- Table 3.6.** *Concentration of the mean values of the elements detected on the bronze pins with the SEM-EDS method* 100
- Table 3.7.** *Concentration of the mean values of the elements detected on the metallurgical wastes with the SEM-EDS method* 101
- Figure 3.5.1.** *Bar chart of the p-XRF, μ XRF and SEM-EDS analyses of the tin content on selected pins; higher tin values are visible during p-XRF analyses* 103
- Figure 3.5.2.** *Scatter plot indicating the perfect correlation for the two axes x and y, for the tin content based on p-XRF, μ XRF and SEM-EDS analyses* 104
- Figure 3.5.3.** *Scatter plot of copper versus tin in selected pins, based on p-XRF, μ XRF and SEM-EDS analytical protocols* 104
- Table 3.8.** *δ relative difference values (%) of the pin's measurements for μ XRF and SEM-EDS* 105
- Table 3.9.** *Standard deviation values (%) on the pin's measurements for the three protocols of elemental analysis* 106
- Table 3.10.** *Precision difference values (%) on the pin's measurements for the three protocols of elemental analysis* 107
- Figure 3.6.1.** *Bar chart of the copper content of the pins, based on μ XRF methodology* 108
- Figure 3.6.2.** *Histogram of the distribution of the pins, regarding their copper content, based on μ XRF methodology* 109
- Figure 3.6.3.** *Bar chart of the copper content on the metallurgical wastes, based on μ XRF methodology* 109
- Figure 3.6.4.** *Histogram of the distribution of the metallurgical wastes, regarding their copper content, based on μ XRF methodology* 109
- Figure 3.6.5.** *Bar chart of the tin content of the pins, based on μ XRF methodology* 110

- Figure 3.6.6.** Histogram of the distribution of the pins, regarding their tin content, based on μ XRF methodology 110
- Figure 3.6.7.** Bar chart of the tin content on the metallurgical wastes, based on μ XRF methodology 110
- Figure 3.6.8.** Histogram of the distribution of the metallurgical wastes, regarding their tin content, based on μ XRF methodology 111
- Figure 3.6.9.** Bar chart of the arsenic content of the pins, based on μ XRF methodology 111
- Figure 3.6.10.** Histogram of the distribution of the pins, regarding their arsenic content, based on μ XRF methodology 112
- Figure 3.6.11.** Bar chart of the arsenic content on the metallurgical wastes, based on μ XRF methodology 112
- Figure 3.6.12.** Histogram of the distribution of the metallurgical wastes, regarding their arsenic content, based on μ XRF methodology 112
- Figure 3.6.13.** Bar chart of the lead content of the pins, based on μ XRF methodology 113
- Figure 3.6.14.** Histogram of the distribution of the pins, regarding their lead content, based on μ XRF methodology 113
- Figure 3.6.15.** Bar chart of the lead content on the metallurgical wastes, based on μ XRF methodology 114
- Figure 3.6.16.** Histogram of the distribution of the metallurgical wastes, regarding their lead content, based on μ XRF methodology 114
- Figure 3.6.17.** Bar chart of the iron content of the pins, based on μ XRF methodology 115
- Figure 3.6.18.** Histogram of the distribution of the pins, regarding their iron content, based on μ XRF methodology 115
- Figure 3.6.19.** Bar chart of the iron content on the metallurgical wastes, based on μ XRF methodology 115
- Figure 3.6.20.** Histogram of the distribution of the metallurgical wastes, regarding their iron content, based on μ XRF methodology 116
- Figure 3.6.21.** Bar chart of the antimony content of the pins, based on μ XRF methodology 116
- Figure 3.6.22.** Histogram of the distribution of the pins, regarding their antimony content, based on μ XRF methodology 117
- Figure 3.6.23.** Bar chart of the nickel content of the pins, based on μ XRF methodology 117
- Figure 3.6.24.** Histogram of the distribution of the pins, regarding their nickel content, based on μ XRF methodology 118
- Figure 3.6.25.** Bar chart of the nickel content on the metallurgical wastes, based on μ XRF methodology 118
- Figure 3.6.26.** Histogram of the distribution of the metallurgical wastes, regarding their nickel content, based on μ XRF methodology 118

- Figure 3.7.1.** Bar chart for the pins analysed, for each period 119
- Figure 3.7.2.** Scatter plot presenting the distribution of Cu versus Sn in pins, based on μ XRF methodology 120
- Figure 3.7.3.** Scatter plot presenting the distribution of Cu versus Sn in selected metallurgical wastes, based on μ XRF methodology 120
- Figure 3.7.4.** Scatter plot presenting the distribution of Cu versus As in pins, based on μ XRF methodology 123
- Figure 3.7.5.** Scatter plot presenting the distribution of Cu versus As concentration in selected wastes, based on μ XRF methodology 124
- Figure 3.7.6.** Scatter plot presenting the range of Cu versus Pb concentration in pins, based on μ XRF technique 125
- Figure 3.7.7.** Scatter plot presenting the distribution of Cu versus Pb concentration in selected wastes, based on μ XRF methodology 125
- Figure 3.7.8.** Scatter plot presenting the distribution of Cu versus Fe in pins, based on μ XRF methodology 127
- Figure 3.7.9.** Scatter plot presenting the distribution of Cu versus Fe in selected metallurgical wastes, based on μ XRF methodology 127
- Figure 3.7.10.** Scatter plot presenting the distribution of Cu versus Sb in pins, based on μ XRF methodology 128
- Figure 3.7.11.** Scatter plot presenting the distribution of Cu versus Ni in pins, based on μ XRF methodology 129
- Figure 3.7.12.** Scatter plot presenting the distribution of Cu versus Ni in selected metallurgical wastes, based on μ XRF methodology 129
- Figure 3.7.13.** Bar chart presenting the concentration of elements in ALEA-P3, based on μ XRF methodology 135
- Figure 3.7.14.** Bar chart presenting the concentration of elements in ALEA-P18, based on μ XRF methodology 136
- Figure 3.7.15.** Bar chart presenting the concentration of elements in ALEA-P4, based on μ XRF methodology 136
- Figure 3.7.16.** Bar chart presenting the concentration of elements in ALEA-P4, based on μ XRF methodology 136
- Figure 4.1.** Scatter plot presenting the distribution of Cu versus Sn on pins and wastes, based on μ XRF methodology 140
- Figure 4.2.** Chart presenting the distribution of pins for Cu versus Sn according to their typology, based on μ XRF methodology 142

Abstract

A collection of 47 copper alloy artifacts from the sanctuary of Athena Alea at Tegea, dating to the 9th-7th centuries BC, was studied and chemically analysed with handheld p-XRF, μ XRF and SEM-EDS to determine the alloy type that was used for their production.

The collection consists of Cu-Sn binary alloys. The relative concentration of the two metals does not seem to have been determined by the type of artifact the alloy was used to produce. The results also imply that fresh rather than scrap metal was used. The majority of the artifacts is made of bronze with an average tin content of approximately 11%. There is, however, an object which was found to have a significantly lower tin concentration, which averages 0.3% Sn. The lead content in the assemblage ranges from 0.5 to 4.94%. Because lead concentrations in the Helladic and the extended Balkan area are significant, their presence is interpreted as a non deliberate addition. The iron content ranges from 0.02 to 1.10%, while nickel exhibits a concentration range between 0.03 - 0.34%. Both elements are believed to be non-intentional additions to the alloys, resulting from the smelting process and originating in the copper ores. Arsenic is detected in all artifacts, in a mean concentration of 0.17%. The limited amount of arsenic may be the result of the use of arsenic-rich copper ores and less likely can be interpreted as evidence for the possible use of recycled metal deriving from artifacts dating to the Bronze Age.

The present study provides evidence concerning the continuity of the use of bronze with high tin content in the area of Tegea during the Geometric and Orientalizing periods.

Introduction

Cultural objects have been processed and used by men, while they have deteriorated by that or during their burial. It was therefore necessary for the archaeological community, to embrace a number of innovative techniques to analyse materials, especially those that constitute heritage materials. The study of ancient objects, thus, requires an integrated approach including knowledge of their archaeological context, typology and classification, interpretation and the scientific analysis of the material itself.

The scientific characterization of cultural heritage materials comprises many different challenges, regarding their analyses. These can be related to various issues like access to materials, representation of assemblage, context and dating, communication with museums and sampling strategies; considering that the materials under analysis are often available in rather small quantities. Although laboratory instruments become more and more powerful and remain the prime equipment for the study of ancient objects, portable instruments have become of major importance, since the necessity of fast and in situ analysis (excavation sites, museums, monuments, etc.) fostered their adaptation to the needs of the cultural heritage materials research. Portable X-ray fluorescence analysis is one of the widely accepted analytical methods nowadays, while Scanning Electron Microscope (SEM) with Energy Dispersive Spectroscopy (EDS) is a classical laboratory technique of chemical analysis, applied to both organic and inorganic materials.

Geometric and Archaic pins from the wider area of the Peloponnese are well typologically classified, though there is little documented comparative information about the nature of raw materials, which were used to produce them. The scope of this thesis is to analyse 26 of the pins excavated at the sanctuary of Athena Alea at Tegea and compare them to 21 of the metallurgical wastes recovered in the same area¹. Their study consists of a) the qualitative and quantitative analysis of the metal, which aims at revealing the main alloy elements, the minor alloying elements as well as impurities and inclusions of the metal, which can provide information on the purity and quality of the raw material; b) the determination of the tin content in the artifacts of the specific period in the area; c) the study of the manufacturing techniques which can reveal the degree of maturity of networking practices. Thus, to understand the metallurgical technology of the pins at the sanctuary, monitoring their evolution in

time and possibly to distinguish features of a possible local technological profile. Although, the number of pins is modest regarding the number revealed in the sanctuary, it is considered as representative of the assemblage. A preliminary analysis can, thus, prove useful given the relative lack of comparative data. The XRF technique along with the use of SEM-EDS method has been chosen in order to analyse the assemblage, without sampling; using only raw spectroscopic intensity data to determine their chemical composition.

The archaeological context of the sanctuary of Athena Alea and the assemblage, along with information regarding the ancient copper metallurgy are reviewed in chapter I. The classification of the assemblage along with the analytical methodology used for its study are presented on chapter II. The obtained results, their interpretation and discussion are comprehensively presented on chapter III, followed by the conclusions on chapter IV.

1. The bronze finds were analysed in accordance with permission (protocol number: ΥΠΠΟΑ/ΓΔΑΠΚ/ΔΣΑΝΜ/ΤΕΕ/Φ77/219908/142273/2264/189) granted by the Directorate of Conservation of Ancient and Modern Monuments of the Hellenic Ministry of Culture and Sports.

I. THE ARCHAEOLOGICAL CONTEXT

1.1. Tegea and the sanctuary of Athena Alea

1.1.1. History of the excavations

The sanctuary was initially identified by Dodwell in 1806, while the first excavations were conducted by the German Archaeological School under the direction of Milchhöfer in 1879 (Grigorakakis et al., 2014a: 58). In 1885 the first drawings of the temple were made by Dörpheld (Dugas, 1921).

Between 1900 and 1902, the French Archaeological School at Athens expropriated the private homes surrounding the sanctuary and began its first systematic excavations. Those were conducted under the direction of Mendel, where more of the temple's foundations, architectural fragments, sculptures, inscriptions along with metallic artifacts and pottery were revealed. The excavations were later continued by Romaios, in 1909 (Romaios, 1911: 276). The French Archaeological School, under the direction of Dugas carried out excavations in the years from 1910 to 1913, while in 1921 he made the first publication of the temple and its findings (Dugas, 1921).

Small-scale research at the beginning of 1960, was carried out by the American School of Classical Studies at Athens with research on the temple proper while the Greek Archaeological Service (under the direction of Christou and Dimakopoulou) brought to light many architectural and sculptured members of the temple. In 1976 and 1977 Steinhauer, also carried out small-scale excavations in the area north of the temple. In the 1980s Østby worked on identifying the foundations of the Early Archaic temple inside the foundations of the of the Classical temple, resulting in directing the excavation research conducted by The Norwegian Archaeological Institute in collaboration with the Greek Archaeological Service between 1990 to 1994 (Voyatzis, 1990: 20-21; Østby et al, 1994: 89-95; Grigorakakis et al., 2014a: 56-59; Grigorakakis, 2014b).

1.1.2. The Sanctuary

Sanctuaries played an important role in the origins, formation and evolution of the ancient city. These are the places where man met the divine, but also the places where human communities met, formed bonds of unity and identity based on common

interests (Tsatsaris et al., 2015). They were also inextricably linked to the concept of territory (De Polignac 1995: 20-25, 64-66; Hall, 2007: 40-52). This is revealed by the richest and most impressive votive offerings, the monumental architecture and the emergence of sculptures around them (Østby, 2014a: 17-18, 20, 52). One of the sanctuaries usually stood out and, as a nucleus, the individual continued in one, the “polis” which continued to evolve (Tsatsaris et al., 2015). The sanctuary of Athena Alea at Tegea was one of the cases where a sanctuary distinguished in a wider area. The evidence concerning the sanctuary indicates that, although in a remote district, it possessed elements of artistic creativity (Voyatzis, 1990: 7). It is located in the heart of the modern community of Alea in the municipality of Tegea, about 8 km southeast of Tripoli (image -I.1-, -I.2-).

According to Pausanias the mythical founder of the sanctuary was Aleos, while the architect of the classical marble temple was one of the most famous sculptors of antiquity, Skopas from Paros. The temple of Athena Alea and the theatre are the only known signs of the topography of the urban territory of the ancient Tegea and its immediate suburban area. Pausanias, based on the topography of these two monuments, determined the position of the stadium and the agora of the ancient polis (Voyatzis, 1990: 13-27).

Regarding the stratigraphy of the sanctuary, there are still layers beneath the excavated areas that have not been investigated. It is considered possible, though, that some kind of human activity, even religious activity, took place during the Mycenaean, Early Helladic and even Final Neolithic eras (Østby, 2014a: 19). By the end of the 8th and in early 7th century BC the first simple buildings intended for the worship of Alea were built (image-I.3-). These were two apsidal, of the wattle-and-daub structural type, huts of successive Geometric dates. Earlier construction dates back to the last quarter of the 8th century BC, while the second wattle-and-daub structure replaced it in the early 7th century BC (image -I.4-). Thus, it is safe to consider the sanctuary as one of the earliest in the Peloponnese (Østby, 2014a: 5). The character of those buildings was cultic; confirmed by the large number of votives as well as from the signs of ritual meals revealed (Østby, 2014a: 19-22).

The erection of the Archaic temple of Athena Alea (the first of its kind in Arcadia) in the last quarter of the 7th century BC creates an historical terminus for the settlement of the nine municipalities in the city of Tegea; considering that the excavations at the wider area bear substantial evidence for polis type structures dating

back to the 6th century BC at least (Østby, 2014a: 51). The monumental temple (image -I.5-) was Doric, 6 x 14 columns, with pronaos, cella and adyton, while it was made of marble and wood (Østby, 2014a: 37,47). The temple was destroyed by fire in 395/4 BC (Østby, 2014a: 35).

The classical temple of Athena Alea (image -I.5-), build in the second quarter of the 4th century BC, remained in use practically without changes until the Roman times (Tarditi, 2005: 201). Dugas believed that the classical temple of Athena Alea was Doric, 6 x 18 columns, made from Dholiana marble; his belief was later confirmed by Østby (2014a: 47). Dugas also uncovered the foundations of a large classical altar, which as Pausanias notes was created by the mythical seer Melampous and the fountain of Auge (Dugas, 1921: 66-71).

Although the sanctuary was functioning during the Hellenistic and Roman periods, there is an almost total lack of evidence of those periods. Only few coins and scraps of Roman glass were discovered, along with a Hellenistic marble statue found, though, in a medieval context; probably since there is indication that during the Late Byzantine times the area was used as the cemetery of a monastic complex (Østby, 2014a: 5; Tarditi, 2005: 202-203, 2014: 99).

The deity originally worshipped in the sanctuary was the local Alea, one of many local deities of Arcadia and is interpreted on the basis of her name, as the goddess of the asylum or of fertility. It is not clear when the process of merging Alea with Athena took place; although it has been mentioned as Alea Athena already since the late 6th century BC, declaring the dominion of the local deity over the Panhellenic; only Pausanias calls it Athena Alea. The merging of the two deities is estimated in the years of the erection of the Archaic monumental temple around 600 BC (Mitsopoulou, 2012: 612-613).

1.1.3. The bronze pin assemblage

Part of the bronze pins assemblage from the sanctuary of Athena Alea derived from the excavations conducted by the French Archaeological School from 1910-13, where, according to Dugas (1924) over a hundred pins were recovered. Voyatzis (1990) notes that in her study concerning the sanctuary she recorded about 400 pins. These were recovered from the older excavations of Dugas, as well as from the excavations conducted by the director of the local Ephorate Steinhauer, in 1976-77

(image-I.6-); a large number were also later unearthed by the excavating archaeological project of the Norwegian Institute of Athens, between the years 1990-94. Although it is not easy to calculate the exact number of pins due to incomplete data, these are estimated at approximately 700 (Mitsopoulou, 2012: 595).

A full study considering the Greek Geometric pins firstly appeared in 1956 by Jacobsthal, who generally classifies them as belonging to the chronological context of the Geometric era, subdivided as Geometric I, II and III. Later, Kilian-Dirlmeier (1984) published a book regarding the Peloponnesian pins where she provides a more detailed analysis and classification subdividing Jacobsthal's initial categorization. According to Voyatzis (1990: 203-209) who generally follows the Jacobsthal classification, providing also some subcategories though, the classification of the Geometric bronze pins of Alea covers a great range of types with some of them being of very early type like ProtoGeometric and Geometric I, while the best represented categories are those belonging to Geometric II, variants of Geometric II and Geometric III.

The pins from the sanctuary of Athena Alea are kept at the National Archaeological Museum in Athens, at the Archaeological Museum of Tripolis and at the Archaeological Museum of Tegea.

1.1.4. The chronological context of the assemblage

In archaeology the term "Geometric" describes a period of decorating style of contemporary pottery vessels, made approximately the ages between circa 900 to 700 BC. Classification concerning the artifacts of the period is made mainly based on this pottery, since there is a continuous sequence of it. The absolute dating of the Geometric style depends on the contexts where the pottery can be connected with recorded historical events from the Helladic space and from elsewhere, although their validity has often been questioned. It has been customary to call in the Thucydidean dates for the Sicilian colonies in order to attach the last phase of Geometric to calendar years, so it is generally agreed the setting of the Geometric style to the ninth and eighth centuries BC.

To think in terms of absolute dating and typology, though, is not profitable when considerable differences of style between the local schools occur in the Helladic space. Arcadia and consequently the Tegea region lacked any independent style,

exhibiting at various times the impact of its larger neighbours, the Argolid and Laconia (Tegea was prone especially to the Laconian Dark Age style), mainly in the first years of the Geometric era. Later on, the finds from Tegea exhibited a Middle Geometric II phase, lacking in Laconia, since there is evidence of persistence there of the local Dark Ages style. Argive influence was still strong in the local Late Geometric; while towards 700 BC Corinthian influences often encountered in the Tegea region (Voyatzis, 1990: 83-84, 209; Coldstream, 2008: 364, 471).

The Archaic period is generally considered to have lasted from the beginning of the seventh century BC until the beginning of the fifth century BC. Orientalizing type is supposedly connected to the seventh century of this new period, although completely different in style (Shapiro, 2007).

Thus, the following approximate dates for each period can be suggested: (Burkert, 1992; Coldstream, 2008: 330, 471):

- Early Geometric: before ca 850 BC
- Middle Geometric I: second half of the ninth century
- Middle Geometric II: early eighth century
- Late Geometric: later eighth century
- Subgeometric: ca 690 BC to first quarter of seventh century
- Orientalizing I: seventh century BC
- Orientalizing II: seventh century BC

All dating information concerning the artifacts, along with relevant contextual information (macroscopic description, dimensions, typological classification, etc.), are presented in chapters 2.1.1. and 2.1.2.

1.2. Ancient copper alloys technology

Copper is the earliest useful metal of mankind; considering its use as a tool making metal. Its production and technology has changed the course of humanity at the end of Neolithic times, giving rise to a new era named Bronze Age. As a metal widely distributed in nature, copper can be found either in the native state or as a mineral. Copper minerals can be divided into two types, the more easily reducible oxide and carbonate ores and the more complex and less easily reduced sulfide ores, which can contain other metals and non-metals. The more easily found and reduced copper oxide and carbonate ores were the first ones worked.

Considering the copper alloys, these are classified in categories according to their composition. The most important of these are the binary systems of Cu-As (arsenical copper alloy), Cu-Sn (bronze) and Cu-Zn (brass). The alloying of copper with arsenic or tin represents a great step forward in metallurgical practice; regardless if this transition was made deliberately or by chance, it changed the properties of the metal and its further use. Impure metals of Late Neolithic period, probably led to bronzes and that to techniques suitable for such bronzes and to the manufacture of deliberately compounded alloys.

Arsenical copper was one of the earliest copper alloys used in the 3rd millennium around the Mediterranean, although its use probably started much earlier and further east (Garfinkel et al, 2014). Gradually, arsenical copper was abandoned in all Mediterranean, in favour of bronze. It was during the last part of the third millennium BC though, that the change from arsenical copper to tin bronze as the main copper alloy took place throughout the Near and Middle East, including Crete, although tin bronzes seem to have been occasionally used in the Aegean and Anatolia from the Early Bronze Age (Craddock, 1976).

Bronze was the main copper alloy used during the Iron Age all over the Mediterranean. The percentage of tin was adjusted, probably by adding cassiterite (SnO_2). The decline in the use of arsenical copper during the Late Bronze Age implies knowledge of the difficulties associated, among other factors, with the adjustment and the toxicity of the arsenic content. Since deliberate alloying would also be very improbable at such an early stage, a natural copper-tin alloy is, at the moment, an interpretation worth considering (Garfinkel et al, 2014). Rarely, copper and tin ores can be found in the same mineral vein; it is this proximity that could spark the interest of prehistoric people on alloying the two metals. Copper sources with a natural tin-copper alloy are known inter alia in Tajikistan. The easy availability of tin and the knowledge of natural tin-copper alloys could be one reason why the alloying of tin-bronze took place in the Caucasus significantly earlier than in neighbouring regions, namely in the 4th millennium (Garfinkel et al, 2014). The origin of the tin for the Aegean, Crete and mainland Greece is not yet confirmed, but the indication is that during the Iron Age when metal trade was flourishing around the Mediterranean, tin was probably imported from as far as Afghanistan and from the Iberian mines, perhaps via Sardinia as an intermediary (Kassianidou et al, 2005).

Tin as a sole metal, was normally not used at all in antiquity except as a constituent of its alloy with copper. The main bronze “recipes” include bronzes with an average 7-9% tin content (hard), an average 11-13% tin content (very hard) and a tin content above 13% (extremely hard). Bronze besides of copper and tin, sometimes may contain smaller amounts of various metals; among others iron, nickel, antimony, zinc and lead (Tselios, 2013:57-61; Mainz, 2015). The fact that tin can be cut into measurable pieces, is resulting to alloys of certain tin content and thus controlled hardness and colour, as opposed to arsenic. Bronze is harder and has a higher tensile strength than copper, but is less malleable. Because it melts at a lower temperature than copper, it is more easily cast than copper.

It is not uncommon for artifacts, made during the long period of change from arsenic to tin alloys with copper, to have appreciable quantities of both metals. Arsenic- rich copper may have continued to be added to the molten metal as a deoxidant which performs better than the tin. Another explanation is that the source of much of the metal used to make tin bronzes would be scrap arsenical copper, and so for a long time one would still expect to find considerable amounts of arsenic in tin bronzes, although much would be lost at each melting because of the extreme volatility of the arsenic in molten copper (Charles, 1967).

Copper in the Helladic mainland during the Iron Age was still based on local ore sources exploitation, mainly from Laurion Andros, Syros, Paros, Seriphos, and Kythnos who all have copper ore deposits; along with imports from the east. Copper from Egypt, Cyprus and the Levant were also used; many of the bronze tripods from Olympia were made from copper originated from the Wadi Arabah in Faynan-Jordan (Gale et al, 1985; Mangou, 1994; Kassianidou et al, 2005; Kiderlen et al, 2016).

Depending on a copper alloy’s formatting processes, bronze objects can be separated into two major categories: hammered and cast.

1.2.1. Analysis of copper alloys

Metal analysis nowadays is conducted by a series of techniques. These techniques -depending on what is the purpose of the analysis- include macro, micro and nanometric characterization of the alloys. For the study of the physical structure and components of metals, the most usually applied techniques are Optical, Metallographic and Scanning Electron Microscopy with energy-dispersive x-ray

analysis (SEM/EDX), Neutron and Proton Activation Analysis and various spectroscopic methods. The non-destructive qualitative analysis techniques like X-ray Fluorescence, Laser-Induced Breakdown Spectroscopy and high-energy PIXE are ideal for elemental analysis.

Although many new analytical techniques have been introduced in the study of metals, there are certain problems remaining. Elemental analysis provides evidence for the type of copper alloys that have been used in artifacts, but it cannot provide evidence for determining the provenance of raw materials. In 1982 it was proposed that the geological technique of lead isotope analysis could be used to study the trace amounts of lead present in all copper ore deposits, since lead isotopes are not affected by human manipulation, thus making this technique more reliable in provenance study than elemental analysis (Gale et al, 1982; Melessanaki et al, 2003).

1.2.2. Copper alloys' corrosion products, selective corrosion and de-alloying phenomena

The terms “corrosion” and “corrosion product” are widely used to describe the products of chemical and electrochemical changes in which the metal passes from the elemental to the combined/oxidized state. A description of the most frequently found corrosion products of copper can be seen in Table 1. Table's data obtained by Gettens, (1963) and Anthony, (2016).

Regarding the corrosion for the rest of the elements of copper alloys, lead also form a variety of corrosion products, with the commonest being cerussite or lead carbonate $PbCO_3$. This is a dense, adherent, warm-grey deposit forming a protective layer on lead, preventing its progressive and complete disintegration. Beside lead carbonates, lead oxides can form on copper alloy objects. Massicot PbO , plattnerite PbO_2 and litharge PbO are the most frequently occurred. Lead sulfides, chlorides and lead sulfates can also be formed and traced under different environments.

Tin mainly forms cassiterite, SnO_2 , while zinc can form hydrozincite $Zn_5(CO_3)_2(OH)_6$ and rosatite $CuZnCO_3(OH)_2$ which is a secondary mineral found in the oxidation zone of copper-zinc deposits (Gettens, 1963).

De-alloying is the selective depletion via corrosion processes of one or more of the components from a solid alloy and into the burial environment. The alloying elements that are more active will be preferentially removed; such as copper over tin.

Table 1.1. Major copper corrosion products

<i>Group</i>	<i>Name/chemical formula</i>	<i>Physical properties</i>	<i>Other information</i>
Copper oxides	Cuprite Cu ₂ O	Dark red to cochineal red colour	Is usually concealed beneath overlying green and blue basic salts of copper and it seems to be an intermediate compound in the conversion of metal to those salts
	Tenorite CuO	Grey-black of metallic appearance mineral	Found as an intermediate layer between copper and malachite
Copper carbonates	Malachite Cu ₂ CO ₃ (OH) ₂	Smooth dark green compact layer on the surface of the objects	Very common secondary copper mineral frequently found as pseudomorphs after azurite (which are generally more tabular in shape), or as alteration pseudomorphs after cuprite. Malachite and azurite are formed by the contact of the object with soil, water or even rain water charged with carbonic acid gas in the presence of atmospheric oxygen
	Azurite Cu ₃ (CO ₃) ₂ (OH) ₂	Vitreous, azure blue to blue colour	Secondary copper mineral frequently found in the oxidized zones of Cu-bearing ore deposits. Similar in composition to malachite although its formation is favoured by less humid conditions
	Chalconatronite Na ₂ Cu(CO ₃) ₂ ·3H ₂ O	Forms a bluish-green, chalky crust	Formed mainly in arid soils where alkali carbonates occur abundantly
Copper chlorides	Atacamite / Paratacamite Cu ₂ Cl(OH) ₃	A sugar-like texture, mineral of emerald to blackish green colour. Paratacamite is a paler green powdery texture mineral	Formed through the oxidation of other copper minerals, especially in arid, saline conditions. Atacamite/paratacamite are identical in chemical composition, but have different crystal forms. Occurrence of paratacamite in an object is known as "Bronze disease"
	Botallackite Cu ₂ (OH) ₃ Cl·H ₂ O	Crusts of minute platy interlaced crystals, bluish green to green colour	May convert almost instantly to either paratacamite or atacamite (alternate crystal structures of botallackite), depending on local water chemistry
	Nantokite CuCl	Colourless, white to greyish, massive, granular mineral	Alters superficially to paratacamite when exposed in air
Copper sulfates	Brochantite Cu ₄ SO ₄ (OH) ₆	Green to emerald green, vitreous mineral	Might be expected on bronzes exposed to sulfate-bearing waters
	Connellite Cu ₃₆ (SO ₄)(OH) ₆₂ Cl ₈ ·6H ₂ O	A sub-vitreous of bright blue and needlelike crystals, mineral	Relatively uncommon secondary copper mineral, occurs mixed with other copper minerals in the bronze corrosion crusts

<i>Group</i>	<i>Name/chemical formula</i>	<i>Physical properties</i>	<i>Other information</i>
Copper sulfides	Chalcocite Cu ₂ S	Blue black to black colour and of metallic appearance	Copper sulfides can be formed when objects have been in contact with sulfur-bearing waters, which may originate from bacterial decomposition of organic debris. Chalcopyrite's weathering may lead to the formation of malachite, azurite, brochantite
	Chalcopyrite Cu ¹⁺ Fe ³⁺ S ₂	Brass yellow	
	Bornite Cu ₅ FeS ₄	Copper-red colour on fresh exposures which quickly tarnishes to an iridescent purple	
	Tetrahedrite Cu ₁₂ Sb ₄ S ₁₃	Steel to iron-grey	
	Covellite Cu ₄ Cu ²⁺ ₂ (S ₂) ₂ S ₂	Indigo-blue to blue-black	
Copper nitrate	Basic copper nitrate [Cu(NO ₃) ₂ ·3Cu(OH) ₂ , BCN]		Rather rare because of their solubility in water, although the nitrates of the alkali metals, sodium and potassium, which are especially soluble, occur abundantly in certain desert regions
Copper phosphate	Libethenite Cu ₃ (PO ₄) ₂ ·3H ₂ O	Sub-vitreous, resinous, waxy, green-blue mass mineral	Secondary mineral, formed by action of copper salt solutions on calcium phosphate of bones. Also, due to the weathering of apatite and other rock-forming phosphates

De-alloying is common in alloys with elements which are far apart in the galvanic series (Jones, 1992). The metal residue that remains in the cases that de-alloying has taken place, often retains its original shape and size, but has altered considerably in its physical characteristics. In the field of archaeological contexts de-alloying is occasionally observed, although is less obvious, mainly because metal objects are usually covered with corrosion products. These may hide any surface features which otherwise would reveal signs of de-alloying such as local colour alterations (Weisser, 1975).

Additionally, selective dissolution of one of the alloying components may have been deliberately carried out during the manufacturing of the object, in order to produce a surface enriched in one of the alloying metals (Meeks, 1986). The most

commonly occurred types of selective dissolution of the elements in copper-based alloys appear in the form of dissolution of copper, tin and zinc. Since these are also the most abundant elements in copper-based alloys, their dissolution may affect the analytical results, especially when techniques of surface investigation are employed.

Destannification is the process where tin is selectively corroded out of a bronze alloy. This process, mainly depends on the environmental conditions and by the tin content of the original alloy (Fontana, 1986), where additives like small amounts of arsenic, antimony and phosphorus may act as effective inhibitors of the de-alloying process (Weisser, 1975; Uhlig, 1971).

Decuprification is the selective corrosion of copper from copper alloys. It has been reported to occur both in brass and bronze. Beside the natural occurring factors that result in decuprification (e.g. galvanic corrosion), they have also been reported cases of deliberate selective dissolution of copper in favour of tin in bronzes (Meeks, 1986).

Beside corrosion products' implications, natural segregation phenomena of the constituent elements in an alloy may also pose a possible cause of elemental analysis discrepancies. When casting, alloys rarely have a uniform composition throughout, unless they are very small or the metal freezes extremely quickly. Normal segregation is where the last metal to freeze contains the material with the lowest melting point. Tin is the element with the lowest melting point in a bronze sample so is the last to freeze and thus its analytical values may appear higher. On gravity segregation phenomena, the heaviest phase of the alloy sinks whilst the metal is still molten in the mould, or after a prolonged time of deposition in the ground. In practice this only considerably affects the distribution of the lead in copper alloys (Craddock, 2009: 138).

II. MATERIALS AND METHODS

On this chapter, the methodology applied for the investigation of the technology of the assemblage will be introduced. Concerning the material under investigation, this is presented through its macroscopic observation and classification regarding to its typology and date, on chapter 2.1. The general principals of operation for the optical microscopy, XRF and SEM-EDS along with the devices and settings used, are presented in chapters 2.2., 2.3., and 2.4.

2.1. Classification of the assemblage

The material under analysis was divided in two groups, according to the type of the artifact. Out of the large assemblage, 26 pins were selected. Of the rest of the metallic finds of the sanctuary 21 metallurgical wastes were also chosen, in order to facilitate the research.

The first group with the name “ALEA” and the abbreviation “P”, followed by a sequence number (from 1 to 26) was used for the pins. The characterization ALEA-“WS” (stands for "waste"), was given to the amorphous metal lumps of the second group which, based on their small size and lack of defined shape, are probable metal spills of secondary metallurgical production. The “WS” abbreviation was also followed by a sequence number from 1 to 21.

Since disdained in a storage area at the Archaeological Museum of Tripolis, the pins have had to be initially categorized according to their typology. The only information available considering the objects was that they were excavated in the Sanctuary of Athena Alea. No information regarding the excavation year, trench, etc. was available. The pins’ typological study, thus, was necessary in order to facilitate the interpretation and the evaluation of the compositional results. Each sample was examined macroscopically through comparison of handbook literature, in order to determine its typological classification and dating (Dugas, 1921, 1924; Kilian-Dirlmeier, 1984; Voyatzis, 1990).

All contextual information concerning the artifacts (macroscopic description, dimensions, typological classification, dating, etc.) is presented in the following catalogue.

2.1.1. Dating of the assemblage

All 26 pins were selected from a pile of metallic artifacts, belonging to the finds of the excavations of the sanctuary of Athena Alea at Tegea. Unfortunately, no other data were available regarding their identity.

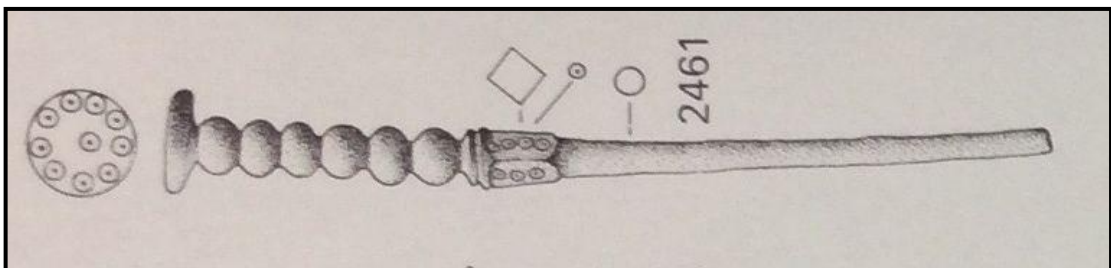
Considering the 21 bronze wastes, the vast majority of them was collected during the excavations of Steinhauer in 1976-77 (the ALEA-WS18 sample belongs to the site findings, but it was recovered from an unknown stratum). The bronze wastes were recovered from trenches A, B, and Γ, north of the temple (image -I.6-) and their recovery depth was up to -2,12m. The available information considering the archaeological context of the trench, since the excavated data are still unpublished, is cited by Voyatzis (1990: 24-25) and is based on information she retrieved by Steinhauer. Thus, it is not possible to date the bronze waste assemblage with accuracy, it is indicated that the 1st layer was Byzantine, followed by a number of layers without finds while down to the 7th and 8th layers the findings were belonging to the classical era. In the 9th layer there existed remains attributed to a seventh century BC context, while the 11th layer of the trench B (the last layer) was of Geometrical context (both ProtoGeometric and Late Geometric pottery and a few shreds attributed to the 10th century BC). Correlating the dates of the excavation of the trenches and the information on the data sheets of the wastes, one can estimate that the top level of the 11th layer was approximately at -1,90m (Tarditi, 2014: 55-86). During the excavations held by the Norwegian Institute it is concluded that in the area, it is common the presence within the same layer of chronologically heterogeneous material, without stratification. Thus, the metallurgical wastes of this assemblage seem to expand from the Geometric to the Classic period. Even it is not quite accurate, this dating of the metallurgical remains allows a rough comparison with the pins.

Regarding the absolute dating of the collection, since it has not yet been developed a scientific method for metal dating (as opposed to 14C method for organically-derived ancient objects, thermo luminescence for ceramics, etc.), this is usually based on the archaeological stratified context and the written sources of the under examination periods. Thus, the dating of the bronze pin's collection was based, as previously written, on the studies of Dugas (1921, 1924), Kilian-Dirlmeier (1984) and Voyatzis (1990). A few decades back they had examined several pins from the

sanctuary; therefore it was possible to identify most of the selected pins through their typology and date them. Although sampling issues guided the selection of the pins, it is quite diverse in its typology covering all of the Geometric and the first decades of the Archaic period. Most pin types, though, date to the Late Geometric period, which is also the most abundantly represented among the sanctuary finds (Voyatzis, 1990: 205).

2.1.2. Bronze pins

ALEA-P1



Description: Bronze Pin with disk (with ten small dotted circles engraved on top) followed by six round globules. Square cross-section with engraved dotted circles and round cross-section on the rest of the rod, part of which is missing.

Excavation data/origin: Sanctuary of Athena Alea

Dimensions: Length (max): 10.2cm, Diameter (max): 1.2cm

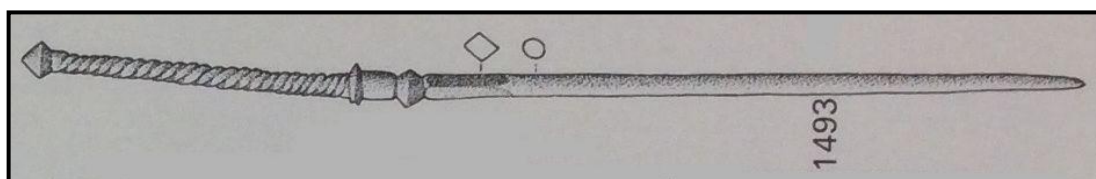
Weight: 13.46gr

Date: Late Geometric- Subgeometric

Typology: Kilian-Dirlmeier (1984), type C, plate 72, n. 2461

Parallels/References: Voyatzis (1990), type Geometric III, plate 159-160; Dugas (1921), figures 40-41, numbers 119-120

ALEA-P2



Description: Bronze Pin with a small biconical bead on the head. The upper part of the rod has been twisted for decorative purposes, followed by a small disc and a biconical bead. Square cross-section followed by a round cross-section on the rest of the rod.

Excavation data/origin: Sanctuary of Athena Alea

Dimensions: Length (max): 15.6cm, Diameter (max): 0.55cm

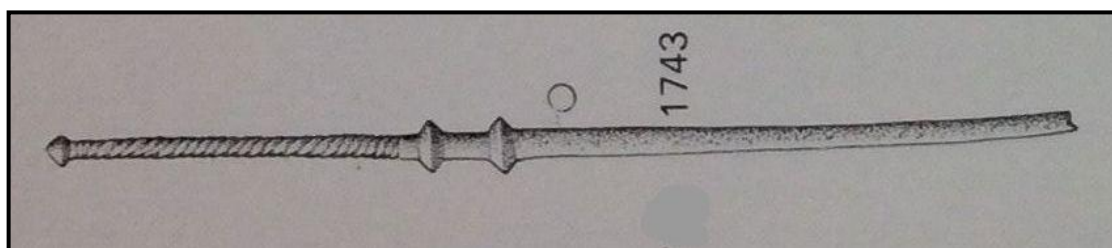
Weight: 7.07gr

Date: Late Geometric

Typology: Kilian-Dirlmeier (1984), type XIIA, plate 50, number 1493

Parallels/References: Voyatzis (1990), type Geometric II variants, plate 154, number B220; Dugas (1921), figures 40-41, numbers 115-118

ALEA-P3



Description: Bronze Pin Bronze Pin with a small biconical bead on the head. The upper part of the rod has been twisted for decorative purposes, followed by two biconical beads. The rest of the rod is of a round cross-section.

Excavation data/origin: Sanctuary of Athena Alea

Dimensions: Length (max): 13cm, Diameter (max): 0.6cm

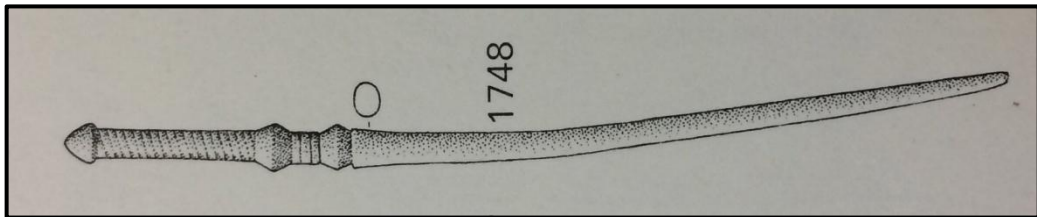
Weight: 5.44gr

Date: Late Geometric

Typology: Kilian-Dirlmeier (1984), type XVIB, plate 59, number 1743

Parallels/References: Voyatzis (1990), type Geometric II variants, plate 153, number B219; Dugas (1921), figures 40-41, numbers 115-118

ALEA-P4



Description: Bronze Pin with a small conical bead on the head. The upper part of the rod has been twisted for decorative purposes, followed by two biconical beads. The rest of the rod is of a round cross-section.

Excavation data/origin: Sanctuary of Athena Alea

Dimensions: Length (max): 12.6cm, Diameter (max): 0.6cm

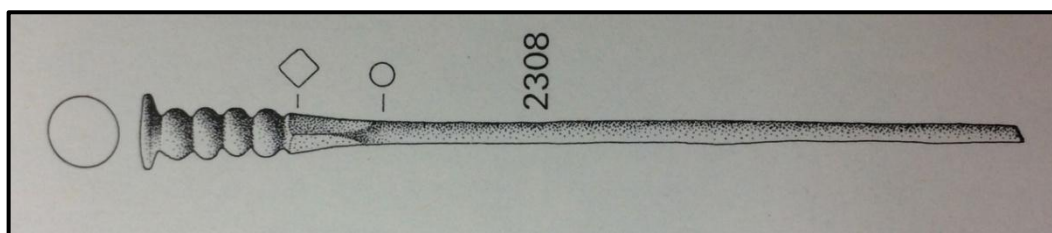
Weight: 7.41gr

Date: Late Geometric

Typology: Kilian-Dirlmeier (1984), type XVIB, plate 59, number 1748

Parallels/References: Voyatzis (1990), type Geometric II variants, plate 153, number B219; Dugas (1921), figures 40-41, numbers 115-118

ALEA-P5



Description: Bronze Pin with disk, followed by four round globules. Square cross-section on the beginning and round cross-section on the rest of the rod, part of which is missing.

Excavation data/origin: Sanctuary of Athena Alea

Dimensions: Length (max): 12.4cm, Diameter (max): 1.0cm

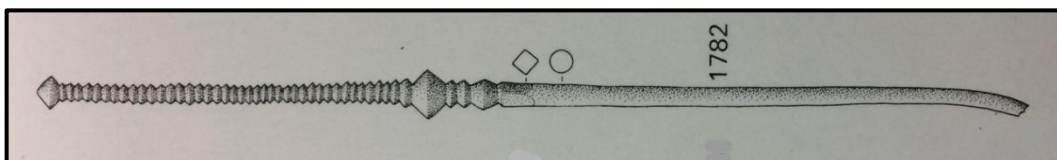
Weight: 10.54gr

Date: Late Geometric - Subgeometric

Typology: Kilian-Dirlmeier (1984), type C, plate 69, number 2308

Parallels/References: Voyatzis (1990), type Geometric III, plate 159, number B235; Dugas (1921), figures 40-41, numbers 119-120

ALEA-P6



Description: Bronze Pin with a small biconical bead on the head. The upper part of the rod has been twisted for decorative purposes, followed by two biconical beads of different size. Square cross-section followed by a round cross-section on the rest of the rod.

Excavation data/origin: Sanctuary of Athena Alea

Dimensions: Length (max): 19.2cm, Diameter (max): 0.9cm

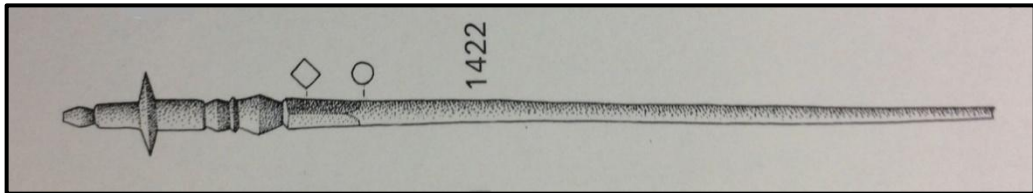
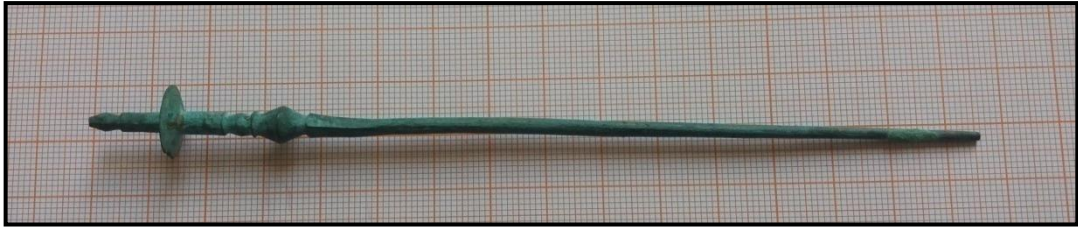
Weight: 14.86gr

Date: Late Geometric - Subgeometric

Typology: Kilian-Dirlmeier (1984), type XVIC, plate 60, number 1782

Parallels/References: Voyatzis (1990), type Geometric II variants, plate 153-154; Dugas (1921), figures 40-41, numbers 115-118

ALEA-P7



Description: Bronze Pin with a small, elongated biconical bead on top, followed by a large biconical “disc” and two biconical beads of different size. Square cross-section followed by a round cross-section on the rest of the rod, part of which is missing.

Excavation data/origin: Sanctuary of Athena Alea

Dimensions: Length (max): 15.4cm, Diameter (max): 1.3cm

Weight: 10.66gr

Date: Late Geometric

Typology: Kilian-Dirlmeier (1984), type IXA, plate 48, number 1422

Parallels/References: Voyatzis (1990), type Geometric II, plate 152, number B216-B217; Dugas (1921), figures 40-41

ALEA-P8



Description: Bronze Pin with a small biconical bead on top, followed by three biconical beads and a large disc. After the disc, two biconical beads of different size. Square cross-section followed by a round cross-section on the rest of the rod, part of which is missing.

Excavation data/origin: Sanctuary of Athena Alea

Dimensions: Length (max): 14.8cm, Diameter (max): 1.4cm

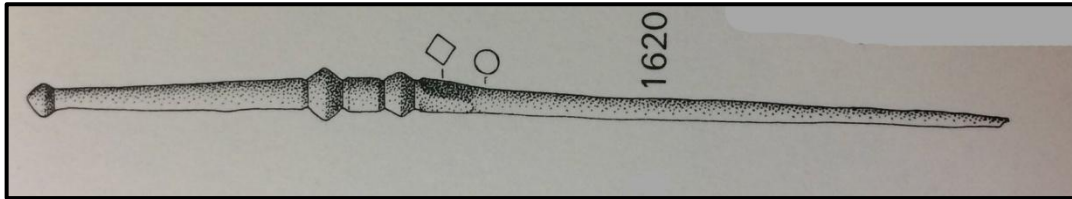
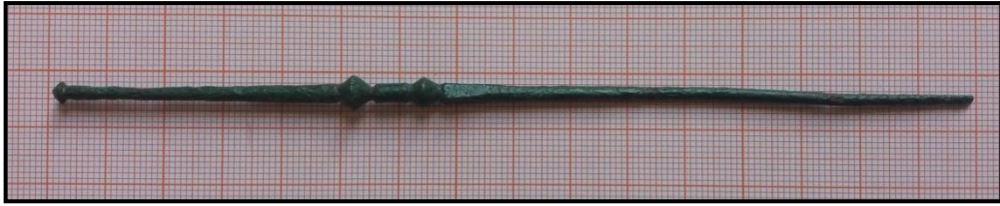
Weight: 14.04gr

Date: Late Geometric

Typology: Kilian-Dirlmeier (1984), type IXA, plate 46-47

Parallels/References: Voyatzis (1990), type Geometric II, plate 152, number B216; Dugas (1921), figures 40-41

ALEA-P9



Description: Bronze Pin with a small biconical bead on the head. The upper part of the rod has been twisted for decorative purposes, followed by two biconical beads of different size. Square cross-section followed by a round cross-section on the rest of the rod.

Excavation data/origin: Sanctuary of Athena Alea

Dimensions: Length (max): 15.7cm, Diameter (max): 0.6cm

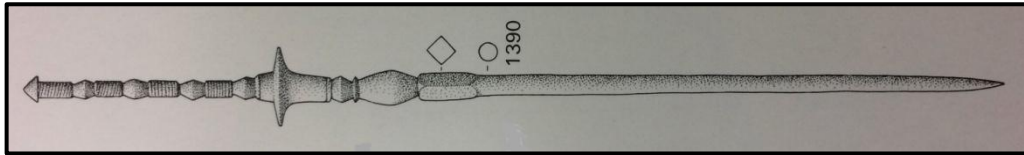
Weight: 7.34gr

Date: Late Geometric – Subgeometric

Typology: Kilian-Dirlmeier (1984), type XVIA, plate 55, number 1620

Parallels/References: Voyatzis (1990), type Geometric II variants, plate 153-154; Dugas (1921), figures 40-41, numbers 115-118

ALEA-P10



Description: Bronze Pin with a small biconical bead on top, followed by four biconical beads and a large disc. After the disc, two biconical beads of different size. Square cross-section followed by a round cross-section on the rest of the rod, part of which is missing.

Excavation data/origin: Sanctuary of Athena Alea

Dimensions: Length (max): 10cm, Diameter (max): 1.25cm

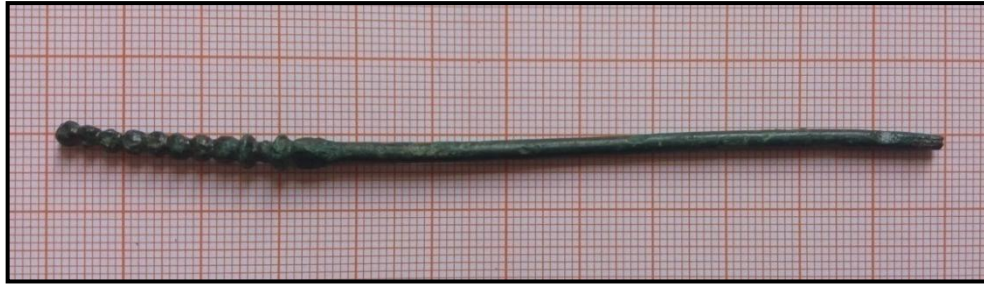
Weight: 15.05gr

Date: Late Geometric

Typology: Kilian-Dirlmeier (1984), type IXA, plate 47, number 1390 (?)

Parallels/References: Voyatzis (1990), type Geometric II, plate 152, number B216-B217; Dugas (1921), figures 40-41

ALEA-P11



Description: Bronze Pin fragment with small globules on the upper part of the rod. The head is not preserved and it is, thus, difficult to assign it to a particular type. Square cross-section followed by a round cross-section on the rest of the rod.

Excavation data/origin: Sanctuary of Athena Alea

Dimensions: Length (max): 11.7cm, Diameter (max): 0.5cm

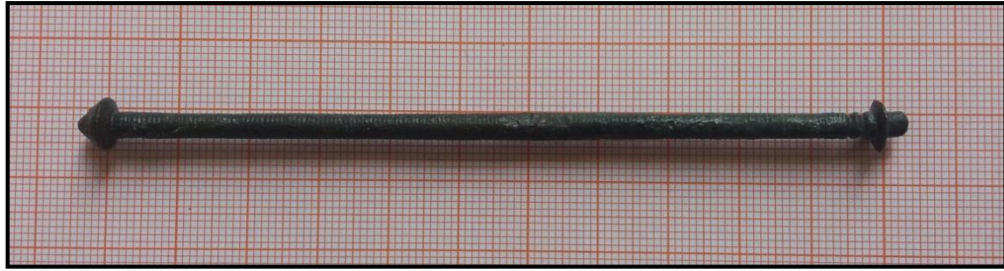
Weight: 5.21gr

Date: Late Geometric

Typology: Kilian-Dirlmeier (1984), type XVIB, plate 58-60

Parallels/References: Voyatzis (1990), type Geometric II variants, plate 153, number B218; Dugas (1921), figures 40-41, numbers 115-118

ALEA-P12



Description: Bronze Pin fragment Bronze Pin with a conical bead on the head. The upper part of the rod has been twisted for decorative purposes, followed by a small disc. The rest of the rod is missing.

Excavation data/origin: Sanctuary of Athena Alea

Dimensions: Length (max): 11.5cm, Diameter (max): 0.75cm

Weight: 10.78gr

Date: Late Geometric

Typology: Kilian-Dirlmeier (1984), type XIVA, plate 54

Parallels/References: Voyatzis (1990), type Geometric II, plate 154, number B220; Dugas (1921), figures 40-41, numbers 115-118

ALEA-P13



Description: Bronze Pin with a very large and thick disk (with a tiny globule on top) followed by a big and a smaller ornate globule, both with horizontal grooves. Round cross-section on the rod, part of which is missing.

Excavation data/origin: Sanctuary of Athena Alea

Dimensions: Length (max): 9.2cm, Diameter (max): 2cm

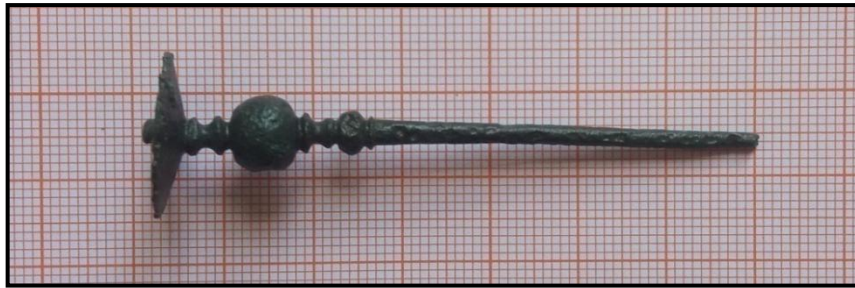
Weight: 25.30gr

Date: Orientalizing

Typology: Kilian-Dirlmeier (1984), type BV, plate 94-96

Parallels/References: Voyatzis (1990), type Orientalizing II, plate 160-161

ALEA-P14



Description: Bronze Pin with a very large disk (with a tiny globule on top) followed by a big and a smaller globule. Round cross-section on the rod, part of which is missing.

Excavation data/origin: Sanctuary of Athena Alea

Dimensions: Length (max): 6.8cm, Diameter (max): 1.8cm

Weight: 8.23gr

Date: Orientalizing

Typology: Kilian-Dirlmeier (1984), type BIV, plate 89

Parallels/References: Voyatzis (1990), type Orientalizing I, plate 160, number B238; Dugas (1921), figure 39, number 135

ALEA-P15



Description: Bronze Pin fragment with two big globular beads, both vertically engraved, followed by a round cross-section rod. Part of the head and rod are missing and it is, thus, difficult to assign it to a particular type.

Excavation data/origin: Sanctuary of Athena Alea

Dimensions: Length (max): 8.7cm, Diameter (max): 1.25cm

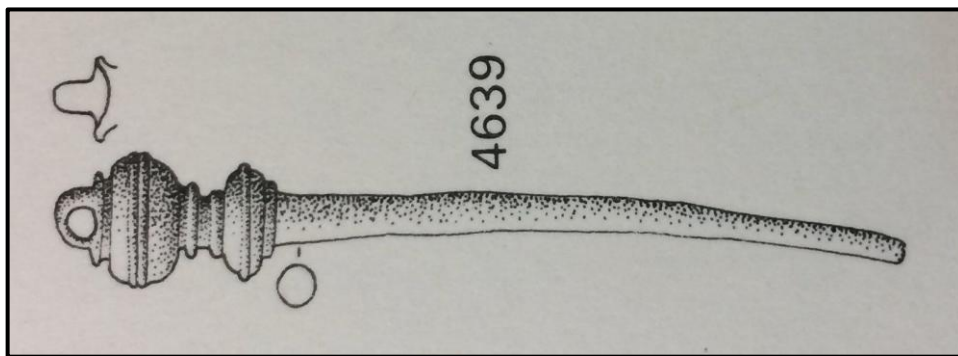
Weight: 13.08gr

Date: Orientalizing

Typology: Kilian-Dirlmeier (1984), type BVI, plate 98-101

Parallels/References: Voyatzis (1990), type Orientalizing II, plate 161, number B240; Dugas (1921), figure 20, number 136

ALEA-P16



Description: Bronze Pin with a medium size loop on top, followed by two big globules of different size, both with horizontal grooves. Round cross-section rod, part of which is missing.

Excavation data/origin: Sanctuary of Athena Alea

Dimensions: Length (max): 7.5cm, Diameter (max): 1.2cm

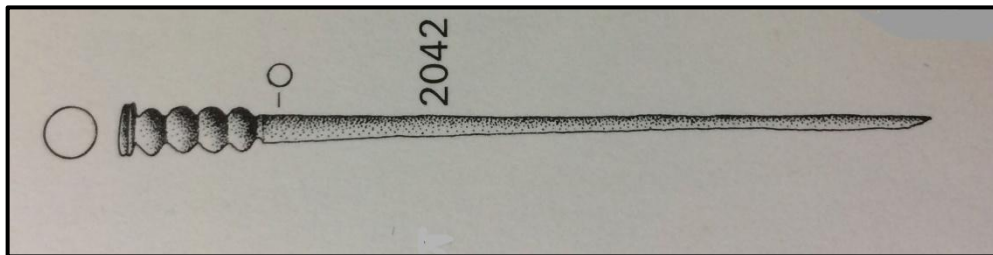
Weight: 9.77gr

Date: Orientalizing

Typology: Kilian-Dirlmeier (1984), type EIII, plate 109, number 4639

Parallels/References: Voyatzis (1990), type Orientalizing I, plate 161, number B241; Dugas (1921), figure 39, number 138

ALEA-P17



Description: Bronze Pin with very small disk followed by four globules. Round cross-section on the rod, part of which is missing.

Excavation data/origin: Sanctuary of Athena Alea

Dimensions: Length (max): 7.1cm, Diameter (max): 0.7cm

Weight: 7.17gr

Date: Late Geometric - Subgeometric

Typology: Kilian-Dirlmeier (1984), type A, plate 65, number 2042

Parallels/References: Voyatzis (1990), type Geometric III, plate 159, number B235; Dugas (1921), figures 40-41, numbers 119-120

ALEA-P18



Description: Bronze Pin fragment, with square cross-section and three biconical beads of different size. The head is not preserved and it is, thus, difficult to assign it to a particular type. Part of the rod is also missing.

Excavation data/origin: Sanctuary of Athena Alea

Dimensions: Length (max): 9.7cm, Diameter (max): 0.9cm

Weight: 13.88gr

Date: Middle Geometric

Typology: Kilian-Dirlmeier (1984), type VA, plate 38

Parallels/References: Voyatzis (1990), type Geometric II

ALEA-P19



Description: Bronze Pin fragment, with square cross-section and three globular beads of different size. The head is not preserved and it is, thus, difficult to assign it to a particular type. Part of the rod is also missing.

Excavation data/origin: Sanctuary of Athena Alea

Dimensions: Length (max): 10.9cm, Diameter (max): 1.25cm

Weight: 23.05gr

Date: Early Geometric- Middle Geometric

Typology: Kilian-Dirlmeier (1984), type IIIA, plate 32-33

Parallels/References: Voyatzis (1990), type Geometric II, plate 151, number B215; Dugas (1921), figure 41

ALEA-P20



Description: Bronze Pin fragment, with round cross-section. One conical and one smaller biconical bead with elongated globules among them. The head is not preserved and it is, thus, difficult to assign it to a particular type. Part of the rod is also missing.

Excavation data/origin: Sanctuary of Athena Alea

Dimensions: Length (max): 10.5cm, Diameter (max): 0.85cm

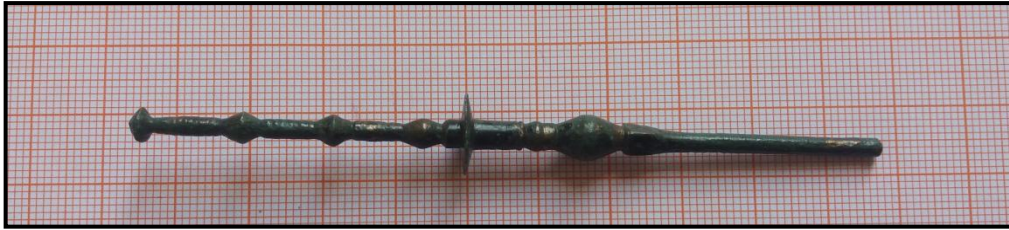
Weight: 9.14gr

Date: Late Geometric- Subgeometric

Typology: Kilian-Dirlmeier (1984), type XIA, plate 50

Parallels/References: Voyatzis (1990), type Geometric III, plate 155, number B223; Dugas (1921), figure 40, number 113

ALEA-P21



Description: Bronze Pin with a small conical bead on top, followed by three biconical beads and a disc. Round cross-section on the beginning of the rod followed by a bigger biconical bead and round cross-section on the rest, part of which is missing.

Excavation data/origin: Sanctuary of Athena Alea

Dimensions: Length (max): 16cm, Diameter (max): 1.5cm

Weight: 8.66gr

Date: Late Geometric

Typology: Kilian-Dirlmeier (1984), type IXA, plate 47

Parallels/References: Voyatzis (1990), type Geometric II, plate 152, number B216; Dugas (1921), figure 41

ALEA-P22



Description: Bronze Pin fragment, with a disc with biconical beds of different size in the upper section. Square cross-section (with an engraved X) on the beginning and round cross-section on the rest of the rod, part of which is missing. The head is not preserved and it is, thus, difficult to assign it to a particular type.

Excavation data/origin: Sanctuary of Athena Alea

Dimensions: Length (max): 6.8cm, Diameter (max): 1cm

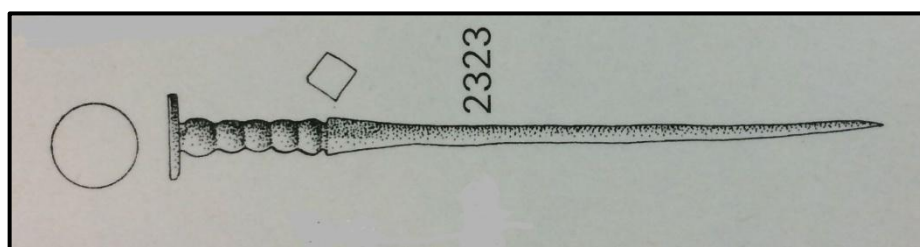
Weight: 7.50gr

Date: Late Geometric

Typology: Kilian-Dirlmeier (1984), type IXA, plate 47

Parallels/References: Voyatzis (1990), type Geometric II, plate 152, number B216; Dugas (1921), figure 41

ALEA-P23



Description: Bronze Pin with disk followed by five round globules of different size. Square cross-section on the beginning and round cross-section on the rest of the rod, part of which is missing.

Excavation data/origin: Sanctuary of Athena Alea

Dimensions: Length (max): 6.6cm, Diameter (max): 1cm

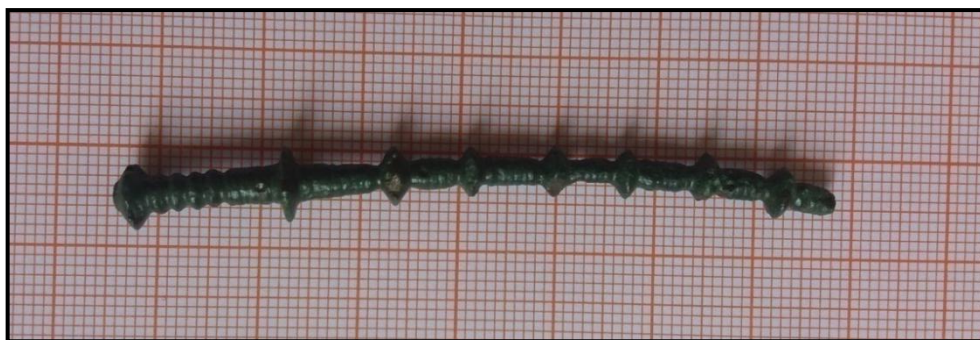
Weight: 2.15gr

Date: Late Geometric- Subgeometric

Typology: Kilian-Dirlmeier (1984), type C, plate 70, number 2323

Parallels/References: Voyatzis (1990), type Geometric III, plate 159-160; Dugas (1921), figures 40-41, numbers 119-120

ALEA-P24



Description: Bronze Pin fragment, with a small biconical bead on top. The upper part of the rod is consisted of four flattened globules, followed by seven also flattened, biconical beads. The rest of the rod is missing.

Excavation data/origin: Sanctuary of Athena Alea

Dimensions: Length (max): 7cm, Diameter (max): 0.75cm

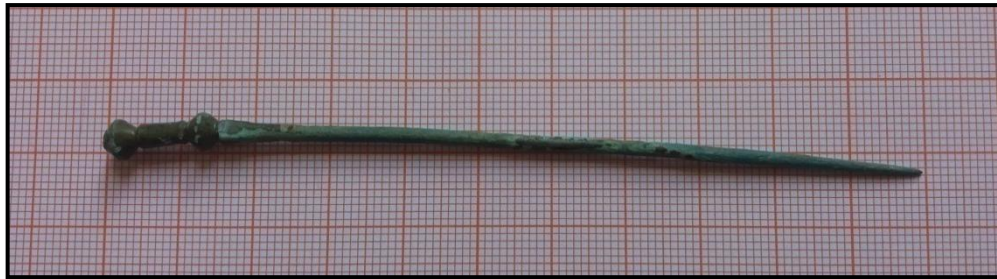
Weight: 5.54gr

Date: Late Geometric

Typology: Kilian-Dirlmeier (1984), type IXB, plate 49

Parallels/References: Voyatzis (1990), type Geometric II, plate 152, number B216; Dugas (1921), figure 41

ALEA-P25



Description: Bronze Pin with two small biconical beads on the head. Square cross-section on the beginning and round cross-section on the rest of the rod.

Excavation data/origin: Sanctuary of Athena Alea

Dimensions: Length (max): 10.9cm, Diameter (max): 0.5cm

Weight: 3.67gr

Date: Late Geometric-Subgeometric

Typology: Kilian-Dirlmeier (1984), type XIXA, plate 62

Parallels/References: Voyatzis (1990), type Geometric II variants

ALEA-PIN-26



Description: Bronze Pin fragment with small globules on the upper part of the rod, followed by three biconical beads. The head is not preserved and it is, thus, difficult to assign it to a particular type. Square cross-section followed by a round cross-section on the rest of the rod.

Excavation data/origin: Sanctuary of Athena Alea

Dimensions: Length (max): 8cm, Diameter (max): 0.5cm

Weight: 5.84gr

Date: Late Geometric

Typology: Kilian-Dirlmeier (1984), type XIIB, plate 52

Parallels/References: Voyatzis (1990), type Geometric II variants, plate 153-154; Dugas (1921), figure 40-41

2.1.3. Metallurgical wastes

ALEA-WS1



Description: Metallurgical waste

Excavation data/origin: Sanctuary of Athena Alea, 07/10/1976, trench A1, depth 1,24m

Dimensions: Length (max): 5.5cm- Width (max): 2.7cm- Thickness (max): 2.5cm

Weight: 50.37gr

ALEA-WS2



Description: Metallurgical waste

Excavation data/origin: Sanctuary of Athena Alea, 12/10/1976, trench A1, depth 1,65m

Dimensions: Length (max): 5.2cm- Width (max): 3.2cm- Thickness (max): 1cm

Weight: 22.37gr

ALEA-WS3



Description: Metallurgical waste

Excavation data/origin: Sanctuary of Athena Alea, 07/10/1976, trench A1, depth 1,24m

Dimensions: Length (max): 3.1cm- Width (max): 2.2cm- Thickness (max): 1.5cm

Weight: 5.71gr

ALEA-WS4



Description: Metallurgical waste

Excavation data/origin: Sanctuary of Athena Alea, 07/10/1976, trench A1, depth 1,24m

Dimensions: Length (max): 3.1cm- Width (max): 2.4cm- Thickness (max): 0.5cm

Weight: 5.46gr

ALEA-WS5



Description: Metallurgical waste

Excavation data/origin: Sanctuary of Athena Alea, 07/10/1976, trench B2

Dimensions: Length (max): 2.9cm- Width (max): 1.6cm- Thickness (max): 2.2cm

Weight: 25.18gr

ALEA-WS6



Description: Metallurgical waste

Excavation data/origin: Sanctuary of Athena Alea, 06/10/1976, trench B2, depth 1,86m

Dimensions: Length (max): 3.4cm- Width (max): 2.3cm- Thickness (max): 0.9cm

Weight: 7.07gr

ALEA-WS7



Description: Metallurgical waste

Excavation data/origin: Sanctuary of Athena Alea, 06/10/1976, trench B2, depth 1,89m

Dimensions: Length (max): 2.3cm- Width (max): 2.3cm- Thickness (max): 1cm

Weight: 9.41gr

ALEA-WS8



Description: Metallurgical waste

Excavation data/origin: Sanctuary of Athena Alea, 28/09/1976, trench B2

Dimensions: Length (max): 4.2cm- Width (max): 2.4cm- Thickness (max): 2cm

Weight: 30.75gr

ALEA-WS9



Description: Metallurgical waste

Excavation data/origin: Sanctuary of Athena Alea, 09/10/1976, trench B2, depth 2,00m

Dimensions: Length (max): 2.4cm- Width (max): 1.4cm- Thickness (max): 1.3cm

Weight: 5.54gr

ALEA-WS10



Description: Metallurgical waste

Excavation data/origin: Sanctuary of Athena Alea, 07/10/1976, trench B2, depth 1,95m

Dimensions: Length (max): 7.4cm- Width (max): 2cm- Thickness (max): 2.1cm

Weight: 23.55gr

ALEA-WS11



Description: Metallurgical waste

Excavation data/origin: Sanctuary of Athena Alea, 04/10/1976, trench B2, 2nd layer

Dimensions: Length (max): 1.2cm- Width (max): 0.9cm- Thickness (max): 1cm

Weight: 1.34gr

ALEA-WS12



Description: Metallurgical waste

Excavation data/origin: Sanctuary of Athena Alea, 22/09/1976, trench B2 (on top of the grave)

Dimensions: Length (max): 1cm- Width (max): 0.7cm- Thickness (max): 0.35cm

Weight: 0.72gr

ALEA-WS13



Description: Metallurgical waste

Excavation data/origin: Sanctuary of Athena Alea, 12/10/1977, trench B2, layer 11 α

Dimensions: Length (max): 3.5cm- Width (max): 1.3cm- Thickness (max): 0.6cm

Weight: 3.86gr

ALEA-WS14



Description: Metallurgical waste

Excavation data/origin: Sanctuary of Athena Alea, 04/10/1976, trench Γ 4

Dimensions: Length (max): 1.6cm- Width (max): 1.2cm- Thickness (max): 1.2cm

Weight: 4.54gr

ALEA-WS15



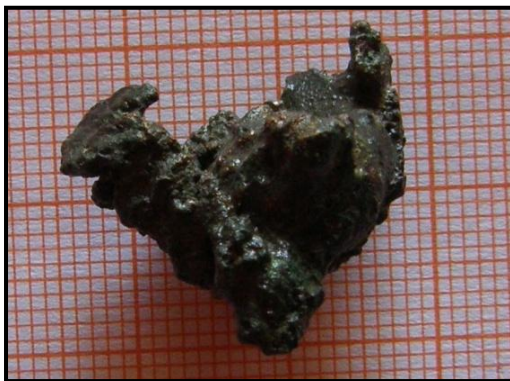
Description: Metallurgical waste

Excavation data/origin: Sanctuary of Athena Alea, 07/10/1976, trench B2

Dimensions: Length (max): 3.9cm- Width (max): 2.3cm- Thickness (max): 2cm

Weight: 19gr

ALEA-WS16



Description: Metallurgical waste

Excavation data/origin: Sanctuary of Athena Alea, 07/10/1976, trench B2 (on red soil), depth 1,90m

Dimensions: Length (max): 2.1cm- Width (max): 1.6cm- Thickness (max): 2cm

Weight: 9.23gr

ALEA-WS17



Description: Metallurgical waste

Excavation data/origin: Sanctuary of Athena Alea, 07/10/1976, trench B2, depth 1,84m

Dimensions: Length (max): 3cm- Width (max): 2.8cm- Thickness (max): 1.5cm

Weight: 20.40gr

ALEA-WS18



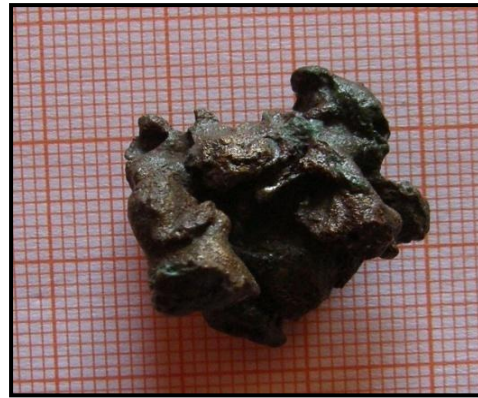
Description: Metallurgical waste

Excavation data/origin: Sanctuary of Athena Alea

Dimensions: Length (max): 5.2cm- Width (max): 4.7cm- Thickness (max): 2.1cm

Weight: 46.48gr

ALEA-WS19



Description: Metallurgical waste

Excavation data/origin: Sanctuary of Athena Alea, 03/10/1976, trench A1, depth 1,79m

Dimensions: Length (max): 2.2cm- Width (max): 2.2cm- Thickness (max): 2cm

Weight: 12.41gr

ALEA-WS20



Description: Metallurgical waste

Excavation data/origin: Sanctuary of Athena Alea, 30/09/1976, trench B2, depth 1,18m

Dimensions: Length (max): 2.4cm- Width (max): 1.9cm- Thickness (max): 1cm

Weight: 7.08gr

ALEA-WS21



Description: Metallurgical waste

Excavation data/origin: Sanctuary of Athena Alea, 06/10/1976, trench Γ4, depth 2,12m

Dimensions: Length (max): 2.3cm- Width (max): 0.7cm- Thickness (max): 1.2cm

Weight: 4.60gr

2.2. Optical Stereomicroscopy

2.2.1. General principles

Low-magnification microscopy is an almost essential precursor to any detailed study or analysis. Stereomicroscopes offer the great advantage of providing a three dimensional view of the sample, usually at low magnifications (typically x5 to x50), an important feature for understanding or inspecting microscopic structures, their spatial extent and nature. During stereomicroscopy, basic features of an object can be observed such as basic materials composition, traces of the manufacturing steps, traces of use, details of ornament or assembly, deposits due to use or burial conditions, evidence of damage or possible active corrosion procedures etc. Stereomicroscope is thus an indispensable tool for the inspection of metallic artifacts. Although may be useful for studying the penetration of corrosion into the metal, it is not suitable for the characterization of the bulk composition and microstructure, since the surface layers of the metal as a whole are not representative (Craddock, 2009: 24).

The stereomicroscope has two complete optical systems from eyepiece to objective, one for each eye. These are mounted at fifteen degrees to each other (seven-and-a-half degrees to the vertical). This reproduces normal vision, where the two images are slightly different in each eye: the human brain interprets this to give a 3-D appreciation of the object to the viewer.

Stereomicroscopes can function under two types:

- Fixed objectives and eyepieces and thus fixed magnifications
- Interchangeable eyepieces and objectives, or zoom magnification capabilities, which can give magnifications from approximately x6 to x200

Increase in magnification, though, may lead to a reduction in the depth of field, typically falling from approximately 22 mm at x6 to 1 mm at x200.

The observation under a stereomicroscope is aided by the use of lighting typically in two modes. Illumination from two angled light sources either side of the object, or under raking light. This uses a single light source falling light across the surface, typically five to forty degrees to the plane of the object, in order to highlight surface relief or/and possible deformations.

Photographs, which can be taken through the stereomicroscopes are usually processed and stored in inbuilt software programs (Caple, 2006: 28-32).

2.2.2. Devices and settings

The examination of the samples from the sanctuary was conducted under a portable Leica (Leica MZ6) stereomicroscope, with a source of Light Emitting Diode system (Volpi Intralux 5100), in visible light. The stereomicroscope was connected to a portable computer for the digital recording, processing and management of photos, using a ProgRes CT3 camera with CapturePro 2.7 software.

The artifacts, after they were microscopically inspected for their morphology, corrosion patterns and general appearance and micro-photographs of areas of interest were obtained, are presented in chapter 3.1.

2.3. X-ray Fluorescence Spectroscopy

2.3.1. General principles

X-ray Fluorescence (XRF) is an analytical technique that uses the interaction of X-rays with a material, in order to determine its elemental composition. XRF is suitable for solids, liquids and powders and in most circumstances is non-destructive (Liritzis et al, 2011; Ferreti et al, 1998; Palamara et al, 2015; Moropoulou et al, 2016). It is an analytical technique involved in the study of ancient objects, sensitive to most elements of the periodic table that are relevant to copper alloys. X-rays form part of the electromagnetic spectrum and are characterized by energies lying between ultra-violet and gamma radiation. Wavelengths are typically in the range 0.01 to 10nm, which is equivalent to energies of 125keV to 0.125keV. Not all the incident X-rays, in XRF spectrometry, result in fluorescence. The ratio of absorption/fluorescence, Compton and Rayleigh scatter and transmission depends on the sample thickness, density, composition and the X-ray energy (Ida, 2004).

X-ray spectrometers bombard the surface with a high energy X-ray beam, causing the excitement and thus expel of electrons from the inner orbital of the atoms. The removal of an electron close to the nucleus from its orbit leaves a gap, which fills with electrons from higher orbital that fall in their position. During the fall, energy in the form of a photon is released. The energy difference between the expelled and replacement electrons is characteristic of the element atom in which the fluorescence process is occurring, thus, the energy of the emitted fluorescent X-ray is directly linked to a specific element being analysed. This characteristic emitted X-ray energy

is collected by a detector, while it is independent of the chemistry of the material. The result of the process is depicted on a spectrum where the peaks are characteristic of the energy produced by the atoms of certain elements (energy line) and of the concentration rate of those elements (number of counts).

The key components of a typical XRF spectrometer are:

- Source of X-rays used to irradiate the sample
- Sample
- Detection of the emitted fluorescent X-Rays

XRF spectrometers fall into two main categories depending on whether they employ a wavelength dispersive approach (WDXRF) or an energy dispersive approach (EDXRF) (Ida, 2004).

The analytical detection range of XRF with the most sophisticated portable instruments covers elements from sodium ($Z=11$) up to uranium ($Z=92$). Its sensitivity to trace low atomic number elements also depends on the environment of the sample. When the analysis is performed under vacuum or helium gas is flushed between the sample and the X-ray detector, light elements below sodium can be detected.

Determination of the amount of an element in a sample by XRF is usually based on a linear relationship between the emitted X-ray intensity and the concentration of the element. Concentrations can range from 100% down to ppm levels. Usually down to ca 0.01%. Limits of detection depend upon the specific element and the sample matrix as stated, but as a general rule, heavier elements will have better detection limits. A simple technique to improve the quality of the excitation beam, especially for portable instruments, is the insertion of an appropriate filter between the source and the analysed sample. The filter can significantly reduce the continuous tube radiation, especially in the energy region up to 15keV. In other portable spectrometers, a crystal or a multilayer is used between the anode and sample, having the property not only to reflect with high efficiency the main K or L emission characteristic X-ray lines of the anode material, but also to focus the exciting beam at the sample position (Karydas et al, 2005).

Large-beam, sub-millimetre or even μ -beam XRF instruments, in combination with polycapillary lenses for focusing the primary beam to less than 100 μ m have been developed for application in the field of analysis of archaeological artifacts (Karydas et al, 2005; Bottaini et al, 2015).

The technique is fast, while its equipment can be transportable and can therefore enable measurements in-situ (Musilek, 2012). Since the consumption or damaging of even a small part of an artifact for analytical purposes must be undertaken only where vital data cannot otherwise be obtained, it is of a major advantage the fact that through XRF analysis artifacts are not harmed by the removal of samples, making it a non-destructive analytical technique (Adriaens, 2005).

For the study of metals and their alloys, the XRF technique offers a highly sensitive analysis of their elemental composition. It can determine the identity and quantity of the elements and distinguishes them from background radiation. It can detect amounts of major, minor, and trace chemical elements and in particular, it is capable of detecting trace amounts (up to a few hundred ppm) of heavy elements, such as antimony and lead. Since the technique exhibits high sensitivity for certain elements, provenance studies can be done not only by means of major elements, but also by using fingerprint trace elements analysis (of Ni, Bi, Ag, As and Sb), usually in combination with isotopic analysis (Pernicka, 1999; Karydas et al, 2005; Liritzis et al, 2011: 109-112; Neff et al, 2013; Kantarelou et al, 2015). Certain limitations arise though, such as possible variations in the composition of the measured areas because of the heterogeneity of the metal core in relation to the substrate and the implication of the corrosion products on the accuracy of the obtained values (Orfanou et al., 2014).

Portable XRF (p-XRF) devices are analytical tools well suited for investigating the major elemental composition of metallic archaeological artifacts (Ida, 2004; Fernandes, 2013). Concerning μ XRF, the small size of its beam is excellent in order to identify decorative details while when used in scanning mode can reveal spatially resolved associations concerning the manufacturing techniques and surface corrosion products. When bulk analysis is required, line or area mode scans can be used. Thus, two-dimensional mapping of element distribution is obtained (Kantarelou et al, 2007b; Kantarelou et al, 2015).

When trying though, to determine qualitative and quantitative composition with the XRF technique certain limitations occur. Knowing the potentials and limitations of the technique thus, these can be easily avoided. The most important limitations of p-XRF in the analysis of archaeological metals includes 1) difficulty in measuring light elements; 2) presence of corrosion layers; 3) grain size of the analysed materials; and 4) geometry of the sample (Liritzis et al, 2011). There has

been a calculation in the effects of the variability of excitation, detection angles and distance from the specimen and possible corrective shape factors have been proposed (Kantarelou et al, 2007b; Musilek, 2012; Trojek, 2014). With the exception of Total Reflection X-ray Fluorescence, all forms of XRF analysis suffer from matrix effects of various types, which increase the overall error, and need to be corrected. Moreover, when X-rays are employed for the detection of arsenic, a possible enhancement of the element's fluorescence intensity in the presence of large amounts of lead, may be the case; the $L\beta$ characteristic lines of which (at 12.011 and 12.620keV) lie just above arsenic's K absorption edge at 11.860keV (Heginbotham et al., 2015).

Regarding the corrosion products which may cover metal artifacts, these may easily reach several tens of mm in thickness; it is easy to understand how strongly these products limit the accuracy of XRF measurements when metal alloys composition is of interest. When a metal surface is corroded, measurements reveal the nature and the composition of the corrosion products and not of the actual metal. Such is the case for copper alloy objects, where almost the entirety of the analytical information for Cu and Pb and almost half of the Sn information comes from the first 20 μ m (Ferretti et al, 2014). Therefore, the interpretation of the measured spectra requires of careful attention and, in some cases, of developing special procedures (Bennallack et al, 2013; Karydas et al, 2014). For the binary Cu–Sn alloy system and for a certain range of Sn concentrations, the factor G_{Sn} (the variation of Sn-K α to Sn-La intensity between non corroded and corroded areas) -which was determined through tests and reference standards- is used, while it is expected to be rather constant and close to unity. Of course, in order to determine a G_{Sn} value the spectrum of Sn-La X-rays must be visible, which is not always the case. Especially when an enrichment of Cu is present in the surface mainly in the form of corrosion products, Sn-La peaks are usually being overlapped (Karydas, 2007; Kantarelou et al, 2015).

For the calibration and check of the accuracy of the technique, reference samples are used. A reference sample must contain all the potential elements included in a material. Thus, the analytical software can associate energies with the characteristic emission of a particular element and calculate the elemental concentration from the measured fluorescence (Hunt et al, 2015). The BCR-691 series by the Community Research of the European Union was up to recently the only set of reference samples close to the values of ancient alloys. Although nine elements were included in the set, only four of them per standard were certified (Pb, Sn, Zn and As).

These are significant shortcomings in its calibration range, covering only typical mean elemental values of ancient alloys; considering that metals pose the problem of ancient extraction and smelting practices, which differed enough from modern practices, using modern standards is not feasible. The CHARM set of reference samples may represent a major step forward in the production of accurate and reliable calibrations for XRF analysis since it includes 12 common heritage alloy types and 20 elements while the lowering of their mean values as close as towards zero may obtain values close to their detection limit and thus smaller uncertainties on the measurements (Heginbotham et al., 2014).

2.3.2. Devices and settings

A handheld portable X-ray fluorescence device (p-XRF) was employed in the determination of the elemental composition of the selected samples from the sanctuary of Athena Alea. The instrument used was a Bruker; model Tracer III-SD (Bruker Company). A portable computer for the storage and processing of the obtained spectra was accompanying the instrument. The system includes software for quantitative analysis (S1P-XRF software), depending on the nature of the measured material; consequently, the metal/alloys program was selected. The settings used, are: an Al/Ti filter (0.012 inches Al plus 0.001 inches Ti) high-energy excitation mode (high voltage set at 40 kV and current of 12 μ A) for the analysis of minor and trace elements with an atomic number $Z > 29$. No vacuum was applied.

The visible corrosion products on the surface were removed, with the use of established conservation methods, before non-invasive analysis was performed. The p-XRF Spectrometer was positioned upward so that the sample table sat horizontally (the X-ray beam vertically upwards). The diameter of the X-ray beam was 3x3mm, thus too big for the analysis of the pins, which have curved surfaces of small diameter. Same applies for the wastes which had rough, uneven surfaces with only a few areas suitable for analysis, with such a large size beam.

Since metals usually exhibit heterogeneities, multiple metered signals were collected from separate corrosion-free, as determined by naked eye, areas of each sample. The number of the measurements taken for each object depended on its size and the geometry of the analysed surface (with the exception of most of the wastes

that had been analysed just one time due to their complex geometries) over a period of 90 seconds.

The accuracy of the applied analytical technique was initially checked by analysing the certified reference copper alloys CDA 360 with a set of determinations: 60.99% Cu, 35.88% Zn, 0.15% Fe and 2.98% Pb. Five measurements were taken from the standard and their mean value was: 61.97% Cu, 35.34% Zn, 0.14% Fe and 2.15% Pb. Since other elements were also detected in very low quantities, it is concluded that there are no significant deviations from the default values of the elements which we are interested in. All raw intensity data (the number of counts) obtained from the samples were normalized to 100% and elements are presented in weight percentage (wt. %). All measurements, including standard deviation values, of the certified reference copper alloy CDA 360 using p-XRF are cited in Appendix II.1.

Another value that was calculated is the standard deviation. It is considered statistically important because it contributes to the clearer evaluation of the results and indicates whether there are significant variations between measurements. The mean values and standard deviation of all measurements of the elemental analysis of the samples from Alea, using p-XRF are presented in chapter 3.2. (tables 3.2. and 3.3.). All performed measurements along with the detection limits, are cited on Appendix II.2 and II.3.

A second round of elemental analysis using XRF was conducted with the employment of the portable micro - XRF instrument of the Institute of Nuclear and Particle Physics of the NCSR Demokritos. The INP μ XRF is a customized version of the commercial μ XRF spectrometer Artax (Bruker-Nano). The spectrometer probe consists of an X-ray micro focus Rh-anode tube (spot size $50\mu\text{m} \times 50\mu\text{m}$, 50kV, 0,6mA, 30W maximum power consumption with 0,2mm Be window thickness) and a polycapillary X-ray lens as a focusing optical element that offers a focal distance of about 21mm and a spatial resolution in the range $40\mu\text{m} - 80\mu\text{m}$, when the unfiltered tube radiation is used as an excitation X-ray beam. The X-ray detection chain consists of a thermo-electrically cooled 10mm^2 silicon drift detector (X-Flash, 1000B) with FWHM equal to 146eV (at $\text{MnK}\alpha$ and 10kcps) coupled with a digital signal processor. The coloured CCD camera that is attached to the spectrometer head can offer live documentary image of the analysed spot, whereas together with a dimmable white LED for sample illumination and a laser beam indicator the reproducible positioning of the measuring probe with respect to the analysed surface is guided. The

spectra obtained, can afterwards be transferred to a portable computer for off-line evaluation.

The apparatus is developed in such a way so it facilitates the movement of the head of the spectrometer, which is equipped with three stepping motors, in three orthogonal directions; in a range of about 50cm. Thus, the analysis spot can be set precisely at the focal distance of the polycapillary lens. The flexible head, which can be also tilted at different orientations in order to better access curved areas and overcome the limitations imposed by the geometry of the artifacts, especially the metals' surface irregularities; so as the beam direction is always perpendicular to the analysed surface. The μ XRF spectrometer head can perform measurements in a helium atmosphere that improves the detection of light elements; however, this option was not used during the measurements of the sanctuary metals. The μ XRF spectrometer has been developed to fulfil certain analytical requirements related to the characterization of metals, overcoming this way the limited spatially resolved analytical performance of XRF spectrometers with a beam spot diameter in the range of a few mm (Kantarelou et al, 2007; Kantarelou et al, 2015).

The accuracy of the applied analytical technique was initially checked by analysing the BCR-691 series of copper alloy standards. The standard consists of five alloys, representative of ancient bronze compositions; with a set of determination as can be seen on Appendix III.1. All areas of the samples were measured at 50kV at 600 μ A using filter no3 (for bronzes). The detection limit at 50s for Co=0.024% wt, for Ni=0.04% wt, Sb=0.3% wt, Pb= 0.002% wt and for Bi=0.019% wt. Two to four measurements from different areas of the samples, in order to avoid various surface heterogeneities, were chosen to be analysed with the μ XRF technique. All raw intensity data (the number of counts) obtained were normalized to 100% and elements are presented as weight percentage (wt. %). The values of the samples from Alea using μ XRF, as presented in chapter 3.3. (table 3.4. and 3.5.) are the mean values of these measurements; the standard deviation is an important factor for the proper evaluation of these results since it may indicate significant variations between measurements. All performed measurements are cited on Appendix III.2 and III.3.

2.4. Scanning Electron Microscope (SEM) with Energy Dispersive Spectroscopy (EDS)

2.4.1. General principles

The scanning electron microscope (SEM) is a method of observation and characterization of heterogeneous organic and inorganic materials. The area under observation may range between nanometer (nm) to micrometer (μm) scale, while the instrument has the capability of obtaining stereoscopic-like, images. The method relates composition to structure, allows the chemical analysis of particular areas, inclusions or phases, provides bulk compositions, as well as features of major importance for the study of metallic artifacts (Bayley, 2008: 32-37). SEM-EDS may also produce quantitative values, with a limit of quantification ca 0.1 wt% (Lankton et al, 2016).

In most cases, no special sampling procedure is required, except for examining insulating materials (for example, areas of non-conducting corrosion products which may be present on metal samples) (Craddock, 2009: 38). In that case a thin film of metal or conducting carbon coating is necessary, in order to avoid material's electrostatic charging when exposed to the electron probe, which may result in image distortions (Egerton, 2005: 147).

The basic components of the SEM are:

- the lens system,
- the electron gun,
- the electron collector,
- the visual and photorecording cathode ray tubes (CRTs)
- the associated electronics (Goldstein et al., 2003, p:3)

The main principle of its operation is based on the irradiation of the- under examination- area with a finely focused electron beam, in an environment of high vacuum (Nixon, 1971). The electron beam is primarily produced by a heated tungsten filament, while it acquires specific wavelength after it has been accelerated by a fixed voltage of 1-50KeV (Goldstein, 2003: 30). The produced electron beam may be used under two forms, a static and a non static. In the non static form the electron beam may be swept in a raster across the surface of the specimen to form images, while in the static form it obtains its data from the analysis of a single surface spot, of a size proportional to the diameter of the initial beam. The electron probe of a SEM is

scanned horizontally across the specimen in two perpendicular (x and y) directions (Egerton, 2005: 127).

The interaction of the electron beam with the materials produces different types of emissions, thus signals to be observed. These types of signals, which can be used to examine different characteristics of the material, are the following:

- **the backscattered electrons**, which derive back from the sample from the elastic scattering of the beam electrons. These have high energies of approximately 50kV, while the intensity of the produced signal depends on the orientation of the crystalline structure and the atomic number of the elements on the sample surface. The contrast, among these energies allows the visualization of the information, thus the image obtained is related to the composition and crystal microstructure on the sample surface (Lloyd, 1987).
- **the secondary electrons**, which derive from the inelastic scattering of the beam electrons and have energy less than 50eV. The number of secondary electrons emitted is proportional to the angle of the incidence of the electron beam, which results in the visualization of the sample surface in high contrast. The image thus produced, is referred to as an ETD (Everhart-Thornley Detector) (Everhart, 1960: 246–248). Along with the backscattered, the secondary electrons are the imaging signals of the greatest importance, because these vary primarily as a result of differences in surface topography (Goldstein et al, 2003:1).
- **the characteristic x-rays** In the SEM, characteristic x-rays are also emitted as a result of electron bombardment. Energy-dispersive spectrometers (EDS) are capable of detecting characteristic x-rays of all from major elements (>10 wt%) above atomic number 4 at typical beam currents used for secondary electron imaging in the SEM. The analysis of the characteristic x-radiation emitted from samples can yield both qualitative identification and quantitative elemental information from regions of a specimen nominally 1 μm in diameter and 1 μm in depth under normal operating conditions (elemental analysis) (Egerton, 2005; Goldstein, 2003: 17).
- **other photons of various energies**

The great depth of field at high magnification is an advantage of SEM over light microscopy. Recognition of features of the topography of naturally weathered and worn surfaces, marks made during deposition or during use (Moropoulou, 2016), or even by tools is clearly of great importance when dealing with ancient metals. One major drawback to its use is that it is impossible to see the natural colours of a material; the obtained image is the product of a value per pixel, that is, the number of electrons retrieved by the detector in a specific period of time.

For the copper alloys analysis, SEM-EDS has been frequently used because of its sensitivity and its capability of detecting lighter elements, in relation to XRF spectroscopy. The detection of light elements is a major aid concerning the recognition of processes that may have been taking place during the deposition of the samples. Since is a technique of elemental analysis, not sensitive to chemical compounds in which the elements are bonded, when dealing with metals, it is through the identification of the object's elemental composition of surface distributed corrosion products, that can be supported significantly the characterization of their mineralogical composition and the subsequent formation of the corrosion products, which often result in obtaining non accurate elemental results.

The beam size can be controlled, enabling very precisely defined areas to be analysed; for metals, these can be as small as 1µm. When bulk analysis is required, line or area mode scans can be used, thus two-dimensional mapping of element distribution can be built up over a specified area, and where several elements are being measured their respective constituents can be represented in false colour. Quantitative x-ray analysis, though, requires that the specimen be perfectly flat with as little surface topography as possible; something that rarely is the case, considering ancient artifacts without sampling abscission and preparation (Goldstein, 2003: 540).

Regarding the reference materials for calibration, the same problems as for the XRF spectroscopy, apply. Another common problem regarding the SEM-EDS quantitative analysis is the detection and quantitative analysis of elements with concentrations under 0,5% (depending on the element), whose spectral lines are just distinguishable from the matrix. The smaller the height of those peaks, the more difficult they are to distinguish, while the value of their concentration resulting from the culmination of the spectrum is not so reliable. This is also dependent on background matrix levels that rarely are the same across the range of the spectrum. Usually a concentration of <0.5% is considered as of low reliability. Concentrations

of elements of low atomic numbers such as carbon, nitrogen, oxygen, fluorine where their K lines are emitted at low energy levels (<1 KeV) are not so reliable. Despite their diligent calibration, these SEM-EDS analyses are referred to as "semi-quantitative".

2.4.2. Devices and settings

Compositional analysis was performed using a SEM JEOL system (JSM-6510LV), coupled with an EDS by Oxford Instruments and software by INCA. The device provides the possibility of a three dimensional imaging and recording of the observation point. Analysis was done in a high vacuum, with secondary electrons, in a small spot size (40). The settings of the analysis were: accelerating voltage 20kV, working distance 15mm, collection time 90sec. The analyses were mostly performed in magnifications 200x and 1400x. The objects were mounted onto a specimen holder and a double-sided carbon tape was used, which improves conductivity and permits analysis. Taking advantage of the presence of the carbon tape for the distinction of free-corroded areas, five to eight measurements of each object were taken.

A certified reference copper alloy with known chemical composition was used in order to check the precision and accuracy of the apparatus and to obtain reliable experimental data. The reference copper alloy was the CDA 360, the same used for the p-XRF technique. Three measurements were taken from the standard and its mean values were: 61.80% Cu, 35.70% Zn, 0.31% Fe and 2.21% Pb. The results of all measurements are displayed on Appendix IV.1. It is concluded that no significant deviations from the default values exist. However, small variances in the values, which are noticed between the two analytical techniques, could be due to the device normalization and were taken into consideration in the discussion of the results. In order to evaluate the aforementioned variances, the relative difference (δ) between the two techniques was calculated by using the formula $\delta = (\mu\text{XRF} - \text{SEM-EDS}) / \text{SEM-EDS}$. The results are given in chapter 3.5., on table 3.8.

The mean value of the measurements on the elemental analyses of the samples from the sanctuary of Athena Alea with the SEM-EDS method, normalized to 100% (the concentrations of O and C have been subtracted), expressed in weight percentage (wt. %); along with the standard deviation are presented in chapter 3.4. (table 3.6. and

3.7.). All performed measurements and photographs obtained during the SEM-EDS analysis, are cited on Appendix IV.2 and IV.3.

III. RESULTS AND DISCUSSION

The results obtained through the microscopic observation, concerning mainly the manufacturing technology and the corrosion products of the assemblage, are presented in chapter 3.1. The chemical analysis of the assemblage under the XRF and SEM-EDS methodologies, is presented in chapter 3.2., 3.3. and 3.4. The comparison of the aforementioned techniques is presented in chapter 3.5., while the results and the discussion regarding the composition of the assemblage on chapters 3.6 and 3.7., respectively.

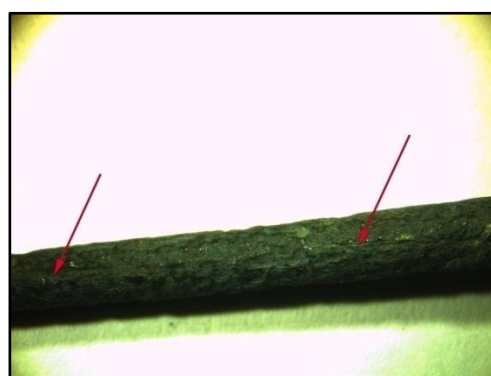
3.1. Stereomicroscopic observation

Using non-invasive scientific techniques, images of optical microscopy and scanning electron microscopy up to x1000 magnification, were captured (appendix IV.2 and IV.3).

The optical microscopy allowed a gross observation on the objects while enabled the identification and recording of the pins' physical features, tool marks and surface textures, which are characteristic of the techniques (cast or forged) used by the copper smiths to manufacture and decorate them. Due to restrictions on ancient objects sampling it was not possible to be documented through a metallographic examination, which could reveal further details. Marks in the form of metal lines running across their rod were identified in most of the pins, characteristic of the manufacturing process. The macroscopic and microscopic observation of the samples, thus, indicated that casting in two moulds was involved, along with possible forging on the edges to improve their properties. The copper smiths attempts to further accentuate the outline and give a finer definition to the designs by chasing and punching the pins directly was not very successful, leaving easily observed marks. These casting marks on some of the pins are indicated on the following images.



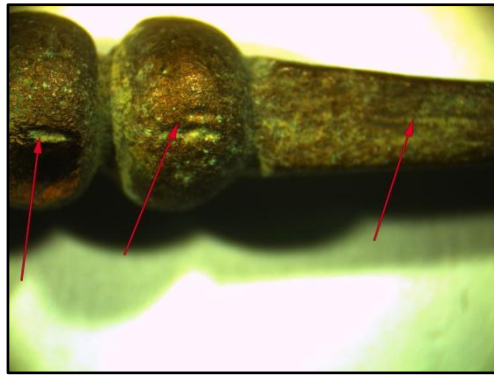
P1



P3



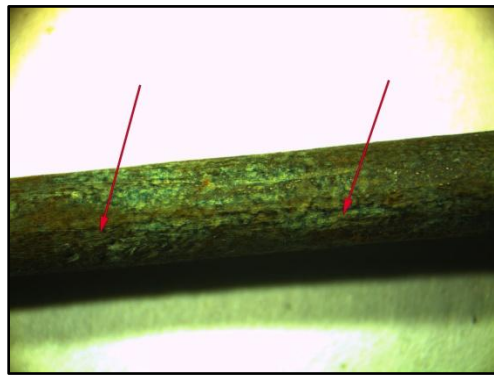
P4



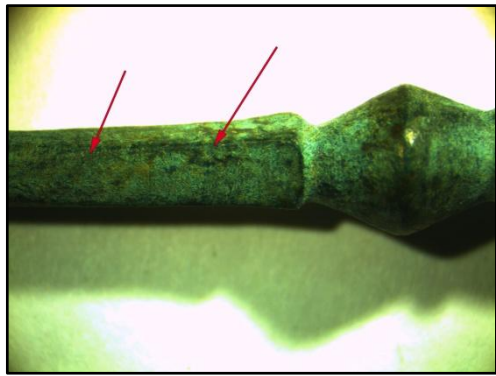
P5



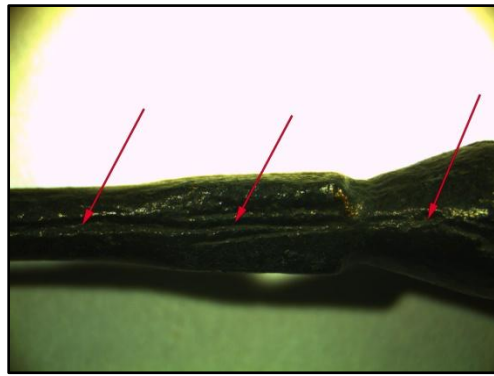
P5



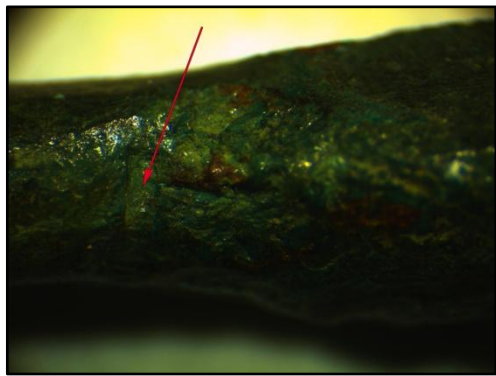
P6



P7



P8



P11



P26

Images 3.1-10. Casting marks on pins ALEA-P1, -P3, -P4, -P5, -P5, -P6, -P7, -P8, -P11, -P26

The corrosion patterns of the pins were also identified and recorded, in order to consider the origin of some of the light elements traced with the SEM-EDS; mainly sulfur, chlorine, phosphorus, chromium and calcium. These elements may be coming from the ore. In most cases, though they either derived from the deposition environment or were the remains of previous conservation, involved in the formation of new corrosion patterns on the samples. Due to lack of data in the Museum of Tripolis, though, it was not possible to investigate/confirm the methods and materials of previous conservation procedures. All pins and wastes were stripped of their varnish coating with the use of acetone, prior to any observation or analysis.

The description of the corrosion products, was based on relative literature (Gettens, 1963: 547-568; Craddock, 2009: 349-352, Anthony, 2016); all related information is presented in the catalogues of the chapters 3.1.1. and 3.1.2. The specification of the corrosion type was based on Rapp's scale (1978: 171-172) and is presented in the following table (table -3.1-)

Type of corrosion	Surface appearance
A	no corrosion (good metallic surface),
B	black patina to very thin green malachite patina present,
C	red cuprous oxide layer,
D	indication of pitting corrosion and light green corrosion layer,
E	heavy corrosion (green malachite patina present)

Table 3.1. *Classification of the corrosion types of bronze alloys*

3.1.1. Bronze pins

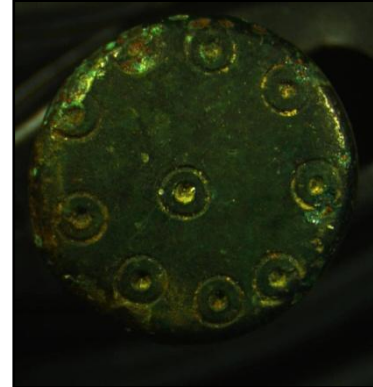
ALEA-P1



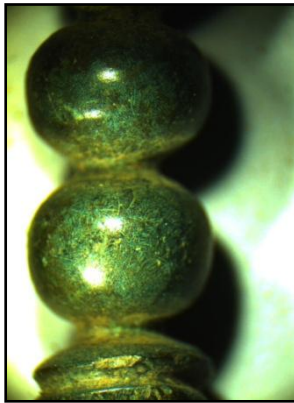
x6



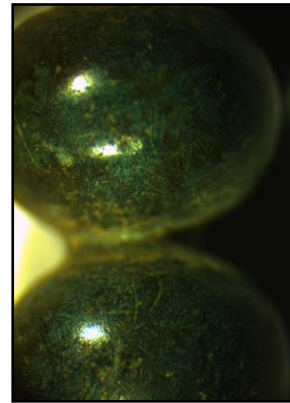
x12



x12



x6



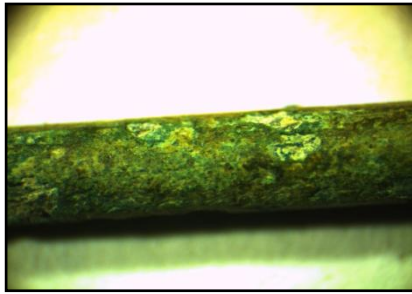
x16

Microscopic observation: The pin holds a thin surface of dark green colour, probably due to copper carbonates' corrosion products (malachite¹). Underneath a layer of grey-black of metallic appearance patina (tenorite), while it maintains its metal core. Casting marks, visible.

Corrosion Type: B

1. The corrosion products which will actually form depend on various parameters such as the composition of the alloy, the acidity of the environment (pH), its oxidation-reduction potential (Eh) and the cations and anions present (Schweizer, 1994: 42). Since their evaluation/identification was performed under optical microscopy all products are described by their physical properties and colour; the name in the parenthesis is indicative, for the corrosion products most likely present.

ALEA-P2



x16



x8

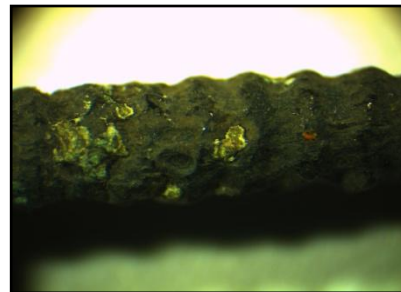
Microscopic observation: The pin holds a thin surface of dark green colour, probably due to copper carbonates' corrosion products (malachite). Underneath a layer of grey-black of metallic appearance patina (tenorite), while it maintains its metal core. Locally, red carbonate corrosion products of great thickness appear (cuprite). Indication of pitting corrosion and formation of loose, light green due to copper chlorides, corrosion products (atacamite/paratacamite). Casting marks, visible.

Corrosion Type: C

ALEA-P3



x6

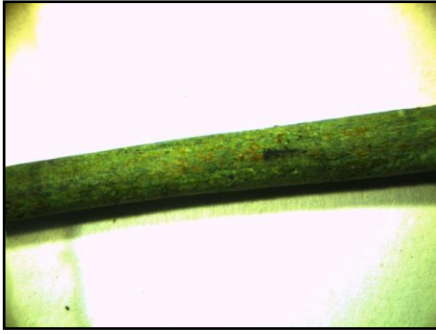


x16

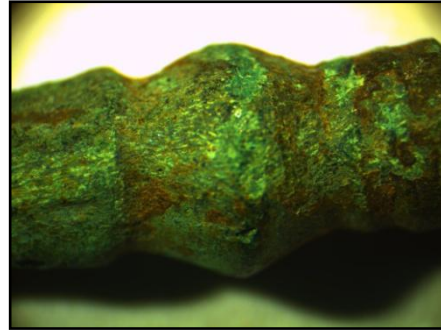
Microscopic observation: The pin holds a thin surface of dark green colour, probably due to copper carbonates' corrosion products (malachite). Underneath a layer of grey-black of metallic appearance patina (tenorite), while it maintains its metal core. Casting marks, visible.

Corrosion Type: C

ALEA-P4



x6



x12

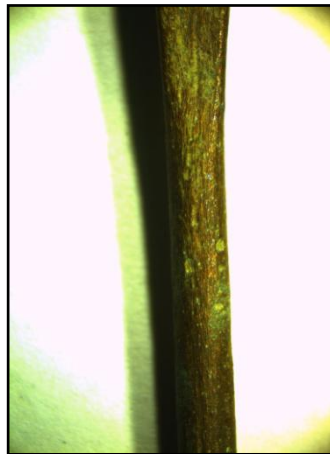
Microscopic observation: The pin holds a thin surface of dark and locally of light green colour, probably due to copper carbonates' corrosion products (malachite). Underneath a layer of grey-black of metallic appearance patina (tenorite), while it maintains its metal core. Locally, there appear areas of soil conglomerates. Casting marks, visible.

Corrosion Type: C

ALEA-P5



x8



x6



x12

Microscopic observation: The pin holds a thin surface of dark and light green colour, probably due to copper carbonates' corrosion products (malachite). Underneath a layer of grey-black of metallic appearance patina (tenorite), while it maintains its metal core. Indication of pitting corrosion and formation of loose, light green due to copper chlorides, corrosion products (atacamite/paratacamite). Casting marks, visible.

Corrosion Type: B

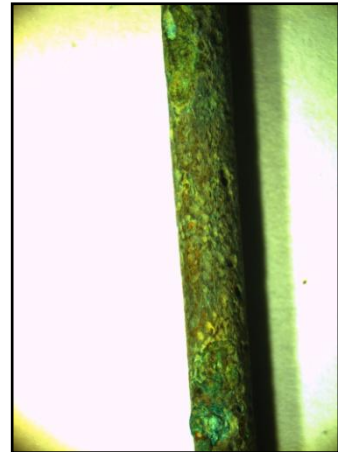
ALEA-P6



x6



x8



x6

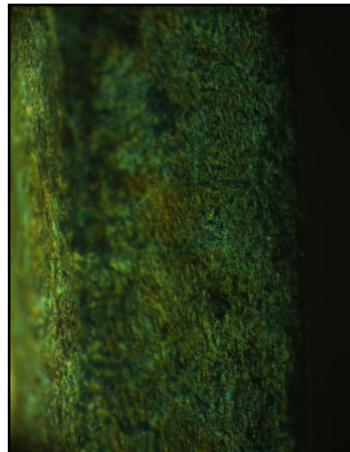
Microscopic observation: The pin holds a thin surface of dark and light green colour, probably due to copper carbonates' corrosion products (malachite). Underneath a layer of grey-black of metallic appearance patina (tenorite), while it maintains its metal core. Casting marks, visible.

Corrosion Type: C

ALEA-P7



x6



x25



x10

Microscopic observation: The pin holds a thin surface of dark and light green colour, probably due to copper carbonates' corrosion products (malachite). Underneath traces of formation of a grey-black of metallic appearance patina (tenorite), while it maintains its metal core. Casting marks, visible.

Corrosion Type: B

ALEA-P8



x6



x6



x8

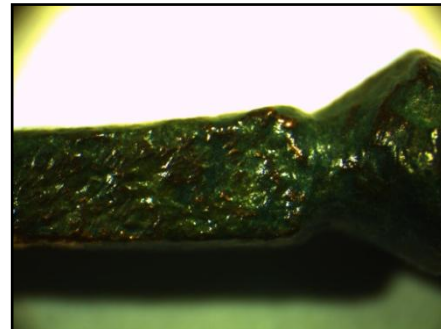
Microscopic observation: The pin holds a grey-black of metallic appearance patina (tenorite), while it maintains its metal core. Locally, few corrosion products of dark green colour, probably due to copper carbonates' (malachite) and thick spots of red corrosion products (cuprite). Casting marks, visible.

Corrosion Type: C

ALEA-P9



x8



x12

Microscopic observation: The pin holds a thin surface of dark green colour, probably due to copper carbonates' corrosion products (malachite). Underneath a layer of grey-black of metallic appearance patina (tenorite), while it maintains its metal core. Indication of stress corrosion, near the needle of the pin.

Corrosion Type: C

ALEA-P10



x10

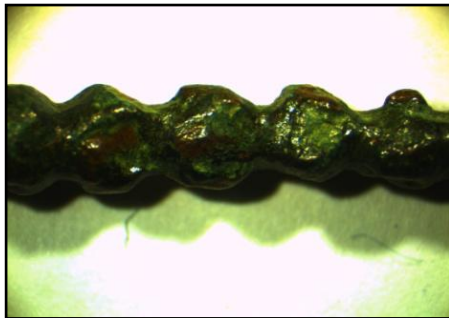


x10

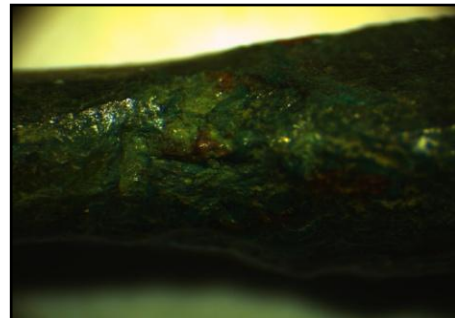
Microscopic observation: The pin holds a surface of grey-black of metallic appearance patina (tenorite), while it maintains its metal core. Casting marks, visible.

Corrosion Type: B

ALEA-P11



x6

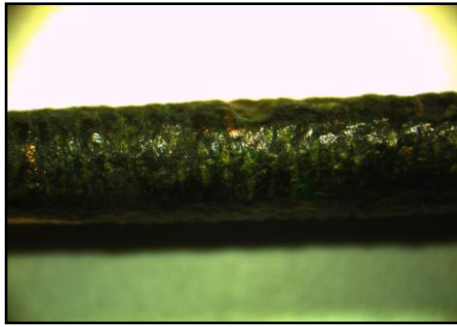


x12

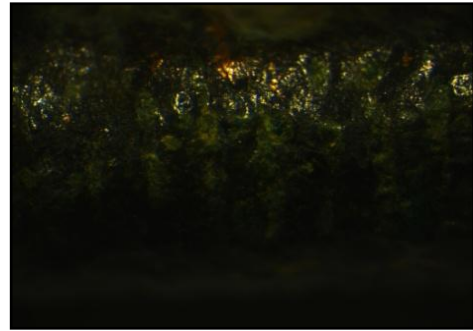
Microscopic observation: The pin holds a thin surface of dark green colour, probably due to copper carbonates' corrosion products (malachite). Underneath a layer of grey-black of metallic appearance patina (tenorite), while it maintains its metal core.

Corrosion Type: C

ALEA-P12



x10

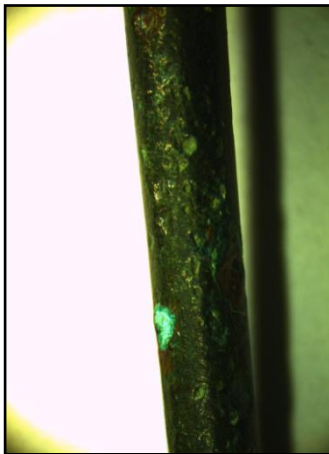


x25

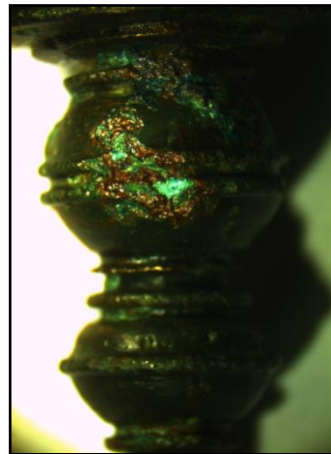
Microscopic observation: The pin holds a thin surface of dark green colour, probably due to copper carbonates' corrosion products (malachite). Underneath a layer of grey-black of metallic appearance patina (tenorite), while it maintains its metal core. Indication of pitting corrosion.

Corrosion Type: C

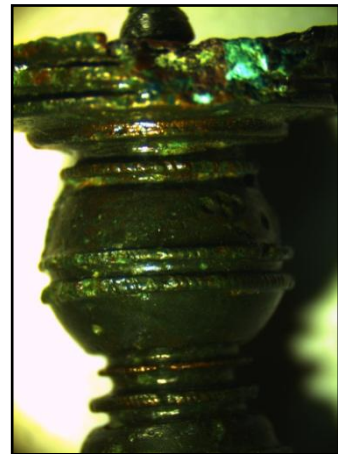
ALEA-P13



x8



x6

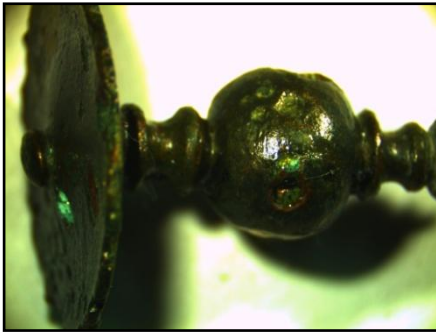


x6

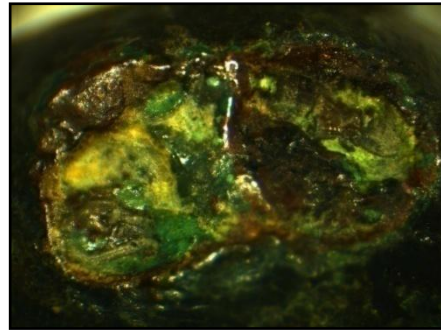
Microscopic observation: The pin holds a thick surface of dark green colour locally, probably due to copper carbonates' corrosion products (malachite). Underneath a layer of grey-black of metallic appearance patina (tenorite), while it maintains its metal core. Thick spots of red corrosion products (cuprite) appear locally. Indication of pitting corrosion and formation of loose, light green due to copper chlorides, corrosion products (atacamite/paratacamite).

Corrosion Type: D

ALEA-P14



x6



x20

Microscopic observation: The pin holds a thick surface of dark green colour locally, probably due to copper carbonates' corrosion products (malachite). Underneath a layer of grey-black of metallic appearance patina (tenorite), while it maintains its metal core. Indication of extensive pitting corrosion and formation of loose, light green due to copper chlorides, corrosion products (atacamite/paratacamite).

Corrosion Type: D

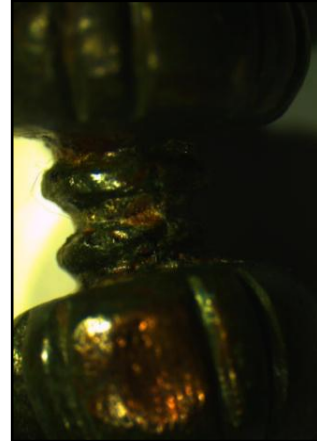
ALEA-P15



x10



x8



x10

Microscopic observation: The pin holds a thick surface of dark green colour locally, probably due to copper carbonates' corrosion products (malachite). Underneath a layer of grey-black of metallic appearance patina (tenorite), while it maintains its metal core. Thick spots of red corrosion products (cuprite) appear locally. Indication of pitting corrosion and formation of loose, light green due to copper chlorides, corrosion products (atacamite/paratacamite). Locally, there appear areas of soil conglomerates.

Corrosion Type: D

ALEA-P16



x6

Microscopic observation: The pin holds a thick surface of dark green colour locally, probably due to copper carbonates' corrosion products (malachite). Underneath a layer of grey-black of metallic appearance patina (tenorite), while it maintains its metal core. Thick spots of red corrosion products (cuprite) appear locally. Indication of pitting corrosion and formation of loose, light green due to copper chlorides, corrosion products (atacamite/paratacamite).

Corrosion Type: D

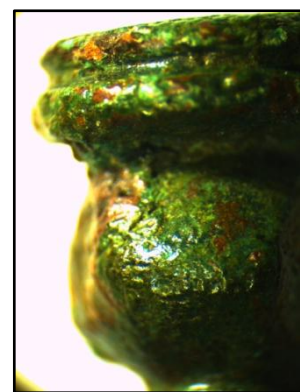
ALEA-P17



x6



x10



x16

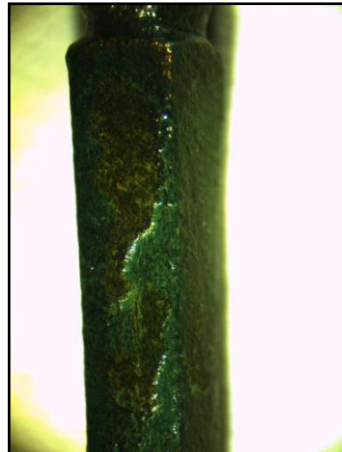
Microscopic observation: The pin holds a thick surface of dark green colour locally, probably due to copper carbonates' corrosion products (malachite). Underneath a layer of grey-black of metallic appearance patina (tenorite), while it maintains its metal core. Thick spots of red corrosion products (cuprite) appear locally. Indication of formation of loose, light green due to copper chlorides, corrosion products (atacamite/paratacamite).

Corrosion Type: C

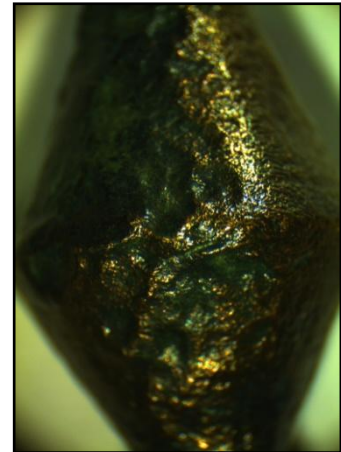
ALEA-P18



x6



x10

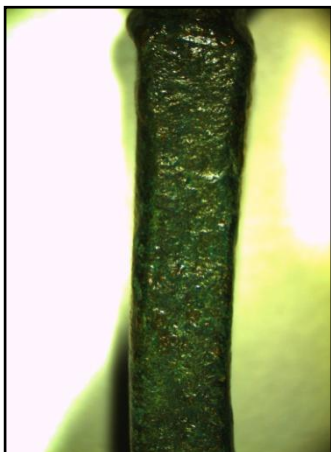


x12

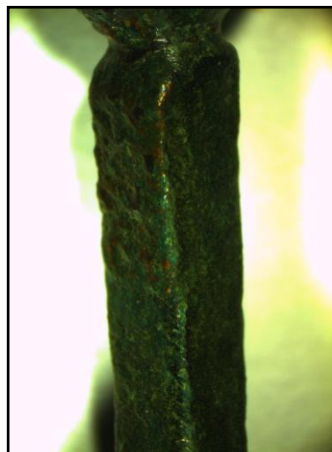
Microscopic observation: The pin holds a thick surface of dark green colour locally, probably due to copper carbonates' corrosion products (malachite) while underneath, it maintains its metal core.

Corrosion Type: C

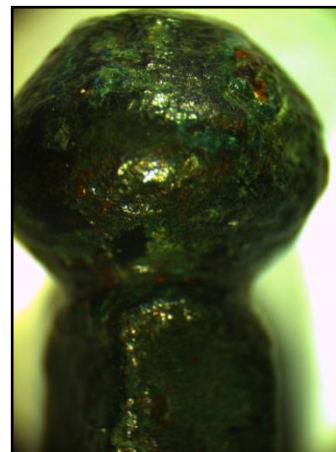
ALEA-P19



x8



x8



x12

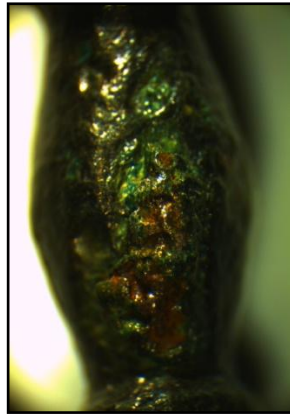
Microscopic observation: The pin holds a thick surface of dark green colour locally, probably due to copper carbonates' corrosion products (malachite). Locally underneath, a layer of grey-black of metallic appearance patina (tenorite), while it maintains its metal core. Thick spots of red corrosion products (cuprite) also appear locally.

Corrosion Type: C

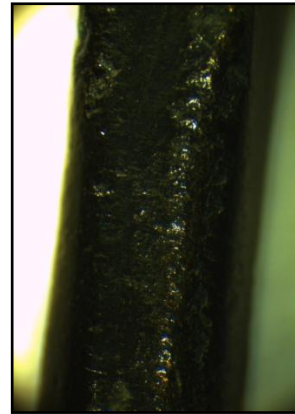
ALEA-P20



x8



x20



x20

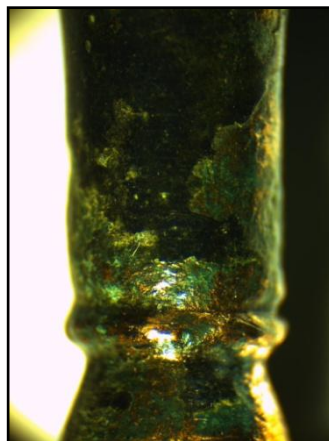
Microscopic observation: The pin holds a thick surface of dark green colour locally, probably due to copper carbonates' corrosion products (malachite). Underneath a layer of grey-black of metallic appearance patina (tenorite), while it maintains its metal core. Thick spots of red corrosion products (cuprite) appear locally.

Corrosion Type: C

ALEA-P21



x6



x16



x10

Microscopic observation: The pin holds a thick surface of dark and light green colour locally, probably due to copper carbonates' corrosion products (malachite). Underneath a layer of grey-black of metallic appearance patina (tenorite), while it maintains its metal core.

Corrosion Type: B

ALEA-P22



x8



x12

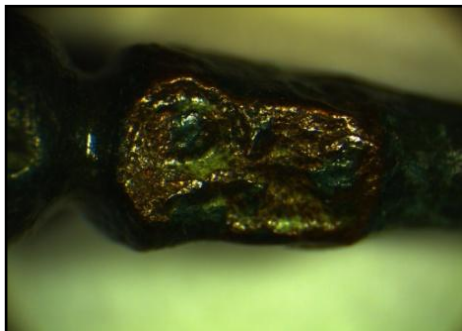


x16

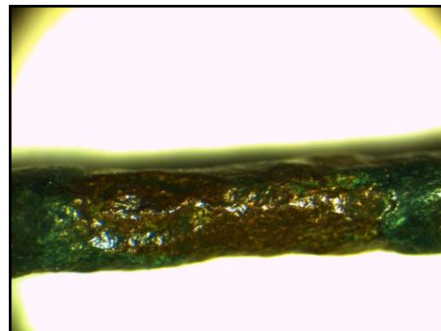
Microscopic observation: The pin holds a thick surface of dark green colour locally, probably due to copper carbonates' corrosion products (malachite). Underneath a layer of grey-black of metallic appearance patina (tenorite), while it maintains its metal core. Thick spots of red corrosion products (cuprite) appear locally. Indication of pitting corrosion and formation of loose, light green due to copper chlorides, corrosion products (atacamite/paratacamite).

Corrosion Type: D

ALEA-P23



x20

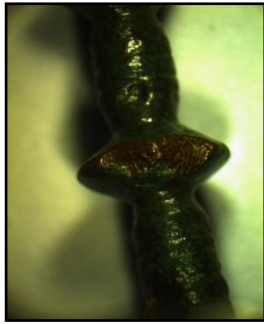


x20

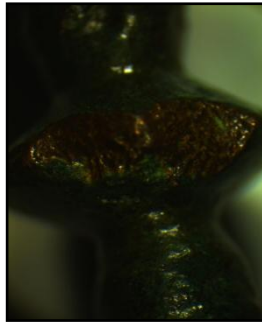
Microscopic observation: The pin holds a thin surface of dark green colour locally, probably due to copper carbonates' corrosion products (malachite). Underneath a layer of grey-black of metallic appearance patina (tenorite), while it maintains its metal core.

Corrosion Type: D

ALEA-P24



x10



x20



x20



x20

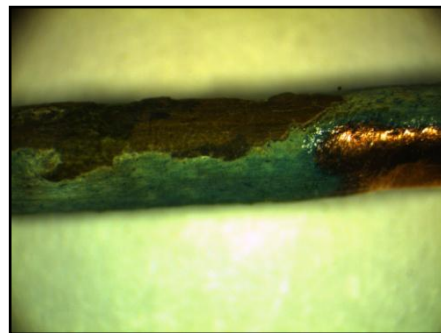
Microscopic observation: The pin holds a thin surface of dark green colour locally, probably due to copper carbonates' corrosion products (malachite). Underneath a layer of grey-black of metallic appearance patina (tenorite), while it maintains its metal core. Thick spots of red corrosion products (cuprite) appear locally.

Corrosion Type: C

ALEA-P25



x16

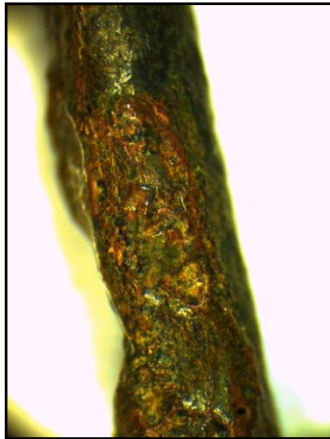


x25

Microscopic observation: The pin holds a thin surface of dark and light green colour locally, probably due to copper carbonates' corrosion products (malachite). Underneath a layer of grey-black of metallic appearance patina (tenorite), while it maintains its metal core. Thick spots of red corrosion products (cuprite) appear locally. Indication of formation of loose, light green due to copper chlorides, corrosion products (atacamite/paratacamite).

Corrosion Type: B

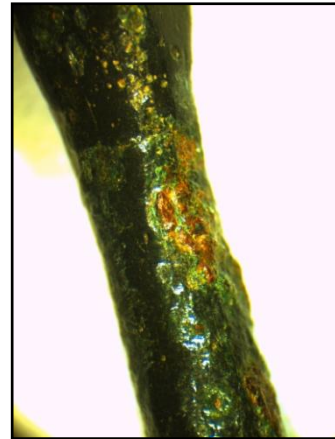
ALEA-P26



x20



x12



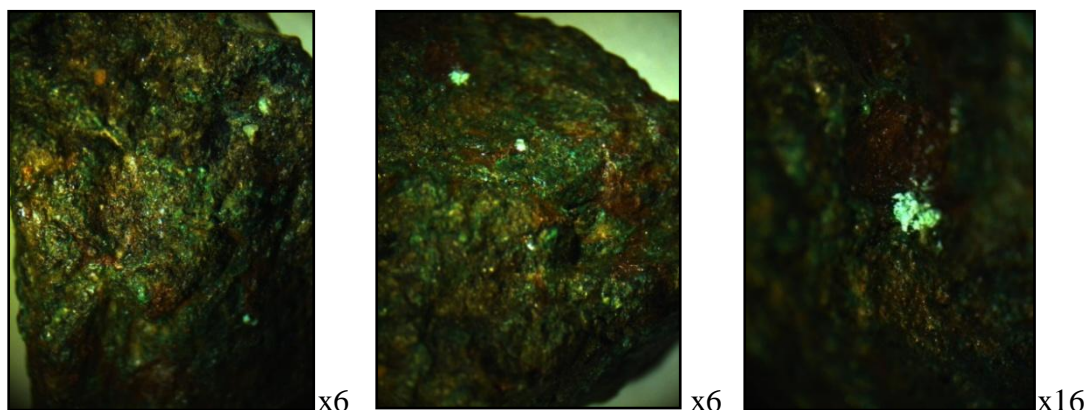
x12

Microscopic observation: The pin holds a thin surface of dark green colour locally, probably due to copper carbonates' corrosion products (malachite). Underneath a layer of grey-black of metallic appearance patina (tenorite), while it maintains its metal core. Thick spots of red corrosion products (cuprite) appear locally. Indication of pitting corrosion.

Corrosion Type: D

3.1.2. Metallurgical wastes

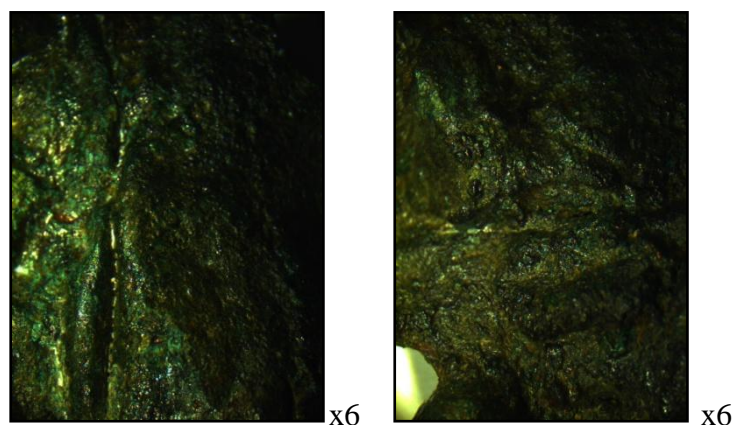
ALEA-WS1



Microscopic observation: The waste holds a very thick surface of dark green colour, probably due to copper carbonates' corrosion products (malachite). Underneath a layer of grey-black of metallic appearance patina (tenorite), while it maintains its metal core. Thick spots of red corrosion products (cuprite) appear locally. Extensive coal inclusions, entrapped among the surface cavities.

Corrosion Type: D

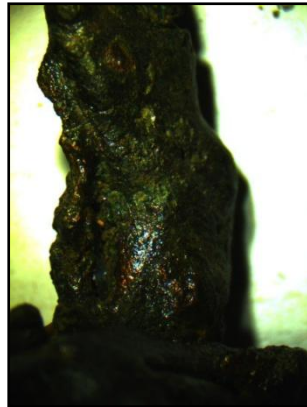
ALEA-WS2



Microscopic observation: The waste holds quite a thick surface of dark green colour, probably due to copper carbonates' corrosion products (malachite). Underneath a layer of grey-black of metallic appearance patina (tenorite), while it maintains its metal core. Thick spots of red corrosion products (cuprite) appear locally. Its general appearance is of fused metal sheets.

Corrosion Type: D

ALEA-WS3

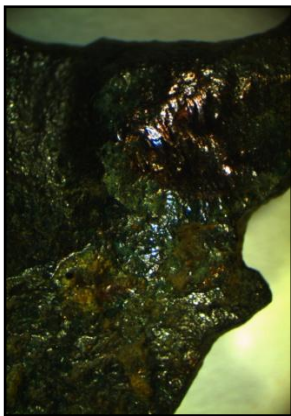


x6

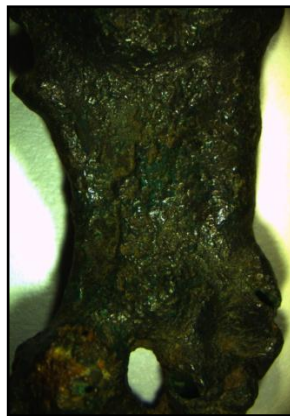
Microscopic observation: The waste holds a very thick surface of dark green colour, probably due to copper carbonates' corrosion products (malachite). Underneath a layer of grey-black of metallic appearance patina (tenorite), while it maintains its metal core. Thick spots of red corrosion products (cuprite) appear locally.

Corrosion Type: D

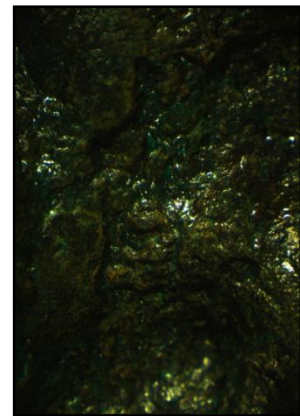
ALEA-WS4



x6



x6

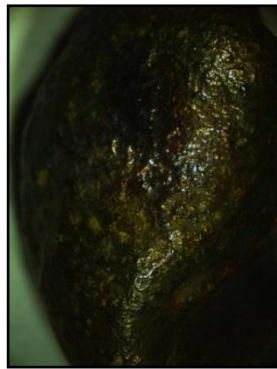


x16

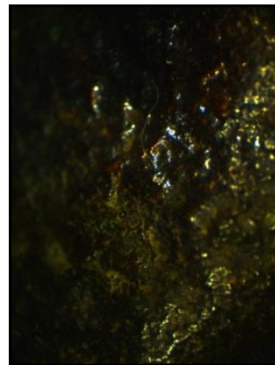
Microscopic observation: The waste holds locally a thin surface of dark green colour, probably due to copper carbonates' corrosion products (malachite). Underneath a layer of grey-black of metallic appearance patina (tenorite), while it maintains its metal core. Thin spots of red corrosion products (cuprite) appear locally. Porous appearance, due to probable gas formation during melting.

Corrosion Type: C

ALEA-WS5



x16



x30

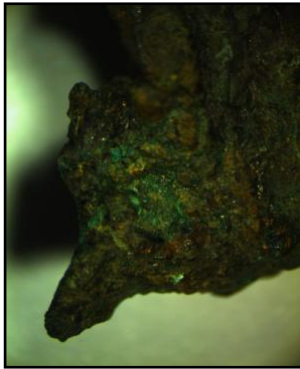


x16

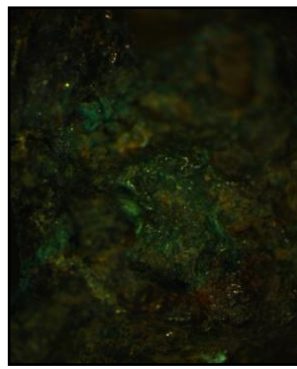
Microscopic observation: The waste holds locally a thin surface of dark green colour, probably due to copper carbonates' corrosion products (malachite). Underneath a layer of grey-black of metallic appearance patina (tenorite), while the waste maintains its metal core.

Corrosion Type: B

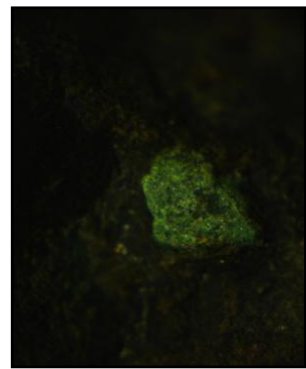
ALEA-WS6



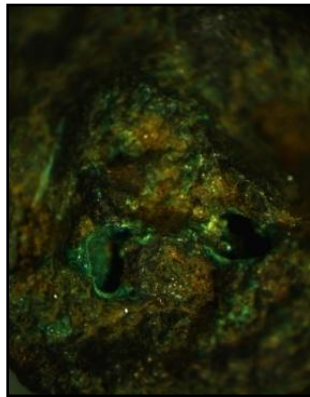
x6



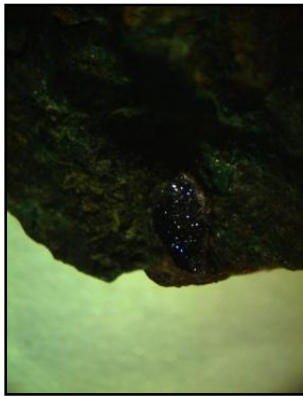
x16



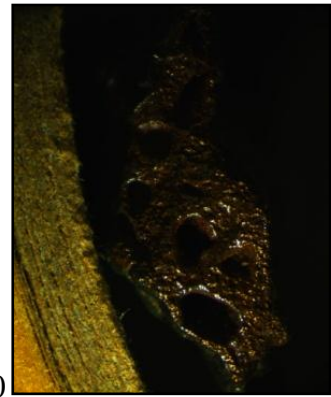
x30



x30



x30

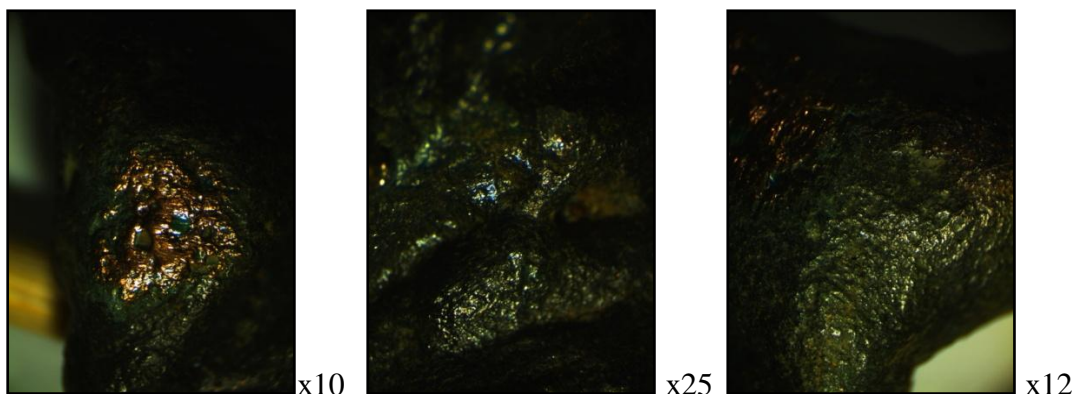


x6

Microscopic observation: The waste holds locally a thin surface of dark green colour, probably due to copper carbonates' corrosion products (malachite). Underneath a layer of grey-black of metallic appearance patina (tenorite), while it maintains its metal core. Porous appearance, due to probable gas formation during melting. In the cross-sections of the waste among the gas formations, red corrosion products (cuprite) appear locally.

Corrosion Type: C

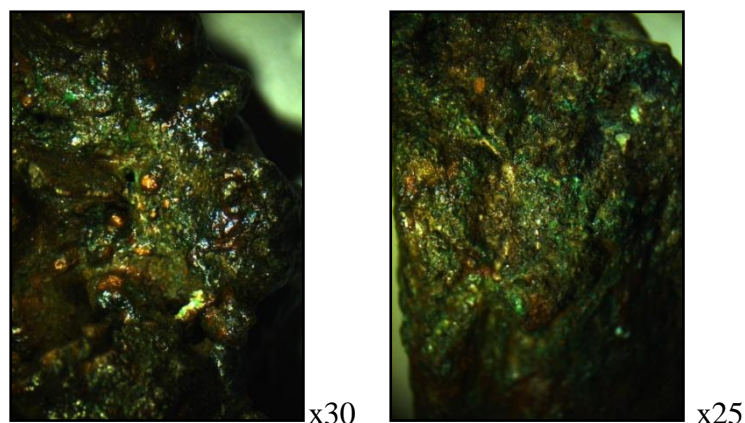
ALEA-WS7



Microscopic observation: The waste holds a thin surface of dark green colour, probably due to copper carbonates' corrosion products (malachite). Underneath a layer of grey-black of metallic appearance patina (tenorite), while it maintains its metal core.

Corrosion Type: B

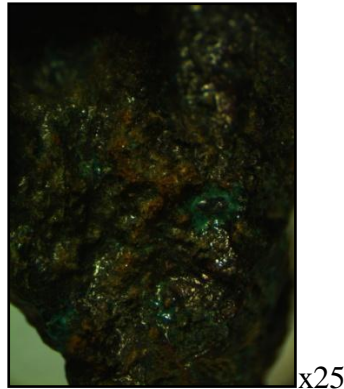
ALEA-WS8



Microscopic observation: The waste holds locally a thick surface of dark green colour, probably due to copper carbonates' corrosion products (malachite). Underneath a layer of grey-black of metallic appearance patina (tenorite), while it maintains its metal core. Exfoliation of metal layers, due to incomplete fusion of the metal sheets that were used during its melting. Porous appearance locally, due to probable gas formation during melting. Inside the gas formations, red corrosion products (cuprite) appear locally.

Corrosion Type: C

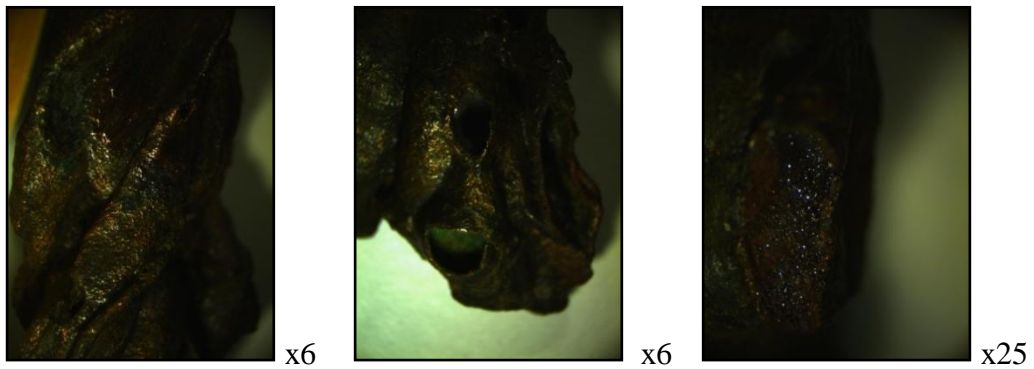
ALEA-WS9



Microscopic observation: The waste holds a very thick surface of dark green colour, probably due to copper carbonates' corrosion products (malachite). Underneath a layer of grey-black of metallic appearance patina (tenorite), while it maintains its metal core. Thick spots of red corrosion products (cuprite) appear locally. Extensive inclusions of white colour conglomerates, entrapped among the surface cavities.

Corrosion Type: C

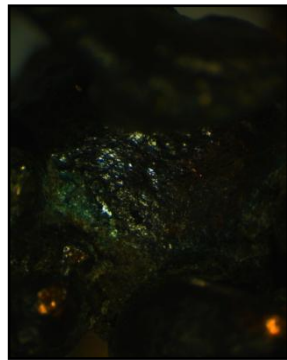
ALEA-WS10



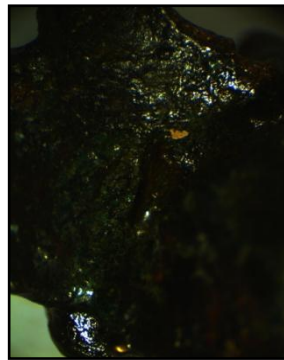
Microscopic observation: The waste holds locally a thin surface of dark green colour, probably due to copper carbonates' corrosion products (malachite). Underneath a layer of grey-black of metallic appearance patina (tenorite), while it maintains its metal core. Porous appearance locally, due to probable gas formation during melting. Inside the gas formations, light green and red corrosion products (malachite-cuprite) appear locally.

Corrosion Type: B

ALEA-WS11



x16

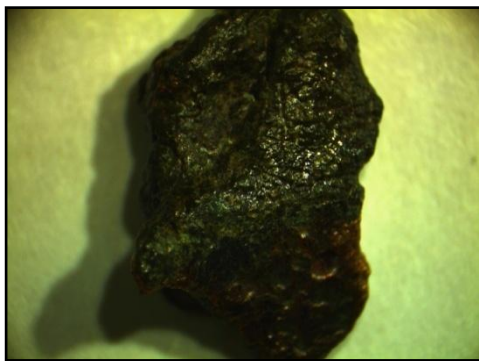


x16

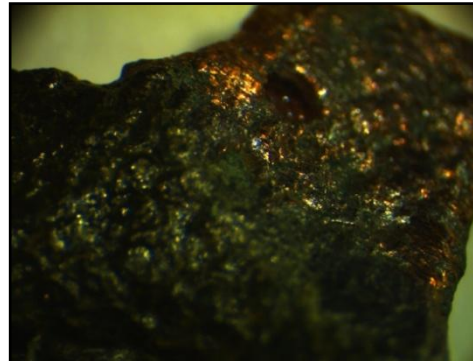
Microscopic observation: The waste holds locally a thin surface of dark green colour, probably due to copper carbonates' corrosion products (malachite). Underneath a layer of grey-black of metallic appearance patina (tenorite), while it maintains its metal core.

Corrosion Type: B

ALEA-WS12



x10

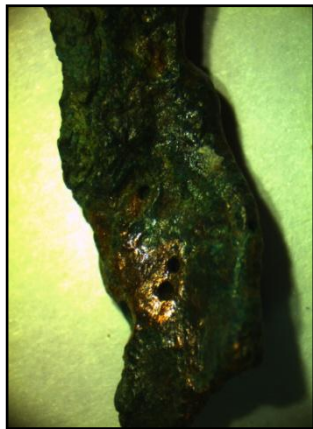


x20

Microscopic observation: The waste holds locally a thick surface of dark green colour, probably due to copper carbonates' corrosion products (malachite). Underneath a layer of grey-black of metallic appearance patina (tenorite), while it maintains its metal core.

Corrosion Type: C

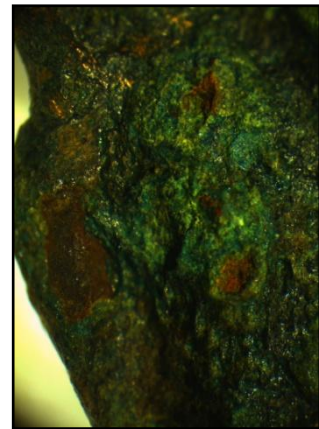
ALEA-WS13



x8



x8



x16

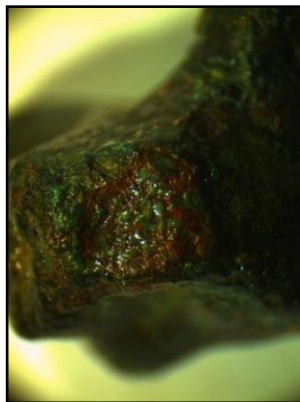
Microscopic observation: The waste holds locally a thick surface of dark green colour, probably due to copper carbonates' corrosion products (malachite), while underneath it maintains its metal core. Indication of extensive pitting corrosion.

Corrosion Type: C

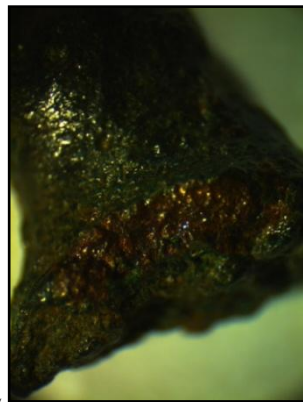
ALEA-WS14



x6



x12

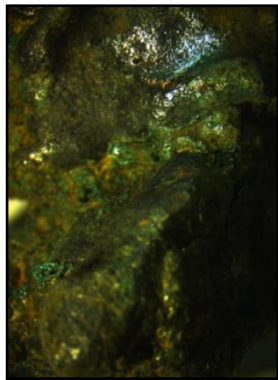


x16

Microscopic observation: The waste holds a thin surface of dark green colour, probably due to copper carbonates' corrosion products (malachite). Underneath a layer of grey-black of metallic appearance patina (tenorite), while it maintains its metal core. Thick spots of red corrosion products (cuprite) appear locally.

Corrosion Type: C

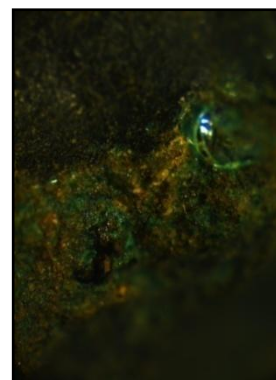
ALEA-WS15



x6



x10

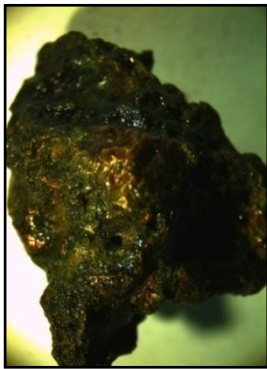


x12

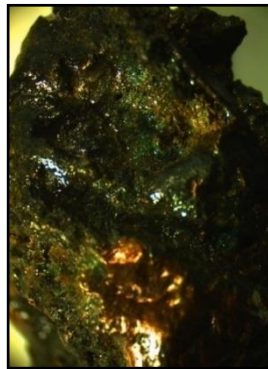
Microscopic observation: The waste holds a very thick surface of dark green colour, probably due to copper carbonates' corrosion products (malachite). Underneath a layer of grey-black of metallic appearance patina (tenorite), while it maintains its metal core. Thick spots of red corrosion products (cuprite) appear locally. Probable iron impurities inside the surface cavities.

Corrosion Type: D

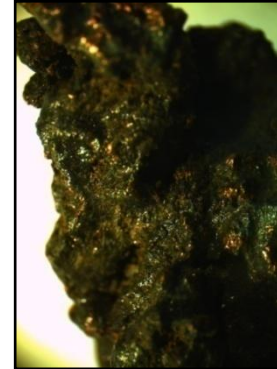
ALEA-WS16



x6



x10

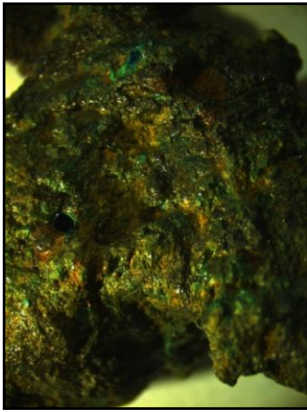


x10

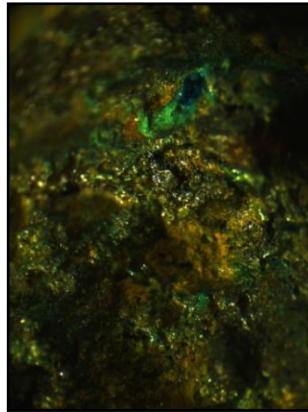
Microscopic observation: The waste holds a surface of dark green colour conglomerates, probably due to copper carbonates' corrosion products (malachite) while underneath, it maintains its metal core.

Corrosion Type: B

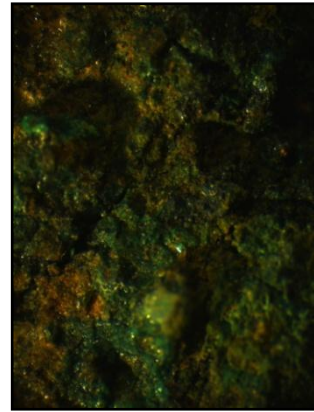
ALEA-WS17



x6



x12

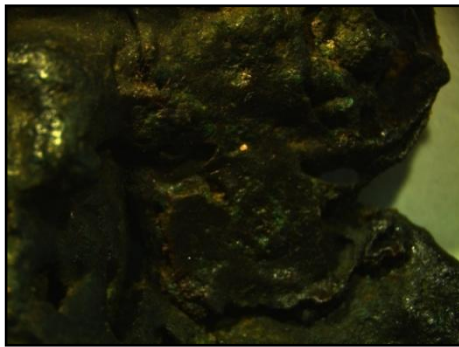


x20

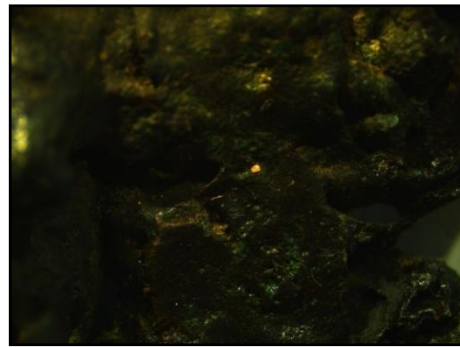
Microscopic observation: The waste holds a surface of dark green colour conglomerates, probably due to copper carbonates' corrosion products (malachite) while underneath, it maintains its metal core. Blue areas of other probable copper carbonates' corrosion products (azurite) appear locally. Soil conglomerates and other mineral inclusion of vitreous appearance, appear among objects' cavities.

Corrosion Type: D

ALEA-WS18



x6

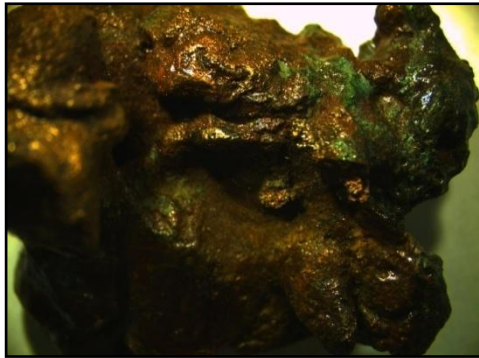


x8

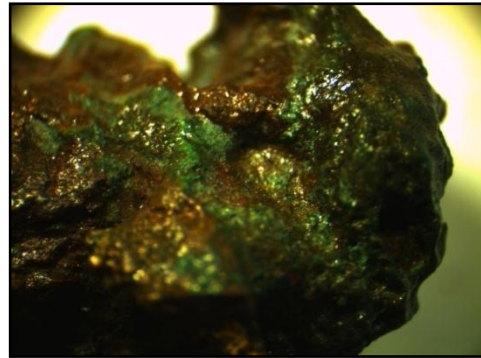
Microscopic observation: The waste holds a thin surface of dark green colour, probably due to copper carbonates' corrosion products (malachite). Underneath a layer of grey-black of metallic appearance patina (tenorite), while it maintains its metal core.

Corrosion Type: B

ALEA-WS19



x6

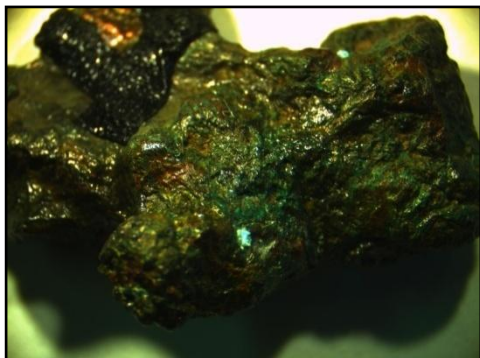


x12

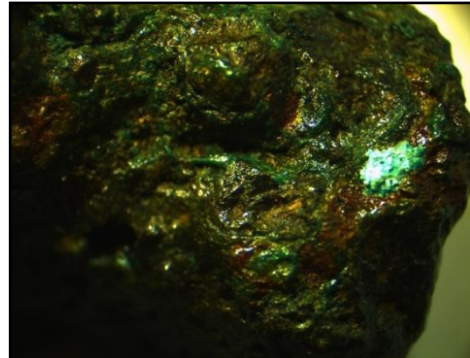
Microscopic observation: The waste holds a very thin surface of dark green colour, probably due to copper carbonates' corrosion products (malachite). Underneath a layer of grey-black of metallic appearance patina (tenorite), while it maintains its metal core. Areas of thin red corrosion products (cuprite) appear locally.

Corrosion Type: C

ALEA-WS20



x6



x12

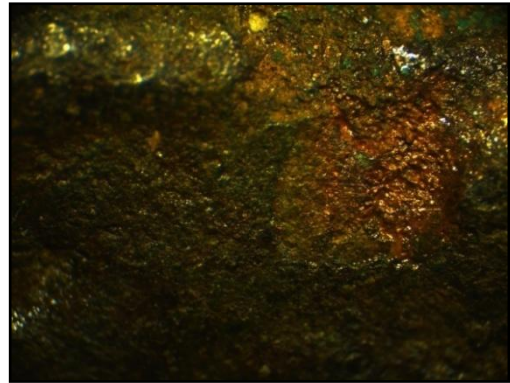
Microscopic observation: The waste holds locally a very thick surface of dark green colour, probably due to copper carbonates' corrosion products (malachite). Underneath a layer of grey-black of metallic appearance patina (tenorite), while it maintains its metal core. Porous appearance locally, due to probable gas formation during melting. Inside the gas formations, red corrosion products (cuprite) appear locally.

Corrosion Type: D

ALEA-WS21



x6



x20

Microscopic observation: The waste holds a thick surface of dark green colour, probably due to copper carbonates' corrosion products (malachite). Underneath a layer of grey-black of metallic appearance patina (tenorite), while it maintains its metal core. Probable iron impurities inside the surface cavities.

Corrosion Type: C

3.2. Elemental analysis using p-XRF

The mean values along with standard deviation of the measurements on the pins and wastes assemblage obtained by portable XRF, concerning the elements Cu, Sn, Fe, As, Pb, Sb, Bi, Ag, Zr, Zn, Mn, Nb, Co, Ni, and Cu, Sn, Fe, As, Pb, Sb, Bi, Ag, Zr, Zn, Mn, Co and Ni respectively, are presented in Tables 3.2. and 3.3.

Table 3.2. Concentration of the mean values of the elements detected on the bronze *pins* with the *p-XRF* method normalized, expressed in % wt. (St. Dev.: standard deviation, n.d.: not detected)

Sample	Cu	Sn	Fe	As	Pb	Sb	Bi	Ag	Zr	Zn	Mn	Nb	Co	Ni
P1	83.6	15.2	0.31	0.19	0.28	0.15	0.11	0.04	0.03	0.07	0.01	n.d.	n.d.	n.d.
St.Dev.	2.9	2.4	0.17	0.14	0.22	0.05	0.04	0.01	0.01	0.01	0.00	-	-	-
P2	86.5	8.8	1.38	1.77	n.d.	0.85	0.19	0.21	0.05	0.16	0.07	n.d.	n.d.	n.d.
St.Dev.	1.7	1.1	0.25	0.12	-	0.17	0.07	0.00	0.01	0.01	0.00	-	-	-
P3	88.7	9.7	0.81	0.15	n.d.	0.20	0.15	0.11	0.04	0.08	0.04	n.d.	n.d.	n.d.
St.Dev.	1.6	1.5	0.10	0.04	-	0.03	0.01	0.02	0.00	0.03	0.01	-	-	-
P4	98.6	0.4	0.26	0.23	n.d.	0.14	0.08	0.21	0.02	0.04	n.d.	n.d.	n.d.	0.05
St.Dev.	0.2	0.1	0.01	0.01	-	0.03	0.04	0.07	0.01	0.00	-	-	-	-
P5	85.8	12.9	0.45	0.33	n.d.	0.18	0.12	0.06	0.03	0.09	0.02	n.d.	n.d.	n.d.
St.Dev.	1.1	1.2	0.04	0.03	-	0.10	0.08	0.05	0.02	0.06	0.00	-	-	-
P6	82.6	16.3	0.30	0.03	0.24	0.18	0.16	0.07	0.05	0.07	n.d.	n.d.	n.d.	n.d.
St.Dev.	3.7	3.6	0.07	0.00	0.04	0.03	0.01	0.00	0.02	0.01	-	-	-	-
P7	84.0	15.0	0.14	0.12	0.20	0.20	0.20	0.05	0.06	0.07	n.d.	n.d.	n.d.	n.d.
St.Dev.	0.2	0.3	0.01	0.01	0.07	0.01	0.02	0.01	0.01	0.00	-	-	-	-
P8	80.3	18.0	0.51	0.23	0.56	0.18	0.11	n.d.	0.04	0.07	0.01	n.d.	n.d.	n.d.
St.Dev.	0.6	0.5	0.02	0.01	0.07	0.05	0.04	-	0.02	0.00	0.01	-	-	-
P9	85.1	12.8	0.05	0.23	1.47	0.13	0.13	0.03	0.04	0.06	n.d.	n.d.	n.d.	n.d.
St.Dev.	1.3	1.2	0.00	0.03	0.09	0.01	0.01	0.02	0.00	0.00	-	-	-	-
P10	75.9	21.1	1.86	0.36	0.16	0.29	0.25	n.d.	0.08	0.09	0.11	n.d.	n.d.	n.d.
St.Dev.	0.7	0.8	0.14	0.03	0.00	0.04	0.04	-	0.02	0.02	0.01	-	-	-
P11	75.1	21.3	0.23	0.53	2.44	0.15	0.11	n.d.	0.04	0.07	n.d.	n.d.	n.d.	n.d.
St.Dev.	0.7	0.6	0.01	0.02	0.01	0.02	0.02	-	0.00	0.00	-	-	-	-
P12	79.8	16.6	1.15	0.20	1.77	0.13	0.13	0.01	0.04	0.13	0.05	n.d.	n.d.	n.d.
St.Dev.	0.5	0.5	0.04	0.02	0.08	0.05	0.04	0.00	0.01	0.02	0.01	-	-	-
P13	75.2	23.1	0.79	0.37	n.d.	0.16	0.17	n.d.	0.06	0.09	0.06	n.d.	n.d.	n.d.
St.Dev.	1.5	1.6	0.08	0.01	-	0.04	0.03	-	0.01	0.02	0.02	-	-	-
P14	84.1	13.4	0.68	0.29	n.d.	0.13	0.15	0.06	0.05	0.10	0.02	n.d.	0.40	0.60
St.Dev.	1.0	0.9	0.01	0.00	-	0.02	0.03	0.00	0.02	0.01	0.00	-	0.01	0.01
P15	81.4	12.7	0.06	1.34	4.02	0.26	0.09	0.09	0.05	0.02	n.d.	n.d.	n.d.	n.d.
St.Dev.	1.4	0.9	0.04	0.47	2.71	0.05	0.05	0.02	0.02	0.01	-	-	-	-
P16	84.2	14.0	0.15	0.26	0.80	0.21	0.17	0.03	0.05	0.15	0.02	n.d.	n.d.	n.d.

Sample	Cu	Sn	Fe	As	Pb	Sb	Bi	Ag	Zr	Zn	Mn	Nb	Co	Ni
St.Dev.	0.3	0.7	0.09	0.01	0.02	0.07	0.05	0.03	0.02	0.10	0.01	-	-	-
P17	80.6	16.1	0.95	1.28	n.d.	0.71	0.20	0.05	0.06	0.09	0.04	n.d.	n.d.	n.d.
St.Dev.	1.2	1.0	0.08	0.24	-	0.01	0.05	0.00	0.01	0.02	0.01	-	-	-
P18	85.3	12.9	0.09	1.29	n.d.	0.20	0.10	0.09	0.02	0.07	n.d.	n.d.	n.d.	n.d.
St.Dev.	0.6	0.5	0.01	0.03	-	0.05	0.01	0.01	0.01	0.01	-	-	-	-
P19	84.6	13.6	0.19	0.21	1.08	0.09	0.07	0.05	0.02	0.10	n.d.	n.d.	n.d.	n.d.
St.Dev.	2.2	2.0	0.06	0.04	0.17	0.03	0.02	0.02	0.01	0.03	-	-	-	--
P20	66.3	27.8	1.57	0.27	3.39	0.13	0.19	n.d.	0.07	0.15	0.07	0.01	0.03	n.d.
St.Dev.	0.9	0.7	0.02	0.04	0.07	0.08	0.08	-	0.03	0.04	0.01	-	0.01	-
P21	78.8	20.3	0.18	0.42	n.d.	0.11	0.13	n.d.	0.04	0.09	n.d.	n.d.	n.d.	n.d.
St.Dev.	0.8	0.7	0.01	0.01	-	0.03	0.02	-	0.01	0.00	-	-	-	-
P22	67.1	31.3	0.47	0.54	n.d.	0.18	0.18	n.d.	0.06	0.08	0.02	n.d.	n.d.	n.d.
St.Dev.	0.3	0.2	0.05	0.00	-	0.00	0.02	-	0.00	0.00	0.01	-	-	-
P23	77.0	21.0	0.58	0.31	0.55	0.24	0.18	n.d.	0.05	0.09	0.02	n.d.	n.d.	n.d.
St.Dev.	0.4	0.3	0.01	0.04	0.08	0.03	0.00	-	0.00	0.01	0.00	-	-	-
P24	79.2	17.4	0.41	0.30	2.17	0.15	0.17	n.d.	0.06	0.10	n.d.	n.d.	n.d.	n.d.
St.Dev.	0.0	0.2	0.01	0.03	0.21	0.03	0.01	-	0.00	0.01	0.01	-	-	-
P25	79.9	17.2	0.19	1.49	n.d.	0.73	0.28	0.03	0.07	0.08	n.d.	n.d.	n.d.	n.d.
St.Dev.	2.4	2.1	0.12	0.12	-	0.02	0.00	0.00	0.00	0.02	-	-	-	-
P26	67.6	28.7	1.84	0.45	0.74	0.30	0.19	n.d.	0.07	0.09	0.09	n.d.	n.d.	n.d.
St.Dev.	0.6	0.5	0.01	0.02	0.08	0.01	0.00	-	0.00	0.01	0.01	-	-	-
Mean	80.7	16.8	0.60	0.51	1.32	0.25	0.15	0.07	0.05	0.09	0.04	0.01	0.22	0.33
Median	81.0	16.2	0.43	0.31	0.80	0.18	0.16	0.05	0.05	0.09	0.04	0.01	0.22	0.33
Max.	98.6	31.3	1.86	1.77	4.02	0.85	0.28	0.21	0.08	0.16	0.11	0.01	0.40	0.60
Min.	66.3	0.4	0.05	0.03	0.16	0.09	0.07	0.01	0.02	0.02	0.01	0.01	0.03	0.05

Table 3.3. Concentration of the mean values of the elements detected on the *metallurgical wastes* with the *p-XRF* method normalized, expressed in % wt
(St. Dev.: standard deviation, n.d.: not detected)

Sample	Cu	Sn	Fe	As	Pb	Sb	Bi	Ag	Zr	Zn	Mn	Co	Ni
WS1	75.1	21.7	1.58	0.37	0.83	0.13	0.10	0.00	0.04	0.09	0.09	n.d.	n.d.
St.Dev.	8.9	9.6	0.64	0.17	0.14	0.01	0.04	0.00	0.01	0.01	0.05	-	-
WS2	78.6	19.3	0.35	0.10	1.36	0.08	0.08	0.00	0.02	0.06	0.01	n.d.	n.d.
St.Dev.	1.0	0.4	0.02	0.03	0.50	0.02	0.01	0.00	0.00	0.01	0.01	-	-
WS3	79.6	18.6	0.88	0.21	0.34	0.10	0.07	n.d.	0.03	0.11	0.05	n.d.	n.d.
WS4	88.5	10.2	0.78	0.22	n.d.	0.10	0.05	0.03	0.01	0.06	0.04	n.d.	n.d.
WS5	69.0	26.6	0.52	1.25	2.13	0.25	0.16	n.d.	0.05	0.09	0.01	n.d.	n.d.
WS6	87.5	11.5	0.25	0.44	n.d.	0.12	0.08	0.04	0.01	0.06	n.d.	n.d.	n.d.
WS7	75.4	22.6	0.63	0.72	n.d.	0.35	0.14	n.d.	0.05	0.07	0.04	n.d.	n.d.
WS8	90.0	8.7	0.92	0.15	n.d.	0.07	0.03	0.04	0.01	0.06	0.05	n.d.	n.d.
WS9	85.2	13.4	0.81	0.17	0.04	0.15	0.09	0.02	0.04	0.09	0.04	n.d.	n.d.
WS10	79.3	19.6	0.39	0.41	0.00	0.09	0.07	0.01	0.02	0.11	0.01	n.d.	n.d.
St.Dev.	6.8	6.4	0.11	0.21	0.00	0.03	0.02	0.00	0.01	0.02	0.02	-	-
WS11	84.8	13.3	0.71	0.30	n.d.	0.20	0.12	0.07	0.04	0.41	0.05	n.d.	n.d.
WS12	88.8	9.7	0.61	0.11	0.43	0.09	0.08	0.05	0.03	0.11	0.01	0.005	n.d.
WS13	75.9	22.6	0.26	0.30	0.71	0.07	0.10	n.d.	0.04	0.06	0.01	n.d.	n.d.
WS14	76.4	19.9	2.84	0.30	n.d.	0.14	0.09	n.d.	0.04	0.07	0.16	n.d.	n.d.
WS15	81.0	15.9	0.62	0.39	1.20	0.60	0.09	n.d.	0.03	0.09	0.03	n.d.	0.001
WS16	87.4	11.2	0.52	0.12	0.41	0.08	0.05	0.04	0.01	0.07	0.02	n.d.	n.d.
WS17	75.6	21.3	1.72	0.34	0.54	0.20	0.10	n.d.	0.03	0.09	0.10	n.d.	n.d.
WS18	79.9	18.4	0.71	0.41	0.07	0.23	0.12	n.d.	0.03	0.08	0.02	n.d.	n.d.
WS19	85.1	13.6	0.35	0.49	n.d.	0.23	0.06	0.01	0.01	0.09	0.01	n.d.	n.d.
WS20	51.6	45.8	1.66	0.48	n.d.	0.06	0.17	n.d.	0.07	0.11	0.09	n.d.	n.d.
WS21	n.d.	75.6	15.75	0.33	3.89	4.97	0.38	0.50	0.02	0.00	0.54	n.d.	n.d.
St.Dev.	-	3.0	0.57	0.31	0.00	0.11	0.04	0.04	0.00	0.00	0.12	-	-
Mean	79.7	18.2	0.86	0.36	0.73	0.17	0.09	0.04	0.03	0.10	0.04	0.005	0.001
Median	79.7	18.5	0.67	0.32	0.54	0.12	0.09	0.04	0.03	0.09	0.04	0.005	0.001
Max.	90.0	45.8	2.84	1.25	2.13	0.60	0.17	0.07	0.07	0.41	0.16	0.005	0.001
Min.	51.6	8.7	0.25	0.10	0.04	0.06	0.03	0.01	0.01	0.06	0.001	0.005	0.001

The ALEA-WS21 although presented in the above table, has not been calculated for the average and median values of the assemblage, due to its extreme values obtained.

3.3. Elemental analysis using μ XRF

The mean values along with standard deviation of the measurements on the pins and wastes assemblage obtained by micro XRF, concerning the elements Cu, Sn, Fe, As, Pb, Sb, Bi, Co, Ni, and Cu, Sn, Fe, As, Pb, and Ni respectively, are presented in Tables 3.4. and 3.5. The detection limit at 50s for Co=0.024%, Ni=0.04%, Sb=0.3%, Pb= 0.002% and Bi=0.019% (wt).

Table 3.4. Concentration of the mean values of the elements detected on the bronze *pins* with the μ XRF method normalized, expressed in % wt (St.Dev.: standard deviation, B.D.L.: below detection limit)

Sample	Cu	Sn	Fe	As	Pb	Sb	Bi	Co	Ni
P1	86.2	12.5	0.17	0.13	0.59	0.36	B.D.L.	B.D.L.	0.03
St.Dev.	0.7	0.8	0.01	0.04	0.11	0.03	-	-	0.04
P2	92.1	4.0	0.82	0.65	2.22	0.43	B.D.L.	B.D.L.	0.04
St.Dev.	1.4	0.2	0.20	0.35	0.84	0.21	-	-	0.00
P3	89.6	9.6	0.64	0.12	0.07	B.D.L.	B.D.L.	B.D.L.	0.04
St.Dev.	0.2	0.2	0.01	0.02	0.00	-	-	-	0.00
P4	98.7	0.3	0.22	0.17	0.42	0.41	B.D.L.	B.D.L.	0.13
St.Dev.	0.1	0.2	0.07	0.09	0.01	0.00	-	-	0.06
P5	87.4	11.8	0.38	0.19	0.24	0.40	B.D.L.	B.D.L.	0.04
St.Dev.	0.1	0.1	0.00	0.03	0.04	0.00	-	-	0.01
P6	88.1	11.5	0.24	0.04	0.05	0.40	B.D.L.	B.D.L.	0.05
St.Dev.	0.3	0.2	0.02	0.02	0.00	0.00	-	-	0.01
P7	89.7	9.9	0.09	0.05	0.11	B.D.L.	B.D.L.	B.D.L.	0.07
St.Dev.	0.7	0.8	0.01	0.03	0.08	-	-	-	0.01
P8	82.1	17.1	0.19	0.08	0.53	B.D.L.	B.D.L.	B.D.L.	0.05
St.Dev.	2.9	2.9	0.01	0.03	0.04	-	-	-	0.00
P9	91.4	7.7	0.02	0.07	0.72	B.D.L.	B.D.L.	B.D.L.	0.11
m,St.Dev.	0.1	0.1	0.01	0.05	0.08	-	-	-	0.01
P10	90.4	8.1	1.07	0.10	0.25	B.D.L.	B.D.L.	B.D.L.	0.03
St.Dev.	0.3	0.4	0.08	0.04	0.08	-	-	-	0.01
P11	84.6	13.8	0.29	0.18	1.34	B.D.L.	B.D.L.	B.D.L.	0.07
St.Dev.	0.0	0.0	0.00	0.00	0.00	-	-	-	0.00
P12	86.7	11.4	0.89	0.05	0.95	0.40	B.D.L.	B.D.L.	0.06
St.Dev.	0.3	0.5	0.09	0.04	0.22	0.00	-	-	0.02
P13	90.4	8.8	0.45	0.04	0.22	0.40	B.D.L.	B.D.L.	0.09
St.Dev.	0.0	0.0	0.01	0.00	0.01	0.00	-	-	0.00
P14	92.0	6.8	0.31	0.09	0.07	B.D.L.	B.D.L.	B.D.L.	0.34
St.Dev.	0.2	0.3	0.05	0.01	0.04	-	-	-	0.42
P15	88.0	6.8	0.10	0.12	4.97	B.D.L.	B.D.L.	B.D.L.	0.08
St.Dev.	1.0	1.1	0.13	0.04	1.82	-	-	-	0.01
P16	90.7	8.6	0.05	0.07	0.46	B.D.L.	B.D.L.	B.D.L.	0.08

Sample	Cu	Sn	Fe	As	Pb	Sb	Bi	Co	Ni
St.Dev.	0.8	0.7	0.02	0.01	0.16	-	-	-	0.01
P17	91.1	7.3	0.44	0.29	0.57	0.33	B.D.L.	B.D.L.	0.11
St.Dev.	1.1	0.9	0.08	0.07	0.18	0.01	-	-	0.10
P18	89.1	9.8	0.13	0.78	B.D.L.	0.25	B.D.L.	B.D.L.	0.06
St.Dev.	0.3	0.3	0.01	0.07	-	0.00	-	-	0.01
P19	91.7	7.1	0.13	0.04	0.86	B.D.L.	B.D.L.	B.D.L.	0.09
St.Dev.	2.5	1.9	0.04	0.02	0.54	-	-	-	0.01
P20	87.9	10.1	0.88	0.02	0.94	B.D.L.	B.D.L.	0.06	0.05
St.Dev.	0.9	0.8	0.10	0.00	0.09	-	-	0.01	0.01
P21	86.2	13.1	0.16	0.14	0.33	B.D.L.	B.D.L.	B.D.L.	0.06
St.Dev.	1.3	1.2	0.04	0.03	0.05	-	-	-	0.01
P22	88.1	11.6	0.09	0.12	0.13	B.D.L.	B.D.L.	B.D.L.	0.04
St.Dev.	1.3	1.3	0.03	0.02	0.04	-	-	-	0.01
P23	90.8	8.4	0.35	0.11	0.29	B.D.L.	B.D.L.	B.D.L.	0.07
St.Dev.	0.0	0.0	0.00	0.00	0.00	-	-	-	0.00
P24	92.1	6.9	0.26	0.03	0.64	B.D.L.	B.D.L.	B.D.L.	0.08
St.Dev.	0.0	0.0	0.00	0.00	0.00	-	-	-	0.00
P25	92.4	6.7	0.07	0.37	0.43	0.34	B.D.L.	B.D.L.	0.05
St.Dev.	0.3	0.2	0.03	0.03	0.01	0.01	-	-	0.01
P26	87.8	10.6	1.03	0.08	0.43	B.D.L.	B.D.L.	B.D.L.	0.05
St.Dev.	0.7	0.6	0.06	0.01	0.03	-	-	-	0.00
Mean	89.4	9.2	0.36	0.16	0.69	0.37	-	0.06	0.08
Median	89.6	9.2	0.25	0.11	0.43	0.4	-	0.06	0.06
Max.	98.7	17.1	1.07	0.78	4.94	0.43	-	0.06	0.34
Min.	82.1	0.3	0.02	0.02	0.05	0.25	-	0.06	0.03

Table 3.5. Concentration of the mean values of the elements detected on the *metallurgical wastes* with the μ XRF method normalized, expressed in % wt (St.Dev.: standard deviation, B.D.L.: below detection limit)

Sample	Cu	Sn	Pb	As	Fe	Ni
WS2	80.0	19.2	0.61	0.03	0.17	0.04
St.Dev.	9.3	9.1	0.18	0.01	0.01	0.01
WS3	89.2	10.3	0.17	0.03	0.27	0.04
St.Dev.	4.0	3.9	0.04	0.01	0.03	0.01
WS8	91.2	8.1	0.05	0.20	0.36	0.04
St.Dev.	0.8	0.6	0.01	0.06	0.20	0.01
WS10	89.4	10.0	0.23	0.09	0.23	0.06
St.Dev.	0.0	0.1	0.05	0.01	0.01	0.03
WS11	81.0	17.4	0.28	0.43	0.85	0.05
St.Dev.	7.9	6.4	0.39	0.33	0.88	0.02
WS21	83.2	14.8	0.66	0.23	1.10	0.03
St.Dev.	18.2	16.0	0.69	0.28	1.23	0.01
Mean	85.6	13.3	0.33	0.17	0.50	0.04
Median	86.2	12.5	0.26	0.15	0.32	0.04
Max.	91.2	19.2	0.66	0.43	1.10	0.06
Min.	80.0	8.1	0.05	0.03	0.17	0.03

3.4. Elemental analysis using SEM-EDS

The mean values along with standard deviation of the measurements on the pins and wastes assemblage obtained by SEM-EDS, concerning the elements Cu, Sn, Fe, As, Pb, Co, Ni, Al, Cl, S, Ca, Cr, P and Cu, Sn, Fe, As, Pb, Cl, Si and P respectively, are presented in Tables 3.6. and 3.7.

Table 3.6. Concentration of the mean values of the elements detected on the bronze pins with the SEM-EDS method normalized, expressed in % wt (St. Dev.: standard deviation, n.d.: not detected)

Sample	Cu	Sn	Fe	As	Pb	Co	Ni	Al	Cl	S	Ca	Cr	P
P2	93.7	3.6	0.70	0.52	1.21	n.d.	n.d.	n.d.	0.33	n.d.	n.d.	n.d.	n.d.
St.Dev.	1.5	0.8	0.06	0.27	0.45	-	-	-	0.16	-	-	-	-
P3	88.5	10.3	0.92	n.d.	n.d.	n.d.	n.d.	n.d.	0.39	n.d.	n.d.	n.d.	0.30
St.Dev.	1.9	1.5	0.15	-	-	-	-	-	0.31	-	-	-	0.22
P4	94.9	2.1	1.33	0.37	0.52	n.d.	n.d.	5.33	0.28	n.d.	0.86	1.56	0.87
St.Dev.	6.8	0.0	1.00	0.09	0.41	-	-	7.26	0.01	-	0.00	0.00	1.15
P13	91.0	8.4	0.41	n.d.	0.20	n.d.	n.d.	n.d.	n.d.	n.d.	n.d.	n.d.	n.d.
St.Dev.	0.8	0.6	0.04	-	0.12	-	-	-	-	-	-	-	-
P14	90.3	7.8	0.33	n.d.	n.d.	0.43	0.65	0.14	0.34	n.d.	n.d.	n.d.	n.d.
St.Dev.	1.1	0.8	0.14	-	0.77	0.04	0.19	0.03	0.00	-	-	-	-
P15	87.8	7.2	0.08	0.12	3.33	n.d.	n.d.	0.11	1.60	n.d.	n.d.	n.d.	n.d.
St.Dev.	1.1	0.1	0.10	0.01	1.32	-	-	0.04	0.36	-	-	-	-
P16	90.6	7.5	n.d.	n.d.	0.41	n.d.	n.d.	0.88	0.64	n.d.	n.d.	n.d.	n.d.
St.Dev.	0.7	1.4	-	-	0.03	-	-	0.94	0.21	-	-	-	-
P20	88.1	10.0	0.89	n.d.	0.94	n.d.	n.d.	n.d.	n.d.	0.40	n.d.	n.d.	n.d.
St.Dev.	1.7	1.4	0.10	-	0.14	-	-	-	-	0.00	-	-	-
P22	89.2	9.2	1.18	n.d.	n.d.	n.d.	n.d.	n.d.	0.54	n.d.	n.d.	n.d.	n.d.
St.Dev.	2.9	2.4	0.25	-	-	-	-	-	0.21	-	-	-	-
P25	91.4	7.8	n.d.	0.57	0.31	n.d.	n.d.	n.d.	n.d.	n.d.	n.d.	n.d.	n.d.
St.Dev.	0.4	0.4	-	0.14	0.10	-	-	-	-	-	-	-	-
Mean	90.5	7.4	0.73	0.40	0.99	0.43	0.65	1.62	0.59	0.40	0.86	1.56	0.59
Median	90.4	7.8	0.80	0.45	0.52	0.43	0.65	0.51	0.39	0.40	0.86	1.56	0.59
Max.	94.9	10.3	1.33	0.57	3.33	0.43	0.65	5.33	1.60	0.40	0.86	1.56	0.87
Min.	87.8	2.1	0.08	0.12	0.20	0.43	0.65	0.11	0.28	0.40	0.86	1.56	0.30

Table 3.7. Concentration of the mean values of the elements detected on the *metallurgical wastes* with the *SEM-EDS* method normalized, expressed in % wt (St.Dev.: standard deviation)

Sample	Cu	Sn	Fe	As	Pb	Cl	Si	P
WS2	83.4	14.2	0.41	0.25	0.53	0.51	0.47	0.41
St.Dev.	2.1	2.0	0.06	0.00	0.05	0.22	0.09	0.20
WS3	83.9	13.2	0.70	0.46	0.30	0.42	0.65	0.59
St.Dev.	1.9	1.2	0.03	0.22	0.20	0.14	0.16	0.17
WS8	89.8	7.6	1.19	0.53	0.12	0.36	0.32	0.22
St.Dev.	2.9	1.9	0.27	0.30	0.12	0.04	0.15	0.14
WS10	83.9	13.9	1.36	0.39	0.59	0.48	0.16	0.39
St.Dev.	2.1	1.7	0.44	0.05	0.00	0.12	0.06	0.22
WS11	83.7	12.3	1.09	0.80	0.57	0.41	1.65	0.41
St.Dev.	1.8	1.6	0.09	0.00	0.00	0.07	0.49	0.14
WS20	70.1	22.2	3.65	0.62	0.43	1.27	0.43	1.97
St.Dev.	1.6	2.0	0.16	0.00	0.00	0.06	0.10	0.15
Mean	82.5	13.9	1.40	0.51	0.42	0.58	0.61	0.67
Median	83.8	13.6	1.14	0.50	0.48	0.45	0.45	0.41
Max.	89.8	22.2	3.65	0.80	0.59	1.27	1.65	1.97
Min.	70.1	7.6	0.41	0.25	0.12	0.36	0.16	0.22

3.5. Methodology-comparison of the techniques

As previously mentioned, three different protocols of elemental analysis were applied on the assemblage; the portable and micro XRF and the SEM-EDS. The p-XRF technique was initially employed because of the fast qualitative and quantitative results that can provide. The SEM-EDS method was employed in order to analyse possibly contained elements lighter or in lower concentrations than those obtained with the p-XRF and check the accuracy of the technique. As discussed above (see Materials and Methods) an aluminium-titanium filter was used in the XRF analysis, which excluded the lighter elements from the measurements. Light elements like aluminium, silicon, sulfur, chlorine and calcium, which may be present in the objects, either naturally or in the form of corrosion products, cannot be detected. Thus the overestimation of particular elements with the XRF may be controverted. The same problem may arise from the fact that the X-rays can penetrate to a greater depth than the electron beam, although the exact penetration depth for each method depends on

the nature of the material to be analysed. Such is the case for copper alloys objects where almost the entirety of the analytical information for copper and lead and almost half of the Sn information comes from the first 20 μm ; for elements with atomic number ca 50 (e.g. Sn, Sb) the respective $K\alpha$ analytical signal may originate from depths up to about 80 μm (Degrigny et al, 2007; Ferretti, 2014). Considering that the corrosion products covering metal artifacts may easily reach several tens of μm in thickness and the substrate of metal artifacts is corroded to variable depths, it is easy to understand how strongly these products limit the accuracy of the measurements when metal alloys composition is of interest; the removal of corrosion layers does not guarantee the removal of all corrosion products until sound metal is revealed, since intergranular corrosion phenomena are quite common (Orfanou et al, 2014). Although, the measurements were taken from areas stripped of their corrosion products using established conservation methods to reveal a visually metallic surface, it is possible that this removal was deficient. The removal of the corrosion products from the samples, due to the fact that permission for only surface analyses was obtained, the fact that they had insufficient surfaces available for analysis (the p-XRF beam was approximately 3x3mm, much greater than the available surfaces under examination); along with the geometry of these surfaces which were curved and irregular, were probably some of the causes for making the p-XRF unsuitable for this analysis under the circumstances. To overcome the problem p-XRF was only used as an initial guide to the possible composition of the alloys, although they likely included some corrosion products.

SEM-EDS analyses were performed on a smaller, focused area of the pin's surface and were more affected by local variations in the concentration of the various elements; thus, the results may differ from the bulk composition of the metal. Accordingly, the XRF technique, although is usually performed on larger areas of the surface may also not be necessarily representative of the whole, since even if there is a thin layer of patina, this is enough to alter the obtained results. A significant problem on the SEM-EDS measurement accuracy may also arise, due to the carbon concentrations subtracted from the compositional values when quantification. These values sometimes may be quite high most likely due to the formed carbonate corrosion products, but also due to possible organic contamination of the samples from handling, or even with from the carbon adhesive tape on which the specimens were stuck, when under SEM-EDS analysis. Carbon or chlorine or other element

subtraction is not a way to by pass corrosion, since corrosion processes, change the metal composition. So even if carbon is subtracted there is a great chance that copper and tin will still be under or overestimated.

A distinction of the ten most characteristic in terms of the high proportion of the various elements was made, in order to be analysed with the SEM-EDS method. These pins were: ALEA-P2, ALEA-P3, ALEA-P4, ALEA-P13, ALEA-P14, ALEA-P15, ALEA-P16, ALEA-P20, ALEA-P22 and ALEA-P25. The adoption of similar reasoning followed the selection of five wastes for SEM-EDS and μ XRF analysis. The number of samples being examined in the SEM-EDS was sufficient for the evaluation of the p-XRF technique. As can be seen in the tables of the chapters 3.2., 3.3. and on the bar chart (fig-3.5.1-) there is a major divergence in the resulted values among the techniques.

The μ XRF technique was later employed for the final analysis of the objects, as it has been confirmed by the literature as a technique more suited for this type of small and rugged surfaces. In the scatter plot (fig-3.5.2-) μ XRF along with SEM-EDS are the techniques that are closer to an ideal correlation, if one considers a perfect correlation the line for the two axes y and x. Considering the limitations on SEM-EDS mentioned above, the discussion considering the pins composition is mainly based on the measurements obtained through μ XRF. The results from the p-XRF and SEM-EDS have been thoroughly considered, though, in order to confirm or reject measurements on elements of interest.

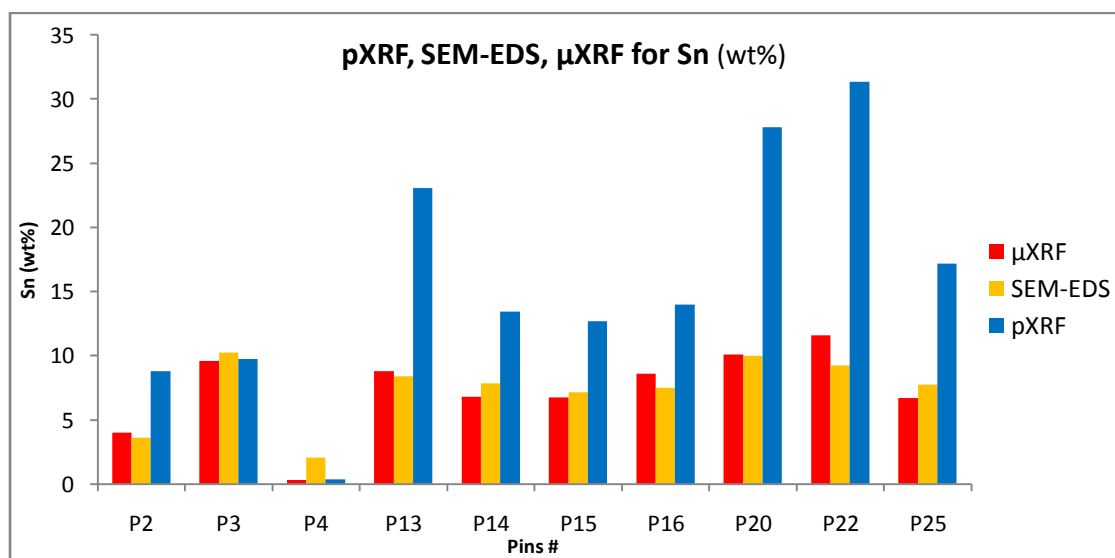


Figure 3.5.1. Bar chart of the p-XRF, μ XRF and SEM-EDS analyses of the tin content on selected pins; higher tin values are visible during p-XRF analyses

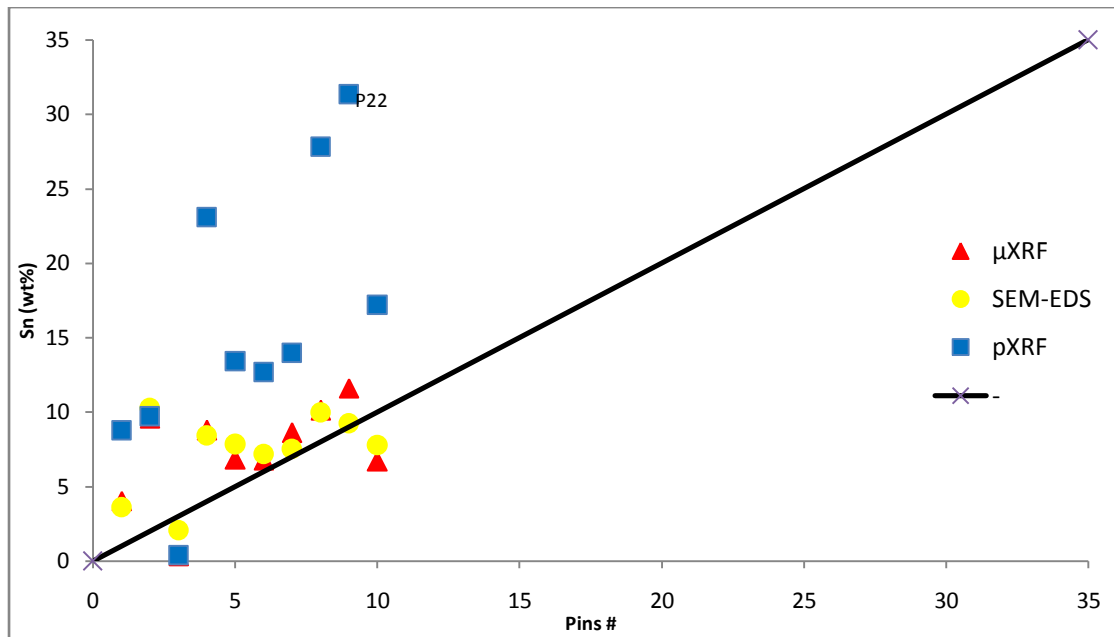


Figure 3.5.2. Scatter plot of the p-XRF, μ XRF and SEM-EDS analyses of the tin content; the black line indicates the ideal correlation for the two axes y and x, so perfect correlation would fall along the line provided. Higher deviation on the values is visible, regarding the p-XRF analysis.

On the following chart visualizing the range of Cu versus Sn concentration in selected pins, the results obtained from p-XRF, μ XRF and SEM-EDS methodologies are presented (Fig-3.5.3-).

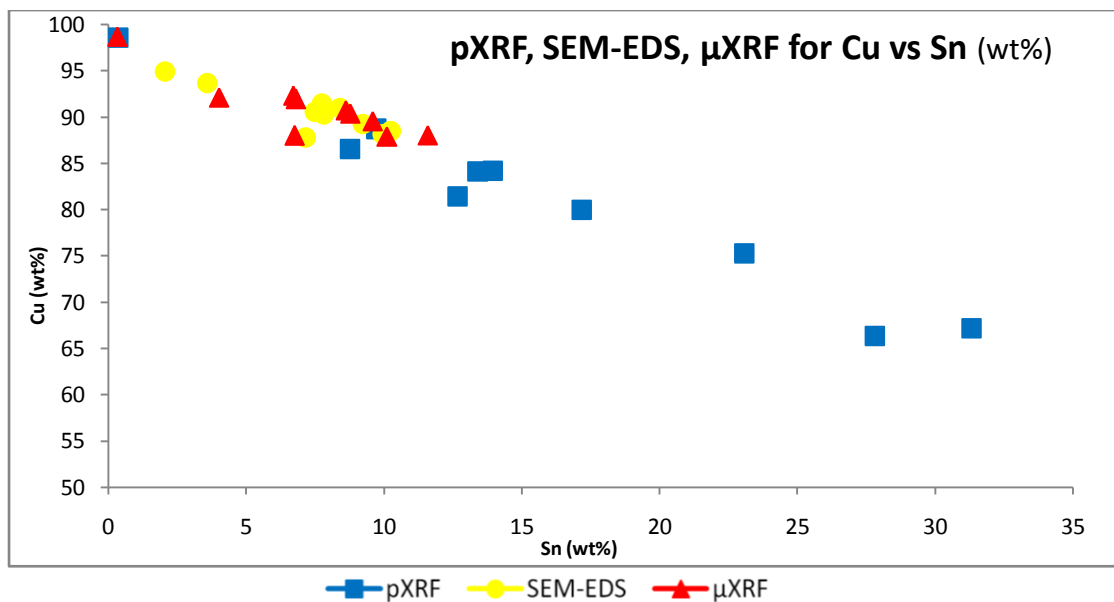


Figure 3.5.3. Scatter plot of copper versus tin in selected pins, based on p-XRF, μ XRF and SEM-EDS analytical protocols; higher tin values are visible during the p-XRF analyses

As can be seen on the charts, there are serious discrepancies of copper versus tin values, among the three sets of analysis. For selected pins, the p-XRF technique has obtained a range of values for the Cu-Sn alloy far from the ones ascertained through the μ XRF and SEM-EDS techniques; thus an overestimation of their tin and an expected underestimation of their copper content.

The relative difference (δ) between the two techniques was calculated, in order to evaluate their variances, by using the formula $\delta=(\mu\text{XRF}- \text{SEM-EDS})/\text{SEM-EDS}$; where for “ μ XRF” and “SEM-EDS” are the accordingly measured values of each element. As can be seen in table 3.8. these relative differences may be either positive, in which case the μ XRF value was greater than the SEM-EDS value, or negative, when the opposite happens. For copper, agreement between the two techniques tends to be very good, since all measurements are close to zero. On the minor elements, though, the values tend to be in higher percentages indicating a variance in the measurements. For example, in tin the values range between -84% to 25%. This indicates that a minus 84% of the μ XRF value was 26% of the SEM-EDS value, thus underestimated. Accordingly a 25% μ XRF value is 75% of the SEM-EDS value which is, in this case, overestimated. The biggest variances considering the pins, are observed on ALEA-P4 which seems to be constantly underestimated under the μ XRF, for all elements except copper; while for ALEA-P2 the exact opposite happens. Its values seem to be overestimated up to 83% for lead and only underestimated on copper. Among elements the biggest variances are observed on lead and iron.

Table 3.8. δ relative difference values (%) of the pin's measurements for μ XRF and SEM-EDS

Sample	Cu	Sn	Pb	As	Fe	Co	Ni
P2	-2	12	83	25	17	-	-
P3	1	-6	-	-	-30	-	-
P4	4	-84	-19	-54	-83	-	-
P13	-1	5	10	-	9	-	-
P14	2	-13	-	-	-5		-47
P15	0	-6	49	0	24	-	-
P16	0	15	12	-	-	-	-
P20	0	1	0	-	-1	-	-
P22	-1	25	-	-	-92	-	-
P25	1	-14	39	-35	-	-	-

The standard deviation of the measurements obtained from the p-XRF had a mean value of 1.1% for the major elements' values, while for the minor elements the mean value of the standard deviation was 0.05%. Its maximum value on copper was 3.7% and on tin 3.6%. The mean value of the standard deviation of the SEM-EDS technique was 2% and 1% for the copper and tin measurements, where in cases were as high as 6.8% and 2.4% respectively. Considering the μ XRF the mean value of the standard deviation for the major elements was 0.7%, although the maximum ascertained values for copper and tin were 2.9%. In the XRF techniques the Pb, in contrast to the rest of the minor elements (with values under 0.5%), showed elevated values of standard deviation on almost every set of measurements (table-3.9-). Not a surprising ascertainment since it is known that lead aggregates and does not mix with the metallic matrix. Its maximum value was 2.71%. On the SEM-EDS measurements though, the biggest deviation was traced on aluminium which had a maximum value of 7.26%, while the lead had a maximum value of 1.32%. Being cognizant that the standard deviation for the major elements of an alloy is acceptable in values close to unit, while for the minor and trace elements the value can be as high as ten, it was apparent that the μ XRF instrument's reproducibility was accurately and thus the most suitable method, for the elemental analysis of this pins assemblage (Lankton et al, 2016).

Table 3.9. *Standard deviation values (%) on the pin's measurements for the three protocols of elemental analysis*

Method/Element	Cu	Sn	Fe	As	Pb	Sb	Co	Ni
p-XRF	1.1	1.0	0.1	0.1	0.2	0.0	0.0	0.0
μ XRF	0.7	0.6	0.0	0.0	0.2	0.0	0.0	0.0
SEM-EDS	2.0	1.0	0.2	0.1	0.5	-	0.1	0.0

The suitability of μ XRF was confirmed after the precision of the methods was also tested. In order to check it and thus tell how close are the results of a series of measurements, regardless of how different they might be from the accepted value, a calculation of the standard deviation divided by the mean compositional value of the samples, presented as a percentage, was used. On table 3.10. are presented the precision difference values for the pins. It is apparent that the values of both the XRF techniques are smaller than the ones obtained through SEM-EDS. In order to consider

a series of measurements as precise, these values should be close to the unit; although in certain methods, values up to 20% are acceptable (Lankton et al, 2016).

Table 3.10. Precision difference values (%) on the pin's measurements for the three protocols of elemental analysis

Method/Element	Cu	Sn	Pb	As	Fe	Sb	Co	Ni
p-XRF	0.01	0.06	0.11	0.11	0.09	0.17	0.00	0.00
μXRF	0.01	0.07	0.27	0.26	0.12	0.07	0.49	0.13
SEM-EDS	0.02	0.13	0.42	0.32	0.32	-	0.08	0.29

Moreover the μXRF can focus on smaller areas and obtain measurements of visually conspicuous corrosion free areas. Since the XRF techniques were both performed under a filtering mode, the SEM-EDS measurements of the light elements were also taken into account; their detection can be a valuable aid in the determination of the accuracy of all measurements, since they are commonly involved in various metal corrosion processes.

3.6. Results of the chemical analysis

The analytical methods confirmed that the assemblage composition was quite homogenous, made of a binary alloy of copper and tin with lead, iron and arsenic being the major metallic impurities. It should be kept in mind, though, that since the surface of the corroded metals exhibits different percentages of the main components of the alloy than they actually are in the compact metal core due to the complex electrochemical processes of corrosion, surface analytical methods usually yield mainly qualitative and secondly quantitative data.

The pins have a mean value of 89.4% regarding their copper content (fig-3.6.1-), a median value of 89.6%, while their maximum and minimum values are 98.7% and 82.1% respectively. The waste assemblage (fig-3.6.3-) has a mean value for copper of 85.6% and a median value of 86.2%. Its maximum value is 91.2% and its minimum 80.0%. The pins and metallurgical wastes distribution, regarding their copper content, are presented on histograms 3.6.2. and 3.6.4, respectively.

The mean value for the tin concentration on the pins assemblage is 9.2% (wt%) while its values vary between 0.3% and 17.1% (fig-3.6.5-). The median value observed, is at 9.2%. The mean value for the concentration of tin on the waste assemblage is 13.3% (wt%) while its range varies between 8.1 and 19.2%. Its median value is estimated at 12.5% (fig-3.6.7-). The pins and metallurgical wastes distribution, regarding their tin content, are presented on histograms 3.6.6. and 3.6.8, respectively.

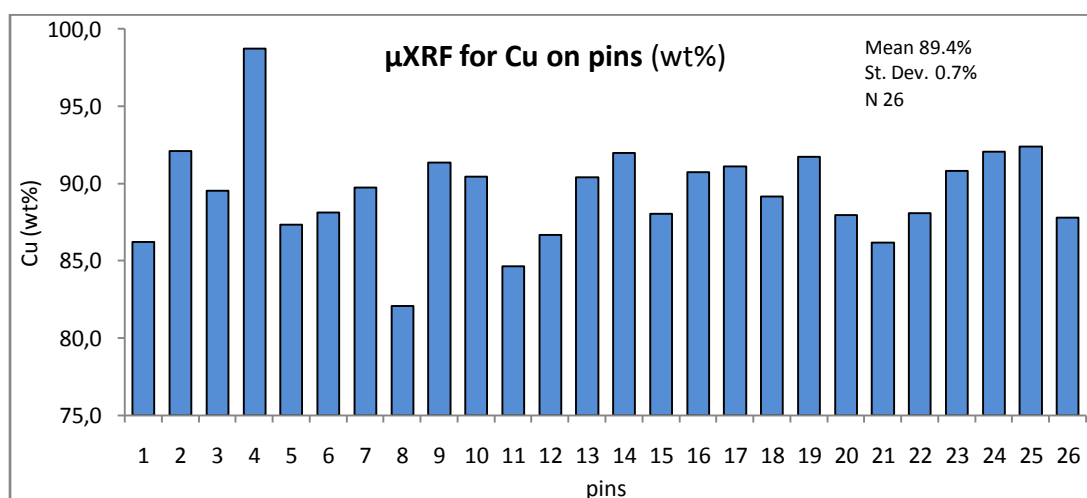


Figure 3.6.1. Bar chart of the copper content of the pins, based on μ XRF methodology

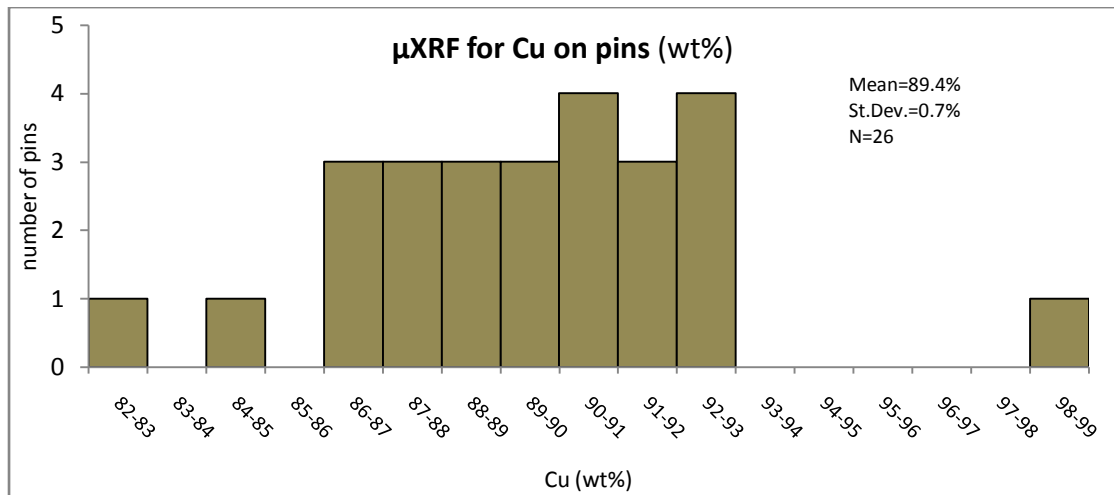


Figure 3.6.2. Histogram of the distribution of the pins, regarding their copper content, based on μ XRF methodology

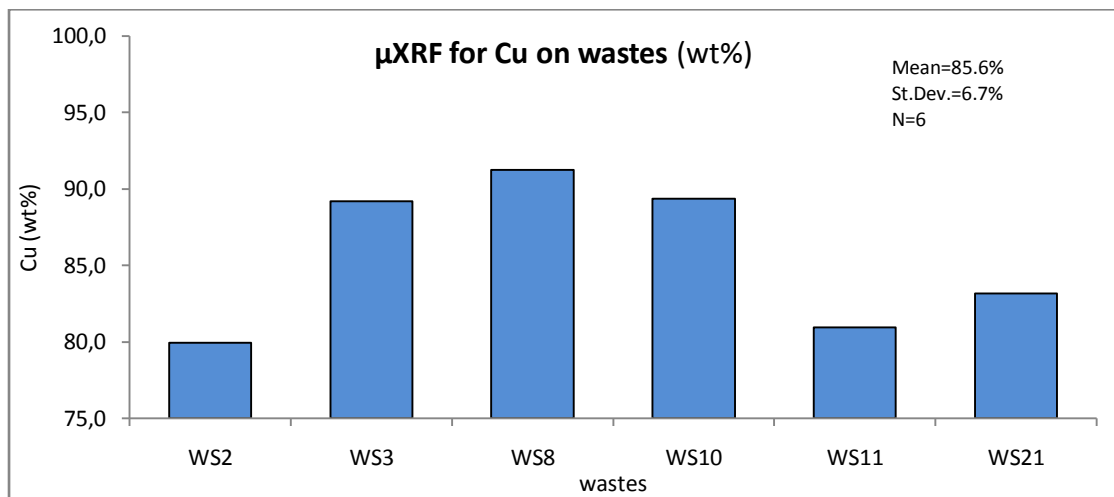


Figure 3.6.3. Bar chart of the copper content on the metallurgical wastes, based on μ XRF methodology

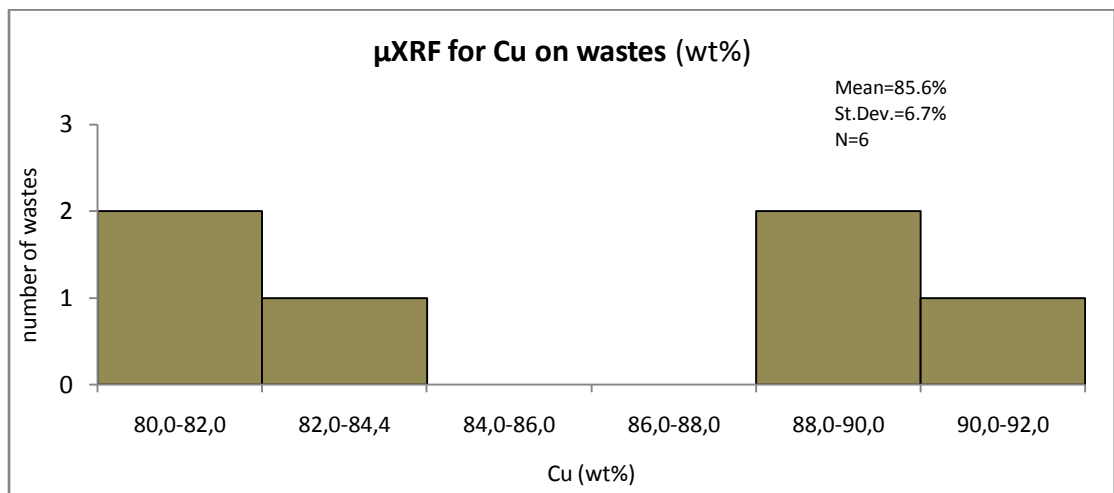


Figure 3.6.4. Histogram of the distribution of the metallurgical wastes, regarding their copper content, based on μ XRF methodology

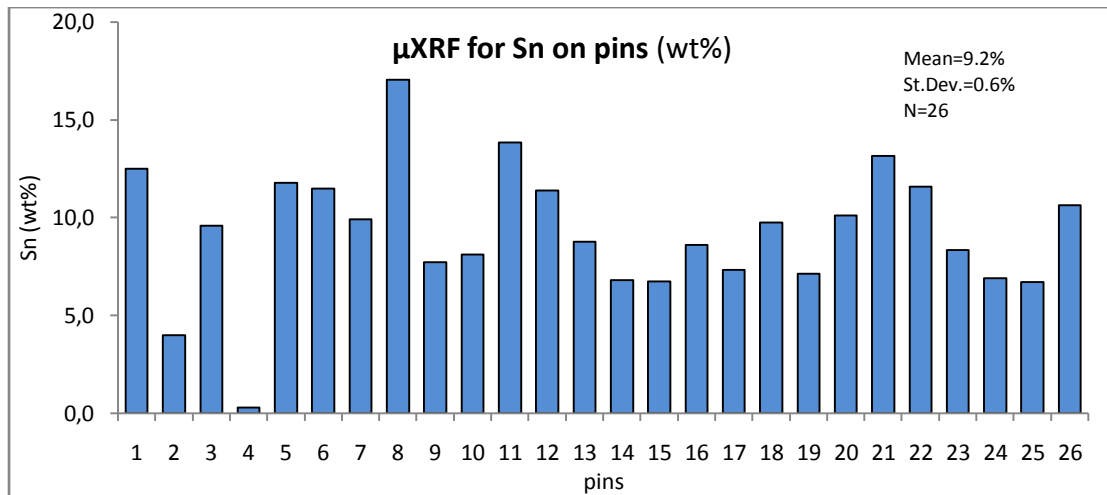


Figure 3.6.5. Bar chart of the tin content of the pins, based on μXRF methodology

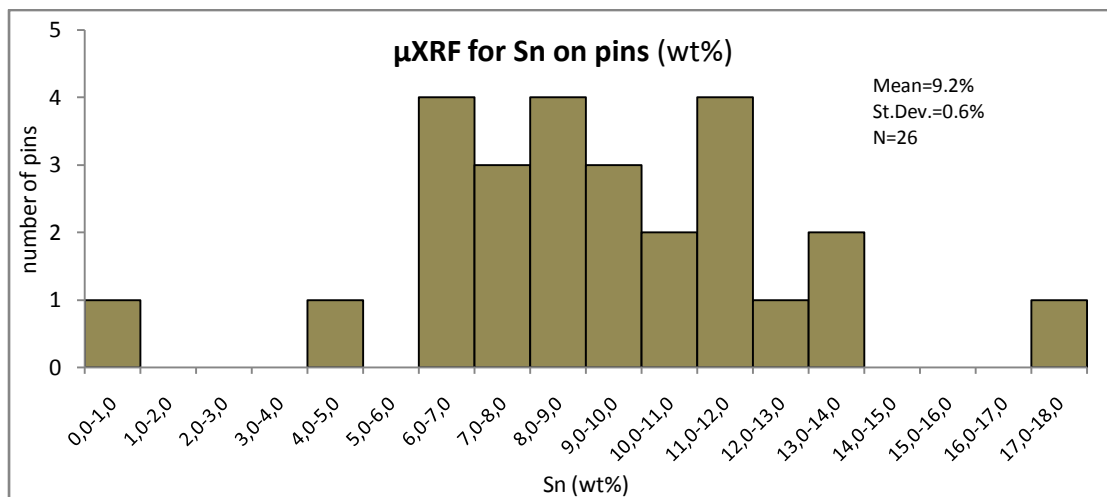


Figure 3.6.6. Histogram of the distribution of the pins, regarding their tin content, based on μXRF methodology

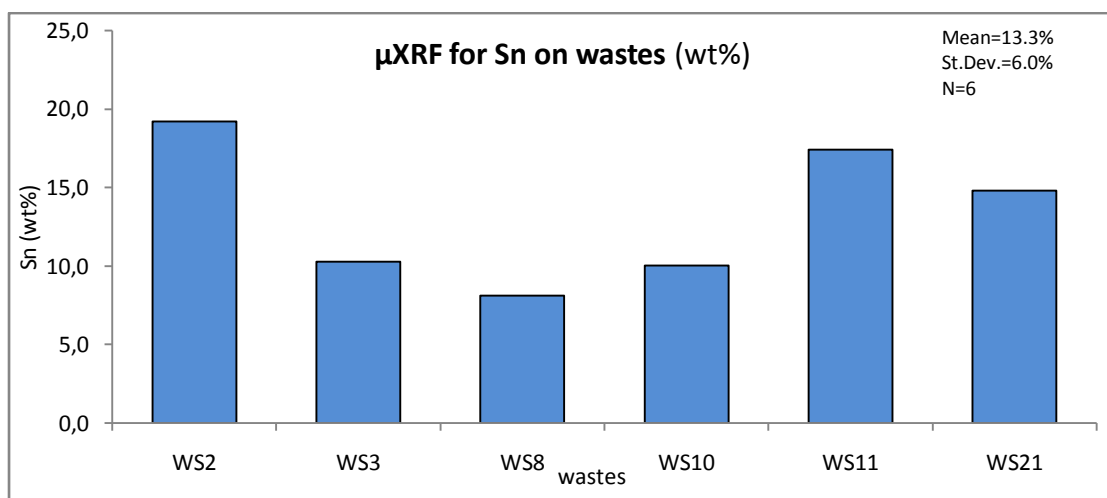


Figure 3.6.7. Bar chart of the tin content on the metallurgical wastes, based on μXRF methodology

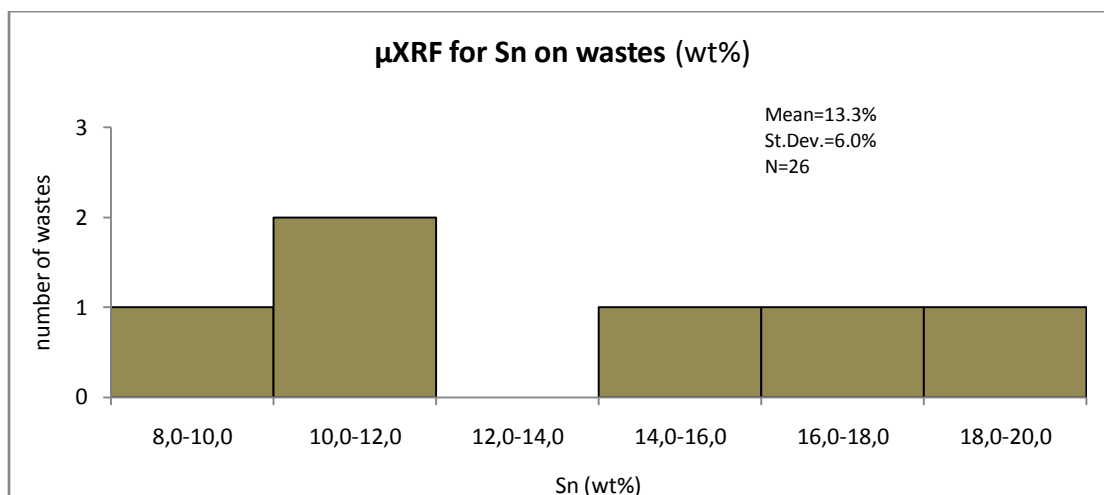


Figure 3.6.8. Histogram of the distribution of the metallurgical wastes, regarding their tin content, based on μ XRF methodology

The presence of arsenic in the bronze pins of this study is very limited in relation to tin. Arsenic can be traced on all pins, having a mean value of 0.16%, while its maximum values at ALEA-P18 and ALEA-P2 pins reach to 0.78% and 0.65% respectively (fig-3.6.9-). The traces of arsenic from the selected metallurgical wastes of the assemblage are found to have a mean value of 0.17%; a minimum value of 0.03% and a maximum of 0.43%. That mean value is in accordance with the mean value obtained from the pins, although in wastes extreme values can be observed between the minimal and maximum values of the set (fig-3.6.11-). The pins and metallurgical wastes distribution, regarding their arsenic content, are presented on histograms 3.6.10. and 3.6.12, respectively.

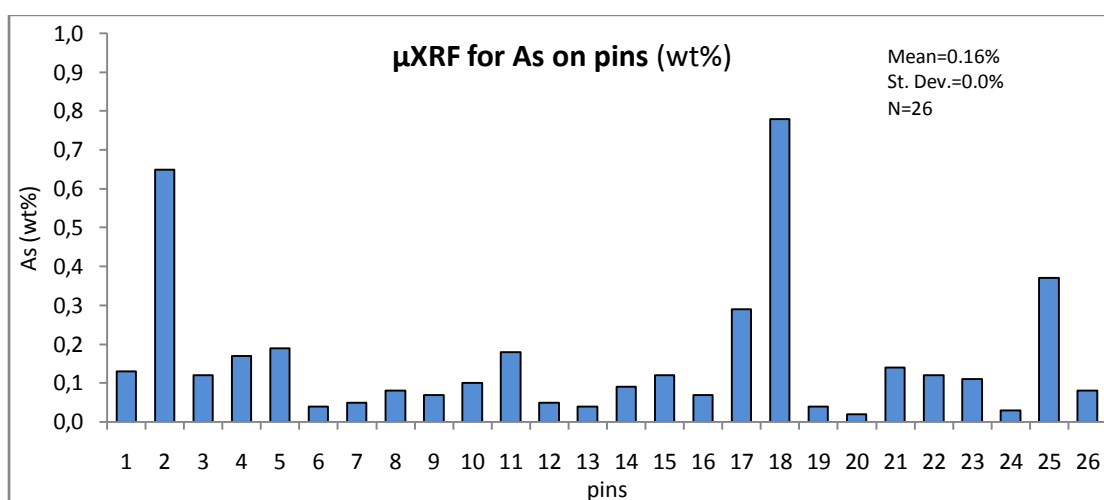


Figure 3.6.9. Bar chart of the arsenic content of the pins, based on μ XRF methodology

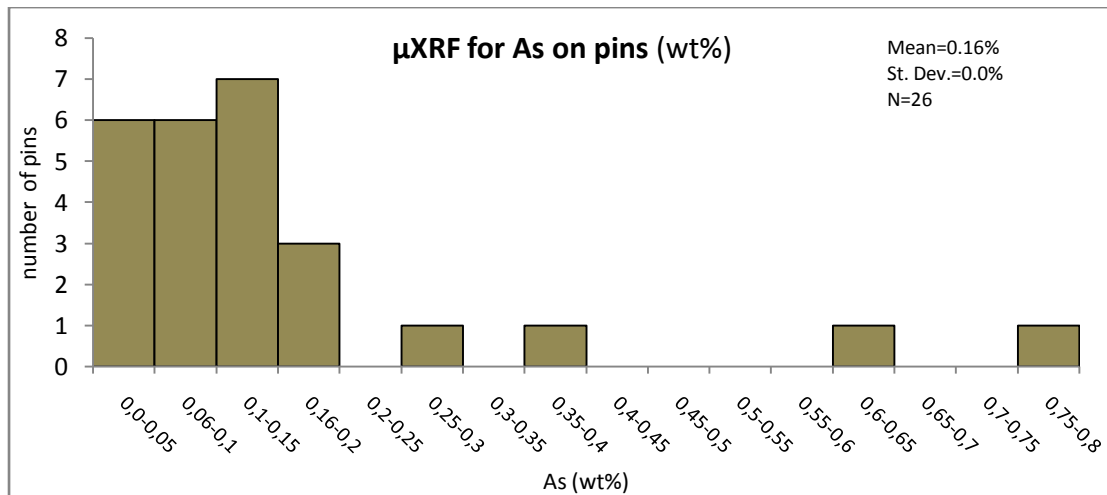


Figure 3.6.10. Histogram of the distribution of the pins, regarding their arsenic content, based on μ XRF methodology

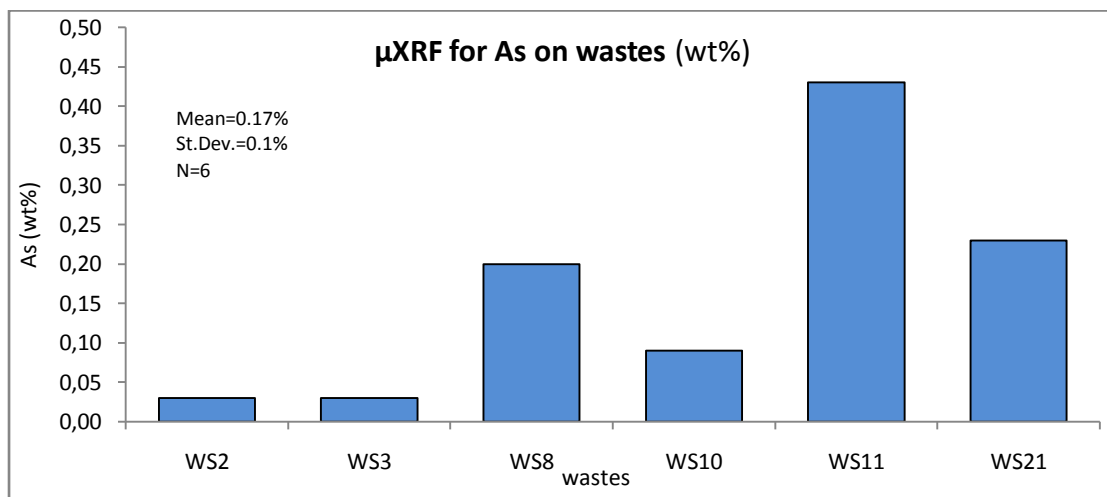


Figure 3.6.11. Bar chart of the arsenic content on the metallurgical wastes, based on μ XRF methodology

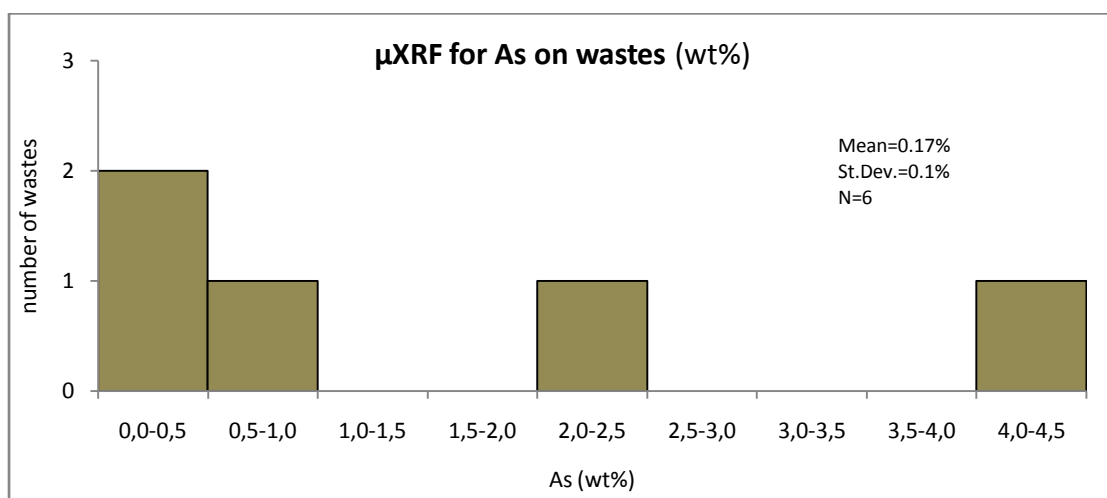


Figure 3.6.12. Histogram of the distribution of the metallurgical wastes, regarding their arsenic content, based on μ XRF methodology

The pins have a mean value of 0.69% regarding their lead content (fig-3.6.13-) a median value of 0.43%, while their maximum and minimum values are 4.97% and 0.05% respectively. Notable exceptions are the pins ALEA-P11 with 1.34%, ALEA-P2 with 2.22% and ALEA-P15 with 4.97%. The wastes assemblage has a mean value of 0.33% (fig-3.6.15-), a median value of 0.26%; their extreme values being at 0.66 and 0.05%. The pins and metallurgical wastes distribution, regarding their lead content, are presented on histograms 3.6.14. and 3.6.16, respectively.

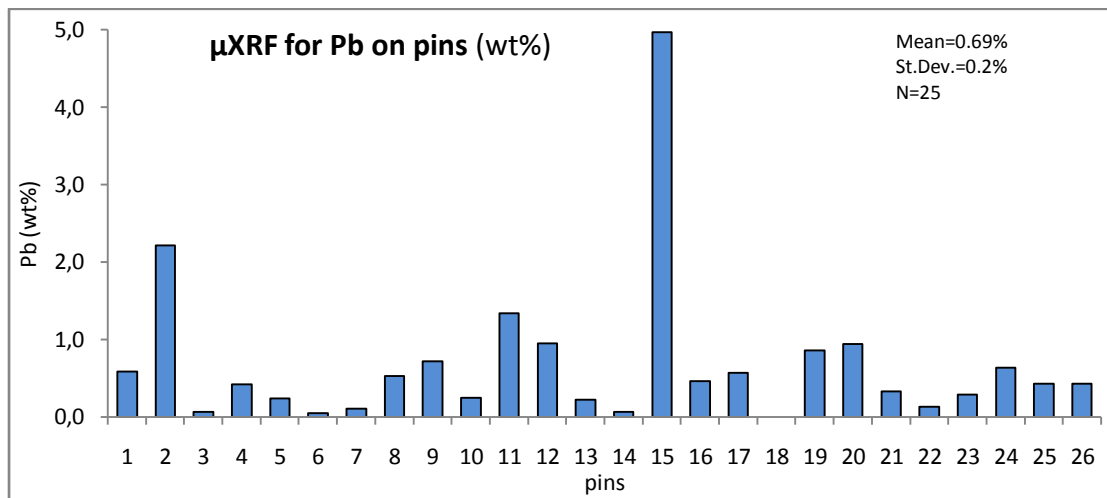


Figure 3.6.13. Bar chart of the lead content of the pins, based on μ XRF methodology

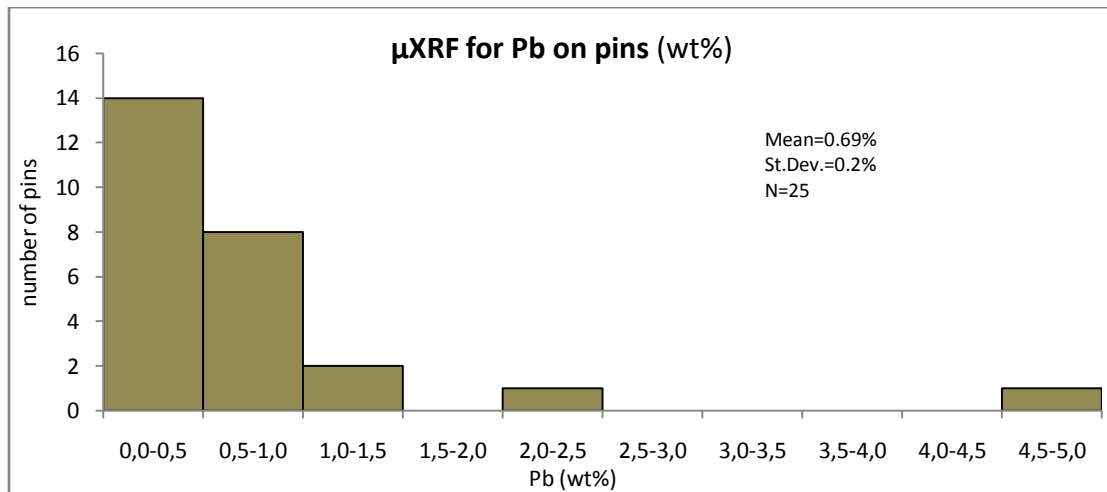


Figure 3.6.14. Histogram of the distribution of the pins, regarding their lead content, based on μ XRF methodology

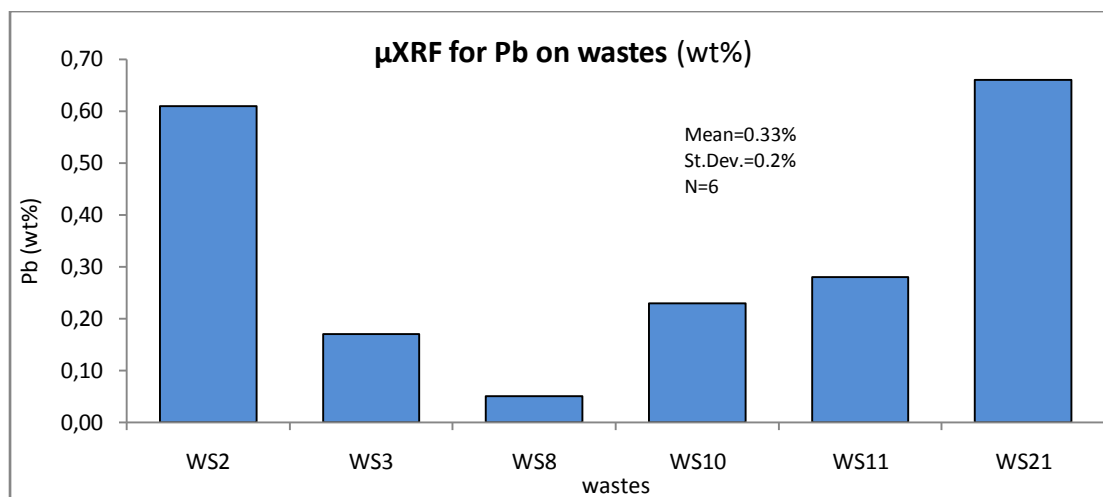


Figure 3.6.15. Bar chart of the lead content on the metallurgical wastes, based on μ XRF methodology

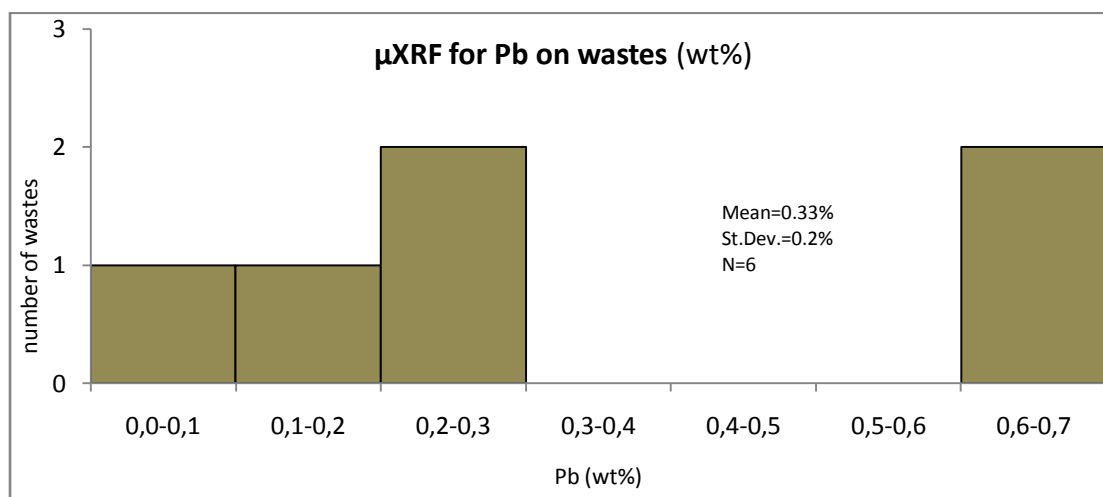


Figure 3.6.16. Histogram of the distribution of the metallurgical wastes, regarding their lead content, based on μ XRF methodology

Iron is estimated as having a mean value of 0.36% in the pins (fig-3.6.17-) and 0.50% in the wastes assemblage (fig-3.6.19-). Their median value is 0.25% and 0.32%, respectively; while their range varies between 0.02 to 1.07% for the pins and 0.17 to 1.10% for the wastes. The pins and metallurgical wastes distribution, regarding their iron content, are presented on histograms 3.6.18. and 3.6.20., respectively.

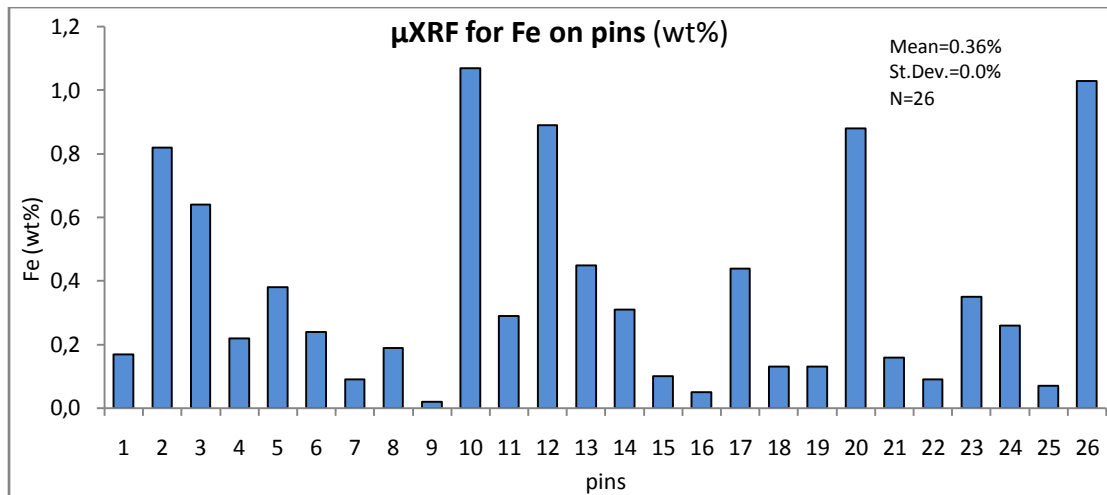


Figure 3.6.17. Bar chart of the iron content of the pins, based on μ XRF methodology

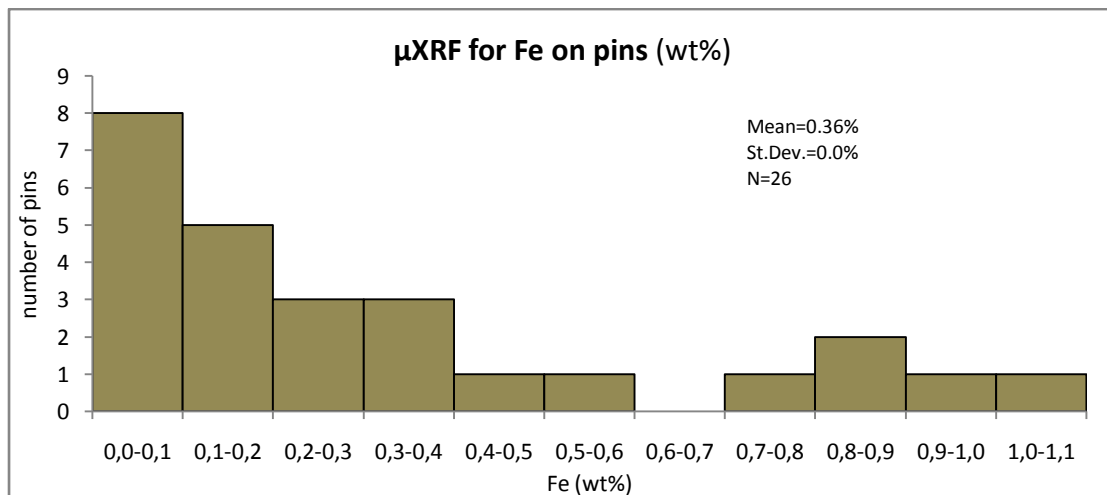


Figure 3.6.18. Histogram of the distribution of the pins, regarding their iron content, based on μ XRF methodology

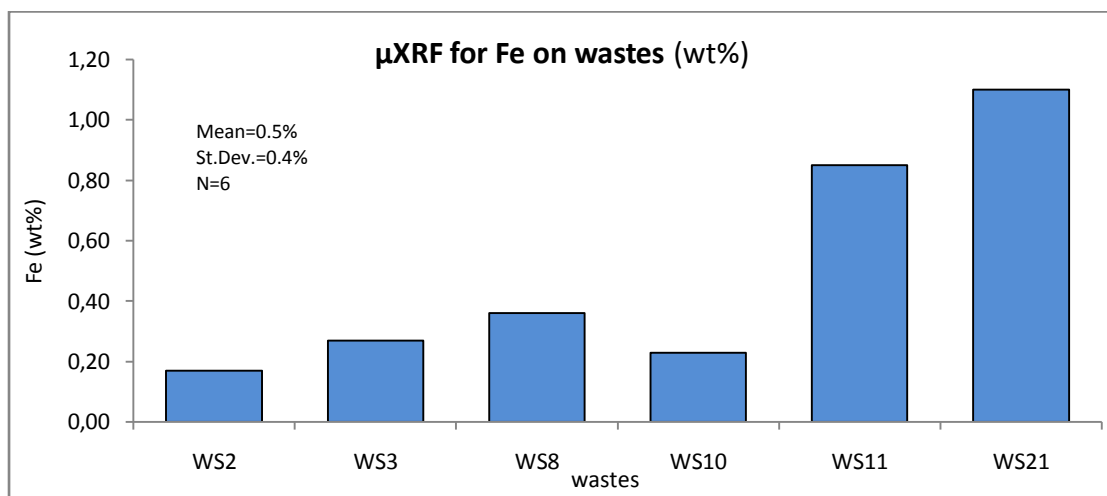


Figure 3.6.19. Bar chart of the iron content on the metallurgical wastes, based on μ XRF methodology

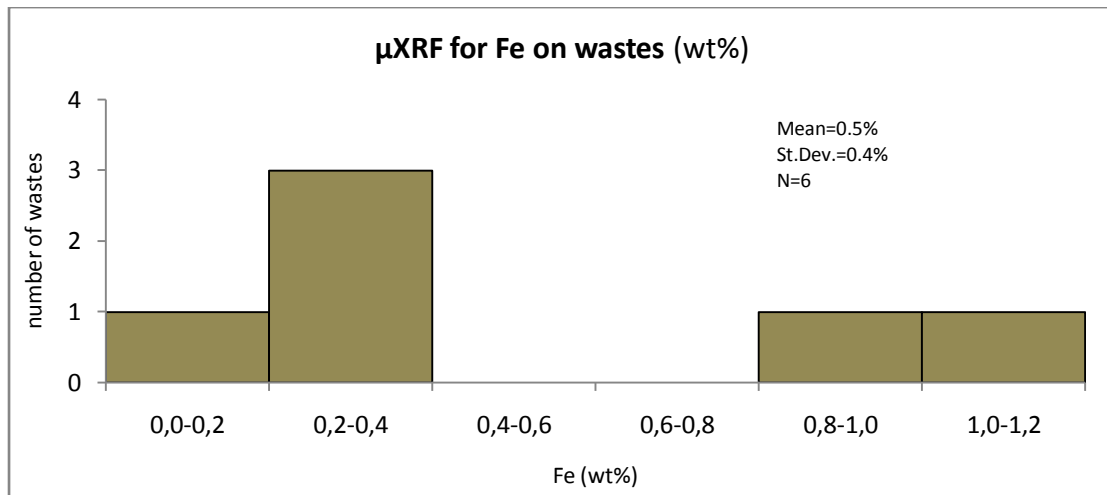


Figure 3.6.20. Histogram of the distribution of the metallurgical wastes, regarding their iron content, based on μ XRF methodology

In the case of the pins assemblage, antimony was traced with both the XRF techniques. Under the μ XRF analysis the antimony was observed in 10 out of the 26 pins having (fig-3.6.21-) values range between 0.25% and 0.50%. The median value was estimated at 0,37%; the maximum and minimum values at 0.43% and 0.25%. Although the element always coexists with copper ores is rarely found in quantities exceeding 0.1%; considering that the detection limit for antimony under μ XRF is 0.3%, it is possible that it might be present on the rest of the pins but it is too low to be detected. The pins distribution, regarding their antimony content, is presented on histogram 3.6.22.

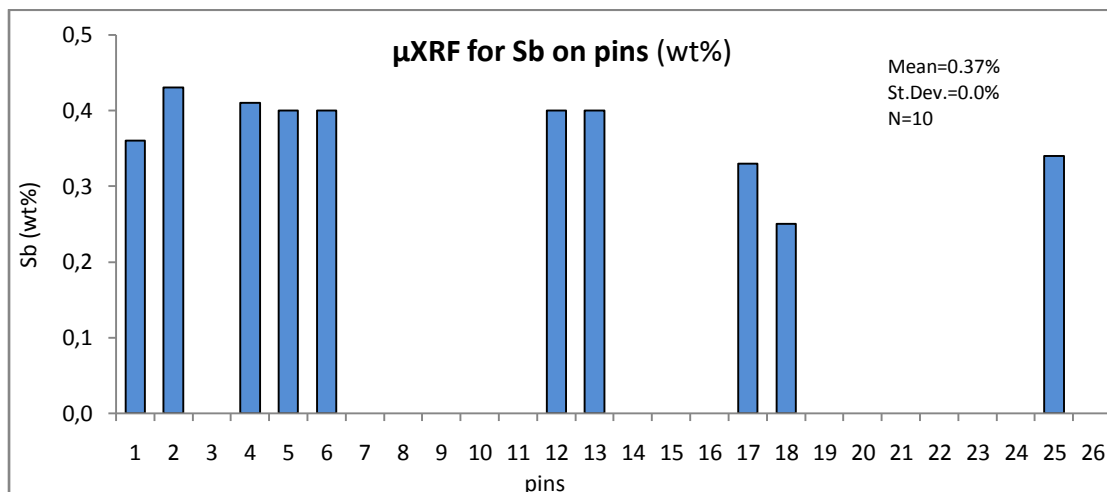


Figure 3.6.21. Bar chart of the antimony content of the pins, based on μ XRF methodology

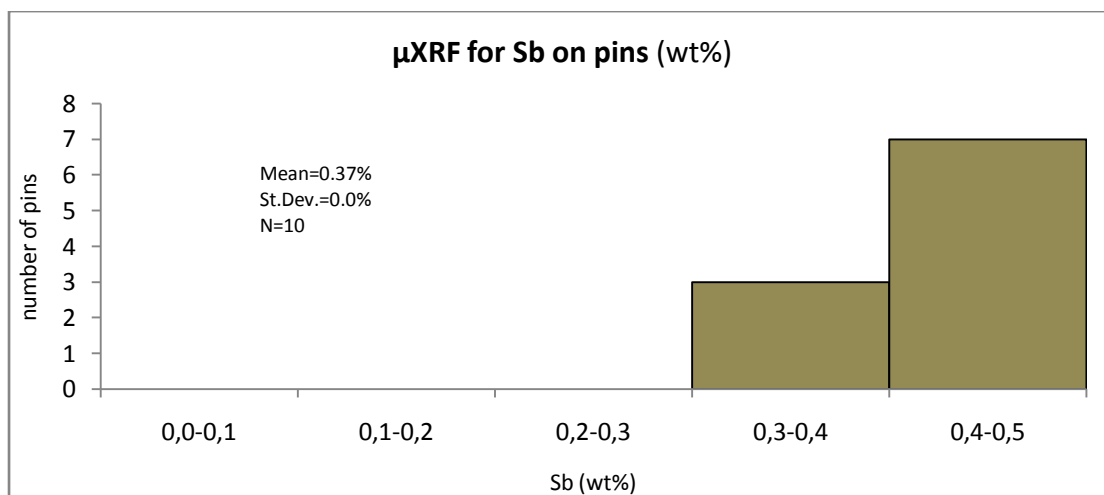


Figure 3.6.22. Histogram of the distribution of the pins, regarding their antimony content, based on μ XRF methodology

Traces of nickel are encountered on all pins (fig-3.6-23-) and wastes (fig-3.6.25-), in quotas under 0.35% and 0.04%, respectively, under the μ XRF analysis. The median value of the pins is 0.06% and for the wastes 0.04%. Their minimum and maximum values range between 0.03 to 0.34% for the pins and 0.03 to 0.06% for the wastes. The pins and metallurgical wastes distribution, regarding their nickel content, are presented on histograms 3.6.24. and 3.6.26, respectively.

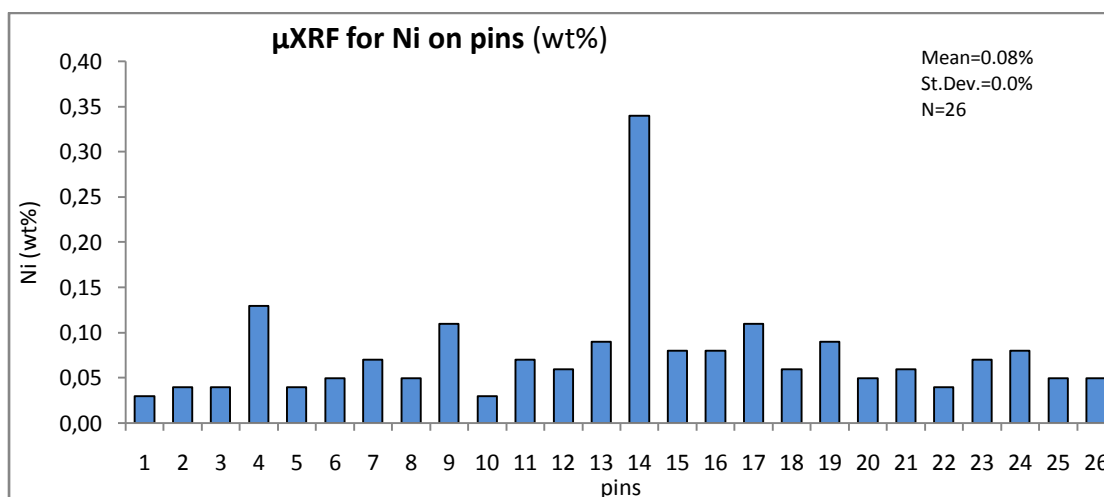


Figure 3.6.23. Bar chart of the nickel content of the pins, based on μ XRF methodology

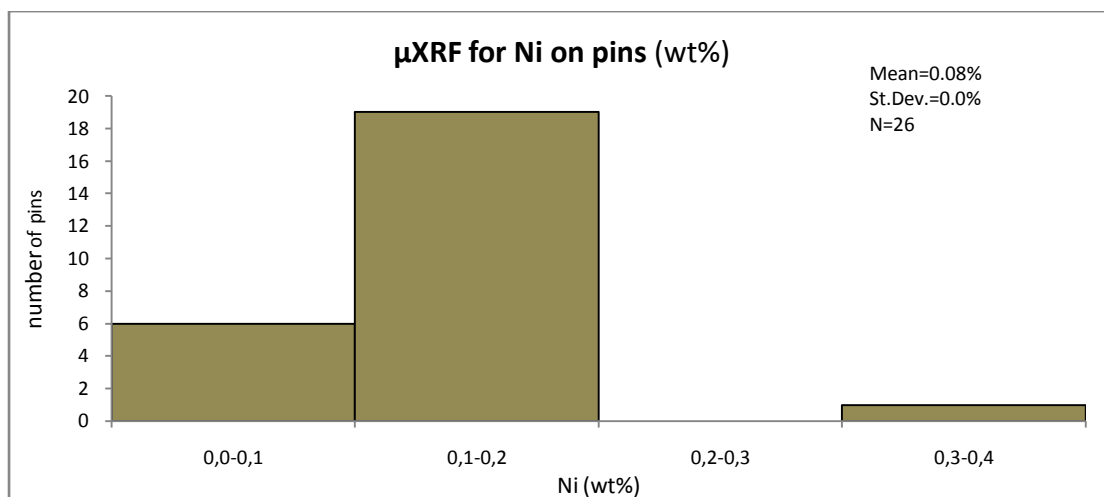


Figure 3.6.24. Histogram of the distribution of the pins, regarding their nickel content, based on μ XRF methodology

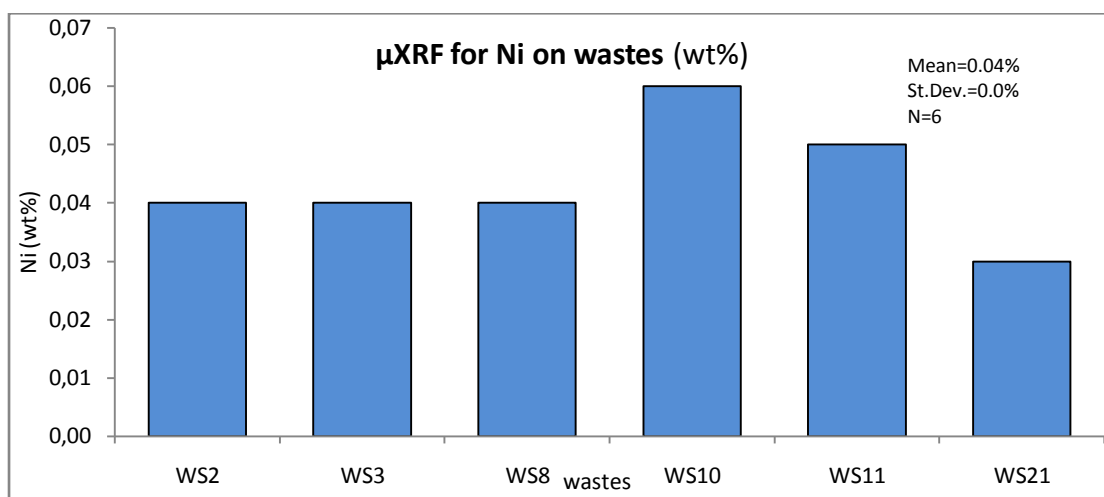


Figure 3.6.25. Bar chart of the nickel content on the metallurgical wastes, based on μ XRF methodology

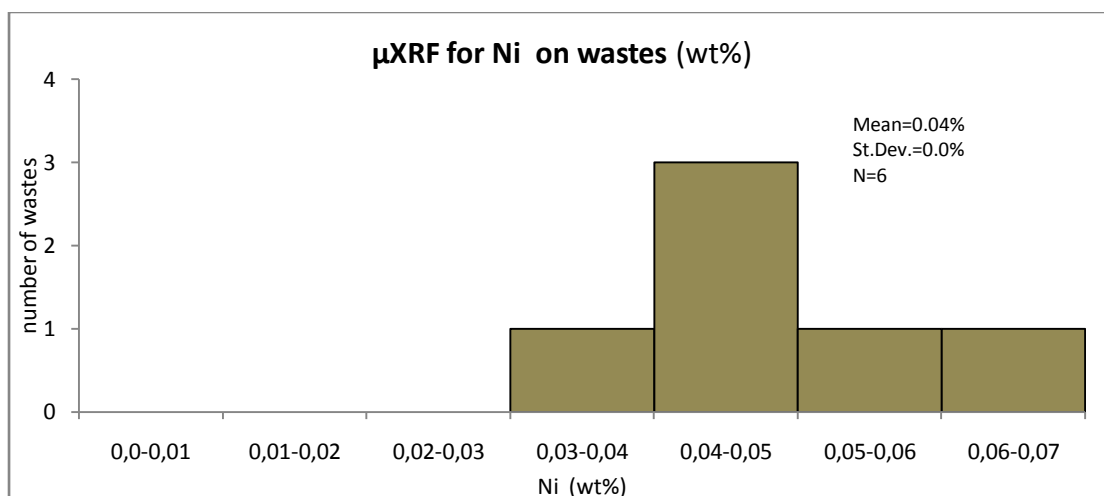


Figure 3.6.26. Histogram of the distribution of the metallurgical wastes, regarding their nickel content, based on μ XRF methodology

3.7. Composition of the assemblage

As discussed on chapter 2.1., all pins were grouped according to their typology and chronology. In the following plots the pins have been visualized, in order to be easily identified with different colours and shapes, each representing a chronological group. There is a discrepancy in the number of the pins represented in each period; although there was an effort to choose pins representing both the Geometric and Archaic years, this was not possible due to difficulties regarding their availability and condition of preservation, making them not suitable for analysis. Albeit, a preliminary conclusion regarding their manufacturing technology throughout the periods, may be extracted. The number of pins of each period is presented in the following figure (fig-3.7.1-). One pin from early to middle Geometric period (ca before 850 BC), one from middle Geometric period (ca 9th BC), twelve from the late Geometric period (ca 750-800 BC), eight from late Geometric to Subgeometric period (ca 675-700 BC) and four from the Orientalizing period (ca 7th BC).

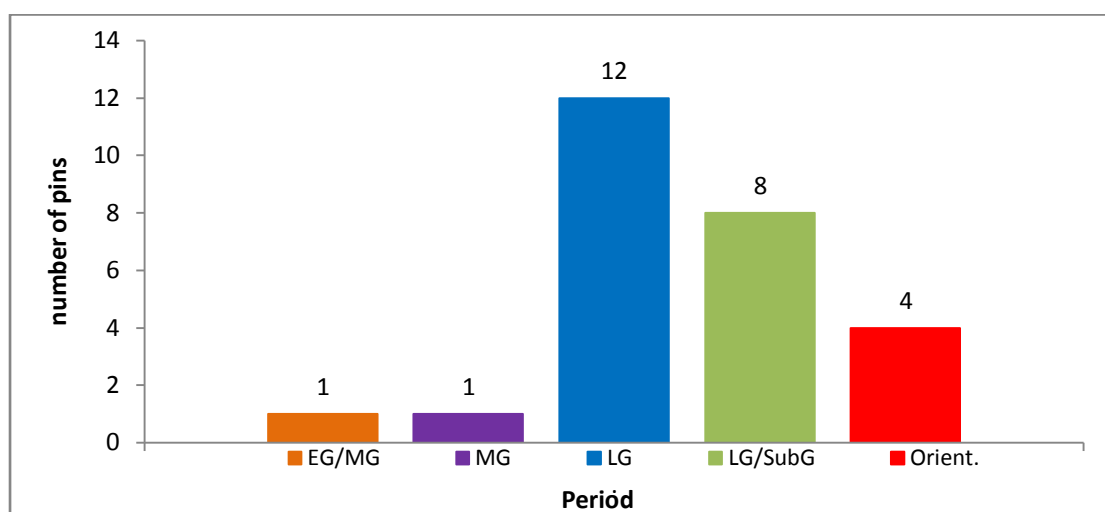


Figure 3.7.1. Bar chart for the pins analysed, for each period

Regarding the range of Cu/Sn concentration under the μ XRF technique (fig-3.7.2-, -3.7.3-), the proportion of added tin on 25 out of 26 pins indicate intentional adding since it exceeds 4% and ca 5% on the wastes; natural copper tin ores contain 1-3% tin (Gale, 1985). It is possible that the values obtained were affected by the corrosion products which, along with the asymmetrical geometry of the assemblage resulted in an overestimation on their tin content. Since tin rarely occurs as native it was introduced into the alloy when intentionally added, in the form of cassiterite.

When unintentionally added, it was usually introduced either through tin-rich copper ores (may contain up to 3% tin) or through fluxes (gossan may introduce 1-3% tin in the alloy). Thus, the low tin bronzes are not necessarily the result of scrap recycling (Gale, 1985).

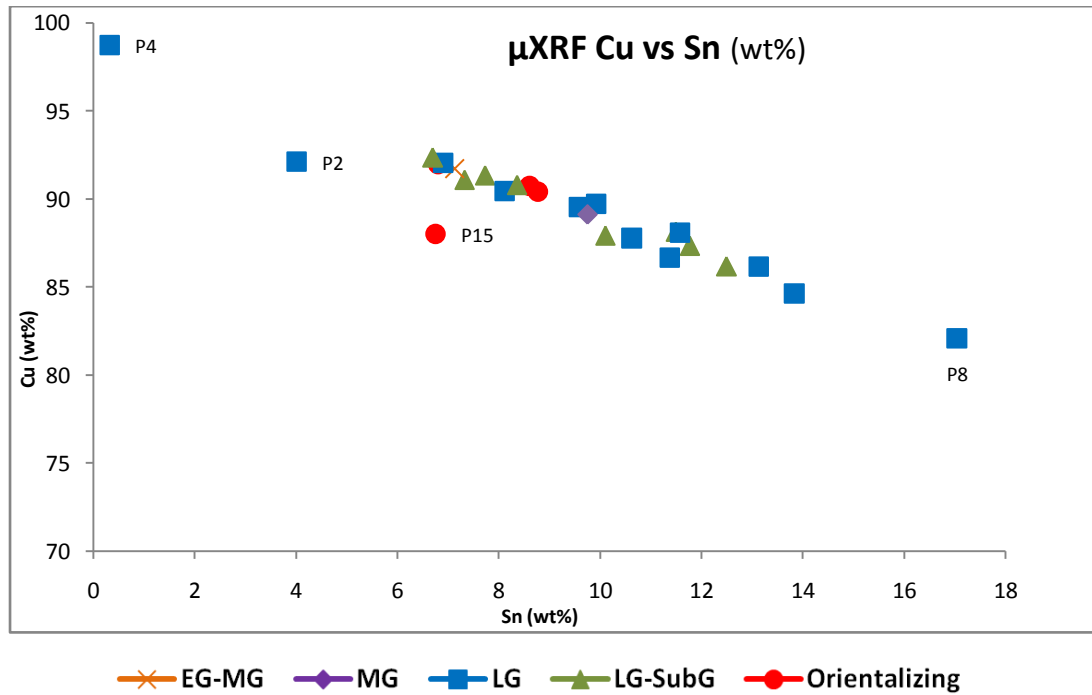


Figure 3.7.2. Scatter plot presenting the distribution of Cu versus Sn in pins, based on μ XRF methodology

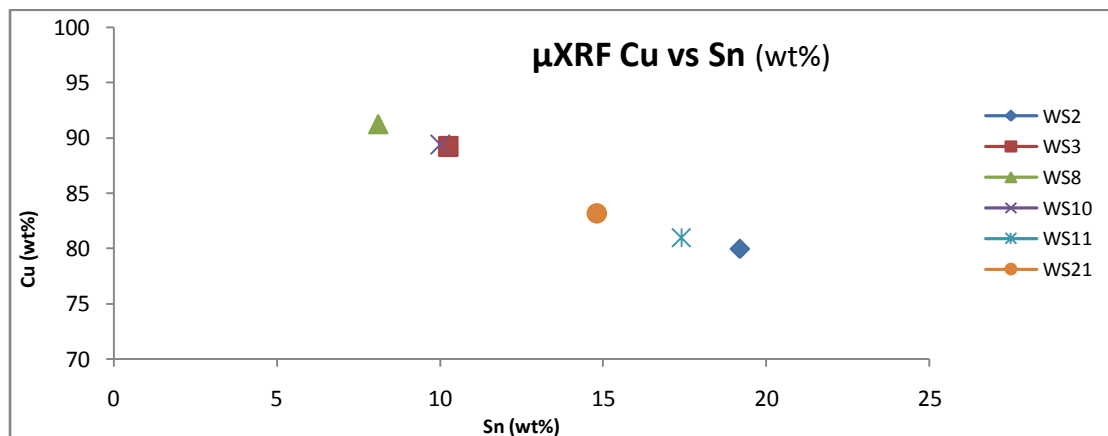


Figure 3.7.3. Scatter plot presenting the distribution of Cu versus Sn in selected metallurgical wastes, based on μ XRF methodology

Tin when intentionally added to copper can reduce its melting temperature, increase the hardness of the alloy, its corrosion resistance (Tylecote, 1992), as well as, to

satisfy the aesthetical needs of the bronze objects' owners (Nordquist, 2014: 195). It should be noted though that the lowest amount of tin in copper that is needed to support a deliberate addition, for the production of bronze is not yet well defined (Charalambous, 2015).

Tin is relatively insoluble in copper. At room temperature, only about 1% Sn can be dissolved in copper, in a solid solution. Cu-Sn alloy is practically a solid solution of good plasticity when the content of tin is up to 14%. Considering a Cu-Sn phase diagram, a casting copper alloy containing tin over 14% belongs to the phase δ which is hard and brittle. When the Sn content ranges between 8 - 11% there is no δ phase. When over 11% tin and slow thawing of the alloy is involved, the phase δ is again present. Thus, the hardness increases proportional to the tin content; though alloys with a content of tin over 20% have a very low workability and greater brittleness (Konofagos, 1967; Charles, 1973; Papandreopoulos, 2012: 38, Tselios, 2013: 61-65). The pins assemblage can be classified in three categories depending on the percentage of tin and thus their hardness. The first group based on a single pin (ALEA-P4) and the second on the rest of the assemblage with analysed tin values between 4 and 14% Sn, since the values seem to present a continuum. The ALEA-P8 pin has an analysed value of 17% tin. Based on the aforementioned, the values of tin along with the observed ratios of copper versus tin, are probably overestimated as a result of possible intergranular corrosion of the pins; considering that the absolute removal of their corrosion products is not possible.

It is almost certain that there are elements missing from the XRF results, because it was not possible for the technique to trace them; either because the filtered mode was used or they were below its detection limits. Therefore, elements like chlorine, oxygen, sulfur ions and nitrates, which are usually critical for the identification and interpretation of the involved corrosion processes of a Cu-Sn alloy and thus for the possible under or overestimation of these major alloying elements, were not identified.

On 25 out of the 26 pins, μ XRF analysis consistently yields a mean tin content of ca. 9.6%. A bronze alloy with a concentration of more than 5% tin, has a reddish tint because of the copper content, but as time passes, it gains a golden-brown hue due to corrosion processes involved. In the process of solidifying the metal in the matrix, in some cases it is seen that the extraneous chain elements, such as tin or arsenic, are extruded on the surface of the objects. The phenomenon of this type of differentiation

is also the cause of the heterogeneity of copper alloys and was possibly exploited by the ancient craftsmen in order to give on the surface of the alloys a colour other than the red of copper; like the colour of more precious materials, usually gold. The aesthetic appearance of metals has long been recognised in archaeometric studies as an important factor in the evolution of metal production. It is also a common assumption by scholars working with aesthetics, the association of distinctive colours and brilliant surfaces with ritual powers and potency (Radivojevic, 2017). Fang and McDonnell (2011) showed that the influence of tin on the colour of tin bronzes may be observed via two trends: 1) the addition of tin up to ca 15%, which significantly reduces the redness of copper, while 2) past this mark and into the high-tin bronze range (ca 18% and more), the increasing tin content reduce both the redness and the yellowness of the alloy, driving it towards a more silvery colour. These objects have poor mechanical properties while when the concentration of tin overcomes 15% its brittleness will increase, however, they have a distinctive colour, which together with their hardness has been argued as one of the reasons for their production (Haynes, 1992; Radivojevic, 2017). Considering the votive demands of a sanctuary, where the individual's offerings become more generous and the hierarchy distinguishes itself through them, one can suppose that hardness was not as essential as the aesthetics (De Polignac, 1995: 20); albeit a theory that these pins were previously used by their owners before deposition, cannot be excluded. Though the 15% tin content, accompanied by the characteristic of brittleness would have been a problem when everyday use was involved.

Based solely on relative literature (Konečná, 2012) regarding the temperature of solidification of the alloying elements, the mean content of ca. 9.6% on 25 out of the 26 pins indicates a Group III cast copper alloy type, which has a wide solidification (freezing range) temperature range of about 110 °C, even up to 170 °C. Bronzes with tin content as high as in Group III of the assemblage have good corrosion resistance, although various parameters such as the acidity of the environment (pH), its oxidation-reduction potential (Eh) and the cations and anions present may influence the corrosion procedures (Schweizer, 1994: 42). This resistance is observed in the samples, considering the duration of their burial along with the high humidity environment of their storage area (based on in-service measurements, the RH of the storage is ranging between 80-90%). Alloys with such wide freezing ranges usually form a delicate zone during solidification, resulting in interdendritic

shrinkages or microshrinkages; so rapid solidification should be ensured during casting. This rapid solidification, as discussed, can be recorded on the pins' microstructure through observation under reflected light microscopy, which is not the case here. Same applies regarding porosity, as can be estimated from the literature may be present, ranging from 1 to 2% of the total volume, resulting in its structural weakening (Konečná, 2012). The ALEA-P4 pin, based on its elements concentration (a copper value of approximately 99%), belongs to the Group I type of alloys; alloys that have a narrow freezing range, approximately of 50 °C between the liquidus and solidus curves.

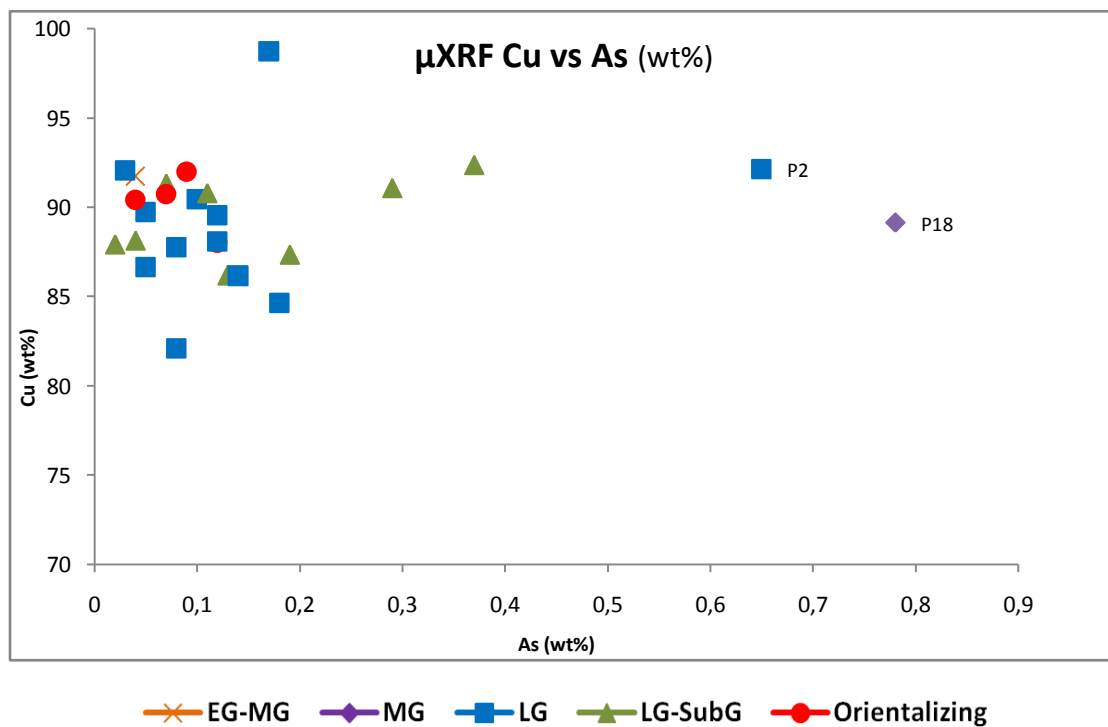


Figure 3.7.4. Scatter plot presenting the distribution of Cu versus As in pins, based on μ XRF methodology

Arsenic, which improves the properties of the alloy mainly resulting in the increase of its ductility and hardness, can be found either as an intentional addition by co-smelting a copper oxide with an arsenical sulphide such as orpiment (As_2S_3), either as deriving from the ore and fluxes or from the recycling of scrap Cu/As metals. The proportion in order to be considered as an intentional addition is not yet well established; Papadimitriou (2001) considers a percentage above 0.5% as intentional adding, while Rapp (1982) refers to native copper with arsenic more than 1% due to the presence of domeykite (Cu_3As). The element may also act as an antioxidant

during the casting process, reducing the oxide content of the oxides while it has the property of altering the red colour of the copper, giving it a tint of white, resembling silver which seems to be a desirable feature by the ancient copper smiths.

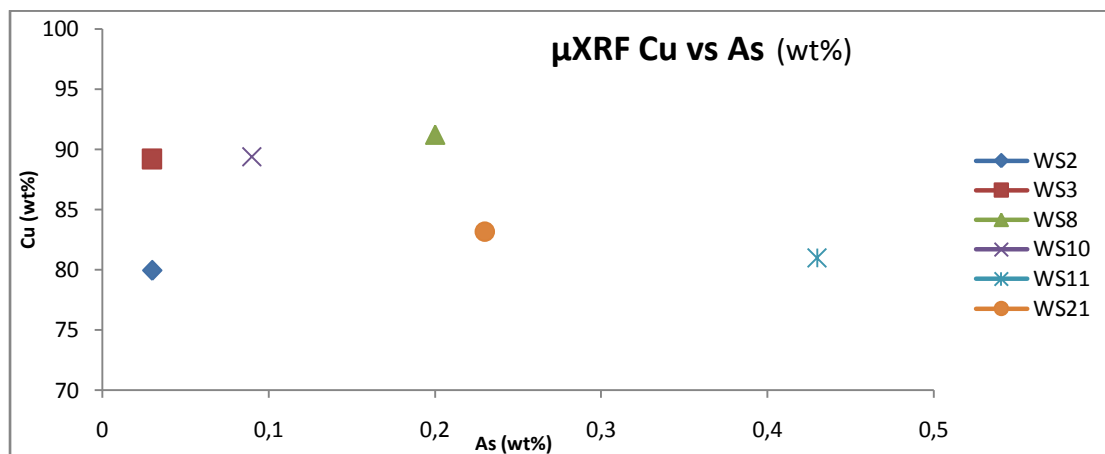


Figure 3.7.5. Scatter plot presenting the distribution of Cu versus As concentration in selected wastes, based on μ XRF methodology

Arsenic along with nickel, antimony, bismuth and silver comprise, up to a certain extent along with lead isotopic study, the main diagnostic elements for the origin of metal artifacts; its composition largely reflects the deposit in which it occurs (Pernicka, 1999). Olivenite $\text{Cu}_2\text{AsO}_4\text{OH}$ and konichalcite $\text{CaCu}[(\text{OH})(\text{AsO}_4)]$ are common copper arsenate minerals, occurred in Laurion and Cyprus. Since in order to be considered as intentionally added, arsenic should be at a percentage above 1%, the mean values of the assemblages may point in the direction of the above mentioned copper arsenate minerals involved (fig-3.7.4-, -3.7.5-); based on the fact that the element is far more easily retained in the copper metal by the direct reduction smelting of such ores than is the case for sulfidic ores, which need an oxidizing roasting step in which arsenic is easily lost. An overestimation, due to corrosion, of its proportion on the assemblage may not be excluded, since these values derived from surface analyses (Gale, 1985; Tylecote, 1992: 10; Charalambous, 2014).

For the 23 out of the 26 pins and the waste assemblage, the effects of such small amounts of lead (smaller than 1%), on the properties of the alloy are minimal (fig-3.7.6-, -3.7.7-). As lead segregates in copper alloys, it may be concentrated in some of its parts by the action of gravity, when the alloy is still in a liquid state. Thus, areas exceptionally diverse in lead are formed; this high or poor concentration may,

therefore, be due to the accidental analysis of one such area (Charalambous, 2014). Ideally the results should be confirmed by bulk chemical analysis on a sample removed from the object. Moreover, the possibility of underestimating the element is always present, due to difficulty in the distinction of its peak related to the peak of arsenic (see chapter 2.3.1., p: 56). This problem concerns both the XRF and the SEM-EDS techniques.

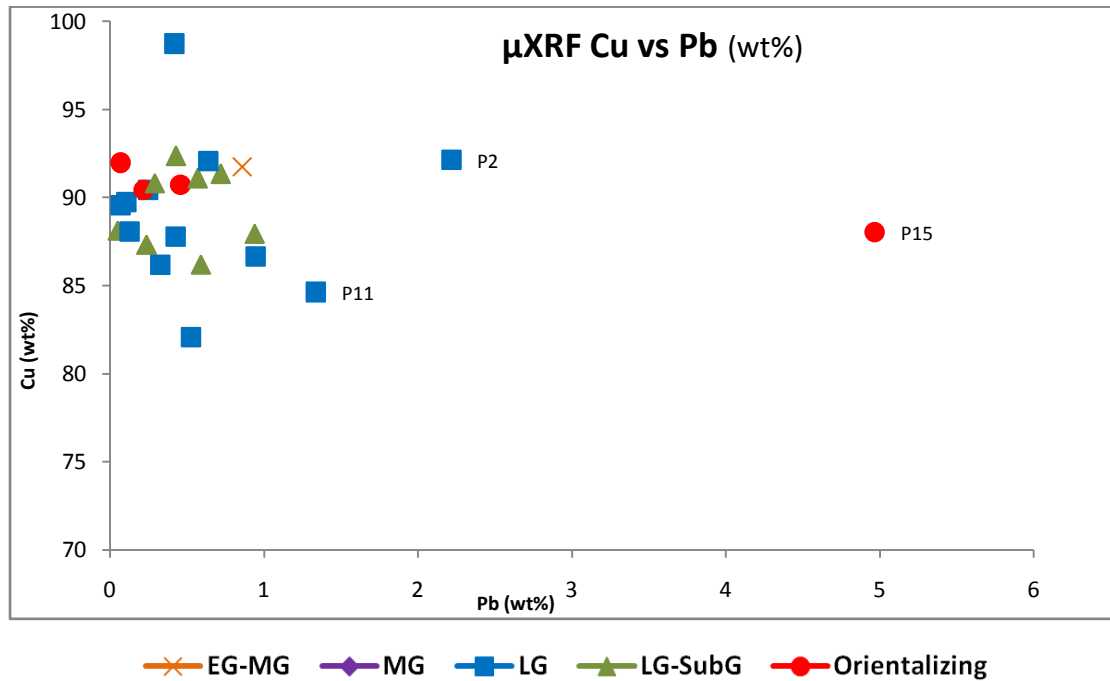


Figure 3.7.6. Scatter plot presenting the range of Cu versus Pb concentration in pins, based on μ XRF technique

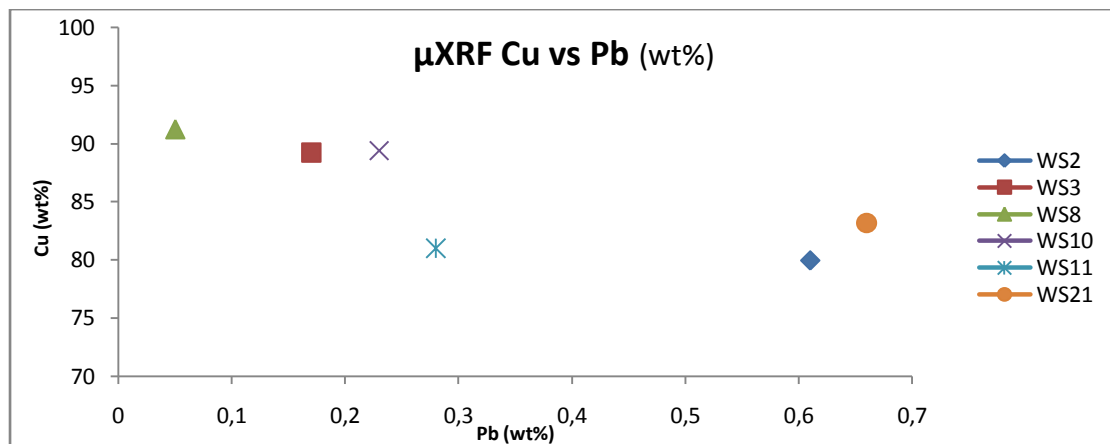


Figure 3.7.7. Scatter plot presenting the distribution of Cu versus Pb concentration in selected wastes, based on μ XRF methodology

The exceptions on the assemblage are the pins ALEA-P11 with 1.34%, ALEA-P2 with 2.22% and ALEA-P15 with 4.97%, which, although seem to belong to two different typologies, it is more likely that their lead originate from lead-rich ores or as a result of mixing of scrap metals. It is less possible that a deliberate addition in order to help casting is involved, since a larger amount of lead would possibly have been preferred (fig-3.7.6-). Lead in about 2% concentration, as in the case of ALEA-P2, is known to help the casting of copper and its alloys. Further increase in lead content (3-4%) does not increase significantly the fluidity of the alloy but there is a lowering in its melting point. This makes leaded bronzes with intricate shapes involved, as in the case of ALEA-P15 easier to cast, but also easier to drill, file or grind. Moreover, as metallic lead oxidizes very quickly and forms a passive oxide layer is regarded as a corrosion resistant alloy (Fernandes, 2013). It is generally considered that lead concentrations up to 4% can be regarded as coming from the ore and are frequently found in copper smelting slags (Mangou et al, 1997: 68-69, Georgakopoulou 2004: 9, Tselios, 2013). Higher concentrations of lead may also result in the alloys' colour alteration (Mangou, 1994:32).

The small amounts of lead traced on the assemblage could have entered in the alloys through the smelting process since as written above copper ores frequently contain lead. Based on the aforementioned, it should be noted that Gale (1985) supports the hypothesis that the concentrations of minor elements like arsenic (up to 7%), lead (up to 4-5%) or tin (up to 1-3%) in a copper alloy, should not be regarded as definite evidence of deliberately produced alloys; since especially for lead, amounts up to that quantity offer only minor advantages on an alloy. It is believed that those additions are not a characteristic of a local mining or workshop tradition, but instead may well be accidentally produced by the smelting of impure ores (Gale, 1985).

Regarding their provenance, lead arsenate ores commonly mixed with oxidized copper ores and other leaded copper ores such as bournonite (PbCuSbS_3) occur in Laurion; the lead (II) sulfide mineral galena (PbS) and its oxidized products (PbSO_4 , PbSO_3 , PbO , PbS_2O_3 , $\text{PbS}_2\text{O}_6 \cdot 4\text{H}_2\text{O}$) are frequently found on various mining sites of the Aegean (Gale 1985, 2008, 2009).

A mean value of 0.36% of iron in the pins (fig-3.7.8-) and 0.50% in the wastes assemblage (fig-3.7.9-) indicate that the mining of the copper derived more likely, either from copper oxide ores or more likely, considering the time of the pins' production, from sulfidic ores (like chalcopyrite or bornite); which were adequately

refined, with strong reducing conditions and temperatures high enough to mobilize iron during smelting, so sufficient de-ironing of the ore was achieved (Kiderlen, 2016).

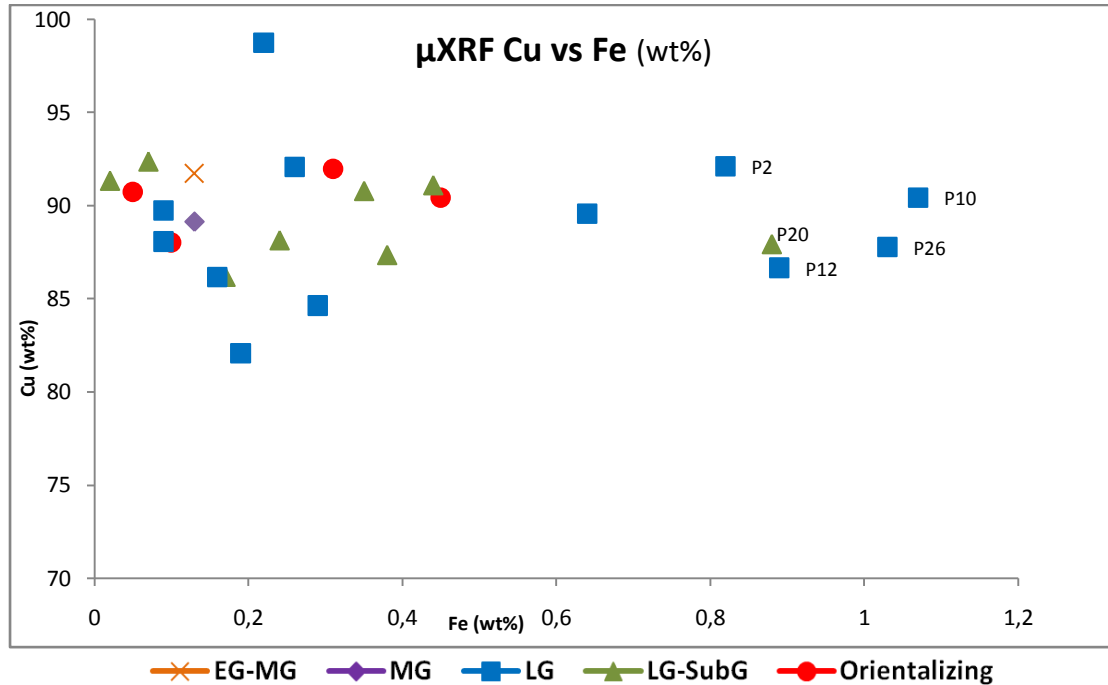


Figure 3.7.8. Scatter plot presenting the distribution of Cu versus Fe in pins, based on μ XRF methodology

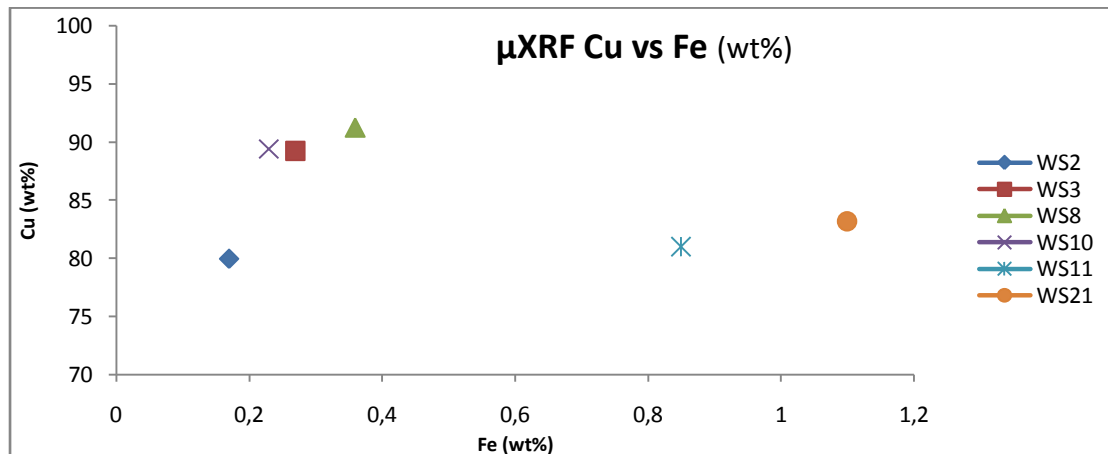


Figure 3.7.9. Scatter plot presenting the distribution of Cu versus Fe in selected metallurgical wastes, based on μ XRF methodology

Iron is probably the most unwanted of the impurities included in a copper alloy; when its concentration is above 0.5% it may cause problems when cold annealing is involved (Tselios, 2012: 56). Albeit, its presence in quantities ranging up

to 1.07% in the pins and 1.10% in the wastes, could indicate, beside the possible use of sulfidic copper ores, the use of iron oxides, mainly limonite, as a flux. This is being advanced by the detection of traces of sulfur in the ALEA-P20 pin (as limonite derives mainly from the oxidation and hydration of iron rich sulfide minerals) (Mangou, 1994: 148,189). The use of limestone as a flux is also possible considering that calcium was traced on ALEA-P4 pin.

Although in earlier periods a ternary copper-antimony-arsenic alloy was used, the quantities measured in the pins assemblage does not justify the identification of such an alloy (fig-3.7.10-). The measured quantities imply that antimony, was probably arisen as impurity, due to the deficient refining of the copper ore (possibly bournonite $PbCuSbS_3$) containing the element (Mangou, 1994: 148).

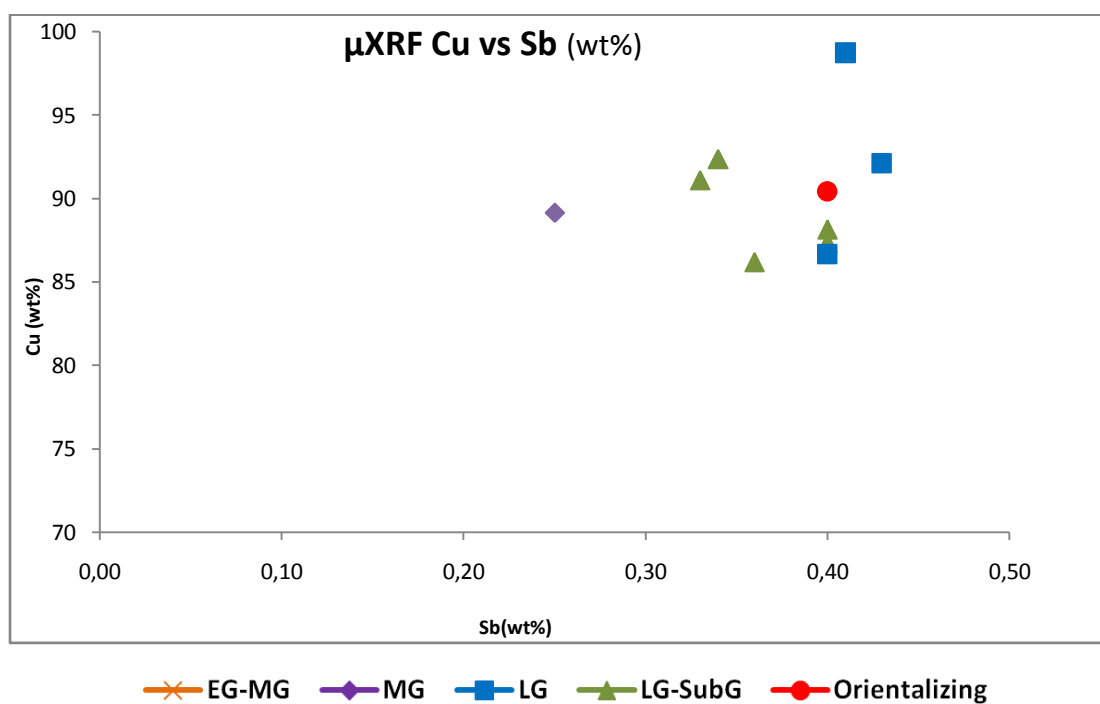


Figure 3.7.10. Scatter plot presenting the distribution of Cu versus Sb in pins, based on μ XRF methodology

Regarding nickel's presence in the assemblage (fig-3.7.11-, 3.7.12-), its quota may be considered as originating from the copper ore or as an admixture of the original ore with a nickeliferous ore, possibly introduced as a flux during copper smelting (Mangou, 1994: 148). Nickel may be a common element in arsenide and sulfarsenide copper ores, encountered in various places around Greece. In copper ores from Crete and Kythnos, the nickel proportion has been quite significant reaching up

to 3%; possibly not the provenance of the ores of this assemblage (Mangou, 2000: 215; Doonan, 2007).

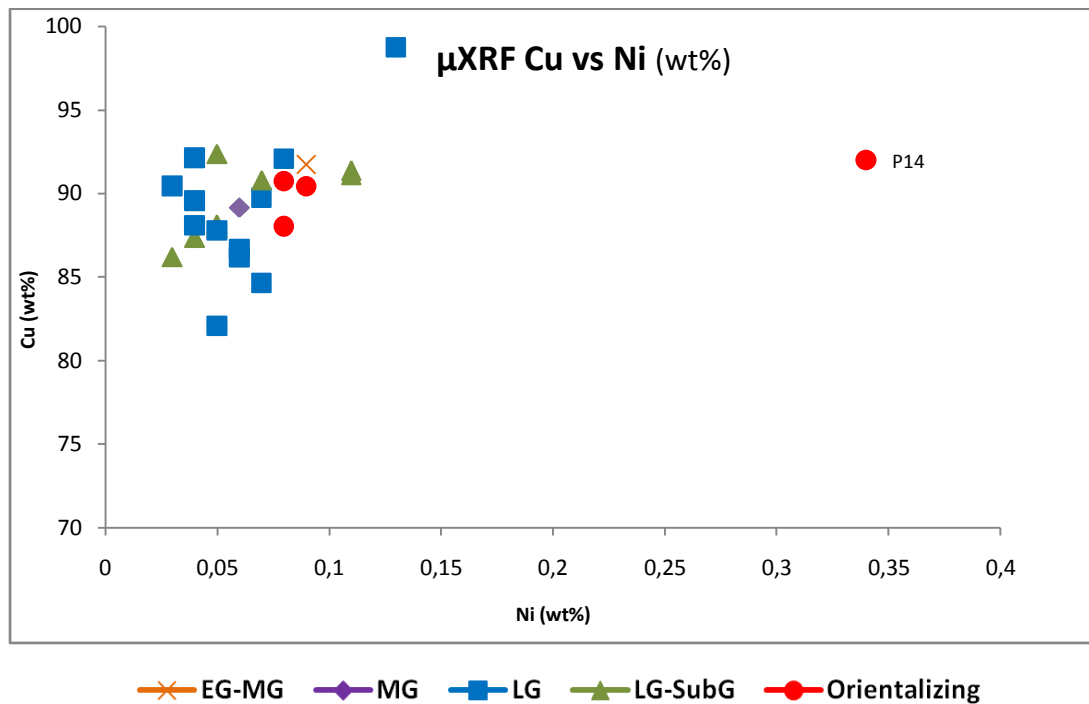


Figure 3.7.11. Scatter plot presenting the distribution of Cu versus Ni in pins, based on μ XRF methodology

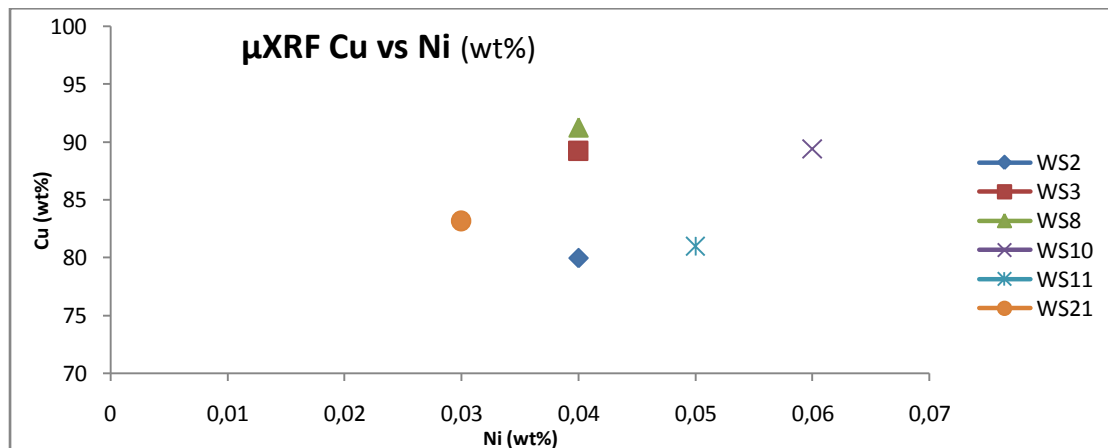


Figure 3.7.12. Scatter plot presenting the distribution of Cu versus Ni in selected metallurgical wastes, based on μ XRF methodology

Cobalt was detected with the μ XRF only on ALEA-P20, having a value of 0.06%. Considering that its detection limit for 50sec excitation is 0.024%, the value lies above it. This amount may be characteristic of the copper ore used or may

attributed to the modern agricultural procedures involved in the enhancement of the soil. Cobalt is an element useful when trace pattern analysis, for provenance, is performed; considering that in some cases, trace element pattern may be more indicative of an ore source than lead isotope ratios (Pernicka, 1999).

The elements of bismuth, zinc and silver are considered important for the study of the technology of the copper alloys; bismuth may also attribute to the origin of provenance through trace pattern analysis study. In the case of the assemblage, these elements were not traced with the μ XRF. They were traced with the p-XRF so they may be attributed to possible enrichment of the surface of the metal, since they are also often involved in bronze's corrosion processes.

Bismuth was traced on the pin assemblage only with the p-XRF technique, in proportions under 0.28%. Its values range between 0.07% and 0.28%. A rather different pattern can be observed for the wastes, which have a mean value for Bi of only 0.09%, although its extreme values range similar to those of the pins, being between 0.03-0.17%. On both assemblages that pattern excludes the intended addition of the element on the alloy; rather it had probably risen from bismuth-bearing sulfidic copper ores and deficient refining of copper during smelting (Mangou, 1994: 149). Bismuth above 0.2% may result in extreme brittleness of the object (Tylecote, 1992), a value close enough to those obtained from the assemblage; considering the era and the technological control achieved in the metal production, one can estimate that the copper smiths involved in their manufacturing were more interested in the aesthetics rather than the mechanical properties of the pins.

All though the presence of zinc is still a matter of debate considering its intentional use during prehistoric eras (Craddock, 2009), it is a fact that there are a number of zinc-rich copper ores in the Mediterranean. Its mean concentration of 0.09% of the pins assemblage and 0.10% of the wastes, traced only, with the p-XRF technique, can possibly consider as unintentional. The element either derived from the ore or the objects were enriched from the burial environment during deposition, not an unusual fact in areas like the sanctuary with anthropogenic activity present.

Silvers' presence was documented only by the p-XRF technique in 16 out of the 26 pins of the assemblage, with a mean value of 0.07%, while in half of the wastes it had a mean value of 0.04%. As a minor enhancement of silver fluorescence intensity might be expected in the presence of large amounts of tin, it is likely the case in certain pins and the wastes of "hard bronze". Silver is an element indicative of the

copper ores used and may contribute to the correlation ore / metal, thus to identify its possible provenance since the ratio of Cu/Ag remains stable under all the processes undergoing copper metallurgy (Tylecote, 1992: 109; Mangou, 1994: 150; Heginbotham et al, 2015).

Light elements as composites of the alloys, could not be detected with the XRF technique, for all measurements as written, were filtered. Moreover, even under vacuum or helium gas flush, elements under sodium can be very hard to trace. The SEM-EDS technique, though, ascertained traces of chlorine, sulfur, phosphorus, aluminium, chromium and calcium.

The presence of sulfur may be attributed to the exploitation of sulfidic or semi oxidized sulfidic ores. The exploitation of cupriferous sulphide minerals occurring in the deep veins, and the roasting of copper ores for making copper matte which is then smelted as easily as the copper oxides, comes as no surprise since it is known that this advanced technology was in use since the Late Bronze Age. The element was confirmed only on the ALEA-P20 pin, having a mean value of 0.4%; an indication of an unsuccessful roasting usually of a stage prior to the smelting, where sulphide ores are roasted under oxidizing conditions to remove the sulfur. Of course, one should not overlook the fact that not all of the potent sulfur-bearing pins were examined under the SEM-EDS. The fact, though, that no sulfur was detected on the rest of the pins examined provides information about the high level of expertise at the time; considering the mining and extraction techniques of the metals involved, since sulfidic copper ores were mainly used as copper sources at the time. It is possible, though, the presence of the element could not be detected due to values which could be under the detection limit of the SEM-EDS technique; considering that even during successful roasting traces of sulfur remain in the metal, in the form of inclusions (Mangou, 1994: 199, Van Brempt, 2015).

Regarding aluminium, it was traced in four out of the ten pins examined under the SEM-EDS technique. In the case of ALEA-P4 its presence was measured at 5.3% of the total value of the alloy. This percentage may indicate a false series of measurements, so it was chosen to be omitted from the discussion. Considering the rest of the pins, aluminium was probably not a component within the original alloys; rather, it likely migrated from the soil into the developing corrosion layers. Rarely, the presence of aluminium may be ascribed to the entrapment of slag remains into the final metal (Mangou, 1994: 190).

Both chromium and calcium were only detected on ALEA-P4 pin. The presence of chromium, which is geochemically bonded to the iron, may be attributed to the corrosion processes or the provenance of the ores. Ores of high proportion of calcium (between 8% to 17%) are known to be extracted in Kythnos. The 0.86% concentration on the pin though, indicate that it was probably originated from the flux added during smelting, from fuel ashes or may existed as eroded furnace material. Another possible explanation for its presence may be attributed to the deposition environment of the pin; soil residues after adhesion on the pins' surface or during the formation of its corrosion products (Mangou, 2000: 215, Tselios, 2013: 193).

The detected chlorine was present on seven out of ten pins examined (mean value 0.59%) under SEM-EDS and in all of the wastes (mean value 0.58%). Its presence may attributed to the corrosion processes of copper. The migration of chloride ions from the environment results in the production of hydrochloric acid, which in the presence of oxygen and humidity interacts with the copper oxides and copper carbonates. Thus a new cuprous chloride product is being formed, namely atacamite/paratacamite which may again react with copper oxides; triggering a cyclic and self-sustaining mechanism (Bozzini, 2016). Atacamite and paratacamite $\text{Cu}_2\text{Cl}(\text{OH})_3$ which are identical in chemical composition but have different crystal forms, are commonly encountered in favourable environments of arid and saline conditions, though they may also be found on bronzes from regions of high humidity (Gettens, 1963: 552-553). The possible occurrence of paratacamite (bronze disease) was observed and recorded on most of the pins bearing chlorine, through the optical microscope (presented in chapter 3.1.).

Phosphorus was traced, in two pins (ALEA-P3 and ALEA-P4) only with SEM-EDS. The characteristic X-rays of phosphorus are low energy, with K lines at 2.013 and 2.142keV, which means that they are (re) absorbed into the sample matrix and/or the detector and scattered as Bremsstrahlung radiation (Hunt, 2015); especially when the element is in very small quantities so the number of characteristic X-ray generated is correspondingly small. A typical phosphorus alloy has a mean composition of: Cu 91%, Sn 5% and P 0.03-0.3%, since the solubility of phosphorus into the copper is only 0.5% (Papandreopoulos, 2012: 37). Small amounts of the element may increase the alloys' tensile strength, though it does not seem possible that this type of alloy was used during the eras of the sanctuary. In the case of the two pins, it might originate from previous, chemically related with the use of phosphoric

acid, conservation treatments or may be present as a secondary mineral in the deposition environment, formed by the action of copper salt solutions on the calcium phosphate of bones (Degriigny et al, 2007). Considering the sanctuary and the presence of votive pits encountered in the area one may assume that ritual dinners refuse or human bones due to its subsequent use as a medieval cemetery, may have provided the necessary amount of phosphorus through weathered apatite; other rock-forming phosphates from the environment may also be present (Tarditi, 2014: 99). Moreover, the whole region of Tegeatis around the sanctuary is an area of heavy agricultural production. Phosphorus may appear in its soil, due to agricultural works and thus deposited bronzes may accumulate it in their corrosion products. The corrosion product formed -libethenite $\text{Cu}_2(\text{PO}_4)(\text{OH})$ - could not possibly identified through the elemental analysis and only indication may be extracted for the presence of phosphorus on the pins (Gettens, 1963: 557).

Silicon was detected only on metallurgical wastes by SEM-EDS. Its mean value was 0.61%. Its presence is probably related to the entrapment of soil remains in the wastes during the formation of their corrosion products. Considering that these wastes are the result of secondary product (metal spills) and not primary (slags) it is more likely that their uneven shape encouraged the entrapment of the soil, in contrast to the smooth surface of the pins. Soil conglomerates were also observed and recorded during the optical microscopic examination on chapter 3.1. Moreover, the presence of iron as previously described enhances the possibility that the wastes were smelted with the use of fluxes rich in silicates (sand). Less likely, its presence may be related to the nature of the ore; considering that copper minerals could have been used for the obtaining of the metal, these may have retained a proportion of silicon (the element is usually detected on slag remains mainly in the form of quartz SiO_2).

Manganese is an element traced only by the p-XRF on half of the pins (mean value 0.04%) and on all of the wastes (mean value 0.04%), which may also attribute to the chemical enhancement of the soil in the area (Nørgaard, 2017). The proportional values obtained for manganese, niobium and zirconium are clearly related to the alloys' corrosion processes. It is probably not a coincidence that those elements were only detected through the p-XRF technique. Its 3x3mm size, beam inevitably analysed corroded areas, although the pins were locally stripped to their original surface. The size of this surface has though been very small, due to the small size of the objects. Therefore, ideally, their quota should be added and the total

subtracted from 100%; since their total mean value was under 0.08% they have been omitted from the discussion.

It should be noted that random or deliberate additions to copper alloys may affect the rate of copper oxidation in a complex way. The trace elements of the assemblage are in quantities under 1%. Some of them, although seem like being in negligible quantities, they may influence the alloys properties. This is easily observed on the corrosion products formed on the objects. For example, nickel of up to 0.1% causes a faster corrosion of copper; conversely nickel on levels above 0.1% can reduce the corrosion mechanisms. Copper alloyed with metals develops protective oxide layers; tin, lead and zinc are oxidized by diffusion outward from the inside of the alloy towards the surface, resulting in a situation where the corresponding oxides of the most upper elements are trapped in the copper oxide layer (Cu_2O) while at the same time accumulate underneath (Papandreopoulos, 2012). Consequently though, the degree of corrosion of ancient copper objects can be determined in addition to their chemical composition by the environmental parameters involved. Considering the spectroscopic analyses of the assemblage an overestimation of the aforementioned metals may have been the case.

Based on the aforementioned results, a statistical correlation between the colour of copper alloy corrosion products and their chemical composition has been proposed under XRF spectroscopy (Kantarelou et al, 2015). These corrosion products usually involve the presence of certain elements like lead, chlorine and carbon. Since C has $Z=6$ and thus it cannot be detected, its presence can be assumed, while the presence of Cu, along with green colour corrosion products of specific texture, may indicate the presence of a carbonate corrosion product, for example malachite. With reference to the presence of Cl, one of the major copper chlorides should be expected. Usually corrosion products like atacamite-paratacamite are expected to be of a loose texture, creating pitting corrosion phenomena and are of a pale green colour, while nantokite is whitish and of a waxy texture. Nantokite's location is of great importance, since it depends on different factors, though it is usually found near the metal surface, among other corrosion products. As regards red colour corroded areas occurrence, cuprite is most likely to be the red product, though if lead is present, minium (lead oxide) cannot be excluded. Other corrosion products can also be present in different colours, incorporating the co-existence of copper, tin, zinc and lead. According to recent studies (Argyropoulos et al, 2002; Arafat et al, 2013; Kantarelou

et al, 2015), seems that Zn is depleted from the surface, while ZnO and Pb_xO_y are found concurrently with tenorite (CuO) and/or cuprite (Cu₂O). Finally, in the corrosion products of a Cu-Sn binary system, the high intensity of Sn-L lines may indicate tin compounds, such as hydrated forms of Sn (SnO₂·nH₂O) or stannic oxide (cassiterite-SnO₂).

Moreover, one cannot possibly establish a solid connection between typology and technology of the pins. The one group formed (fig-3.7.2-) indicates a common technology throughout the periods observed; the tin proportion of ca 9% indicates a trend towards the “hard bronze” technology for the group. Thus, the pins ALEA-P3 and ALEA-P18 were chosen to be presented because of the values of their major elements (Cu and Sn) which are very close to the mean values of the pins examined under the μXRF technique. Their composition can be regarded as the typical composition of the alloy of the pins recovered in the sanctuary, although belonging to different typology and periods; the ALEA-P18 (fig-3.7.14-) belongs to the Middle Geometric while the ALEA-P3 (fig-3.7.13-) to the Late Geometric era. It is probably a common technological choice of a hard copper-tin alloy, for the casting of the pins assemblage; either this casting was performed at the sanctuary or elsewhere. The ALEA-P8 (fig-3.7.15-) pin has an analysed value of 17% tin. Its value is probably overestimated as a result of possible intergranular corrosion of the pin; considering that the absolute removal of corrosion products from a metal is not possible. The elements involved have already been presented in this chapter.

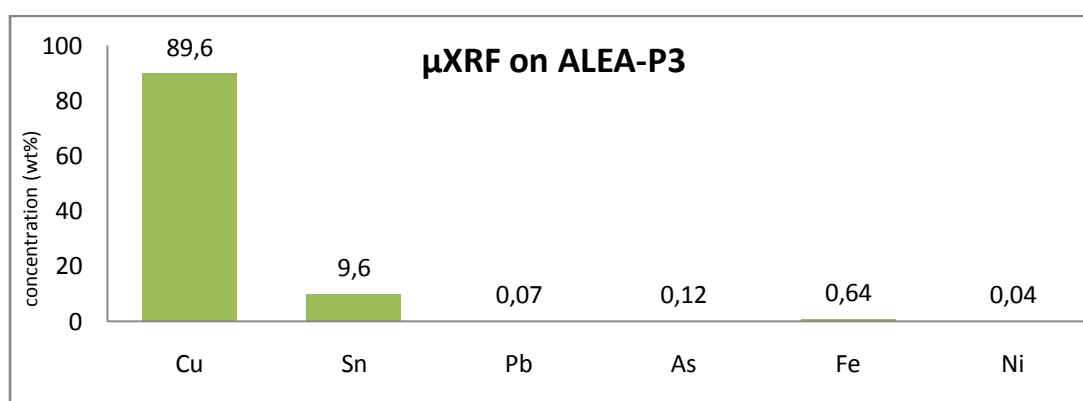


Figure 3.7.13. Bar chart presenting the concentration of elements in ALEA-P3, based on μXRF methodology

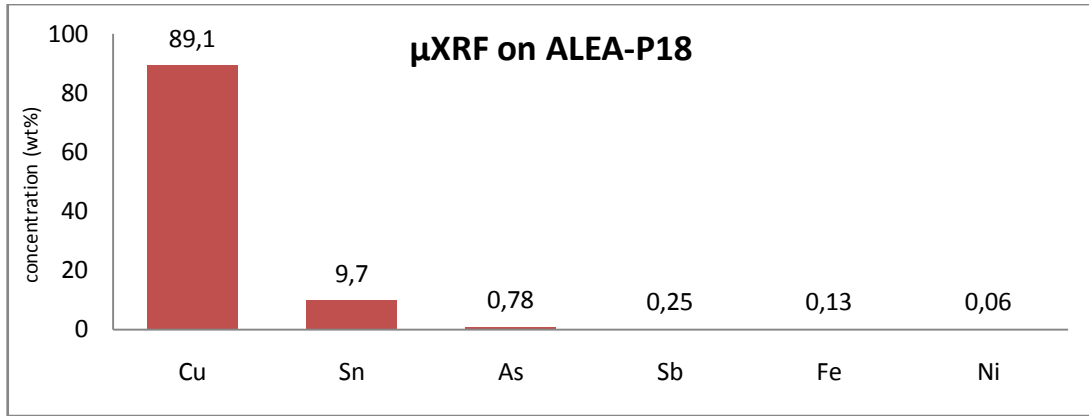


Figure 3.7.14. Bar chart presenting the concentration of elements in ALEA-P18, based on μ XRF methodology

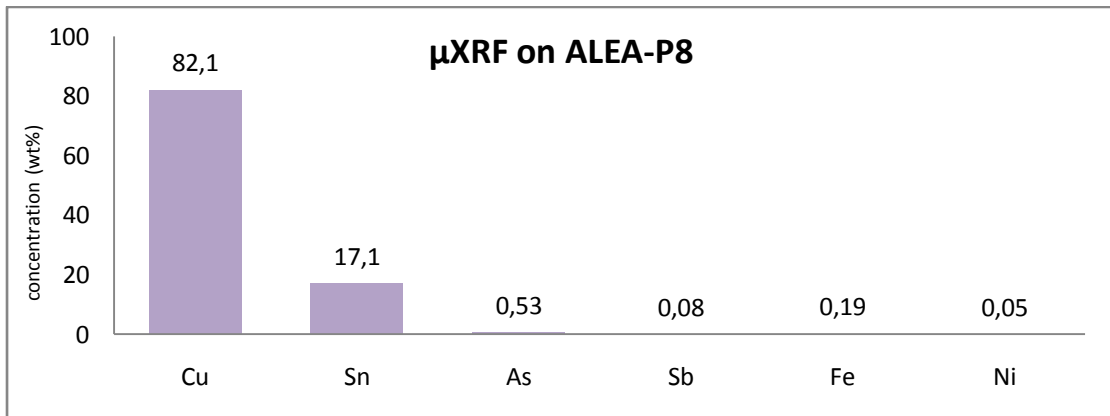


Figure 3.7.15. Bar chart presenting the concentration of elements in ALEA-P4, based on μ XRF methodology

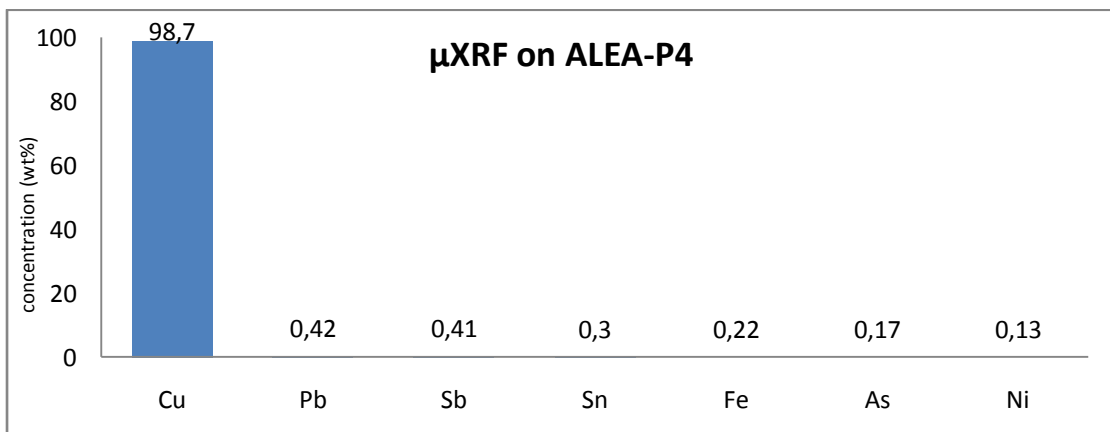


Figure 3.7.16. Bar chart presenting the concentration of elements in ALEA-P4, based on μ XRF methodology

The ALEA-P4 pin is a peculiar case worth examining, since its composition is far from the average; made of almost pure copper, as can be seen on the Cu/Sn chart

(fig-3.7.16-). The mean value of copper is 98.7% (± 0.1), while for the rest of the elements combined the percentage is less than ca 1.5%. As copper was rarely used unalloyed at the time and considering that the object belongs to the late Geometric period (chapter 2.1.), the proportion of the alloy used, is quite strange.

Although one could consider the object as made of native copper since it contains traces of tin and arsenic, which, rarely may exist in native copper (Gale, 1985), this is not likely the case. The amount of lead and antimony, which is higher than the ratio of the rest of the elements combined, is indicative of the nature of the ore; considering that the overwhelming majority of native copper is very pure. Besides, smelting was practiced at the time, and bronze alloys were known and almost exclusively used. Moreover, there seem to be major difficulties involved in the casting of objects made of almost pure copper (Pernicka, 1999). Shrinking phenomena during their solidification may occur; while the dissolving of a considerable amount of gasses due to high temperatures during the solidification process can be released into the metal, resulting in the increase of its porosity and thus the decrease of its strength (Konečná, 2012). Thus, the pin was either the result of recycling scrap of low tin bronzes, which is not very likely considering the very small amount of the included tin; either a poor technological choice, resulting from the deficient smelting of sulfidic or even oxide copper ore. Calcium and chromium, traced under SEM-EDS (not visualized on fig-3.7.16-), they may be indicative of this smelting process. Tin shortage during the time of its casting could be a factor worth considering, but based on its typology one should expect a similar pattern on the rest of the pins of the assemblage, which is not the case. The possibility that the pin may be the product of a completely different technology, of a different metal shop, made outside of the sanctuary cannot be excluded.

IV. CONCLUSIONS

From the ninth century onwards and especially during the Geometric period, metals constitute the majority of votive offerings at Athena Alea. Moreover, it is broadly recognised that bronze is the dominant alloy of the Geometric period; the warrior aristocracy of the times took an effort on accumulating bronzes, presumably as a symbol of high status (De Polignac 1995: 6, 14). Thus, the type of votives in relation to the total percentage of other findings in the sanctuary may be revealing of the type of worship and those involved in it. Jewellery and in particular pins, as objects closely linked with feminine and domestic life, although they are sporadically found in male deities sanctuaries or in other contexts, appear to be basically votives of women to female deities; in the extent of their powers goddesses appear to outshine even the gods. (De Polignac 1995: 26; Mitsopoulou, 2012: 595). Although, it is necessary to have a full compositional documentation of those findings, this is not the case. Even so, it is not always simple to evaluate and interpret the people involved- due to the complexity of the social, political or economic situation, the changes that took place or the role of the sanctuary on the local community- during that time. At early Tegea as in the larger sanctuaries of the period, this domination of bronze offerings may be an indication that the society in general had at its disposal greater wealth and many more materials than previously.

As already discussed, the applied methods of elemental analysis on the bronzes assemblage were the portable and micro XRF technique and the Scanning Electron Microscope (SEM) with Energy Dispersive Spectroscopy (EDS) technique. Based on the compositional results (chapter 3.6.), the mean value of copper on the alloy used for the pins and the wastes, based on μ XRF methodology, was 89.4% and 85.6% respectively. The large amount of tin on the assemblage, suggests that the majority of the objects under study were not produced with scrap metal, since the use of recycled bronze results to a much lower tin content in the analysed material. This is enhanced by the fact that quite significant amounts of antimony are observed in ten pins (ALEA-P1, -P2, -P4, -P5, -P6, -P12, -P13, -P17, -P18, -P25), reaching up to 0.43%. Since older bronzes were not correspondingly high in antimony, the use of fresh metal is more likely (Craddock, 1976). The fact that antimony was also detected on all of the wastes supports the hypothesis. The presence of arsenic, though, in the alloy seems to complicate the decision considering the origin of the metal used; it is

clearly limited in relation to tin, since its percentage is generally less than 1%. Thus, the use of arsenic was probably accidental, resulting from the melting of scrap or more likely to the choice of mining arsenate copper ores. Based on the aforementioned respecting antimony and its lack on older arsenical bronzes, the use of fresh metal from arsenical copper ores for the assemblage is strengthening.

Besides, the discovery of such large number of votives, as well as the presence of a votive pit in the sanctuary, for the discard of older metal offerings is an indication that not extensive recycling was taking place. This votive pit (bothros) represents one of the best stratigraphic contexts in the sanctuary and bears evidence of use from the ProtoGeometric to Late Geometric period, with the vast majority of its material dating to the Geometric, particularly the Middle and Late Geometric periods. Thus, around that time it was covered, on purpose with silt and the metalshop was installed above it. The metalshop was used as such in the Late Geometric and into the Early Archaic period. The absence of slag in the workshop of the sanctuary indicates that secondary production, which involved the melting and shaping of metal objects, was taking place (Nordquist, 2014: 176-195). The presence of the bothros along with the results of the chemical analysis on the small assemblage indicate, as previously mentioned, that perhaps only a small proportion of the votives was recycled. That of course does not exclude the import of scrap in the sanctuary from elsewhere, albeit the analysis seem to point in the direction of fresh metal use.

Copper and tin concentrations of the pins fall within the range of both the Geometric and Archaic years (Craddock, 1976; 1977) but based on the propositions of the alloys no attribution to a specific era can be made, since the analysis could not consistently yield a typical tin content on the majority of the assemblage for each period. Thus, the main ascertainment is that the Iron Age copper smiths seem to continue the Late Bronze Age metalworking tradition of using standard binary bronzes; albeit tin content around 10% is the alloying element, instead of the previously used arsenic (Tylecote, 1982; Mangou, 1994: 173). Although, as aforementioned, the wide range of tin proportions falls into the categories of typical archaeological bronzes of the period, some outliers appear. On the chart (fig.-4.1-) presenting the assemblage for copper versus tin, one can notice that there is basically one large group of pins, formed. The ALEA-P4 is an exception among the analysed pins, consisting of almost pure copper. Based on the presence and percentages of trace elements in the analysis, the metal used cannot be of native copper; since the native

copper is, in general, purer with characteristic impurities. The very low tin content of the artifact (0.3%), possibly indicates the smelting of a natural copper-tin ore or the melting of fresh copper metal with a quantity of bronze scrap, originally containing a higher amount of tin (Gale et al, 1985; Charalampous et al, 2014). Moreover, the ALEA-P15 differs in its lead proportion; the value of Cu versus Sn corresponds well to the mean prices of the rest of the group. The ALEA-P2 has a high proportion of trace elements, while the ALEA-P8 contains the maximum amount of tin. The trace element pattern of the pins, along with the iron and lead concentration that do not systematically vary with the rise of the tin concentration, points rather to an intentional addition of tin to the copper than to a reuse of bronze scrap (Kiderlen, 2016).

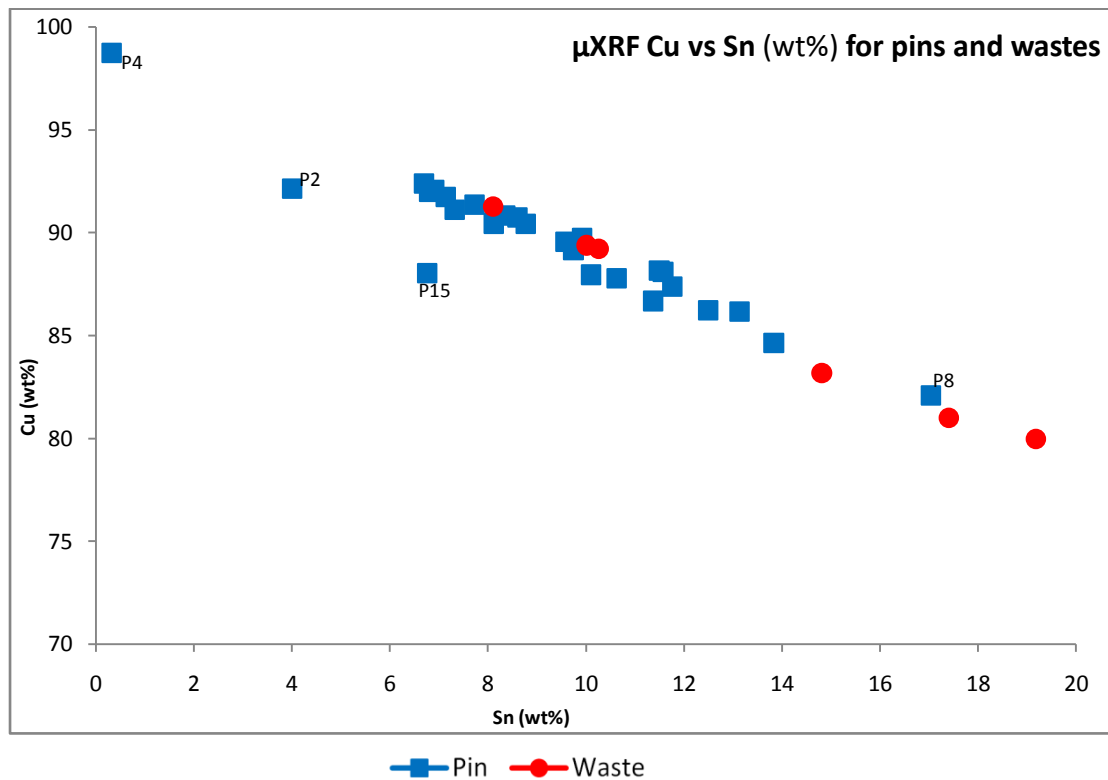


Figure 4.1. Scatter plot presenting the distribution of Cu versus Sn on pins and wastes, based on μ XRF methodology

Accordingly, for the wastes two distinct groups can be observed. The first is composed of hard bronze with values for tin ranging between 8-11%, clearly not belonging to the hard phase δ of an alloy while the second group ranges between 14-20%, belonging to extremely hard but at the same time very brittle bronzes. On the chart (fig.-4.1-), one can see that the wastes are overlapping the pins values on half of

the occasion; not necessarily interpreted as common technology or origin, mainly because the wastes cannot be classified. Moreover, the sample of this study is limited compared to the whole of the excavation bronze finds. Thus, statistically it cannot accurately reflect the image of the metallurgy in the sanctuary.

The variety of tin concentration in the assemblage does not reflect the copper smith's intention to use the hardness and durability of bronze proportional to the use of the objects; although it seems that they were able to control the percentages of added tin in copper. This practice appears to be a deliberate one, irrespectively of time or workshop attributions, but also not particularly associated with a specific type of object, since the wastes seem to contain almost equal amounts of the element. Seems more likely that the copper smiths who produced them had the intention to obtain a yellowish, "gold like", colour, probably in an attempt to imitate the appearance of similar artifacts made of the precious metal, since the colour and the imitation of precious materials was a desirable effect of the metal offerings of the sanctuary of Athena Alea (De Polignac, 1995: 20; Bassiakos, 2014: 589). Even though, there is a suggestion from various scholars regarding a tin shortage during the EIA, its proportions on the assemblage indicate abundance of the element. It is probably not a coincidence, since tin is the most common alloying element of copper during the Iron Age and has been traced on various types of objects around Greece (Orfanou, 2015: 311); the origin of tin used in the extended Hellenic space and more generally in the Eastern Mediterranean area at the time remains a subject of research.

From the microscopic observation on the pins assemblage it is concluded that these were originally cast, probably into two separate open moulds and then forged; considering that the objects bear traces of further attenuation on their casting marks.

Additionally, it seems that there was not even a consistent use of the same alloy for the pins belonging to the same typology (after Kilian-Dirlmeier, 1984) (fig. 4.2-). The only group that is clearly formed is the one belonging to the Orientalizing era; overlapping, though, other periods. Thus, the BV (ALEA-P13) and EIII (ALEA-P16) having a tin proportion of 8.6 and 8.8%, respectively; leading to the conclusion of their possible origin of the same workshop. The rest of the pins, though, may also originate from technology acquired locally; something that does not seem to apply to the case of the ALEA-P4 pin, since it seems like been of a completely different technology. The Orientalizing along with the Late Geometric-Subgeometric type of

pins seems to be in a steady proportion of their tin content, the former ranging between 6.8 to 8.8% of tin and the latter range between 6.7 to 12.5% tin.

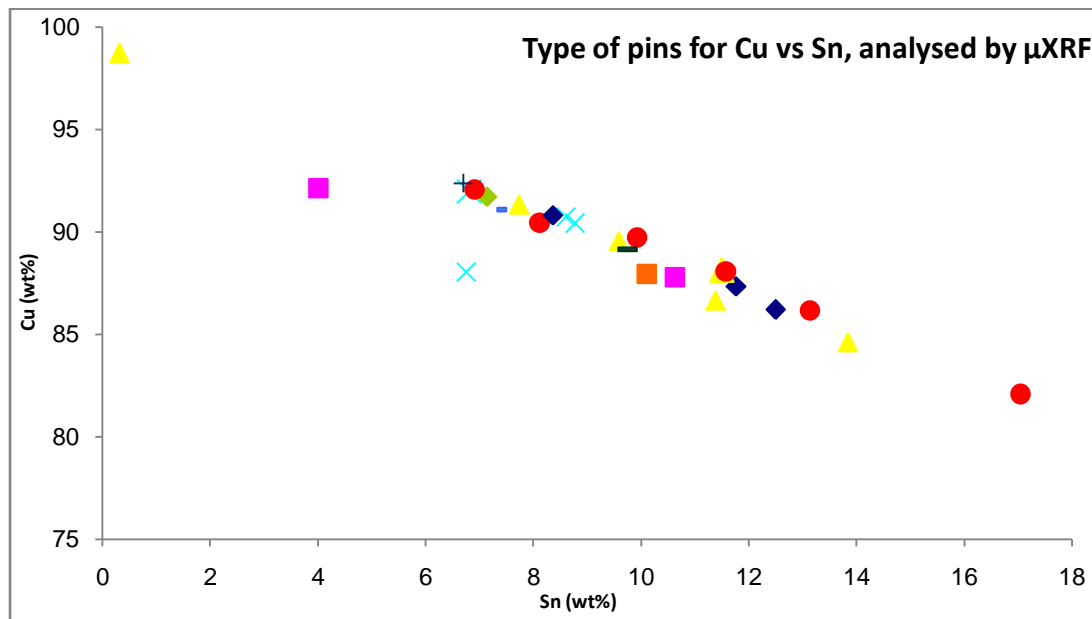


Figure 4.2. Chart presenting the distribution of pins for Cu versus Sn according to their typology, based on μ XRF methodology

The fact that the pins consist of similar alloys, as well as, to alloys of earlier periods, indicating either: a) a steady technology throughout the duration of more than two centuries, either b) a conservative point of view of the seasonal or permanent operation of a local workshop, either c) that the pins in question should be dated in different periods. The answer goes beyond the scope of this thesis, but in any case it is possible that the pin types were used since much earlier than the proposed time frame. Possibly, this dispersion across time and compositional values of the assemblage indicates that the phenomenon of high tin content should not be attributed to particular workshops or the preferences of particular individuals, but was instead a marked feature, widely dispersed in time.

Making an effort to establish a frame of origin for the assemblage based on its alloy composition, any conclusion can be rather unsubstantiated; if appropriate sampling and testing does not take place beforehand. In order to trace the origin of the metals, up to date, the lead isotope method must be engaged, although the results of

the method are still under dispute among scholars, since the obtained results usually fall on around 20% of certainty (Gale et al, 1985). Certain minor elements included in a copper ore can be very helpful on its correlation with a specific area of mining; especially when combined with lead isotope compositional data (Pernicka, 1999). Albeit, these elements (Ni, Sb, Bi, As, Ag) may be indicative of the ore sources, at least to a certain extent. Moreover, not only do the minor elements usually vary widely in content through a given ore body, but during the smelting of an ore, disturbances between the minor elements in the ore and the metal come from added fluxes, type of fuel etc. may occur (Gale et al, 1985). In the case of the bronze assemblage, the minor elements originating either from the original copper ore or from use of scrap bronze, mainly characterized by the presence, besides tin, of arsenic, lead and antimony. Based on this, one can roughly estimate that these metals could possibly have been derived from copper mined in the extended Aegean and Balkan area, where there exist relatively high rates of arsenic, tin and also of traceable trace elements; although Eastern areas of the Mediterranean cannot be excluded, considering the trade mechanisms that have been developed since the Bronze Age, around the Mediterranean. It is less likely though, to origin from Cyprus, where tin does not exist on copper ores (Craddock, 1976; Charalambous et al, 2014).

Regarding the protocols of analysis applied, the most important question is not how close are the p-XRF, μ XRF and SEM-EDS measurements, but rather how do the three datasets lead to the same answers to the questions of interest. In general, normalized XRF analyses could not be confirmed by the corresponding SEM-EDX due to the different sensitivity of the technique, the unevenness of the surfaces of the samples and their different degree of corrosion products cover. SEM-EDX and XRF analysis thus, despite different variance ranges for each alloy and excluding some extreme values, they can be related to the main volume alloys. The XRF technique can trace elements of minor quantities, but not light elements; the corrosion products of the metals involved always pose a challenge. The missing elements such as chlorine, oxygen and sulfur ions, nitrates and carbon dioxide; are the elements usually involved in corrosion processes. The parameter that decisively influenced the composition of the specimens after their excavation from the sanctuary was the degree of their surface coverage with soil and corrosion products. Although the analytical techniques performed are widely used in heritage materials, the nature of ancient metal corrosion causes several problems, resulting in significant data constraints. As

regards, the investigation of possible corrosion products based on optical microscopy observation and analysis on mostly "large" surfaces analysed under SEM-EDS (e.g. x50-x200), at least in terms of bronze alloys dominated by the combination of Cu₂O and CuO; while locally (on the parts of the surfaces that were high concentrations of Si, Al, Ca, Fe, etc.) were probably formed oxides of these elements, such as: SiO₂, Al₂O₃, CaCO₃, FeO, Fe₂O₃, et al.. Thus, regarding the spectroscopic analyses of the assemblage an overestimation of the aforementioned elements may have been the case; although a surface removal of the observed corrosion products down to the original metal was attempted. This fact, though, may become the trigger for exploring the possibility of approaching an alloy composition by determining the composition of its corrosion products.

Ultimately, it should be held in mind that spectroscopic techniques like XRF and SEM-EDS can perform qualitative and quantitative elemental analysis under proper handling and interpretation, when clear questions are made and reasonable expectations are formulated by the user; and that in general, the solution to any cultural heritage problem rarely depends on the application of a single technique and an interdisciplinary approach is always requisite.

V. REFERENCES

- Adriaens, A., (2005), Non-destructive analysis and testing of museum objects: An overview of 5 years of research, *Spectrochimica Acta Part B* 60, Elsevier Ltd, p.1503 – 1516
- Anthony, J. W., Bideaux, R.A., Bladh, K.W., and Nichols, M.C., (Eds), (2016), *Handbook of Mineralogy*, Mineralogical Society of America, [ebook] Available at: <http://www.handbookofmineralogy.org/search.html?p=all> [Accessed 3 Nov. 2017]
- Arafat, A., Na'es, M., et al., (2013), Combined in situ micro-XRF, LIBS and SEM-EDS analysis of base metal and corrosion products for Islamic copper alloyed artefacts from Umm Qais museum, Jordan, *Journal of Cultural Heritage* 14, Elsevier Ltd, p. 261–269
- Argyropoulos, V., Karydas, A.G., et al., (2002), A scientific approach for the conservation of the outdoor bronze monument of Theodoros Kolokotronis, *Conservation Science* 2002, p. 141-147
- Bassiakos, Y., (2014), Metals and slagged residues from Tegea: an analysis and metallurgical notes, in *TEGEA I-Investigations in the Temple of Athena Alea 1991–94*, Østby, E., (editor), *Papers and Monographs from the Norwegian Institute at Athens Volume 3*
- Bayley, J., et al., (2008), *Metals & Metalworking: A research framework for archaeometallurgy*, The Historical Metallurgy Society Ltd., (Bayley, J., Crossley D., and Ponting, M., Eds), Occasional Publication No 6, ISBN 978-0-9560225-0-9
- Bennallack, K., Hahn, L., et al., (2013), Field applications of p-XRF for cultural heritage diagnostics: Rapid in-field archaeological analyses in the Faynan ancient copper production zone, Jordan, *JCPDS-International Centre for Diffraction Data*, ISSN 1097-0002
- Bottaini, C., Mirão, J., (2015), Energy dispersive X-ray fluorescence spectroscopy/Monte Carlo simulation approach for the non-destructive analysis of corrosion patina-bearing alloys in archaeological bronzes: The case of the bowl from the Fareleira 3 site (Vidigueira, South Portugal), *Spectrochimica Acta Part B* 103–104, Elsevier Ltd, p. 9–13
- Bozzini, B., Alemán, B., et al., (2016), Novel insight into bronze disease gained by synchrotron-based photoelectron spectromicroscopy, in support of electrochemical treatment strategies, *Studies in Conservation*, DOI:10.1080/00393630.2016.1235339
- Burkert, W., (1992), *The Orientalizing Revolution- Near Eastern Influence on Greek Culture in the Early Archaic Age (Revealing Antiquity)*, Harvard University Press
- Caple, C., (2006), *Objects: reluctant witnesses to the past*, Routledge, ISBN10: 0-415-30589-6

- Charalambous A., Kassianidou V., Papassavas G., (2014), A compositional study of Cypriot bronzes dating to the Early Iron Age using portable X-ray fluorescence spectrometry (p-XRF). *Journal of Archaeological Science* 46, p. 205–216, <http://dx.doi.org/10.1016/j.jas.2014.03.006>
- Charalambous, A., (2015), A diachronic study of Cypriot copper alloy artefacts, *Journal of Archaeological Science: Reports*, <http://dx.doi.org/10.1016/j.jasrep.2015.12.010>
- Charles, J.A., (1967), Early Arsenical Bronzes-A Metallurgical View, *American Journal of Archaeology*, Vol. 71, No. 1, p. 21-26
- Charles, J.A., (1973), Heterogeneity in Metals, *Archaeometry* 15:1, p. 105-114
- Coldstream, J.N., (2008), *Greek Geometric Pottery-A survey of ten local styles and their chronology*, 2nd edition, Bristol Phoenix Press
- Craddock, P., T., (1976), The Composition of the Copper Alloys used by the Greek, Etruscan and Roman Civilizations-1.The Greeks before the Archaic Period, *Journal of Archaeological Science*, 3, p. 93-113
- Craddock, P.T., (2009), *Scientific investigation of copies, fakes and forgeries*, Elsevier Ltd
- De Polignac, F., (1995), *Cults, Territory and the Origins of the Greek City*, State University Of Chicago Press
- Degrigny, Ch., Karydas, A.G., et al.,(2007), Methodology for the in-situ analyses of historic steel armours with portable milli and micro-XRF spectrometers, *Proceedings-METAL 07*, vol. 2. Innovative investigation of metal artefacts, p. 26-34
- Doonan R., Day P. M. et al, (2007), Lane excuses for emerging complexity in Early Bronze Age Crete: the metallurgical finds from Poros Katsambas and their context, in M. P. Day and R. Doonan, *Metallurgy in the Early Bronze Age Aegean*, Sheffield Studies in Aegean Archaeology, Great Britain, Oxbow, 98-122.
- Dugas, C., (1921), Le Sanctuaire d'Alea Athena a Tegee avant le IV siecle, *BCH* 45, p.335-435
- Dugas, C. Berchmans J., Clemmensen, M., (1924), *Le sanctuaire d'Aléa Athéna à Tégée au IVe siècle*. P. Geuthner, Paris
- Egerton, R.F., (2005), *Physical Principles of Electron Microscopy. An Introduction to SEM, TEM and AEM*, Springer Science &Business Media, Inc., New York, ISBN-13: 978-0387-25800-0, 158-165, 167.
- Everhart, T.E., Thornley, R.F.M., (1960), Wide-band Detector for Micro-microampere Low-energy Electron Currents, *J.Sci.Instrum.* 37 (7), 246–248.
- Fang J.L., and McDonnell, G., (2011), The colour of copper alloys, *Historical Metallurgy* 45 (1), p. 52-61

- Fernandes et al., (2013), The use of Hand-Held XRF for investigating the composition and corrosion of Roman copper-alloyed artefacts, *Heritage Science*, 1:30, DOI: doi:10.1186/2050-7445-1-30
- Ferretti, M., Muioli, P., (1998), The use of portable XRF systems for preliminary compositional surveys on large bronze objects-A critical review after some years' experience, *Proceedings of the international conference on metals conservation*, Mourey, W., Robbiola, L., (Eds.), James&James Ltd, p. 39-44
- Ferretti, M., (2014), The investigation of ancient metal artefacts by portable X-ray fluorescence devices, *J. Anal. At. Spectrometry*. 29, p. 1753-1766
- Fontana, N.M., (1986), *Corrosion engineering*, 3rd edition, New York: McGraw-Hill Inc
- Gale, N.H., Stos-Gale, S.A., (1982), Bronze Age Copper Sources in the Mediterranean: A New Approach, *Science*, v.216, n.4541, p. 11-19
- Gale N. H. et al., (1985), Alloy types and Copper sources of Anatolians Copper alloy artifacts, *Anatolian Studies*, vol. 35, p. 143- 173
- Gale H. N., Kayafa M. and Stos-Gale Z. A., (2008), Early Helladic Metallurgy at Raphina, Attica, and the Role of Lavrion, in I. Tzachili, *Aegean Metallurgy in the Bronze Age, Proceedings of an International Symposium Held at the University of Crete, Rethymnon, Greece, 2004, I. Ta Pragmata*, p. 87-104.
- Gale H. N., Kayafa M. and Stos-Gale Z. A., (2009), Further Evidence for Bronze Age Production of Copper from Ores in the Lavrion Ore District, Attica, Greece, *Proceedings of the 2nd International Conference Archaeometallurgy in Europe, Aquileia 2007, Milan*, p. 158-176
- Georgakopoulou M., (2004), Examination of Copper Slags from the Early Bronze Age Site of Daskaleio-Kavos on the island of Keros (Cyclades,Greece), *Institute of Archaeo-Metallurgical Studies* 24, p. 3-12
- Gettens, R. J., (1963), The corrosion products of metal antiquities, *Annual Report of the Board of Regents of the Smithsonian Institution*, vol. 1
- Garfinkel Y, Klimscha F, Shalev S, Rosenberg D., (2014), The Beginning of Metallurgy in the Southern Levant: A Late 6th Millennium CalBC Copper Awl from Tel Tsaf, Israel, *PLoS ONE* 9(3): e92591, DOI:10.1371/journal.pone.0092591
- Grigorakakis, G., Ioannidis, P., Tsatsaris, A., (2014a), Αρχαιολογικό Μουσείο Τεγέας. Ένα καινοτόμο τεχνολογικό ταξίδι στη γη του Μύθου και της Ιστορίας / *Archaeological Museum of Tegea: An innovative technological journey to the land of myth and history*, p. 23-82.

- Grigorakakis, G., (2014b), Η Ιστορική και Αρχαιολογική Έρευνα στην Πελοπόννησο, όπως προκύπτει από τα αρχεία των Γ.Α.Κ. Νομών Πελοποννήσου και αρχεία άλλων φορέων, Αρχαιολογικό Ινστιτούτο Πελοποννησιακών Σπουδών: Η Αρχαιολογία στην Πελοπόννησο 2, Τρίπολη, p. 71-87
- Goldstein J.I. et al., (2003), Scanning Electron Microscopy and X-Ray Microanalysis, 3rd edition, Kluwer Academic/Plenum Publishers, New York, ISBN: 0-306-47292-9
- Hall, J.M., (2007), Polis, Identity and Ethnic Community, in The Cambridge Companion to Archaic Greece, Shapiro, H.A (editor), Cambridge Companions to the Ancient World
- Haynes, D., 1992. The Technique of Greek Bronze Statuary. Mainz am Rhein: Verlag Phillip von Zabern
- Heginbotham, A., Bassett, J., et al., (2015), The Copper CHARM Set: A New Set of Certified Reference Materials for the Standardization of Quantitative X-Ray Fluorescence Analysis of Heritage Copper Alloys*. *Archaeometry*, 57: 856–868. doi: 10.1111/arc.12117.
- Hunt, A.M.W, Speakman, R.J., (2015), Portable XRF analysis of archaeological sediments and ceramics, *Journal of Archaeological Science* 53, p.626-638 <http://dx.doi.org/10.1016/j.jas.2014.11.031>
- Ida, H., (2004), X-ray fluorescence analysis with portable instruments, PhD thesis, Department of Materials Science and Engineering, Kyoto University
- Jones, D.A., (1992), Principles and prevention of corrosion, New York: MacMillan Publishing Company
- Kantarelou, V., Zarkadas, Ch., et al., (2007), A novel approach on the combined in-situ application of LIBS and μ -XRF spectrometers for the characterization of copper alloy corrosion products, *Proceedings- METAL 07*, vol. 2. Innovative investigation of metal artefacts, p. 35-41
- Kantarelou, V., Karydas, A.G., et al., (2007b), Micro-XRF Analysis of High Tin Bronze Mirrors at the museum of Ancient Messene in Greece, *Proceedings of the International Conference on Conservation Strategies for Saving Indoor Metallic Collections*, p. 93-99
- Kantarelou, V., Karydas, A.G., et al., (2015), In situ scanning micro-XRF analyses of gilded bronze figurines at the National Museum of Damascus, *J. Anal. At. Spectrom.*, 30, p. 1787-1798
- Karydas, A.G., Brecoulaki, X., et al., (2005), Importance of in-situ EDXRF Measurements in the Preservation and Conservation of Material Culture, *X-rays for Archaeology*, M. Uda et al. (eds.), p. 27–53

- Karydas, A.G., (2007), Application of a portable XRF spectrometer for the noninvasive analysis of museum metal artefacts, *Annali di Chimica*, 97, 2007, by Società Chimica Italiana, p. 419-432
- Karydas, A.G., Padilla-Alvarez, R., et al., (2014), Handheld XRF analysis of the old Mexican feather headdress in the Weltmuseum Vienna, *X-Ray Spectrometry* 43, John Wiley & Sons, Ltd, p. 138–145
- Kassianidou, V. and Knapp, A. B., (2005), Archaeometallurgy in the Mediterranean: The Social Context of Mining, Technology, and Trade, in *The Archaeology of Mediterranean Prehistory* (Eds E. Blake and A. B. Knapp), Blackwell Publishing Ltd, Oxford, UK. doi: 10.1002/9780470773536.ch9
- Kiderlen, M., Bode, M., et al (2016), Tripod cauldrons produced at Olympia give evidence for trade with copper from Faynan (Jordan) to South West Greece, c. 950–750 BCE, *Journal of Archaeological Science: Reports* 8, p.303–313, doi.org/10.1016/j.jasrep.2016.06.013
- Kilian-Dirlmeier, I., (1984), *Nadeln der frühhelladischen bis archaischen Zeit von der Peloponnes*, PBF 13,8, Munich
- Konečná, R., Fintová, S., (2012), Copper and Copper Alloys: Casting, Classification and Characteristic Microstructures, *Copper Alloys - Early Applications and Current Performance – Enhancing Processes*, Dr. Luca Collini (Ed.), InTech, ISBN: 978-953-51-0160-4
- Konofagos, K., (1967), *Μεταλλογνωσία- Τα Βιομηχανικά κράματα*, τόμος III, 1η έκδοση, Αθήνα
- Lankton, J.W., Gratuze, B., et al., (2016), Scientific analysis of ancient glass: Answering the questions and questioning the answers. In: F. Gan, Q. Li and J. Henderson, eds., *Recent Advances in the Scientific Research on Ancient Glass and Glaze. Series on Archaeology and History of Science in China*, Vol. 2. Singapore: World Scientific, p. 267-301
- Liritzis, I., Zacharias, N., (2011), Portable XRF of Archaeological Artifacts: Current Research, Potentials and Limitations, ch.6, in M. S. Shackley, *X-Ray Fluorescence Spectrometry (XRF) in Geoarchaeology*, USA, Springer, p. 109-142.
- Lloyd, G.E., (1987), Atomic Number and Crystallographic Contrast Images with the SEM: a Review of Backscattered Electron Techniques, *Mineral Mag* 51, p. 3-19.
- Mainz, V.V., (2015), The Metals of Antiquity and Their Alloys, In *Chemical Technology in Antiquity*; Rasmussen, Seth C.; ACS Symposium Series; American Chemical Society: Washington, DC, DOI:10.1021/bk-2015-1211.ch005
- Mangou E., (1994), *Μελέτη αρχαίων χάλκινων αντικειμένων από τον Ελλαδικό χώρο*, Διδακτορική διατριβή, Πανεπιστήμιο Πατρών

- Mangou E., Ioannou, P.V., (1997), On the Chemical Composition of Prehistoric Greek copper-based artefacts from the Aegean region, *The Annual of the British School at Athens*, 92, p.59-72, DOI:10.1017/S0068245400016634
- Meeks, N.D., (1986), Tin-rich surfaces on bronze-Some experimental and archaeological considerations, *Archaeometry*, 28, 2, Oxford: Research laboratory for archaeology and the history of art, p. 133-162
- Melessanaki, K. Mastrogiannidou, A. et al., (2003), Analysis of Archaeological Objects with LM^{NT}I, a new Transportable LIBS Instrument, *Proceedings of the 4th Symposium of the Hellenic Society for Archaeometry*, Facorellis, Y., Zacharias, N., Polikreti, K. (editors), p. 441-444
- Mitsopoulou, E., (2012), Τα ιερά της Αθηνάς στην Πελοπόννησο, Διδακτορική διατριβή, Αριστοτέλειο Πανεπιστήμιο Θεσσαλονίκης, Θεσσαλονίκη
- Moropoulou, A., Zacharias, N., et al, (2015), Analytical and Technological Examination of Glass Tesserae from Hagia Sophia, *Microchemical Journal* (2015), doi: 10.1016/j.microc.2015.11.020
- Musilek, L., Cechak, T., Trojek, T., (2012), X-ray fluorescence in investigations of cultural relics and archaeological finds, *Applied Radiation and Isotopes* 70, Elsevier Ltd, p. 1193–1202
- Neff, D., Reguer, S., Dillmann, P., (2013), Analytical techniques for the study of corrosion of metallic heritage artefacts: from micrometer to nanometer scales, *Corrosion and conservation of cultural heritage metallic artefacts*, Woodhead Publishing Ltd, p. 55-81,
- Nixon, W.C., (1971), *The General Principles of Scanning Electron Microscopy*, Philosophical Transactions of the Royal Society of London. Series B, Biological Sciences, Vol 261, No 837
- Nordquist, G.C., (2014), Results of the fieldwork in the temple sector, in *TEGEA I- Investigations in the Temple of Athena Alea 1991–94*, Østby, E., (editor), *Papers and Monographs from the Norwegian Institute at Athens Volume 3*, p. 57-195
- Nørgaard, H.W., (2017), Portable XRF on Prehistoric Bronze Artefacts: Limitations and Use for the Detection of Bronze Age Metal Workshops, *Open Archaeology* 2017; 3: 101–122, <https://doi.org/10.1515/opar-2017-0006>
- Orfanou V., Rehren, Th., (2014), A (not so) dangerous method: p-XRF vs. EPMAWDS analyses of copper-based artefacts, *Archaeological and Anthropological Sciences*, DOI 10.1007/s12520-014-0198-z
- Orfanou V., (2015), *Early Iron Age Greek copper-based technology: votive offerings from Thessaly*, PhD thesis, University College London- Institute of Archaeology

- Østby, E., Luce, J.M., et al, (1994), The Sanctuary of Athena Alea at Tegea: First Preliminary Report (1990–1992), *OpAth* 20(8)
- Østby, E., (2014), The Norwegian excavation project in the sanctuary of Athena Alea at Tegea: an introduction, in *TEGEA I-Investigations in the Temple of Athena Alea 1991–94*, Østby, E., (editor), *Papers and Monographs from the Norwegian Institute at Athens* Volume 3, p. 1-10
- Østby, E.,(2014), The sanctuary of Alea at Tegea in the pre-classical period, in *TEGEA I-Investigations in the Temple of Athena Alea 1991–94*, Østby, E., (editor), *Papers and Monographs from the Norwegian Institute at Athens* Volume 3, p. 11-56
- Palamara, E., Zacharias, N. et al, (2016), Studying a Funerary Roman Vessel Glass Collection from Patras, Greece: An Interdisciplinary Characterisation and Use Study, *STAR: Science & Technology of Archaeological Research*, 2:2, p. 203-216, DOI: 10.1080/20548923.2016.1239868
- Papadimitriou, G.D., (2001), Η εξέλιξη των Κραμάτων Χαλκού στον Ελλαδικό Χώρο μέχρι το Τέλος της Γεωμετρικής Εποχής: Κραματικές Προσμίξεις και Τεχνολογική Εξέλιξη", *Αρχαιομετρικές Μελέτες για την Ελληνική Προϊστορία και Αρχαιότητα* (Μπασιάκος, Ι., Αλούπη, Ε., Φακορέλης, Γ., επιμ.), Αθήνα, p. 596-597
- Papandreopoulos, P., (2012), Διερεύνηση της φυσικοχημικής συμπεριφοράς και των μηχανισμών των προϊόντων επιφανειακής διάβρωσης κραμάτων χαλκού με καταστρεπτικές και μη μεθόδους, Διδακτορική διατριβή, Ε.Μ.Π., Αθήνα
- Pernicka, E., (1999), Trace Element Fingerprinting of Ancient Copper: A Guide to Technology or Provenance? in *Metals in Antiquity*, Young, S., Pollard, A.M., Budd P.M, and Ixer R., (eds), *BAR International Series* 792, p. 163-171
- Radivojevic, M., et al., (2017), Experimental design of the Cu-As-Sn ternary colour diagram, *Journal of Archaeological Science*, <https://doi.org/10.1016/j.jas.2017.12.001>
- Rapp, G.Jr., Jones, R.E., et al., (1978), *Analyses of the Metal Artifacts, Excavations at Nichoria in Southwest Greece, Vol. I, Site, Environs, and Techniques*, (Rapp, G.Jr., Aschenbrenner, S., Eds), Published by the University of Minnesota Press, Minneapolis, ISBN 0-8166-0824-5
- Rapp. G., (1982), Native Copper and the Beginning of Smelting: Chemical Studies, in *Early Metallurgy in Cyprus*, (Eds Muhly, J. D., Maddin, R., and Karageorghis, V.), Nicosia
- Romaios, K., (1911), Γενική έκθεσις περί των εν Τεγέα ανασκαφών εν έτει 1910, Η εν Αθήναις Αρχαιολογική Εταιρεία (εκδότης), Πρακτικά της εν Αθήναις Αρχαιολογικής Εταιρείας σελ.274-276
<http://digi.ub.uni-heidelberg.de/diglit/prakt1910/0276>

- Schreiner, M., Frühmann, B., (2004), X-rays in art and archaeology-an overview, International Centre for Diffraction Data 2004, *Advances in X-ray Analysis*, Volume 47, p. 1-17
- Schweizer, F., (1994), Bronze Objects from Lake Sites: From Patina to “Biography” on “Ancient & historic metals: conservation and scientific research”, Scott, D.A., Podany, J., Considine, B.B. (editors), Proceedings of a symposium organized by the J.Paul Getty Museum and the Getty Conservation Institute, November 1991
- Tarditi, C., (2005), The sanctuary of Athena Alea: Recent excavation in the northern area. Results and problems. In *Ancient Arcadia. Papers from the third international seminar on ancient Arcadia, held at the Norwegian Institute at Athens, 7-10 May 2002* (Papers from the Norwegian Institute at Athens 8), edited by E. Østby
- Tarditi, Ch., (2014), The Sanctuary of Athena Alea at Tegea: Excavations in the Northern Sector 2004 in TEGEA II-Investigations in the Sanctuary of Athena Alea 1990–94 and 2004, Østby, E., (editor), *Papers and Monographs from the Norwegian Institute at Athens Volume 4*
- Trojek, T., Musilek, L., Cechak, T., (2014), X-ray fluorescence analysis of cultural artefacts — Applications to the Czech heritage, *Radiation Physics and Chemistry 95*, Elsevier Ltd, p. 381–384
- Tsatsaris, A., Grigorakakis, G., (2015), Τεγεάτις: Ένα Χαρτογραφικό Ταξίδι στη Γη του Μύθου και της Ιστορίας, στο "Χαρτογραφίες Νου, Ψυχής και Γνώσης"- Τιμητικός Τόμος Ομότιμου Καθηγητή Μύρωνα Μυρίδη, Θεσσαλονίκη, p. 176-189
- Tselios, Ch., (2013), Η Μεταλλουργία και η Μεταλλοτεχνία του Χαλκού κατά την Υστεροελλαδική Περίοδο στη Νοτιοδυτική Πελοπόννησο, Αρχαιομετρική Μελέτη των Χαλκών Τεχνέργων της Υστεροελλαδικής Μεσσηνίας, PhD thesis, Αθήνα
- Tylecote, R. F., (1992), A history of metallurgy, 2nd edition, The Institute of Materials, Maney Publishing, ISBN 1-902653-79-3
- Uhlig, H.H., (1971), Corrosion and corrosion control, 2nd edition, New York: John Wiley & Sons Inc
- Van Brempt, L., Kassianidou, V., (2015), Facing the complexity of copper-sulphide ore smelting and assessing the role of copper in south-central Cyprus: A comparative study of the slag assemblage from Late Bronze Age Kalavassos-Ayios Dhimitrios, *Journal of Archaeological Science: Reports*, <http://dx.doi.org/10.1016/j.jasrep.2015.08.022>
- Voyatzis, M., (1990), The early sanctuary of Athena Alea at Tegea, Paul Åströms förlag, Göteborg

Weisser, T.D., (1975), The de-alloying of copper alloys, in Leigh, D., Moncrieff, A., Oddy, W.A., & Pratt, P., (eds), Conservation in archaeology and the applied arts-reprints of the Stockholm congress, June, 1975, London: IIC, p. 207-214

APPENTICES

Appendix I

Charts and Images



Image I.1. Map of the Tegea region (Tsatsaris et al, 2015)



Image I.2. Aerial photograph of the sanctuary of Athena Alea (Photo: Archaeological Museum of Tegea)

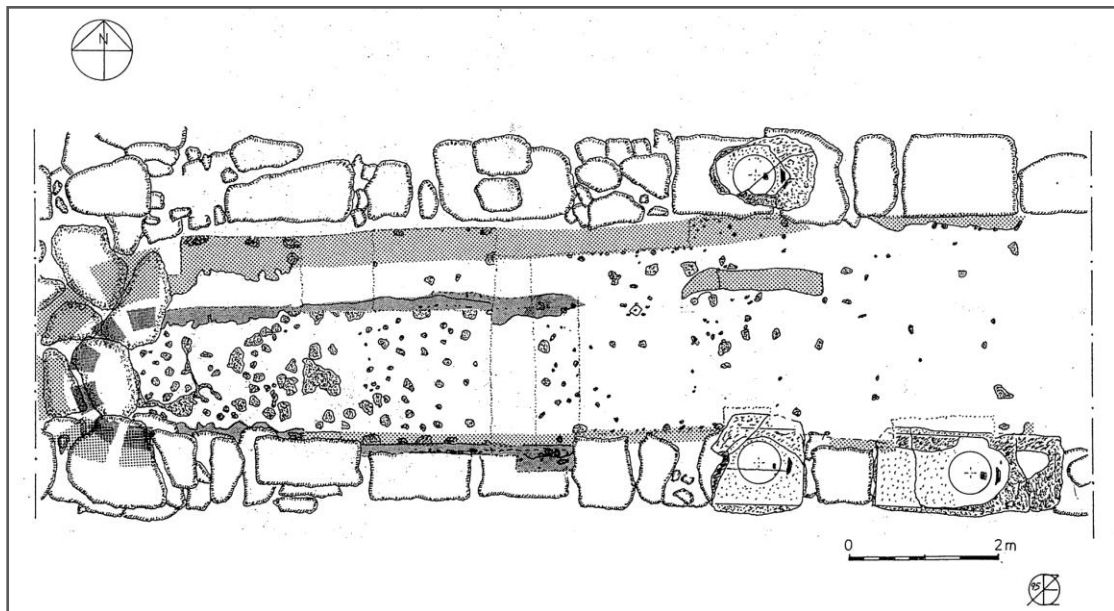


Image I.3. Plan of the two Geometrical cult buildings as indicated by the actual remains. Building 1 (lighter) and Building 2 (darker) among the foundations of the Archaic inner colonnades (Drawing: Østby) (Østby, 2014a: 20)

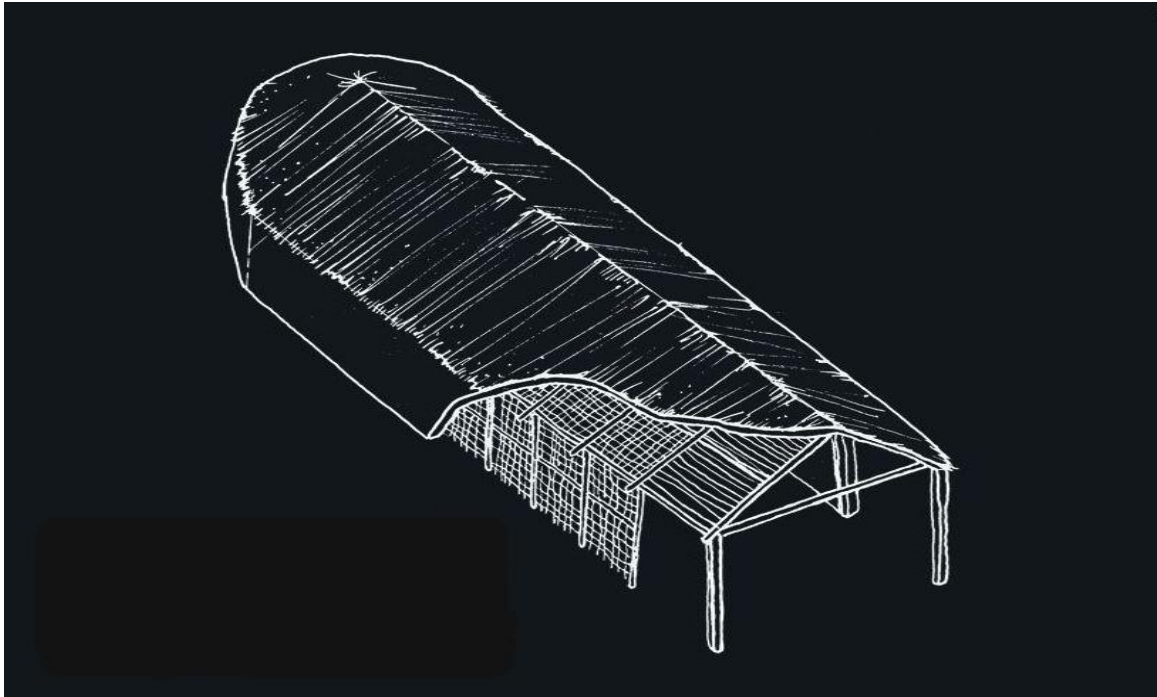


Image I.4. Sketch of the apsidal wattle-and-daub edifice of the Late Geometric-Early Archaic period in the sanctuary of Alea (Drawing: M. Varnava, G. Grigorakakis; Photo: Archaeological Museum of Tegea)

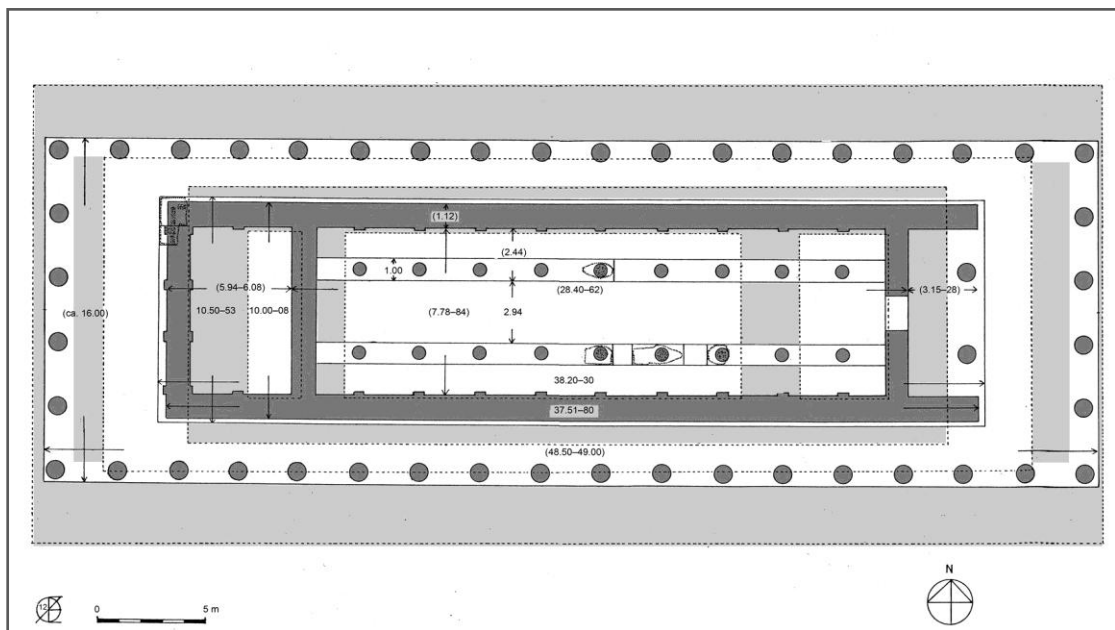


Image I.5. Plan of the foundations of the Archaic (darker) and classical temple (lighter), as indicated by the actual remains (Drawing: Østby) (Østby, 2014a: 36)

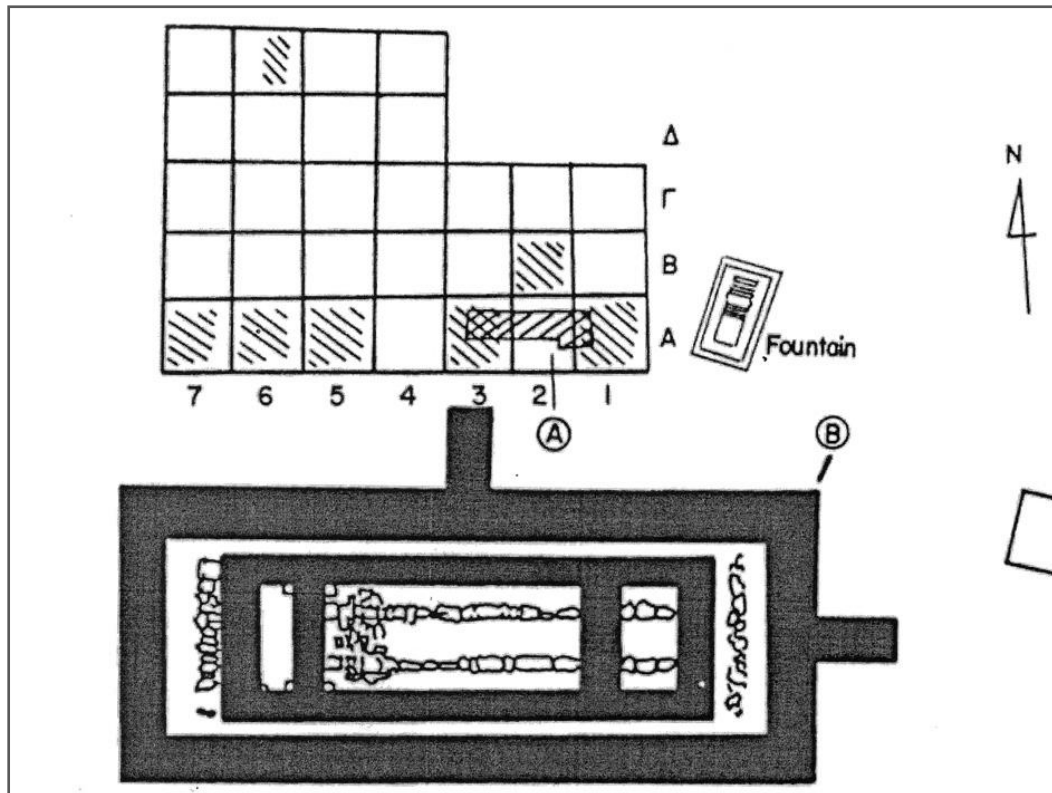


Image I.6. Plan of the trenches excavated by Steinhauer in 1976-77, shaded (Voyatzis, 1990: 350)



Image I.7. The bronze pins assemblage (Photo: Klaus-Valtin Von Eickstedt)

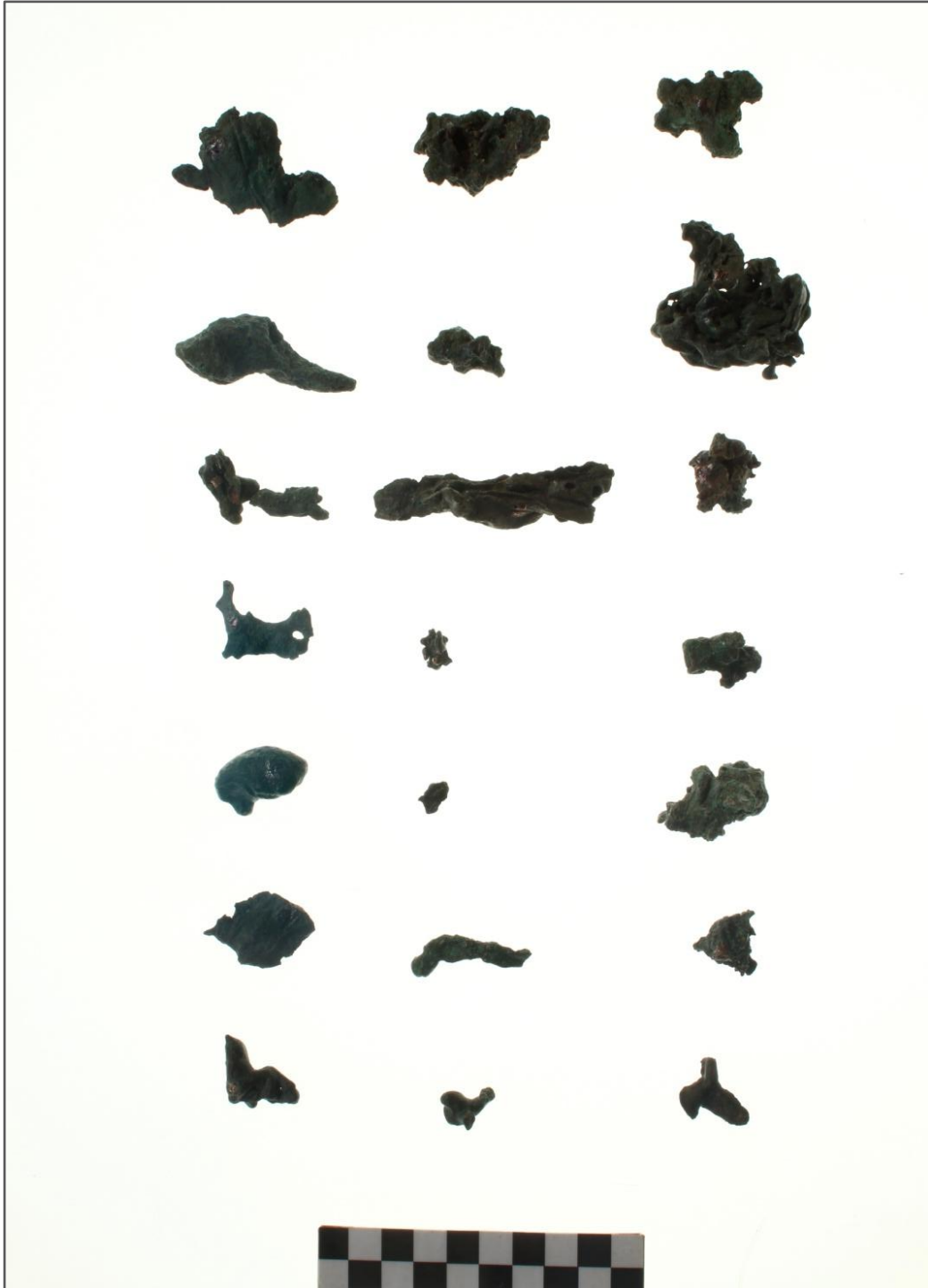


Image I.8. The metallurgical wastes assemblage (Photo: Klaus-Valtin Von Eickstedt)

Appendix II.1

Table II.1 Concentration of measured values of the elements detected on the *reference sample CD-360* with the *p-XRF* method, normalized and expressed in % wt
(*St. Dev.*: standard deviation, *Max.*: maximum, *Min.*: minimum)

Nominal values for CD-360: 0.15% Fe, 60.99% Cu, 35.88% Zn, 2.98% Pb

Spectrum #	Fe	Co	Ni	Cu	Zn	Nb	Sn	Pb
1	0.15	0.01	0.07	62.03	35.31	0.11	0.18	2.13
2	0.15	0.02	0.07	62.02	35.22	0.10	0.18	2.23
3	0.13	0.02	0.08	61.91	35.42	0.10	0.20	2.13
4	0.13	0.02	0.09	61.95	35.38	0.10	0.20	2.12
5	0.13	0.02	0.09	61.97	35.33	0.11	0.20	2.14
6	0.14	0.02	0.09	61.95	35.36	0.10	0.20	2.14
St. Dev.	0.01	0.00	0.01	0.05	0.07	0.01	0.01	0.04
Mean	0.14	0.02	0.08	61.97	35.34	0.10	0.19	2.15
Median	0.14	0.02	0.09	61.96	35.35	0.10	0.20	2.14
Max.	0.15	0.02	0.09	62.03	35.42	0.11	0.20	2.23
Min.	0.13	0.01	0.07	61.91	35.22	0.10	0.18	2.12

Appendix II.2

Table II.2. Concentration of the measured values of the elements detected on the **bronze pins** with the **p-XRF** method, normalized and expressed in % wt. (n.d.: not detected)

Sample	File #	Cu	Sn	Fe	As	Pb	Sb	Bi	Ag	Zr	Zn	Mn	Nb	Co	Ni
P1	1883	61.95	35.56	0.38	1.22	n.d.	0.36	0.31	n.d.	0.10	0.11	0.02	n.d.	n.d.	n.d.
P2	1885	87.76	7.98	1.20	1.69	n.d.	0.73	0.15	0.21	0.04	0.16	0.07	n.d.	n.d.	n.d.
P2	1886	85.30	9.56	1.55	1.86	n.d.	0.97	0.24	0.22	0.06	0.16	0.08	n.d.	n.d.	n.d.
P1	1888	84.50	14.33	0.18	0.31	0.17	0.21	0.16	0.03	0.04	0.07	n.d.	n.d.	n.d.	n.d.
P3	1889	89.84	8.66	0.74	0.12	n.d.	0.17	0.15	0.12	0.04	0.11	0.04	n.d.	n.d.	n.d.
P3	1890	87.59	10.77	0.88	0.18	n.d.	0.22	0.14	0.09	0.04	0.06	0.03	n.d.	n.d.	n.d.
P4	1892	98.78	0.31	0.25	0.23	n.d.	0.12	0.05	0.16	0.01	0.04	n.d.	n.d.	n.d.	0.05
P4	1893	98.43	0.43	0.27	0.22	n.d.	0.17	0.11	0.25	0.02	0.04	n.d.	n.d.	n.d.	0.06
P5	1895	86.56	12.06	0.42	0.31	n.d.	0.26	0.18	0.09	0.05	0.05	0.02	n.d.	n.d.	n.d.
P5	1896	78.30	19.93	0.78	0.48	n.d.	0.21	0.15	n.d.	0.04	0.08	0.03	n.d.	n.d.	n.d.
P5	1897	85.04	13.77	0.48	0.35	n.d.	0.11	0.06	0.02	0.01	0.14	0.02	n.d.	n.d.	n.d.
P6	1899	80.03	18.81	0.35	0.03	0.27	0.20	0.17	n.d.	0.06	0.08	n.d.	n.d.	n.d.	n.d.
P6	1900	85.26	13.79	0.25	0.03	0.21	0.15	0.15	0.07	0.04	0.06	n.d.	n.d.	n.d.	n.d.
P7	1902	84.16	14.73	0.13	0.11	0.25	0.21	0.22	0.05	0.07	0.07	n.d.	n.d.	n.d.	n.d.
P7	1903	83.87	15.18	0.14	0.13	0.14	0.19	0.19	0.04	0.05	0.07	n.d.	n.d.	n.d.	n.d.
P8	1905	79.68	18.42	0.53	0.22	0.63	0.24	0.16	n.d.	0.06	0.08	n.d.	n.d.	n.d.	n.d.
P9	1907	86.00	11.90	0.05	0.21	1.40	0.13	0.14	0.05	0.04	0.06	n.d.	n.d.	n.d.	n.d.
P9	1908	84.14	13.65	0.06	0.25	1.53	0.12	0.13	0.02	0.04	0.07	n.d.	n.d.	n.d.	n.d.
P10	1910	75.53	21.34	2.01	0.39	n.d.	0.25	0.20	n.d.	0.06	0.10	0.11	n.d.	n.d.	n.d.
P10	1911	79.61	17.77	1.69	0.28	0.05	0.20	0.17	n.d.	0.05	0.08	0.09	n.d.	n.d.	n.d.

Sample	File #	Cu	Sn	Fe	As	Pb	Sb	Bi	Ag	Zr	Zn	Mn	Nb	Co	Ni
P11	1913	74.64	21.75	0.24	0.51	2.45	0.16	0.13	n.d.	0.04	0.07	n.d.	n.d.	n.d.	n.d.
P11	1914	78.13	18.47	0.16	0.55	2.14	0.23	0.16	n.d.	0.05	0.11	n.d.	n.d.	n.d.	n.d.
P12	1916	80.21	16.21	1.12	0.19	1.71	0.17	0.16	0.01	0.05	0.12	0.05	n.d.	n.d.	n.d.
P12	1917	73.41	21.71	1.35	0.25	2.40	0.18	0.17	n.d.	0.06	0.40	0.07	n.d.	n.d.	n.d.
P13	1919	74.83	23.61	0.75	0.37	n.d.	0.11	0.15	n.d.	0.04	0.08	0.05	n.d.	n.d.	n.d.
P13	1920	76.87	21.28	0.88	0.37	n.d.	0.19	0.15	n.d.	0.05	0.12	0.08	n.d.	n.d.	n.d.
P14	1922	77.19	20.04	1.06	0.42	n.d.	0.09	0.11	n.d.	0.04	0.14	0.04	n.d.	0.35	0.52
P14	1923	84.81	12.76	0.69	0.29	n.d.	0.11	0.13	0.05	0.03	0.10	0.02	n.d.	0.40	0.60
P15	1925	82.70	13.03	0.08	1.71	2.11	0.20	0.02	0.08	0.04	0.02	n.d.	n.d.	n.d.	n.d.
P15	1926	79.88	11.61	0.02	0.81	7.13	0.27	0.11	0.09	0.05	0.03	n.d.	n.d.	n.d.	n.d.
P16	1928	83.96	14.48	0.09	0.26	0.79	0.16	0.13	0.01	0.04	0.07	0.01	n.d.	n.d.	n.d.
P16	1929	84.43	13.44	0.21	0.27	0.82	0.26	0.20	0.05	0.07	0.22	0.03	n.d.	n.d.	0.01
P17	1931	81.45	15.35	0.89	1.11	n.d.	0.71	0.24	0.05	0.06	0.10	0.04	n.d.	n.d.	n.d.
P18	1933	84.82	13.23	0.09	1.31	n.d.	0.24	0.11	0.09	0.03	0.08	n.d.	n.d.	n.d.	n.d.
P18	1934	77.65	19.45	0.16	2.07	n.d.	0.32	0.21	n.d.	0.05	0.09	n.d.	n.d.	n.d.	n.d.
P19	1936	81.30	16.50	0.27	0.27	1.33	0.09	0.08	n.d.	0.03	0.14	0.01	n.d.	n.d.	n.d.
P19	1937	86.07	12.24	0.16	0.19	0.97	0.13	0.09	0.06	0.03	0.07	n.d.	n.d.	n.d.	n.d.
P20	1939	66.91	27.30	1.56	0.25	3.44	0.08	0.13	n.d.	0.05	0.17	0.08	n.d.	0.02	n.d.
P20	1940	61.20	32.21	1.92	0.38	3.64	0.11	0.18	n.d.	0.06	0.15	0.10	n.d.	0.05	n.d.
P21	1942	79.35	19.74	0.17	0.41	n.d.	0.09	0.12	n.d.	0.03	0.09	n.d.	n.d.	n.d.	n.d.
P21	1943	70.85	27.87	0.20	0.57	n.d.	0.15	0.20	n.d.	0.07	0.09	n.d.	n.d.	n.d.	n.d.
P22	1945	62.11	34.80	0.92	0.37	0.24	0.80	0.38	n.d.	0.23	0.10	0.05	n.d.	n.d.	n.d.
P22	1946	66.91	31.51	0.50	0.54	n.d.	0.18	0.19	n.d.	0.06	0.08	0.02	n.d.	n.d.	n.d.
P23	1948	76.69	21.25	0.57	0.29	0.60	0.26	0.18	n.d.	0.05	0.09	0.02	n.d.	n.d.	n.d.
P24	1950	79.24	17.57	0.40	0.31	2.02	0.13	0.16	n.d.	0.05	0.10	0.01	n.d.	n.d.	n.d.

Sample	File #	Cu	Sn	Fe	As	Pb	Sb	Bi	Ag	Zr	Zn	Mn	Nb	Co	Ni
P24	1951	87.59	10.27	0.32	0.19	1.28	0.09	0.12	0.04	0.04	0.05	n.d.	n.d.	n.d.	n.d.
P25	1953	89.80	8.31	0.11	0.68	n.d.	0.53	0.24	0.19	0.07	0.07	n.d.	n.d.	n.d.	n.d.
P25	1954	78.27	18.68	0.28	1.57	n.d.	0.75	0.28	n.d.	0.07	0.10	n.d.	n.d.	n.d.	n.d.
P26	1956	67.95	28.33	1.83	0.47	0.68	0.31	0.19	n.d.	0.06	0.08	0.10	n.d.	n.d.	n.d.
P1	2004	63.07	34.82	0.31	1.13	n.d.	0.24	0.22	n.d.	0.06	0.12	0.02	n.d.	n.d.	n.d.
P1	2005	83.59	15.40	0.19	0.40	n.d.	0.18	0.13	n.d.	0.03	0.07	0.01	n.d.	n.d.	n.d.
P6	2006	85.95	13.28	0.25	0.03	0.14	0.11	0.09	0.05	0.02	0.06	0.01	n.d.	n.d.	n.d.
P8	2007	80.44	17.94	0.51	0.23	0.54	0.14	0.08	n.d.	0.03	0.07	0.02	n.d.	n.d.	n.d.
P8	2008	80.90	17.52	0.49	0.23	0.50	0.17	0.09	n.d.	0.03	0.07	0.01	n.d.	n.d.	n.d.
P10	2009	75.39	21.62	1.75	0.36	n.d.	0.31	0.27	n.d.	0.08	0.11	0.11	n.d.	n.d.	n.d.
P10	2010	76.68	20.18	1.80	0.33	0.16	0.32	0.26	n.d.	0.09	0.07	0.10	n.d.	n.d.	n.d.
P11	2011	75.59	20.86	0.23	0.55	2.44	0.13	0.10	n.d.	0.04	0.07	0.01	n.d.	n.d.	n.d.
P12	2012	79.46	16.89	1.18	0.21	1.82	0.09	0.10	n.d.	0.03	0.14	0.06	n.d.	n.d.	n.d.
P13	2013	73.96	24.34	0.73	0.38	n.d.	0.19	0.21	n.d.	0.07	0.08	0.05	n.d.	n.d.	n.d.
P14	2014	73.82	23.01	0.97	0.44	n.d.	0.25	0.29	n.d.	0.11	0.16	0.04	n.d.	0.36	0.55
P14	2015	83.41	14.06	0.68	0.28	n.d.	0.15	0.17	0.06	0.06	0.10	0.02	n.d.	0.40	0.61
P15	2016	81.60	13.39	0.08	1.49	2.82	0.30	0.12	0.11	0.07	0.02	n.d.	n.d.	n.d.	n.d.
P17	2017	79.70	16.80	1.01	1.44	n.d.	0.72	0.17	n.d.	0.05	0.08	0.03	n.d.	n.d.	n.d.
P18	2018	85.72	12.51	0.08	1.27	n.d.	0.16	0.09	0.09	0.01	0.06	n.d.	n.d.	n.d.	n.d.
P18	2019	78.08	19.19	0.14	2.00	n.d.	0.28	0.18	n.d.	0.04	0.08	0.01	n.d.	n.d.	n.d.
P19	2020	84.88	13.43	0.17	0.22	1.07	0.05	0.05	0.03	0.02	0.09	n.d.	n.d.	n.d.	n.d.
P19	2021	86.02	12.37	0.15	0.17	0.98	0.09	0.07	0.05	0.02	0.08	n.d.	n.d.	n.d.	n.d.
P20	2022	65.68	28.33	1.59	0.30	3.34	0.19	0.25	n.d.	0.09	0.12	0.06	0.01	0.03	n.d.
P21	2023	78.21	20.76	0.19	0.43	n.d.	0.13	0.15	n.d.	0.04	0.09	0.01	n.d.	n.d.	n.d.
P22	2024	67.38	31.16	0.44	0.53	n.d.	0.17	0.17	n.d.	0.06	0.07	0.02	n.d.	n.d.	n.d.

Sample	File #	Cu	Sn	Fe	As	Pb	Sb	Bi	Ag	Zr	Zn	Mn	Nb	Co	Ni
P23	2025	77.22	20.80	0.59	0.34	0.49	0.22	0.18	n.d.	0.05	0.08	0.03	n.d.	n.d.	n.d.
P24	2026	79.24	17.26	0.42	0.28	2.32	0.18	0.17	n.d.	0.06	0.09	n.d.	n.d.	n.d.	n.d.
P25	2027	81.61	15.68	0.11	1.41	n.d.	0.72	0.29	0.03	0.07	0.07	n.d.	n.d.	n.d.	n.d.
P26	2028	67.15	29.03	1.85	0.44	0.80	0.30	0.19	n.d.	0.07	0.09	0.09	n.d.	n.d.	n.d.

Appendix II.3

Table II.3. Concentration of the measured values of the elements detected on the *metallurgical wastes* with the *p-XRF* method, normalized and expressed in % wt. (n.d. not detected)

Sample	File #	Cu	Sn	Fe	As	Pb	Sb	Bi	Ag	Zr	Zn	Mn	Co	Ni
WS2	1958	79.34	19.00	0.34	0.08	1.01	0.07	0.08	n.d.	0.02	0.05	0.01	n.d.	n.d.
WS2	1959	77.88	19.63	0.37	0.12	1.72	0.09	0.09	n.d.	0.03	0.06	0.02	n.d.	n.d.
WS3	1961	79.57	18.64	0.88	0.21	0.34	0.10	0.07	n.d.	0.03	0.11	0.05	n.d.	n.d.
WS4	1963	88.52	10.18	0.78	0.22	n.d.	0.10	0.05	0.03	0.01	0.06	0.04	n.d.	n.d.
WS5	1965	68.99	26.55	0.52	1.25	2.13	0.25	0.16	n.d.	0.05	0.09	0.01	n.d.	n.d.
WS6	1967	87.50	11.48	0.25	0.44	n.d.	0.12	0.08	0.04	0.01	0.06	n.d.	n.d.	n.d.
WS7	1969	75.40	22.59	0.63	0.72	n.d.	0.35	0.14	n.d.	0.05	0.07	0.04	n.d.	n.d.
WS8	1971	89.96	8.69	0.92	0.15	n.d.	0.07	0.03	0.04	0.01	0.06	0.05	n.d.	n.d.
WS9	1973	85.16	13.39	0.81	0.17	0.04	0.15	0.09	0.02	0.04	0.09	0.04	n.d.	n.d.
WS10	1975	74.50	24.14	0.47	0.56	n.d.	0.11	0.08	n.d.	0.02	0.10	0.03	n.d.	n.d.
WS10	1976	84.06	15.10	0.31	0.26	n.d.	0.07	0.05	0.01	0.02	0.12	n.d.	n.d.	n.d.
WS1	1978	68.74	28.47	1.13	0.49	0.73	0.13	0.13	n.d.	0.04	0.08	0.06	n.d.	n.d.
WS1	1979	81.39	14.96	2.03	0.26	0.92	0.12	0.07	n.d.	0.03	0.10	0.13	n.d.	n.d.
WS11	1981	84.77	13.33	0.71	0.30	n.d.	0.20	0.12	0.07	0.04	0.41	0.05	n.d.	n.d.
WS12	1983	88.77	9.72	0.61	0.11	0.43	0.09	0.08	0.05	0.03	0.11	0.01	n.d.	n.d.
WS13	1985	75.89	22.57	0.26	0.30	0.71	0.07	0.10	n.d.	0.04	0.06	0.01	n.d.	n.d.
WS14	1987	76.42	19.94	2.84	0.30	n.d.	0.14	0.09	n.d.	0.04	0.07	0.16	n.d.	n.d.
WS15	1989	80.99	15.94	0.62	0.39	1.20	0.60	0.09	n.d.	0.03	0.09	0.03	n.d.	n.d.
WS16	1991	87.45	11.22	0.52	0.12	0.41	0.08	0.05	0.04	0.01	0.07	0.02	n.d.	n.d.

Sample	File #	Cu	Sn	Fe	As	Pb	Sb	Bi	Ag	Zr	Zn	Mn	Co	Ni
WS17	1993	75.63	21.26	1.72	0.34	0.54	0.20	0.10	n.d.	0.03	0.09	0.10	n.d.	n.d.
WS18	1995	79.91	18.42	0.71	0.41	0.07	0.23	0.12	n.d.	0.03	0.08	0.02	n.d.	n.d.
WS19	1997	85.14	13.62	0.35	0.49	n.d.	0.23	0.06	0.01	0.01	0.09	0.01	n.d.	n.d.
WS20	1999	51.57	45.80	1.66	0.48	n.d.	0.06	0.17	n.d.	0.07	0.11	0.09	n.d.	n.d.
WS21	2001	n.d.	73.43	16.15	0.11	3.89	4.89	0.35	0.53	0.02	n.d.	0.62	n.d.	n.d.
WS21	2003	n.d.	77.70	15.35	0.55	n.d.	5.04	0.42	0.48	0.02	n.d.	0.45	n.d.	n.d.

Appendix III.1

Table III.1 Concentration of the measured values of the elements detected on the **reference samples of the BCA series**, under the μ XRF method, normalized and expressed in % wt (SD: standard deviation, DL indicates that for the particular element the quantification is not possible either due its low content below the detection limits of the analysis or due to interference problems)

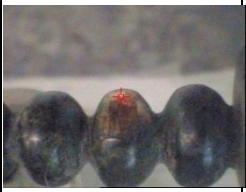

Elements	BCR _A			BCR _B		
	Nominal	Measured	SD(%)	Nominal	Measured	SD(%)
Cu	78.73	80	- 1.5	82.7	81	1.8
Zn	6.02	6.0	0.5	14.8	16	-7.4
As	0.19	DL	-	0.099	DL	-
Sn	7.16	7.2	- 0.8	2.06	2.1	-0.5
Pb	7.9	7.6	4	0.39	DL	-



Elements	BCR _C			BCR _D			BCR _E		
	Nominal	Measured	SD(%)	Nominal	Measured	SD(%)	Nominal	Measured	SD(%)
Cu	95.5	89	6.0	80.3	84	- 4.5	92.4	92.8	- 0.4
Zn	0.06	DL	-	0.148	DL	-	0.157	DL	-
As	4.06	5.6	- 23	0.285	DL	-	0.194	0.16	16.5
Sn	0.2	0.27	- 36	10.1	8.7	13.5	7	6.8	2.9
Pb	0.18	DL	-	9.2	7.2	21	0.204	0.22	- 6.4



Appendix III.2



Table III.2 Microphotographs and concentration of the measured values of the elements detected on the **bronze pins** with the μ -XRF method, normalized and expressed in % wt. All areas were measured at 50kV_600uA using filter #3 (for bronzes).



Detection limit at 50s for Co=0.024%wt, Ni=0.04%wt, Sb=0.3%wt, Pb= 0.002%wt, Bi=0.019%wt. B.D.L= Below Detection Limit




Sample #	Image of the analysed area	Time (s)	Norm. factor	Concentration (%wt)								Bi
				Fe	Co	Ni	Cu	As	Sn	Sb	Pb	
1a		50	1,07	0.17	B.D.L.	0.06	86.70	0.10	11.90	0.38	0.67	B.D.L.
1c		50	1,23	0.18	B.D.L.	0.00	85.70	0.15	13.10	0.34	0.51	B.D.L.
P1 mean				0.17		0.03	86.20	0.13	12.50	0.36	0.59	



Sample #	Image of the analysed area	Time (s)	Norm. factor	Concentration (%wt)								Bi
				Fe	Co	Ni	Cu	As	Sn	Sb	Pb	
2a		50	1.19	0.96	B.D.L	0.04	91.14	0.89	4.15	0.58	2.81	B.D.L.
2c		50	1.23	0.68	B.D.L	0.04	93.10	0.40	3.87	0.28	1.62	B.D.L.
P2 mean				0.82		0.04	92.12	0.65	4.01	0.43	2.22	



Sample #	Image of the analysed area	Time (s)	Norm. factor	Concentration (%wt)								
				Fe	Co	Ni	Cu	As	Sn	Sb	Pb	Bi
3b		50	1.61	0.64	B.D.L	0.04	89.40	0.10	9.71	B.D.L.	0.07	B.D.L.
3c		50	1.68	0.65	B.D.L	0.04	89.69	0.13	9.47	B.D.L.	B.D.L.	B.D.L.
P3 mean				0.64		0.04	89.55	0.12	9.59		0.07	



Sample #	Image of the analysed area	Time (s)	Norm. factor	Concentration (%wt)								
				Fe	Co	Ni	Cu	As	Sn	Sb	Pb	Bi
4b		50	1.26	0.17	B.D.L	0.17	98.80	0.24	0.20	0.41	0.42	B.D.L.
4c		50	1.24	0.27	B.D.L	0.09	98.66	0.11	0.44	B.D.L.	0.43	B.D.L.
P4 mean				0.22		0.13	98.73	0.17	0.32	0.41	0.42	



Sample #	Image of the analysed area	Time (s)	Norm. factor	Concentration (%wt)								
				Fe	Co	Ni	Cu	As	Sn	Sb	Pb	Bi
5a		50	1.18	0.38	B.D.L	0.05	87.30	0.21	11.84	0.40	0.21	B.D.L.
5b		50	1.16	0.38	B.D.L	0.04	87.40	0.17	11.70	B.D.L.	0.27	B.D.L.
P5 mean				0.38		0.04	87.35	0.19	11.77	0.40	0.24	


Sample #	Image	Time (s)	Norm. factor	Concentration (%wt)								Bi
				Fe	Co	Ni	Cu	As	Sn	Sb	Pb	
6a		50	1.06	0.27	B.D.L	0.06	87.86	0.06	11.75	B.D.L.		B.D.L.
6b		50	0.97	0.23	B.D.L	0.05	88.18	0.03	11.46	B.D.L.	0.05	B.D.L.
6c		50	1.1	0.23	B.D.L	0.04	88.37	0.04	11.30	0.40		B.D.L.
P6 mean				0.24		0.05	88.14	0.04	11.50	0.40	0.05	





Sample #	Image	Time (s)	Norm. factor	Concentration (%wt)								
				Fe	Co	Ni	Cu	As	Sn	Sb	Pb	Bi
7b		50	0.99	0.08	B.D.L	0.07	90.25	0.03	9.39	B.D.L.	0.17	B.D.L.
7c		50	1.17	0.09	B.D.L	0.08	89.21	0.07	10.48	B.D.L.	0.05	B.D.L.
P7 mean				0.09		0.07	89.73	0.05	9.93		0.11	




Sample #	Image	Time (s)	Norm. factor	Concentration (%wt)								
				Fe	Co	Ni	Cu	As	Sn	Sb	Pb	Bi
8a		50	1.06	0.18	B.D.L	0.05	80.00	0.10	19.13	B.D.L.	0.50	B.D.L.
8b		50	1.37	0.19	B.D.L	0.05	84.16	0.06	14.97	B.D.L.	0.55	B.D.L.
P8 mean				0.19		0.05	82.08	0.08	17.05		0.53	


Sample #	Image	Time (s)	Norm. factor	Concentration (%wt)								
				Fe	Co	Ni	Cu	As	Sn	Sb	Pb	Bi
9a		50	1.11	0.03	B.D.L	0.11	91.28	0.10	7.81	B.D.L.	0.66	B.D.L.
9b		50	0.922	0.02	B.D.L	0.10	91.41	0.03	7.65	B.D.L.	0.77	B.D.L.
P9 mean				0.02		0.11	91.35	0.07	7.73		0.72	



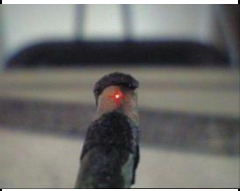
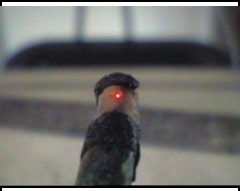
Sample #	Image	Time (s)	Norm. factor	Concentration (%wt)								
				Fe	Co	Ni	Cu	As	Sn	Sb	Pb	Bi
10a		50	0.95	1.12	B.D.L	0.03	90.63	0.07	7.83	B.D.L.	0.30	B.D.L.
10c		50	1.07	1.01	B.D.L	0.04	90.23	0.12	8.40	B.D.L.	0.19	B.D.L.
P10 mean				1.07		0.03	90.43	0.10	8.12		0.25	


Sample #	Image	Time (s)	Norm. factor	Concentration (%wt)								
				Fe	Co	Ni	Cu	As	Sn	Sb	Pb	Bi
P11		50	1.09	0.29	B.D.L	0.07	84.63	0.18	13.84	B.D.L.	1.34	B.D.L.



Sample #	Image	Time (s)	Norm. factor	Concentration (%wt)								Bi
				Fe	Co	Ni	Cu	As	Sn	Sb	Pb	
12a		150	0.93	1.01	B.D.L	0.08	86.77	0.03	10.96	B.D.L.	1.14	B.D.L.
12b		50	1.11	0.87	B.D.L	0.04	86.57	0.04	11.58	B.D.L.	0.87	B.D.L.
12b2		150	1.06	0.87	B.D.L	0.05	86.99	0.02	10.93	0.40	1.12	B.D.L.
12c		50	1.75	0.80	B.D.L	0.05	86.32	0.10	12.05	B.D.L.	0.68	B.D.L.
P12 mean				0.89		0.06	86.66	0.05	11.38	0.40	0.95	


Sample #	Image	Time (s)	Norm. factor	Concentration (%wt)								Bi
				Fe	Co	Ni	Cu	As	Sn	Sb	Pb	
13a		150	1.21	0.46	B.D.L	0.09	90.42	0.04	8.76	0.40	0.21	B.D.L.
13b		150	1.1	0.44	B.D.L	0.09	90.41	0.04	8.79	B.D.L.	0.23	B.D.L.
												
P13 mean				0.45		0.09	90.42	0.04	8.78	0.40	0.22	


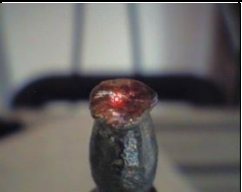
Sample #	Image	Time (s)	Norm. factor	Concentration (%wt)								
				Fe	Co	Ni	Cu	As	Sn	Sb	Pb	Bi
14b		150	1.24	0.35	B.D.L	0.64	91.85	0.10	6.63	B.D.L.	0.04	B.D.L.
14c		150	1.04	0.28	B.D.L	0.05	92.08	0.08	6.99	B.D.L.	0.09	B.D.L.
P14 mean				0.31		0.34	91.97	0.09	6.81		0.07	

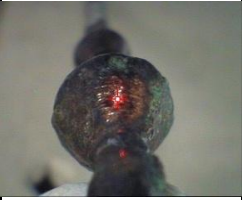

Sample #	Image	Time (s)	Norm. factor	Concentration (%wt)								Bi
				Fe	Co	Ni	Cu	As	Sn	Sb	Pb	
15a		150	1.11	0.29	B.D.L	0.08	88.63	0.08	5.67	B.D.L.	5.49	B.D.L.
15a2		150	1.27	0.06	B.D.L	0.09	86.53	0.13	5.88	B.D.L.	7.31	B.D.L.
15c		150	0.96	0.02	B.D.L	0.07	88.13	0.17	7.87	B.D.L.	3.72	B.D.L.
		150	1.01	0.02	B.D.L	0.07	88.80	0.12	7.60	B.D.L.	3.36	B.D.L.
P15 mean				0.10		0.08	88.02	0.12	6.76		4.97	



Sample #	Image	Time (s)	Norm. factor	Concentration (%wt)								
				Fe	Co	Ni	Cu	As	Sn	Sb	Pb	Bi
16a		150	1.4	0.01	B.D.L	0.07	91.91	0.08	7.52	B.D.L.	0.38	B.D.L.
16b		150	1.33	0.05	B.D.L	0.08	90.39	0.06	8.79	B.D.L.	0.61	B.D.L.
16c		150	1.36	0.04	B.D.L	0.08	91.07	0.08	8.42	B.D.L.	0.31	B.D.L.
P16 mean				0.05		0.08	90.73	0.07	8.61		0.46	



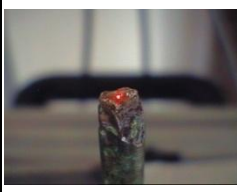
Sample #	Image	Time (s)	Norm. factor	Concentration (%wt)								Bi
				Fe	Co	Ni	Cu	As	Sn	Sb	Pb	
17a		150	1.34	0.38	B.D.L	0.04	91.90	0.24	6.66	0.34	0.44	B.D.L.
17c		150	1.17	0.50	B.D.L	0.18	90.29	0.34	7.99	0.32	0.69	B.D.L.
P17 mean				0.44		0.11	91.10	0.29	7.33	0.33	0.57	


Sample #	Image	Time (s)	Norm. factor	Concentration (%wt)								
				Fe	Co	Ni	Cu	As	Sn	Sb	Pb	Bi
18a		150	1.27	0.13	B.D.L	0.06	88.90	0.73	9.94	B.D.L.	B.D.L.	B.D.L.
18c		150	1.08	0.14	B.D.L	0.07	89.38	0.83	9.56	0.25	B.D.L.	B.D.L.
P18 mean				0.13		0.06	89.14	0.78	9.75	0.25		


Sample #	Image	Time (s)	Norm. factor	Concentration (%wt)								
				Fe	Co	Ni	Cu	As	Sn	Sb	Pb	Bi
19a		150	1.13	0.09	B.D.L	0.10	93.23	0.02	5.96	B.D.L.	0.60	B.D.L.
19b		150	1.59	0.15	B.D.L	0.09	88.86	0.06	9.35	B.D.L.	1.48	B.D.L.
19c		150	1.22	0.17	B.D.L	0.08	93.10	0.02	6.11	B.D.L.	0.51	B.D.L.
P19 mean				0.13		0.09	91.73	0.04	7.14		0.86	

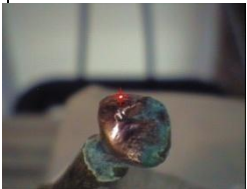
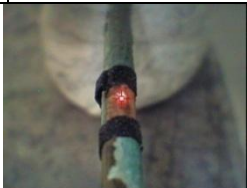
Sample #	Image	Time (s)	Norm. factor	Concentration (%wt)								
				Fe	Co	Ni	Cu	As	Sn	Sb	Pb	Bi
20a		150	1.37	1.00	0.05	0.04	88.86	0.02	9.12	B.D.L.	0.90	B.D.L.
20b		150	1.09	0.81	0.06	0.05	88.63	0.02	9.57	B.D.L.	0.85	B.D.L.
20c		150	1.17	0.94	0.07	0.05	87.24	0.02	10.64	B.D.L.	1.03	B.D.L.
P20 mean				0.88	0.06	0.05	87.94	0.02	10.11		0.94	



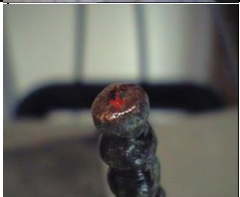
Sample #	Image	Time (s)	Norm. factor	Concentration (%wt)								
				Fe	Co	Ni	Cu	As	Sn	Sb	Pb	Bi
21a		150	1.77	0.16	B.D.L	0.05	84.91	0.18	14.32	B.D.L.	0.38	B.D.L.
21b		150	1.42	0.12	B.D.L	0.06	87.52	0.13	11.86	B.D.L.	0.29	B.D.L.
21c		150	1.38	0.19	B.D.L	0.06	86.06	0.12	13.25	B.D.L.	0.31	B.D.L.
P21 mean				0.16		0.06	86.16	0.14	13.14		0.33	

Sample #	Image	Time (s)	Norm. factor	Concentration (%wt)								
				Fe	Co	Ni	Cu	As	Sn	Sb	Pb	Bi
22a		150	1.41	0.11	B.D.L	0.04	87.97	0.10	11.67	B.D.L.	0.10	B.D.L.
22b		150	1	0.05	B.D.L	0.04	89.39	0.13	10.20	B.D.L.	0.16	B.D.L.
22c		150	5.47	0.10	B.D.L	0.05	86.84	0.14	12.86	B.D.L.	B.D.L.	B.D.L.
P22 mean				0.09		0.04	88.07	0.12	11.58		0.13	

Sample #	Image	Time (s)	Norm. factor	Concentration (%wt)								Bi
				Fe	Co	Ni	Cu	As	Sn	Sb	Pb	
P23		150	1.1	0.35	B.D.L	0.07	90.81	0.11	8.36	B.D.L.	0.29	B.D.L.


Sample #	Image	Time (s)	Norm. factor	Concentration (%wt)								Bi
				Fe	Co	Ni	Cu	As	Sn	Sb	Pb	
P24		150	0.95	0.26	B.D.L	0.08	92.06	0.03	6.91	B.D.L.	0.64	B.D.L.



Sample #	Image	Time (s)	Norm. factor	Concentration (%wt)								
				Fe	Co	Ni	Cu	As	Sn	Sb	Pb	Bi
25a		150	0.98	0.05	B.D.L	0.05	92.55	0.35	6.57	0.35	0.43	B.D.L.
25c		150	1.26	0.09	B.D.L	0.06	92.18	0.39	6.83	0.34	0.44	B.D.L.
P25 mean				0.07		0.05	92.37	0.37	6.70	0.34	0.43	



Sample #	Image	Time (s)	Norm. factor	Concentration (%wt)								Bi
				Fe	Co	Ni	Cu	As	Sn	Sb	Pb	
26a1		150	1.19	1.03	B.D.L	0.05	88.48	0.07	9.92	B.D.L.	0.45	B.D.L.
26a2		150	1.24	0.98	B.D.L	0.05	87.63	0.08	10.84	B.D.L.	0.40	B.D.L.
26c		150	1.07	1.09	B.D.L	0.05	87.19	0.08	11.12	B.D.L.	0.46	B.D.L.
P26 mean				1.03		0.05	87.77	0.08	10.63		0.43	



Appendix III.3



Table III.3. Microphotographs and concentration of the measured values of the elements detected on the *metallurgical wastes* with the μ -XRF method, normalized and expressed in % wt. All areas were measured at 50kV_600uA using filter #3 (for bronzes).
 Detection limit at 50s for Co=0.024%wt, Ni=0.04%wt, Sb=0.3%wt, Pb= 0.002%wt, Bi=0.019%wt.



Sample #	Image of the analysed area	Time (s)	Norm. factor	Concentration (%wt)					
				Cu	Sn	As	Pb	Fe	Ni
ws2a		150	1.33	86.52	12.72	0.02	0.49	0.18	0.05
ws2b		150	1.7	73.38	25.66	0.03	0.74	0.16	0.03
WS2 mean				79.95	19.19	0.03	0.61	0.17	0.04

Sample #	Image	Time (s)	Norm. factor	Concentration (%wt)					
				Cu	Sn	As	Pb	Fe	Ni
ws3a		150	1.11	92.02	7.49	0.04	0.15	0.25	0.03
ws3b		150	1.27	86.38	13.05	0.02	0.20	0.29	0.05
WS3 mean				89.20	10.27	0.03	0.17	0.27	0.04

Sample #	Image	Time (s)	Norm. factor	Concentration (%wt)					
				Cu	Sn	As	Pb	Fe	Ni
ws8a		150	1.25	90.65	8.50	0.24	0.06	0.50	0.05
ws8b		150	1.59	91.83	7.71	0.16	0.04	0.22	0.03
WS8 mean				91.24	8.11	0.20	0.05	0.36	0.04

Sample #	Image	Time (s)	Norm. factor	Concentration (%wt)					
				Cu	Sn	As	Pb	Fe	Ni
ws10a		150	1.09	89.37	10.06	0.10	0.19	0.23	0.04
ws10b		150	1	89.36	9.98	0.09	0.26	0.22	0.08
WS10 mean				89.37	10.02	0.09	0.23	0.23	0.06

Sample #	Image	Time (s)	Norm. factor	Concentration (%wt)					
				Cu	Sn	As	Pb	Fe	Ni
ws11a		150	1.75	75.35	21.91	0.66	0.56	1.47	0.03
ws11b		150	0.93	86.59	12.90	0.19	0.01	0.23	0.06
WS11 mean				80.97	17.41	0.43	0.28	0.85	0.05

Sample #	Image	Time (s)	Norm. factor	Concentration (%wt)					
				Cu	Sn	As	Pb	Fe	Ni
ws21a		150	2.54	95.99	3.54	0.03	0.17	0.23	0.03
ws21b		150	1.39	70.31	26.10	0.43	1.15	1.97	0.02
WS21				83.15	14.82	0.23	0.66	1.10	0.03

Appendix IV.1

Table IV.1 Concentration of measured values of the elements detected on the **reference sample CD-360** with the **SEM-EDS** method, normalized and expressed in % wt
(*St. Dev.*: standard deviation, *Max.*: maximum, *Min.*: minimum)

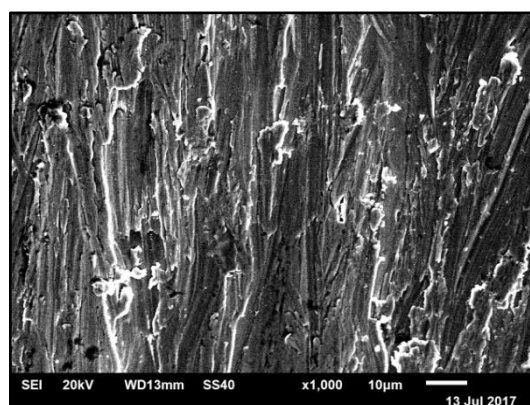
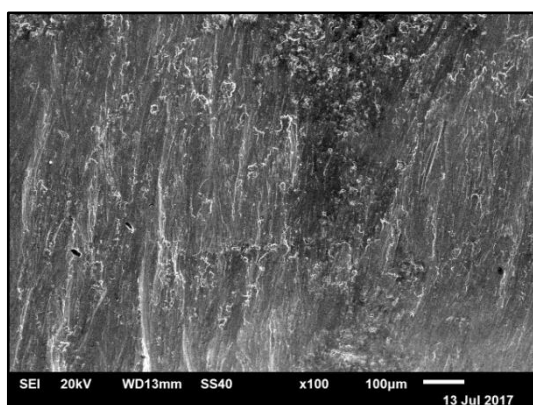
Nominal values for CD-360: 0.15% Fe, 60.99% Cu, 35.88% Zn, 2.98% Pb

Spectrum #	Fe	Cu	Zn	Pb
1	0.20	61.97	35.49	2.34
2	0.34	62.63	33.92	3.11
3	0.42	61.89	34.67	3.01
4	0.02	61.73	34.05	4.20
5	0.21	61.65	34.75	3.40
6	0.34	62.01	34.71	2.94
St. Dev.	0.14	0.35	0.57	0.61
Mean	0.26	61.98	34.60	3.17
Median	0.27	61.93	34.69	3.06
Max.	0.42	62.63	35.49	4.20
Min.	0.02	61.65	33.92	2.34

Appendix IV.2

Table IV.2.1. Concentration of the measured values of the elements detected on the *Alea-P2* pin with the *SEM-EDS* method, normalized and expressed in % wt. (*m.*: measurement, *St. Dev.*: standard deviation, *n.d.*: not detected)

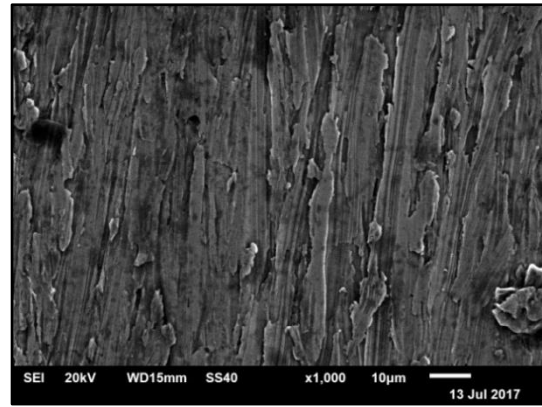
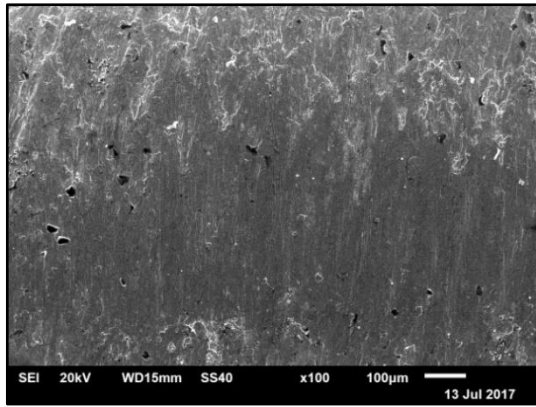
Alea-P2	Cu	Sn	As	Pb	Fe	Cl
m1	92.39	4.14	0.85	1.46	0.69	0.47
m2	92.63	3.95	0.62	1.71	0.62	0.46
m3	93.97	3.87	0.33	0.88	0.75	0.21
m4	95.61	2.40	0.28	0.78	0.75	0.19
Mean	93.65	3.59	0.52	1.21	0.70	0.33
St. Dev.	1.48	0.80	0.27	0.45	0.06	0.16



Images 1-2: Backscattered electron images in the SEM for the object *Alea-P2*.

Left: Magnification 200x. Head of the pin. Compositional contrast that results from different atomic number elements and their distribution is displayed

Right: Magnification 1000x. Head of the pin.



Images 3-4: Backscattered electron images in the SEM for the object **Alea-P2**.
Left: Magnification 100x. Needle of the pin.
Right: Magnification 1000x. Needle of the pin.

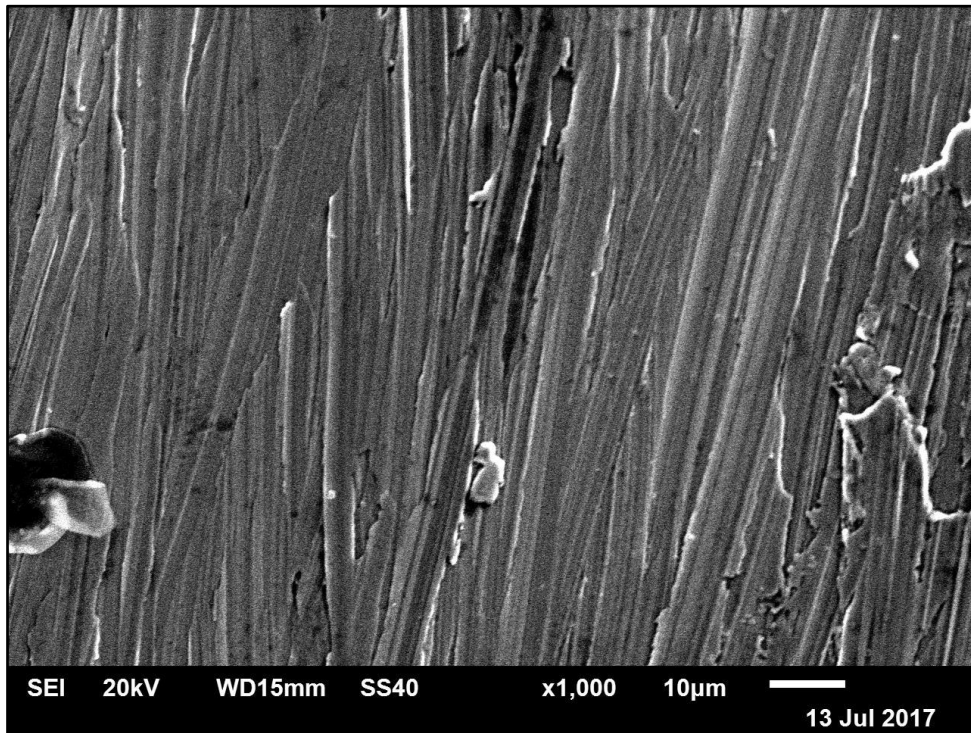


Image 5: Backscattered electron image in the SEM for the object **Alea-P2**.
Magnification 1000x. Center of the pin.

Table IV.2.2. Concentration of the measured values of the elements detected on the *Alea-P3* pin with the *SEM-EDS* method, normalized and expressed in % wt. (*m.*: measurement, *St. Dev.*: standard deviation, *n.d.*: not detected)

Alea-P3	Cu	Sn	Fe	Cl	P
m1	90.08	8.96	0.74	0.23	n.d.
m2	86.55	11.71	0.99	0.75	n.d.
m3	87.76	10.92	1.12	0.20	n.d.
m4	89.97	8.93	0.84	n.d.	0.25
m5	86.24	12.17	1.05	n.d.	0.54
m6	90.33	8.78	0.78	n.d.	0.11
Mean	88.49	10.25	0.92	0.39	0.30
St. Dev.	1.87	1.54	0.15	0.31	0.22

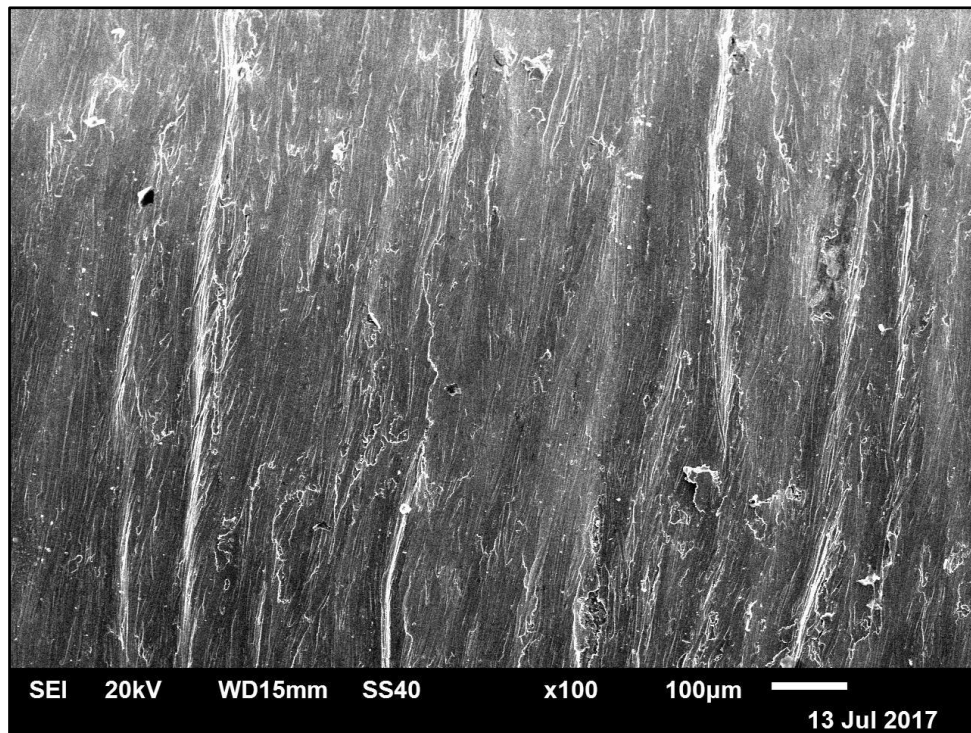
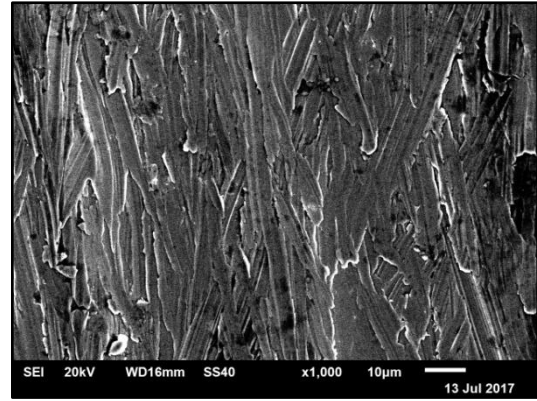
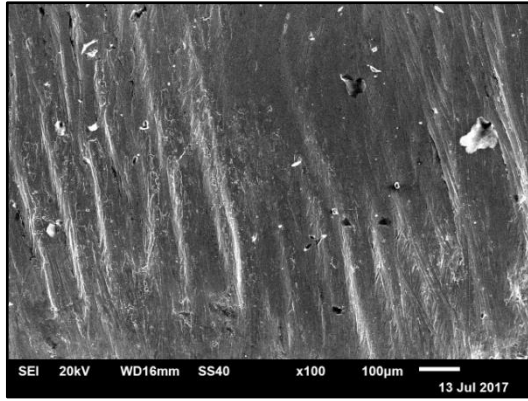


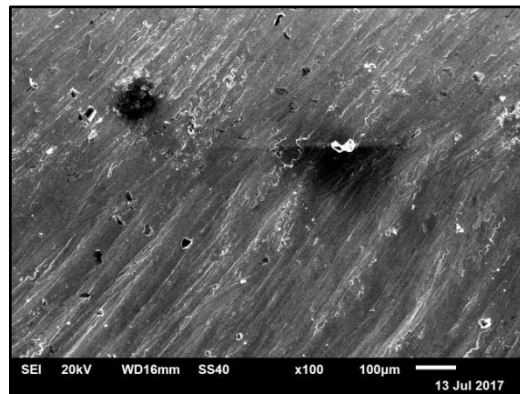
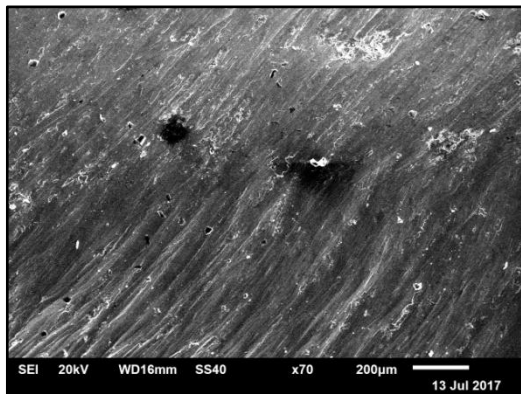
Image 6: Backscattered electron image in the SEM for the object *Alea-P3*. Magnification 100x. Center of the pin



Images 7-8: Backscattered electron images in the SEM for the object **Alea-P3**.
Left: Magnification 100x. Needle of the pin
Right: Magnification 1000x. Needle of the pin

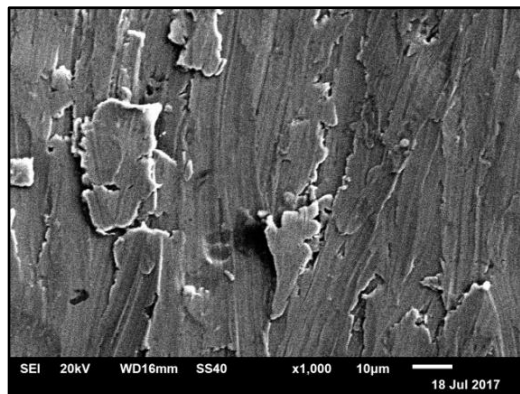
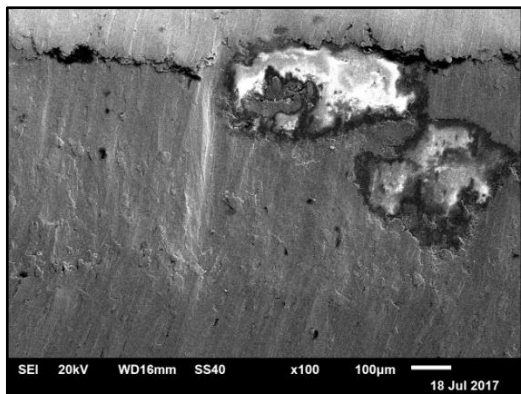
Table IV.2.3. Concentration of the measured values of the elements detected on the **Alea-P4** pin with the **SEM-EDS** method, normalized and expressed in % wt. (*m.*: measurement, *St. Dev.*: standard deviation, *n.d.*: not detected)

Alea-P4	Cu	Sn	As	Pb	Fe	Cl	Al	P	Ca	Cr
m1	99.17	n.d.	0.48	0.35	n.d.	n.d.	n.d.	n.d.	n.d.	n.d.
m2	99.32	n.d.	0.40	0.28	n.d.	n.d.	n.d.	n.d.	n.d.	n.d.
m3	10n.d.	n.d.	n.d.	n.d.	n.d.	n.d.	n.d.	n.d.	n.d.	n.d.
m4	79.56	n.d.	n.d.	n.d.	n.d.	0.28	20.17	n.d.	n.d.	n.d.
m5	90.73	n.d.	n.d.	n.d.	n.d.	n.d.	9.27	n.d.	n.d.	n.d.
m6	99.11	n.d.	0.38	0.51	n.d.	n.d.	n.d.	n.d.	n.d.	n.d.
m7	96.28	n.d.	0.22	n.d.	0.44	0.27	2.79	n.d.	n.d.	n.d.
m8	85.49	2.06	n.d.	1.24	2.75	n.d.	3.60	2.44	0.86	1.56
m9	97.91	n.d.	0.36	0.24	n.d.	0.29	1.20	n.d.	n.d.	n.d.
m10	97.71	n.d.	n.d.	n.d.	1.25	n.d.	n.d.	1.04	n.d.	n.d.
m11	98.85	n.d.	n.d.	n.d.	0.87	n.d.	0.29	n.d.	n.d.	n.d.
Mean	94.92	2.06	0.37	0.52	1.33	0.28	5.33	0.87	0.86	1.56
St. Dev.	6.76	0.00	0.09	0.41	1.00	0.01	7.26	1.15	0.00	0.00



Images 9-10: Backscattered electron images in the SEM for the object **Alea-P4**.

Left: Magnification 70x. Center of the pin Right: Magnification 100x. Center of the pin



Images 11-12: Backscattered electron images in the SEM for the object **Alea-P4**.

Left: Magnification 70x. Needle of the pin Right: Magnification 100x. Needle of the pin

Table IV.2.4. Concentration of the measured values of the elements detected on the *Alea-P20* pin with the *SEM-EDS* method, normalized and expressed in % wt. (*m.*: measurement, *St. Dev.*: standard deviation, *n.d.*: not detected)

Alea-20	Cu	Sn	Pb	Fe	S
m1	88.58	9.52	1.01	0.89	n.d.
m2	85.19	12.33	1.14	0.93	0.40
m3	87.61	10.66	0.71	1.01	n.d.
m4	89.92	8.29	0.90	0.89	n.d.
m5	89.31	9.04	0.94	0.71	n.d.
Mean	88.12	9.97	0.94	0.89	0.40
St. Dev.	1.66	1.41	0.14	0.10	0.00

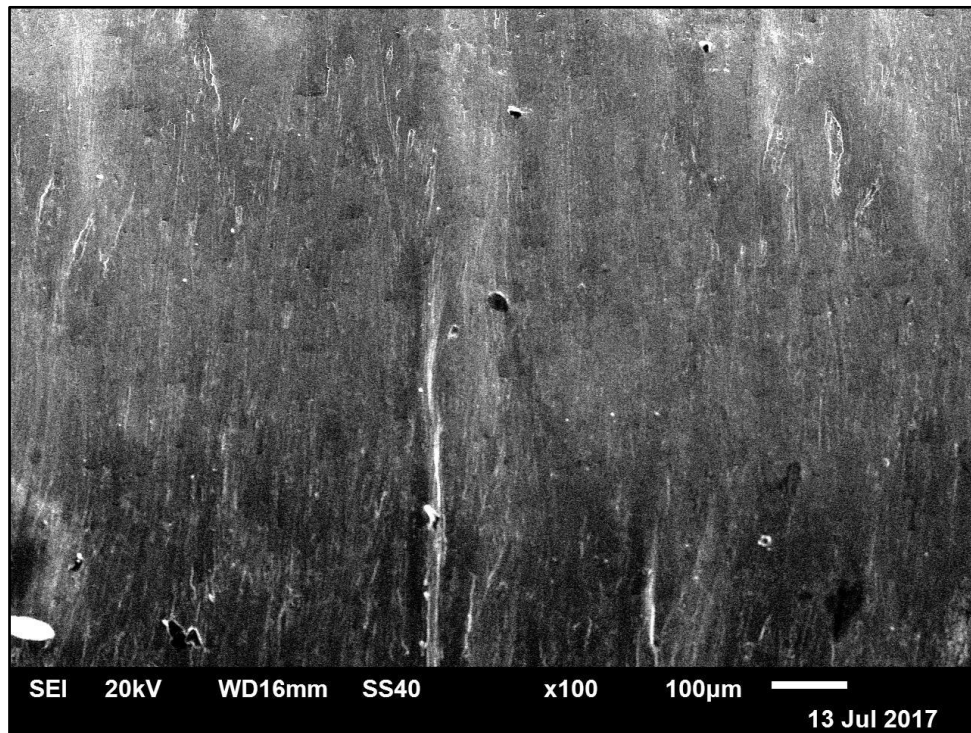


Image 13: Backscattered electron image in the SEM for the object *Alea-P20*. Magnification 100x. Needle of the pin

Table IV.2.5. Concentration of the measured values of the elements detected on the *Alea-P22* pin with the *SEM-EDS* method, normalized and expressed in % wt. (*m.*: measurement, *St. Dev.*: standard deviation, *n.d.*: not detected)

Alea-P22	Cu	Sn	Fe	Cl
m1	91.02	7.92	1.05	n.d.
m2	92.69	6.43	0.88	n.d.
m3	84.11	13.31	1.62	0.96
m4	89.42	9.38	1.20	n.d.
m5	88.14	10.08	1.11	0.66
m6	89.88	8.33	1.24	0.55
Mean	89.21	9.24	1.18	0.54
St. Dev.	2.94	2.36	0.25	0.21

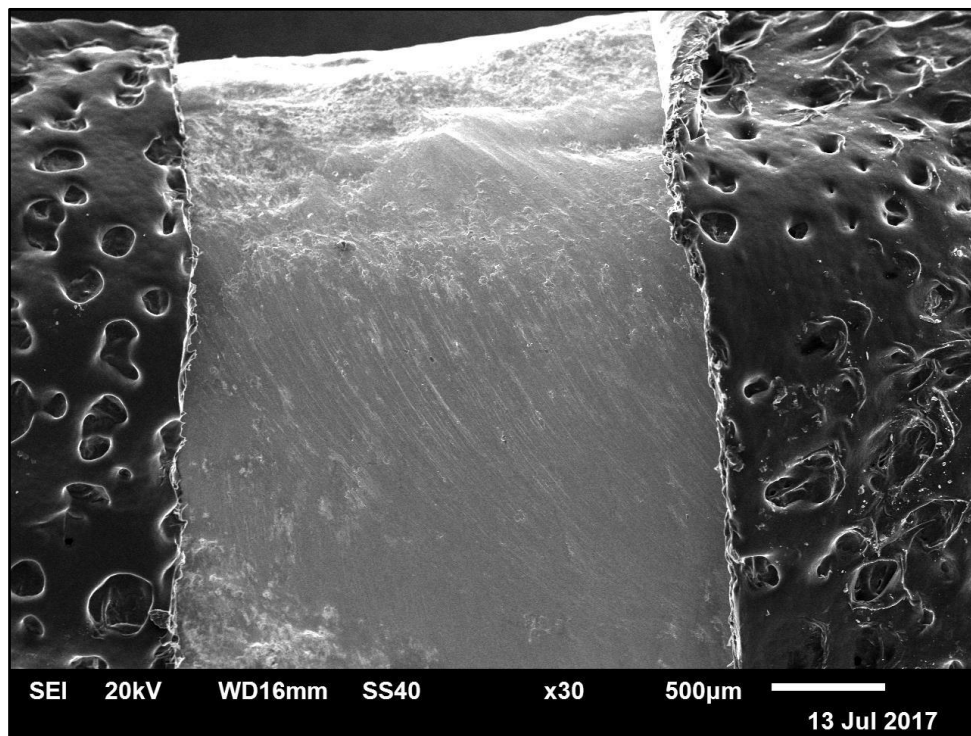
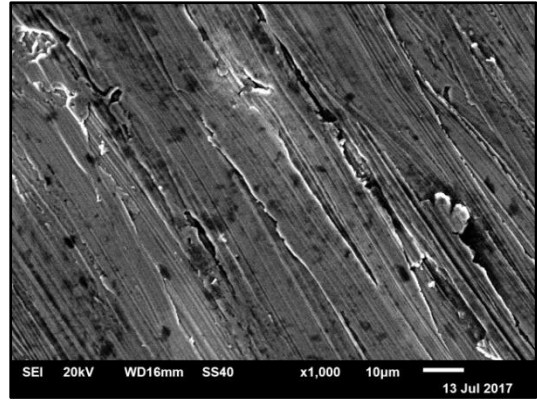
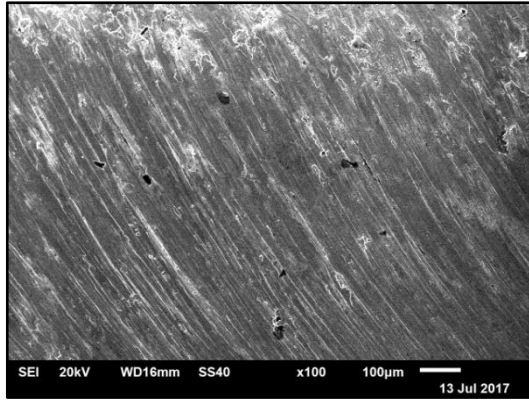


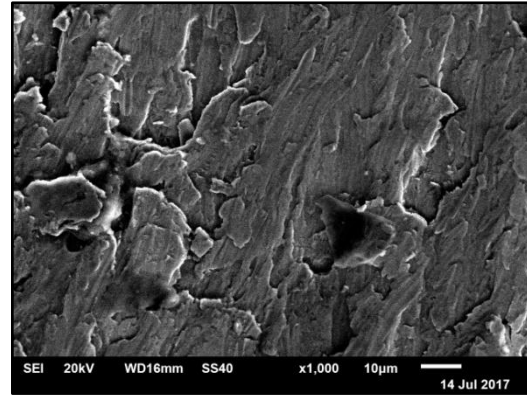
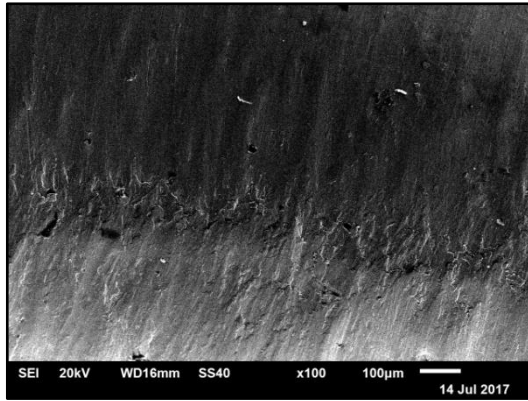
Image 14: Backscattered electron image in the SEM for the object *Alea-P22*. Magnification 30x. Head of the pin



Images 15-16: Backscattered electron images in the SEM for the object **Alea-P22**.
Left: Magnification 100x. Head of the pin Right: Magnification 1000x. Head of the pin

Table IV.2.6. Concentration of the measured values of the elements detected on the *Alea-P13* pin with the *SEM-EDS* method, normalized and expressed in % wt. (*m.*: measurement, *St. Dev.*: standard deviation, *n.d.*: not detected)

Alea-P13	Cu	Sn	Fe	Pb
m1	91.48	8.06	0.33	0.14
m2	91.91	7.67	0.26	0.16
m3	90.34	8.97	0.56	0.13
m4	90.20	8.91	0.50	0.39
Mean	90.98	8.40	0.41	0.20
St. Dev.	0.84	0.64	0.04	0.12



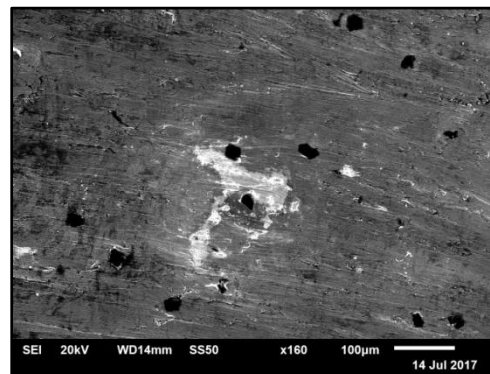
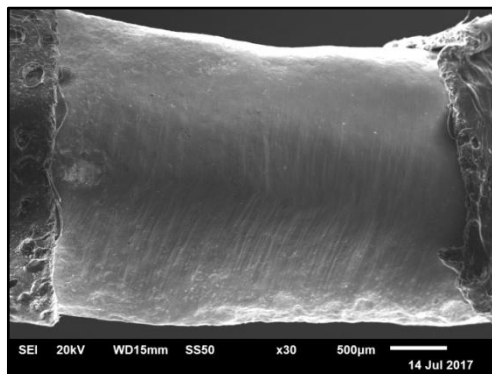
Images 17-18: Backscattered electron images in the SEM for the object *Alea-P13*.
Left: Magnification 100x. Needle of the pin Right: Magnification 1000x. Needle of the pin

Table IV.2.7. Concentration of the measured values of the elements detected on the *Alea-P14* pin with the *SEM-EDS* method, normalized and expressed in % wt. (*m.*: measurement, *St. Dev.*: standard deviation, *n.d.*: not detected)

Alea-P14	Cu	Sn	Fe	Cl	Al	Co	Ni
m1	89.51	8.37	0.43	0.34	0.13	0.45	0.78
m2	91.07	7.28	0.23	0.34	0.16	0.40	0.51
Mean	90.29	7.83	0.33	0.34	0.14	0.43	0.65
St. Dev.	1.11	0.77	0.14	0.00	0.03	0.04	0.19

Table IV.2.8. Concentration of the measured values of the elements detected on the *Alea-P15* pin with the *SEM-EDS* method, normalized and expressed in % wt. (*m.*: measurement, *St. Dev.*: standard deviation, *n.d.*: not detected)

Alea-P15	Cu	Sn	As	Pb	Fe	Cl	Al
m1	86.43	7.23	0.11	4.74	0.15	1.34	n.d.
m2	87.40	7.06	0.12	4.15	0.01	1.25	n.d.
m3	88.24	7.22	n.d.	2.41	n.d.	1.99	0.14
m4	88.94	7.15	n.d.	2.03	n.d.	1.81	0.07
Mean	87.75	7.16	0.12	3.33	0.08	1.60	0.11
St. Dev.	1.08	0.08	0.01	1.32	0.10	0.36	0.04



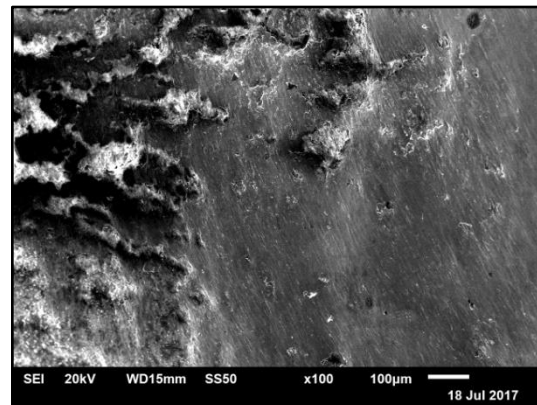
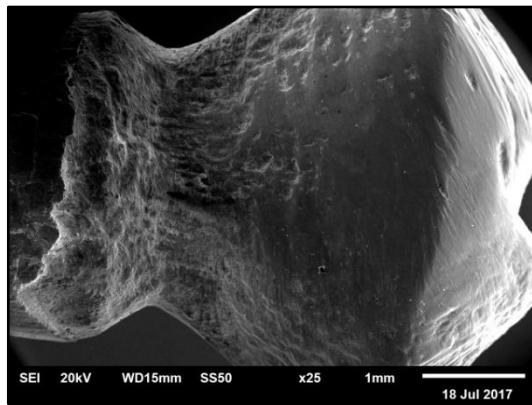
Images 19-20: Backscattered electron images in the SEM for the object *Alea-P15*. Left: Magnification 30x. Needle of the pin Right: Magnification 160x. Head of the pin

Table IV.2.9. Concentration of the measured values of the elements detected on the *Alea-P16* pin with the *SEM-EDS* method, normalized and expressed in % wt. (*m.*: measurement, *St. Dev.*: standard deviation, *n.d.*: not detected)

Alea-P16	Cu	Sn	Pb	Cl	Al
m1	90.10	8.42	0.44	0.81	0.23
m2	91.38	5.85	0.40	0.40	1.96
m3	90.23	8.21	0.39	0.70	0.46
Mean	90.57	7.50	0.41	0.64	0.88
St. Dev.	0.71	1.43	0.03	0.21	0.94

Table IV.2.10. Concentration of the measured values of the elements detected on the *Alea-P25* pin with the *SEM-EDS* method, normalized and expressed in % wt. (*m.*: measurement, *St. Dev.*: standard deviation, *n.d.*: not detected)

Alea-P25	Cu	Sn	As	Pb
m1	91.19	7.87	0.53	0.41
m2	91.91	7.17	0.65	0.28
m3	91.81	7.37	0.81	n.d.
m4	91.42	7.78	0.46	0.34
m5	91.46	8.09	0.45	n.d.
m6	90.74	8.21	0.54	0.51
Mean	91.42	7.75	0.57	0.31
St. Dev.	0.43	0.40	0.14	0.10



Images 21-22: Backscattered electron images in the SEM for the object **Alea-P25**.
Left: Magnification 25x. Head of the pin Right: Magnification 100x. Head of the pin

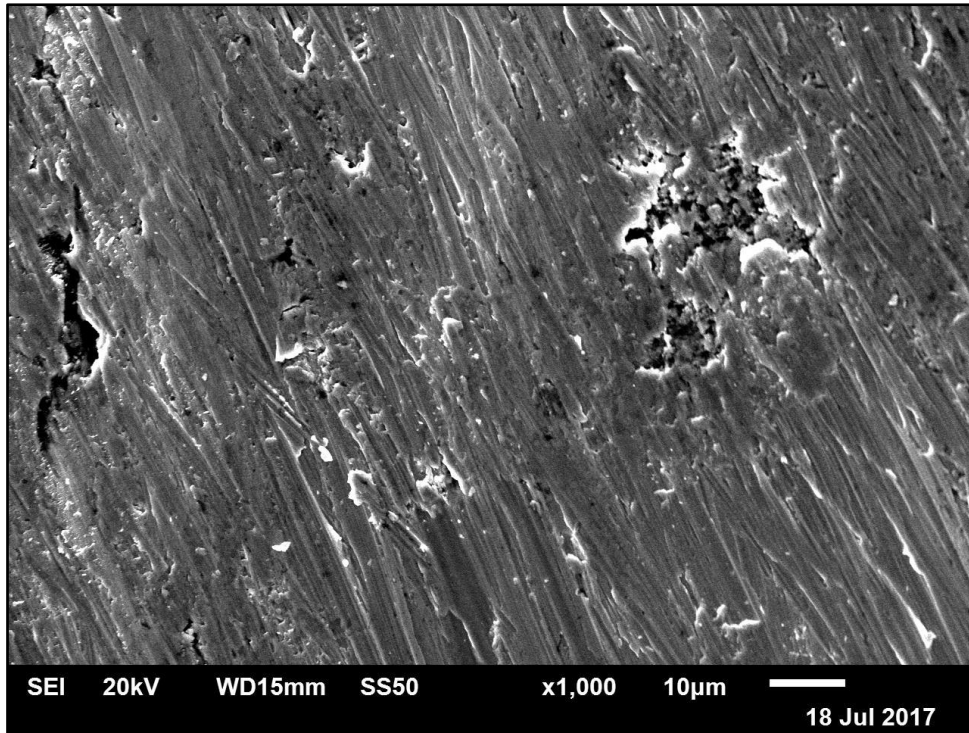
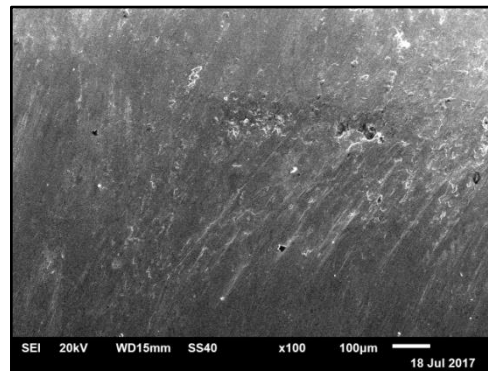
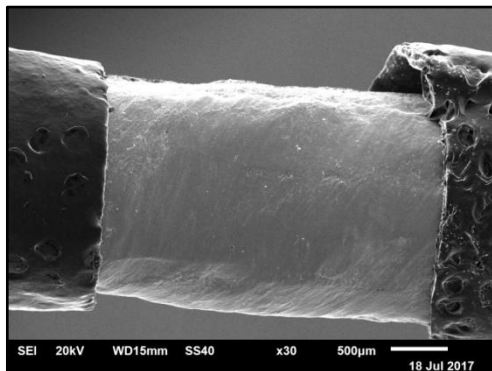


Image 23: Backscattered electron image in the SEM for the object **Alea-P25**. Magnification 1000x. Head of the pin



Images 24-25: Backscattered electron images in the SEM for the object **Alea-P25**. Left: Magnification 30x. Needle of the pin Right: Magnification 100x. Needle of the pin

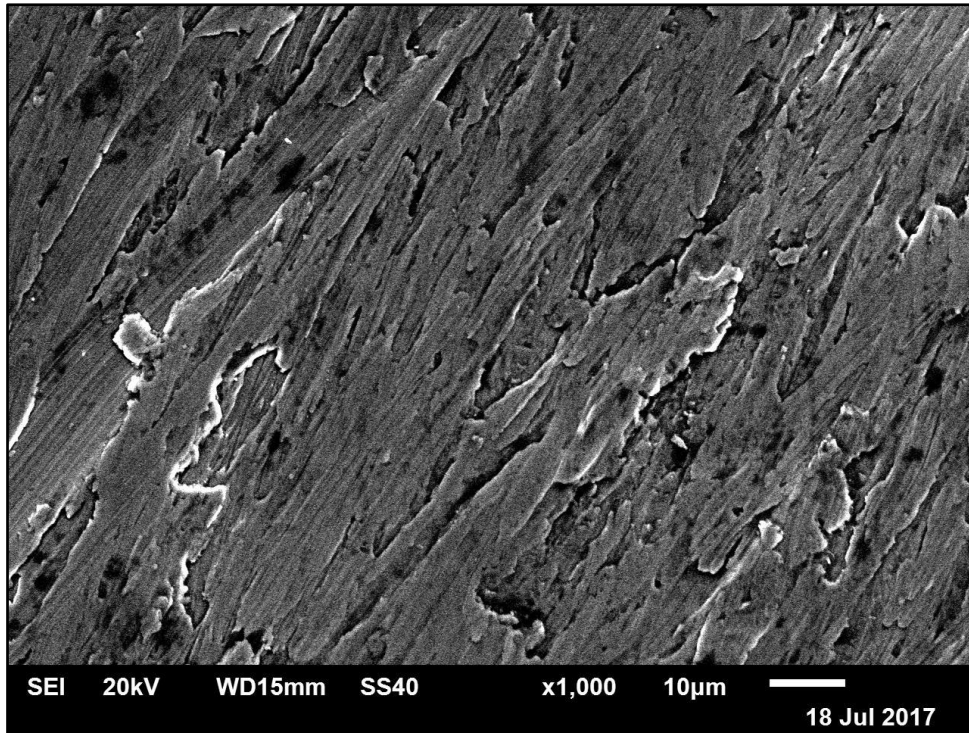


Image 26: Backscattered electron image in the SEM for the object **Alea-P25**. Magnification 1000x. Needle of the pin

Appendix IV.3

Table IV.3.1. Concentration of the measured values of the elements detected on the *Alea-WS2* pin with the *SEM-EDS* method, normalized and expressed in % wt. (*m.*: measurement, *St. Dev.*: standard deviation, *n.d.*: not detected)

Alea-WS2	Cu	Sn	Fe	As	Pb	Cl	P	Si
m1	80.29	17.05	0.48	n.d.	0.58	0.38	0.70	0.52
m2	84.98	12.62	0.43	0.25	0.47	0.28	0.40	0.57
m3	84.42	13.31	0.36	n.d.	0.54	0.75	0.25	0.35
m4	83.98	13.76	0.37	n.d.	0.53	0.63	0.29	0.45
Mean	83.42	14.19	0.41	0.25	0.53	0.51	0.41	0.47
St.Dev	2.13	1.97	0.06	0.13	0.05	0.22	0.20	0.09

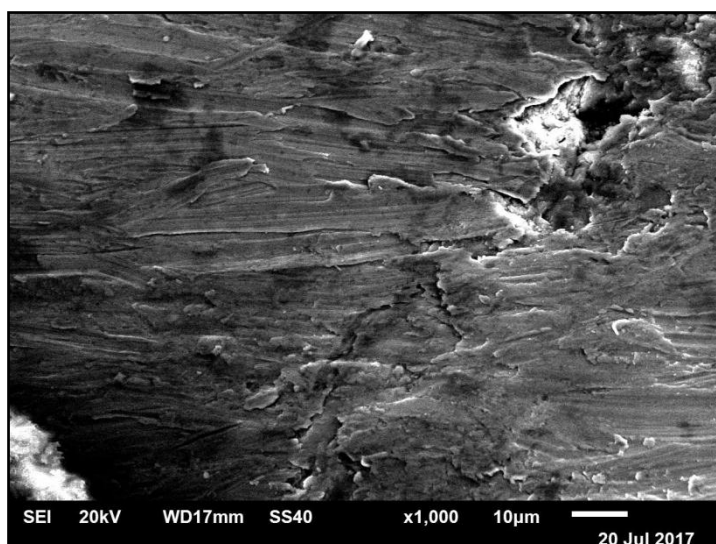
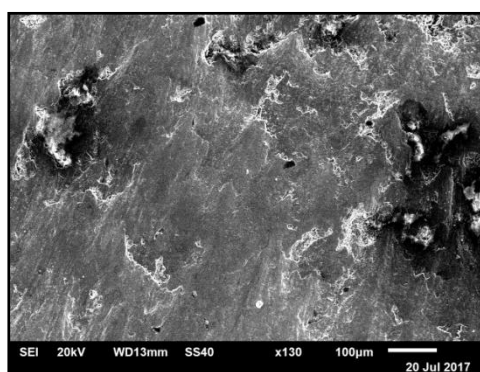
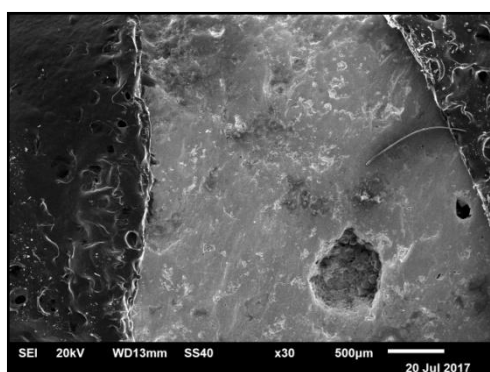


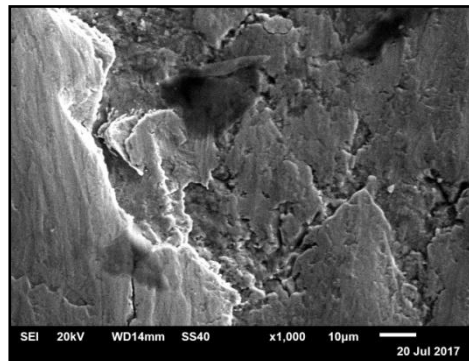
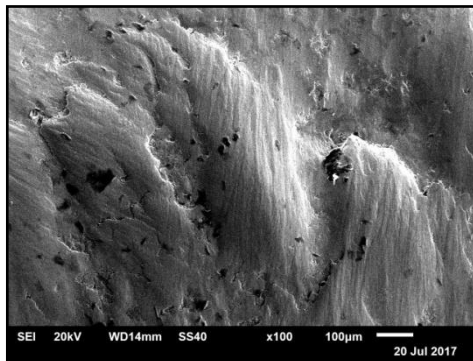
Image 1: Backscattered electron image in the SEM for the object *Alea-WS2* Magnification 1000x.



Images 2-3: Backscattered electron images in the SEM for the object *Alea-WS2* Left: Magnification 30x. Right: Magnification 130x

Table IV.3.2. Concentration of the measured values of the elements detected on the *Alea-WS3* pin with the *SEM-EDS* method, normalized and expressed in % wt. (*m.*: measurement, *St. Dev.*: standard deviation, *n.d.*: not detected)

Alea-WS3	Cu	Sn	Fe	As	Pb	Cl	P	Si
m1	82.91	13.56	0.73	0.62	0.44	0.58	0.59	0.56
m2	82.72	14.25	0.69	0.30	0.16	0.30	0.75	0.82
m3	86.05	11.91	0.69	n.d.	n.d.	0.38	0.42	0.56
Mean	83.89	13.24	0.70	0.46	0.30	0.42	0.59	0.65
St.Dev.	1.87	1.20	0.03	0.31	0.22	0.14	0.17	0.16



Images 4-5: Backscattered electron images in the SEM for the object *Alea-WS2*
Left: Magnification 30x. Right: Magnification 130x

Table IV.3.3. Concentration of the measured values of the elements detected on the *Alea-WS8* pin with the *SEM-EDS* method, normalized and expressed in % wt. (*m.*: measurement, *St. Dev.*: standard deviation, *n.d.*: not detected)

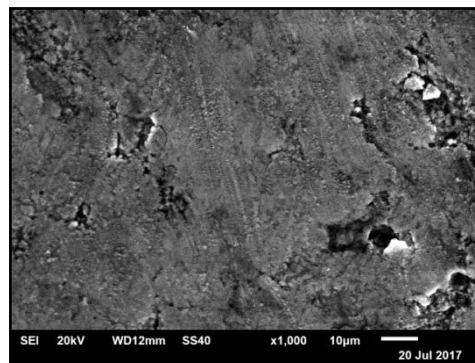
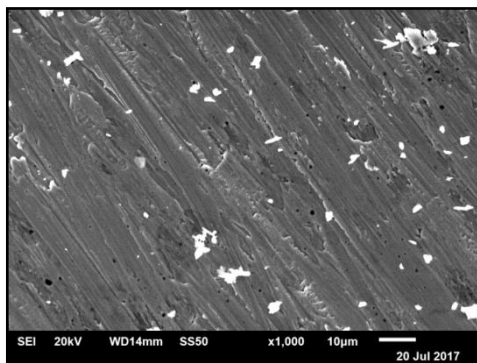
Alea-WS8	Cu	Sn	Fe	As	Pb	Cl	P	Si
m1	88.72	8.35	1.31	0.57	0.20	0.38	0.26	0.21
m2	93.15	5.39	0.88	0.21	n.d.	0.31	0.06	n.d.
m3	87.63	8.99	1.37	0.81	0.04	0.39	0.34	0.43
Mean	89.83	7.58	1.19	0.53	0.12	0.36	0.22	0.32
St.Dev.	2.92	1.92	0.27	0.30	0.11	0.04	0.14	0.21

Table IV.3.4. Concentration of the measured values of the elements detected on the *Alea-WS10* pin with the *SEM-EDS* method, normalized and expressed in % wt. (*m.*: measurement, *St. Dev.*: standard deviation, *n.d.*: not detected)

Alea-WS10	Cu	Sn	Fe	As	Pb	Cl	P	Si
m1	82.75	13.49	1.85	0.44	0.59	0.44	0.35	0.09
m2	85.22	14.78	n.d.	n.d.	n.d.	n.d.	n.d.	n.d.
m3	85.99	11.66	0.98	0.39	n.d.	0.62	0.20	0.16
m4	81.47	15.70	1.25	0.34	n.d.	0.39	0.63	0.21
Mean	83.86	13.91	1.36	0.39	0.59	0.48	0.39	0.16
St.Dev.	2.11	1.75	0.77	0.20	0.30	0.26	0.27	0.09

Table IV.3.5. Concentration of the measured values of the elements detected on the *Alea-WS11* pin with the *SEM-EDS* method, normalized and expressed in % wt. (*m.*: measurement, *St. Dev.*: standard deviation, *n.d.*: not detected)

Alea-WS11	Cu	Sn	Fe	As	Pb	Cl	P	Si
m1	84.99	10.56	1.04	n.d.	0.57	0.48	0.28	2.06
m2	84.52	12.42	1.03	n.d.	n.d.	0.37	0.56	1.10
m3	81.69	13.79	1.19	0.80	n.d.	0.37	0.40	1.77
Mean	83.73	12.26	1.09	0.80	0.57	0.41	0.41	1.65
St.Dev.	1.79	1.62	0.09	0.46	0.33	0.07	0.14	0.49



Images 6-7: Backscattered electron images in the SEM for the object *Alea-WS11*
 Left: Magnification 1000x. Right: Magnification 1000x

Table IV.3.6. Concentration of the measured values of the elements detected on the *Alea-WS20* pin with the *SEM-EDS* method, normalized and expressed in % wt.
(*m.*: measurement, *St. Dev.*: standard deviation, *n.d.*: not detected)

Alea-WS20	Cu	Sn	Fe	As	Pb	Cl	P	Si
m1	71.88	2n.d.	3.59	0.62	0.43	1.34	1.81	0.32
m2	69.43	23.00	3.83	n.d.	n.d.	1.23	2.00	0.51
m3	68.90	23.74	3.52	n.d.	n.d.	1.25	2.11	0.47
Mean	70.07	22.25	3.65	0.62	0.43	1.27	1.97	0.43
St.Dev.	1.59	1.98	0.16	0.36	0.25	0.06	0.15	0.10

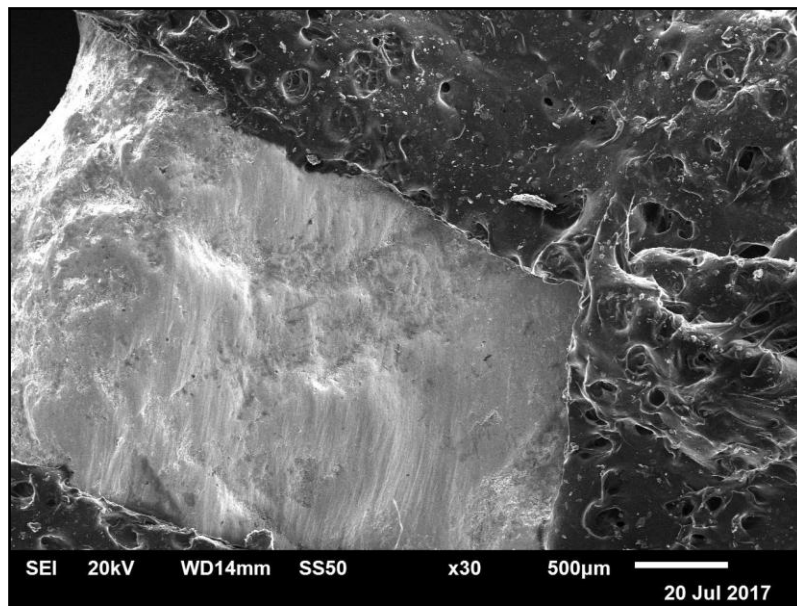


Image 8: Backscattered electron image in the SEM for the object *Alea-WS20*
Magnification 30x